BNIP3 Regulates Excessive Mitophagy in the Delayed Neuronal Death in Stroke

By

Ruoyang Shi

A Thesis submitted to the Faculty of Graduate Studies of

The University of Manitoba

in partial fulfillment of the requirements of the degree of

DOCTOR OF PHILOSOPHY

Department of Human Anatomy & Cell Science

University of Manitoba

Winnipeg

SPRINGER LICENSE
TERMS AND CONDITIONS

Dec 30, 2013

This is a License Agreement between Ruoyang Shi ("You") and Springer ("Springer") provided by Copyright Clearance Center ("CCC"). The license consists of your order details, the terms and conditions provided by Springer, and the payment terms and conditions.

All payments must be made in full to CCC. For payment instructions, please see information listed at the bottom of this form.

License Number	3299111424390
License date	Dec 30, 2013
Licensed content publisher	Springer
Licensed content publication	Springer eBook
Licensed content title	Caspase-Independent Stroke Targets
Licensed content author	Ruoyang Shi
Licensed content date	Jan 1, 2012
Type of Use	Thesis/Dissertation
Portion	Full text
Number of copies	1
Author of this Springer article	Yes and you are the sole author of the new work
Order reference number	
Title of your thesis / dissertation	BNIP3 Regulates Excessive Mitophagy in the Delayed Neuronal Death in Stroke
Expected completion date	Jan 2014
Estimated size(pages)	200
Total	0.00 CAD
Terms and Conditions	

Introduction

The publisher for this copyrighted material is Springer Science + Business Media. By clicking "accept" in connection with completing this licensing transaction, you agree that the following terms and conditions apply to this transaction (along with the Billing and Payment terms and conditions established by Copyright Clearance Center, Inc. ("CCC"), at the time that you opened your Rightslink account and that are available at any time at

JOHN WILEY AND SONS LICENSE TERMS AND CONDITIONS

Feb 14, 2014

This is a License Agreement between Ruoyang Shi ("You") and John Wiley and Sons ("John Wiley and Sons") provided by Copyright Clearance Center ("CCC"). The license consists of your order details, the terms and conditions provided by John Wiley and Sons, and the payment terms and conditions.

All payments must be made in full to CCC. For payment instructions, please see information listed at the bottom of this form.

License Number	3327760514728
License date	Feb 14, 2014
Licensed content publisher	John Wiley and Sons
Licensed content publication	CNS: Neuroscience & Therapeutics
Licensed content title	Excessive Autophagy Contributes to Neuron Death in Cerebral Ischemia
Licensed copyright line	© 2012 Blackwell Publishing Ltd
Licensed content author	Ruoyang Shi,Jiequn Weng,Ling Zhao,Xin-Min Li,Tian-Ming Gao,Jiming Kong
Licensed content date	Mar 11, 2012
Start page	250
End page	260
Type of use	Dissertation/Thesis
Requestor type	Author of this Wiley article
Format	Print and electronic
Portion	Full article
Will you be translating?	No
Title of your thesis / dissertation	BNIP3 Regulates Excessive Mitophagy in the Delayed Neuronal Death in Stroke
Expected completion date	Feb 2014
Expected size (number of pages)	200
Total	0.00 USD
Terms and Conditions	

ABSTRACT

Autophagy is a physiological process by which the cell eliminates damaged organelles, toxic agents, and long-lived proteins by degradation through lysosomal system. Mitophagy, the specific autophagic elimination of mitochondria, regulates mitochondrial number to match metabolic demand and is a core machinery of quality control to remove damaged mitochondria. A neuroprotective role of physiological autophagy/mitophagy has been discovered. However, recent studies suggested that highly accelerated autophagy/mitophagy might contribute to neuronal death in various pathological situations including cerebral ischemia. In this study, we aimed to investigate the activation of excessive autophagy, particularly, the more specific mitophagy, in neuronal tissues and its contribution to ischemia/hypoxia (I/H)-induced delayed neuronal death. I/H injury was induced by oxygen and glucose deprivation (OGD) followed by reperfusion (RP) on primary cortical neurons *in vitro*. Cerebral ischemia was induced by unilateral common carotid artery occlusion and hypoxia in neonatal mice in *vivo*.

In order to determine the extent to which autophagy contributes to neuronal death in cerebral ischemia, we performed multiple methods and found that in both primary cortical neurons and SH-SY5Y cells exposed to OGD for 6 h and RP for 24, 48, and 72 h, respectively, an increase of autophagy was observed as determined by the increased ratio of LC3-II to LC3-I and Beclin 1 expression. Using Fluoro-Jade C and monodansylcadaverine double-staining, and electron microscopy we found the increment in autophagy after OGD/RP was accompanied by increased autophagic cell death, and this increased cell death was inhibited by the specific autophagy inhibitor, 3-methyladenine. The presence of large autolysosomes and numerous autophagosomes in cortical neurons were confirmed by electron microscopy. Autophagy activities were increased dramatically

in the ischemic brains 3-7 days postinjury from a rat model of neonatal cerebral I/H as shown by increased punctate LC3 staining and Beclin-1 expression. We thus obtained the conclusion that excessive activation of autophagy contributes to neuronal death in cerebral ischemia.

BNIP3 (Bcl-2/adenovirus E19 kD interacting protein 3), a member of a unique subfamily of death-inducing mitochondrial proteins, is highly associated with mitochondrial dysfunction and delayed neuronal death in stroke. It is known that BNIP3-induced neuronal death is caspase-independent and characterized by early mitochondrial damage. Recent evidence suggested that the BNIP3 family of proteins might be important regulators of mitophagy. Here, using both stroke models, we found that homodimer (60 kD) of BNIP3/NIX (BNIP3L) were highly expressed in a 'delayed' manner. Particularly, significant mitophagic activation was confirmed by electron microscopy. In contrast, both neonatal mitophagy and apoptosis were significantly inhibited in the BNIP3 knockout (KO) mice after I/H, which was also accompanied by a significantly increased autophagic response. In addition, the infarct volume in the BNIP3 KO mice was significantly reduced as compared to wild-type (WT) mice after 7 or 28 days recovery, showing a prominent neuroprotection of BNIP3 gene silencing. A protein-to-protein interaction of mitochondria-localized BNIP3 (60 kD) with the autophagosome marker, LC3, was confirmed by co-ip, immunocytochemistry and further quantified by ELISA, indicating BNIP3 was an effective LC3-binding target on damaged mitochondria. These data demonstrated a novel role of BNIP3 in regulating neuronal mitophagy and cell death during ischemic stroke.

ACKNOWLEDGEMENTS

I would like to express my sincere gratitude and appreciation to the precious opportunity provided by the Department of Human Anatomy and Cell Science, University of Manitoba. I have enjoyed an exceptionally productive and critical six years of my life studying and striving here. This experience not only establishes my foundation in the academic career, but also makes my staying in Canada unforgettably challenging and uniquely inspiring. I would like to acknowledge the Manitoba Health Research Council (MHRC), the Manitoba Institute of Child Health (MICH), and the Canadian Stroke Network (CSN) for their generous and continuing financial supports to my graduate studies.

This thesis would never be possible without the tremendous instructions and inputs from my supervisor, Dr. Jiming Kong. To me, he is not merely a supervisor on lab techniques and academic merits, but also a mentor of life, and a role model who taught me how to become a successful scientist as well as a responsible person from his own experiences. I want to show my deepest gratefulness for all his guidance and support for the past six years. I am extremely fortunate to be supported by my other advisory committees throughout my studies. Greatly gratitude is given to Dr. Maria Vrontakis-Lautatzis, Dr. Fiona Parkinson, Dr. Mike Namaka and my external examiner, Dr. Ruth Slack, who provide close supervisions and critical guidance for the progression and conduction of my project all year long. Without their contributions, I could never make this far to become a qualified PhD candidate. Their constant encouragement and belief in myself motivates me to always look forward, especially when I was facing difficulties. These unreserved trust and help grants me ample confidence to continue my journey in the neuroscience research.

I greatly appreciated the help from all the professors in the Anatomy Department. I would like to thank Dr. Thomas Klonisch, the departmental head, for his generosity in supporting leaderships and academic exposures of graduate students. I am also enormously grateful for Dr. Maria Vrontakis-Lautatzis, Dr. Sabine Hombach-Klonisch and Dr. Hugo Bergen for their dedication and enthusiasm in teaching anatomy. They not only taught me the concrete knowledge of human anatomy, but also showed me the significance of teaching itself as an indispensable component of professionism.

Outside of the department, I am also appreciated for the mentorship of Dr. Xin-min Li, who constantly provides insightful comments for my project and constructive advices for my career development. Special thanks are given to Dr. Michael F Jackson for his advice and assistance in editing my manuscripts and thesis.

Throughout my training track, numerous people have helped and taught me so much inside and outside of the lab. I am very lucky to meet all of the students and post-doc fellows at the Drs Kong and Li's lab. Those keen discussions with everyone of them are particularly inspiring for the improvement of studies, and it is them who taught me the value of teamwork and collaboration. Gratitude also goes to my dearest friends in the department, spending time and having fun together with them during holiday seasons brings true happiness and bliss to my life. Their wonderful friendship makes me feel warm even in the coldest winter of Winnipeg.

Last but importantly, I want to express my huge appreciation to my family. Their unconditional and unwavering love is always my strength source and spiritual dependence. To my husband, who is also my dearest colleague and friend, Shenghua Zhu, I extend my thanks for what he has done and sacrificed for me. He not only supports me in every aspect

of the daily life, but also uses his knowledge and expertise to back up and solve technical issues in my experiments. To my parents, I am so blessed to have their accompanies and understandings during these years. Without all your support, I could never have accomplished this much. Your love means everything to me and my achievement belongs to all of you as well.

I wish to dedicate this thesis to
My family, for your continued support and
Encouragement.

And to my beloved grandpa,
Wish you rest in peace in heaven.

Table of Contents

List of Figures

List of Tables

List of Abbreviations

(ce)BNIP3	Caenorhabditis elegans ortholog BNIP3
2-VO	two-vessel occlusion
3-MA	3-methyladenine
4-VO	four-vessel occlusion
CSF	cerebrospinal fluid
AIF	apoptosis inducing factor
ATP	adenosine triphosphate
AMPA	2-amino-3-(5-methyl-3-oxo-1, 2- oxazol-4-yl) propanoic acid
ABT-737	pharmacological BH3 mimetic
Apaf-1	apoptosis interacting factor-1
Atgs	autophagy-related genes
BBB	Blood Brain Barrier
BNIP3	BCL2/adenovirus E1B 19 kDa protein-interacting protein 3
BNIP3 ΔTM	dominant-negative form of BNIP3
BSA	bovine serum albumin
EBSS	Earle's balanced salt solution
CA1	cornu ammonis 1
CAD	caspase-activated deoxyribonuclease
CBF	cerebral blood flow
CCA	common carotid artery
COX IV	cytochrome c oxidase subunit IV
CT	computed tomography
CypA	cyclophilin A
Cyto c	cytochrome c
DIABLO	direct IAP binding protein with low pI
DNA	Deoxyribonucliei acid
DND	delayed neuronal death
Drp1	Dynamin-related protein-1
EM	electron microscopy
Endo G	Endonuclease G
ER	endoplasmic reticulum
GST	glutathione S-transferase
GFP	green fluorescence protein
HGF	hepatocyte growth factor
HIF-1	hypoxia-inducible factor-1
HIFdn	dominant-negative form of HIF-1α
HRE	hypoxia responsive elements
HtrA2	High temperature requirement protein A2

Hsp70	heat-shock protein70
Ac-YVAD-cmk	tyrosine-valine-alanine-aspartate-chloromethyl ketone
AO	acridine orange
AVs	autophagic vacuoles
CMA	chaperone-mediated autophagy
CNS	central nervous system
EB	ethidium bromide
EM	electron microscopy
Et-1	Endothelin-1
ELISA	Enzyme-linked immunosorbent assay
Grp78/Bip	ER-specific member of heat shock protein 70 family
I/H	Ischemia/Hypoxia
ISEL	in situ end-labeling
IRE1	inositol-requiring kinase 1
JNK	c-JunN-terminal kinase
KA	kainic acid
LC3	microtubule-associated protein 1 light chain 3
LDH	Lactate dehydrogenase
LACI	lacunar infarct
LAMP-2	lysosome-associated membrane protein 2
MCA	middle cerebral artery
MCAO	middle cerebral artery occlusion
MDC	monodansylcadaverine
MEFs	mouse embryonic fibroblasts
MMP	mitochondrial membrane potential
MOMP	mitochondrial outer membrane permeabilization
MOI	multiplicity of infection
MPTP	mitochondrial permeability transition pore
MRI	magnetic resonance imaging
mTOR	mammalian target of rapamycin
NIX	BNIP3 like protein X
NMDA	N-methyl-D-aspartate
NOS	nitric oxide synthase
OGD	oxygen glucose deprivation
OCSP	Oxford Community Stroke Project classification
Opa1	optic atrophy 1
OSC	organotypic slice culture
PARP-1	poly (ADP-ribose) polymerase-1
Parkin	E3 ubiquitine ligase
PACI	partial anterior circulation infarct
PBS	phosphate buffered saline

PCD	programmed cell death
PERK	RNA-dependent protein kinase (PKR)-like ER kinase
PGC-1a	mitochondrial transcription factor A and nuclear respiratory factor 1
PI	propidium iodide
POCI	posterior circulation infarct
PINK1	PTEN-induced putative protein kinase 1
PCD	programmed cell death
PTD	protein transduction domain
PTPC	permeability transition pore complex
RNAi	RNA interference
ROS	reactive oxygen species
RP	reperfusion
SH-SY5Y	human neuroblastoma cell line
siRNA	small interference RNA
Smac	second mitochondria-derived activator of caspases
STAIR	Stroke Therapy Academic Industry Roundtable
SOD1	superoxide dismutase 1
SVZ	subventricular zone
TACI	total anterior circulation infarct
tBid	truncated Bid
TBS	Tris-buffered saline
TEM	transmission electron microscopy
tFCI	transient focal cerebral ischemia
TIA	transient ischemic attack
TM domain	transmembrane domain
TNF	tumor necrosis factor
TNF-α	tumour necrosis factor-α
TOM	mitochondrial translocase of outer membrane
TOMM22	human mitochondrial import receptor subunit
TTC	2, 3, 5-triphenyltetrazolium chloride
TUDCA	bile acid tauroursodeoxycholic acid
TUNEL	in situ terminal deoxytransferase-mediated dUTP nick end labeling
UPR	unfolded protein response
XIAP	X chromosome-linked inhibitor of apoptosis
WT	wild-type
KO	knockout

Chapter 1. Introduction

1.1 Major Types of Stroke (Ischemic/Hemorrhagic)

Stroke is a medical emergency which causes permanent neurological damage, complications, and death. There are two types of stroke: ischemic stroke, which is mainly due to the interruption of the blood flow inside the brain; and hemorrhagic stroke, which is caused by the rupture of brain blood vessels.[1] Stroke is the second leading cause of death for people above the age of 60, and the fifth leading cause in people aged 15 to 59.[2] Among all strokes, 88% are ischemia-induced, only 9% involve an intracerebral hemorrhage, and 3% involve a subarachnoid hemorrhage. Ischemic strokes, including the atherothrombotic stroke (61%) and embolic stroke (22%), are the most prevalent types in humans. The main risk factors of ischemic strokes include old age, hypertension, obesity, stress, previous stroke or transient ischemic attack (TIA), diabetes, high cholesterol, tobacco smoking and atrial fibrillation. High blood pressure is the most important modifiable risk factor of stroke.[3] Most stroke survivors develop lasting symptoms, such as physical and intellectual limitations, leading to high social costs.

1.2 Characteristics of Ischemic Stroke

1.2.1 The Anatomical Basis of Brain Vasculature

The human brain has a peculiar vasculature scheme. Blood supplement of the human brain is forced by the two major circulation systems including the anterior bilateral carotid arteries circulation and the posterior vertebrobasilar circulation. At several points blood vessels are divided into different circulation

territories and finally return to these two systems.[4] Other higher order animals such as monkeys also share a similar anatomic arrangements, with the anterior-medial side of both hemispheres supplied mainly by the anterior cerebral arteries, the most lateral territory of the cerebral cortex as well as deep brain structures supplied by the middle cerebral arteries, and the posterior part of the brain (mainly the occipital lobe, the thalamus inside and part of the temporal lobe) supplied by the posterior cerebral arteries.[5] Another extremely important structure related to the stroke pathology is the Circle of Willis, which is responsible for the communication between the anterior and posterior circulation by connecting several arteries into a well-distinguished loop. [6, 7] These arteries include the anterior and posterior cerebral arteries and the anterior and posterior communicating arteries. Through the posterior communicating artery, the posterior cerebral artery (posterior circulation) are efficiently connected to the internal carotid artery (anterior circulation). The vertebral arteries unite to form the basilar artery and plays a crucial role to the brain blood supply. [8]

1.2.2 Pathophysiology of Ischemic Stroke

The pathophysiology of ischemic stroke is closely related to the dysfunction of the arterial supplies inside the brain. There are four reasons that may contribute to the obstruction of the blood supply to brain. In thrombotic stroke, a thrombus (blood clot) usually forms around atherosclerotic plaques. Since blockage of the artery is gradual, onset of symptomatic thrombotic strokes is slower.[9] In embolic stroke, the blockage of an artery is due to an arterial embolus, a travelling particle or debris in the arterial bloodstream originating from elsewhere. An embolus is most frequently a thrombus, but it can also be a

number of other substances including fat, air, cancer cells or clumps of bacteria.[3] In systemic hypoperfusion, where blood flow is reduced to all parts of the body, heart failure from cardiac arrest or reduced cardiac output as a result of myocardial infarction, pulmonary embolism, pericardial effusion, or bleeding are the main causes. [10] Finally, cerebral venous sinus thrombosis will also lead to stroke due to locally increased venous pressure, which exceeds the pressure generated by the arteries. Infarcts are more likely to undergo hemorrhagic transformation (leaking of blood into the damaged area) than other types of ischemic stroke.[11] Various classification systems for ischemic stroke have also been established. The Oxford Community Stroke Project classification (OCSP, also known as the Oxford classification) classified stroke as total anterior circulation infarct (TACI), partial anterior circulation infarct (PACI), lacunar infarct (LACI) or posterior circulation infarct (POCI) based on the extent of the stroke, the area of the brain affected, the underlying causes, and the prognosis.[12, 13]

1.2.3 Diagnosis and Clinical Symptoms of Ischemic Stroke

Stroke can be diagnosed through several techniques, such as a neurological examination (Nihss), CT or MRI scans, Doppler ultrasound, and angiography. By using angiography, an obstruction of a specific blood vessel in the brain can be clearly distincted by injecting a radio-opaque contrast agent into the blood vessel and imaging using X-ray based techniques such as CT. [14] Accordingly the symptoms may vary due to the different location of the blood supply decrease. [15] For example, symptoms in anterior cerebral artery occlusion include contralateral hemiplegia in lower limb, impaired sensation in contralateral leg and mental confusion; symptoms in middle cerebral artery

occlusion include contralateral hemiplegia in upper limb and lower face, general contralateral sensory loss, and aphasia; symptoms in posterior cerebral artery occlusion include complex visual deficits due to lesion of the occipital lobe and disturbance of memory (amnesia); symptoms in vertebral artery occlusion ('brain stem' stroke) include the loss of pain and temperature sensation, difficulties in swallowing, phonation, and dizziness, cerebellar ataxia or nystagmus. Loss of consciousness, headache, and vomiting usually occurs more often in hemorrhagic stroke than in ischemic stroke because of the increased intracranial pressure from the leaking blood compressing the brain. If symptoms are maximal at onset, the cause is more likely to be a subarachnoid hemorrhage or an embolic stroke.

1.3 Systems Used to Study Ischemic Stroke

1.3.1 Biological Evidence of Ischemic Stroke Modeling in Different Animal Species

Clinical variability of stroke, mainly in terms of causes, duration, localization, and severity of ischemia and coexisting systemic diseases, raises the need for very large patient group sizes in clinical research to avoid confounding effects of the diversity. Certainly, there is not 'one' ideal ischemic stroke model since human stroke itself is a diverse condition. [16] Realizing that it is impossible to set up a single universally proper model for stroke, the first aspect to consider of selecting animal stroke model should be: how much does the model match with the clinical problem that will be taken under investigation? Criteria for selection of the 'ideal' animal model have been proposed. First of all, the ischemic processes and pathophysiologic responses of the selected

model should be relevant to human stroke, and the ischemic lesion size in the brain should be reproducible. Secondly, the technique used to perform the modeling should be relatively easy and minimally invasive, with physiologic variables easily monitored and maintained within normal range. Thirdly, the brain samples should be readily available for outcome measurements such as histopathological, biochemical, and molecular biological evaluation. Lastly, the cost and effort of producing the model should be reasonable and acceptable. To date, the majority of ischemic stroke models are carried out in small animals, especially in rodents[17] due to the relatively lower cost, ease of performing genetic modifications and limited ethical concerns.[18] However, in recent years, several well-designed stroke models in higher order species such as non-human primates have also been reported.[19, 20] Although models carried out in large animals are much more labor intensive and costly because of the usage of complicated invasive surgery for ischemia, combined with a high mortality rate, the advantages of these animals are indubitable since they are much closer to humans in terms of brain structure and function. [21, 22] That's why it is recommended that once a positive result is achieved from a therapeutic study in small animals, the study should be later replicated in higher species before proceeding to clinical trials on human (STAIR, 1999).

The success of stroke research requires parallel studies to identify the best animal model for each form of stroke. Therefore, detailed anatomical knowledge of the encephalic vessels of various species is essential for developing a reliable and useful model of the pathology.[4] Comparing the brain structures between different species, it can be easily observed that the rodent brain is characterized by smooth cortex without sulcus, and a higher

gray/white matter ratio when compared to brain of non-human primate. The latter species (e.g. *Cynomolgus Macaque*) demonstrates clearly identified multiple sulcus and gyrus with cortical pial vasculature, organized white matter tracts, as well as subcortical nuclei in its brain, implying great structural similarities to the human brain. Angiography of monkey brain also shows the similar arrangement of circle of Willis, anterior cerebral artery, middle cerebral artery and so on, demonstrating an exact same pattern of cerebral circulation as in human. [20] Although there is significant difference between rodent and primate in terms of complexity of cortical motor organization, a growing appreciation of certain functional similarities, [23, 24] including the cortical and basal-ganglia circuits controlling the development, maintenance and selection of adaptive motor response, is also present. [25, 26] Moreover, recent studies have revealed that despite all of the changes that arterial branches have undergone during development of the brain, their vascular territories have remained constant throughout the evolutionary process. [4] This consistency in brain vasculature can be further confirmed by the consistent anatomic structure of the Circle of Willis between different species.

1.3.2 *In Vivo* Animal Models of Ischemic Stroke (Three Major Types)

Experimental animal models of ischemic stroke are characterized as global, focal, and hypoxia/ischemia in nature.[27] Global ischemic stroke models are designed to mimic the clinical situation where cerebral blood flow (CBF) is reduced throughout most or all of the brain, which is commonly caused by cardiac arrest and asphyxia in humans. [28] Focal ischemic stroke models are intended to mimic a reduction in blood flow to a very distinct,

specific brain region, which actually has a greater relevance than other models to the typical human stroke situation. [29] The hypoxia/ischemia stroke models are almost exclusively used in young animals to mimic the neonatal (perinatal) stroke in human, when vessel occlusion is combined with breathing in a hypoxic environment.[30, 31] In particular, these models are also used to reproduce permanent or transient, complete or incomplete, as well as focal or multifocal ischemia. Ischemic lesion size varies greatly according to the ischemia duration. Permanent stroke refers to the long-lasting cerebral ischemia with no reperfusion; while the transient stroke happens when an occluded artery is recanalized as in most of human stroke, consequently the effects of reperfusion in the ischemic territory (i.e. reperfusion injury) can be assessed.[16, 32, 33]

1.3.2.1 Global Ischemic Stroke Models

To date, there are 4 major global ischemic stroke models.[27, 28, 34, 35] In 1979, Pulsinelli and Brierley developed the four-vessel occlusion (4-VO) model in rats. This model uses permanent coagulation of the vertebral arteries, plus temporary ligation of the two common carotid arteries to provide a method of reversible forebrain stroke.[36] Blood flow was found decrease to 3% of control values in hippocampus, striatum, and cortex resulting in a rather extensive pathological change. After 30 minutes of ischemia, damaged striatal neurons were detected, with hippocampal injury detectable in 3 to 6 hours and cortex damage in 1 to 3 days after reperfusion.[37, 38] This model provides a high rate of predictable ischemic neuronal damage and a low incidence of seizures, and does not require anesthesia at the time of carotid occlusion.[39] It has been recognized as a useful tool to study the delayed neuronal damage in

global ischemic stroke and to test the neuroprotective efficacy of drugs by many studies.[28, 40] The two-vessel occlusion (2-VO) combined with hypotension model in rat and mice were carried out by ligation of both common carotid arteries along with a whole-body blood pressure reduction to 50 mm Hg to produce a reversible forebrain stroke.[41-44] It is an improved alternative to the 4-VO model, since the animals recovering from 2-VO have less respiratory problems than from 4-VO due to a minimal injury on the Purkinje fibers of the cerebellar brain stem.[45] Besides, the 2-VO model is more easily handled as the ischemia and reperfusion can be achieved instantly.[28] Another useful model should not be neglected is the Gerbil 2-VO model.[46] Uniquely, gerbil has no posterior communicating arteries developed throughout the evolution, so in this species the anterior circulation of the brain is completely independent from the posterior vertebral system.[47] By temporarily ligating the carotid arteries with no reduction in blood pressure in gerbils, the CBF in cortex can be reduced to ~1%, while in hippocampus reduced to ~4%.[48] This model is widely accepted and used in the last decade due to its high efficiency in producing a profound forebrain ischemia and relatively less requirement of surgical techniques. Finally, complete global ischemia models are also available in stroke research. It could be achieved by decapitation, neck cuff, cardiac arrest, or by ligation or compression of all arteries from the heart.[49] The blood flow to the whole brain in these models can be reduced to zero or <1%. However, due to a very high mortality rate, the complete global ischemia models are not widely used today despite the long history they had since their early invention in 1960s.[27, 50]

1.3.2.2 Focal Ischemic Stroke Models

It is commonly agreed that the focal ischemic stroke models are more relevant to the typical human stroke. Especially, most animal stroke models were developed to induce cerebral ischemia within the middle cerebral artery (MCA) territory, in order to be pertinent to the clinical fact that around 80% of cerebral ischemia happens in the MCA territory in human. [51, 52] Focal ischemic stroke is different from global ischemic stroke in two aspects. First of all, longer insults are usually required to cause damage in focal ischemia due to the fact that the blood flow is always higher even in the ischemic core than during global ischemia. Secondly, there is a marked gradation of ischemic injury from the core of the lesion to its farthest border, consequently there are altered metabolic conditions in the damaged area. Although the insult of the focal ischemia is much more complicated than in global ischemia because of its duration and heterogeneity, it is a valuable and reasonable model for human stroke and is most widely used today.[27] Certainly, there are sub-types of focal ischemic stroke as well, among which the blood vessel is occluded either permanently or transiently, and damage results from either ischemia alone or combined with reperfusion. For the past several decades, a variety of methods to induce the brain vessel occlusion and trigger the focal ischemic stroke have been developed. Seven of them are the most well-described and well-validated ones. In the following sections, I summarized from recent literature and described each of these methods briefly in term of procedures, preferred applications as well as strengths and weaknesses, respectively, and made comparison and contrast between them.

1.3.2.2.1 Tamura's model (Tamura et al., 1981)

In 1981, Tamura et al. devised a permanent proximal MCA occlusion model in rats by using electrocoagulation, which also involved sub-temporal craniotomy.[53] This model has been applied widely since it allows access to the more proximal regions of the MCA and results in a focal ischemic infarction of both the cortex and striatum in the MCA territory.[54] For the Tamura's model, it is important to make sure that the MCA be occluded at the proximal site in order to yield both cortical and sub-cortical damage. By using this permanent MCAO model, it was found that local CBF in cortical areas in which histological abnormalities occur was approximately 25 mL/100 g/min, and the region of ischemic damage corresponded to the area of marked reduction in CBF.[55] Afterwards, modifications[56] have been made on this model to allow reperfusion by using microclips[57] or ligature snares[58] instead of electrocoagulation, thus being compatible with preclinical drug development studies. The main disadvantage of this model includes the requirement of craniotomy, which expose the brain to the atmosphere and affect intracranial pressure and blood-brain barrier (BBB) function. Also, drilling or electrocoagulation may lead to thermal and mechanical damage of the brain and cause an inconsistent infarct size.[16]

1.3.2.2.2 Intraluminal suture MCAO model (Koizumi et al., 1986)

Middle Cerebral Artery Occlusion (MCAO) models have been used extensively because of their purported relevance to human thromboembolic stroke.[59] After first reported by Koizumi et al. in 1986,[60] the intraluminal suture MCAO model developed through the decades and became the most frequently used model of focal ischemic stroke to date. It is most commonly

used in rats and mice, while the technique engages approaching a monofilament through the internal carotid artery to specifically block the blood flow to MCA. Various methods of intraluminal occlusion of the MCA have been reported, including the cap method (Cam), common carotid artery route by Koizumi et al, as well as external carotid artery route by Zea Longa et al.[61] It provides reproducible MCA territory infarctions involving both frontoparietal cortex and striatum and allows reperfusion by simply retracting the suture from the targeted area. Since the technique is less invasive and easy to perform, it is advantageous for studies of pharmacological neuroprotection and cellular mechanisms of brain injury after stroke. It has been proved that brain damage of this model is controllable, since the size of the filament correlates well with the size of the infarct,[62] and the lesion size of the brain grows when the suture insertion goes deeper.[63, 64] When Belayev et al. coated the intraluminal suture with poly-L-lysine to make the suture more adherent to the surrounding endothelium; they found that this coating technique resulted in a more consistent infarction.[65] Using the intraluminal suture MCAO method, CBF decreased by 80% in the cortex and caudoputamen and to remain at this reduced level for even up to 180 min.[66] Reperfusion is usually performed by withdrawing the thread, and the animals will survive for days, weeks, and months, allowing functional outcomes to be measured.[67] This technique is also widely applied in transgenic mice to explore the involvement of a variety of genes and proteins in the mechanism of ischemic injury and neuroprotection.

However, besides those obvious advantages of this model, it actually may cause the vessel rupture and subsequent subarachnoid hemorrhage during the surgical procedure. Several studies showed that the silicone-coated suture

may produce more consistent infarcts with good reproducibility and reliability in contrast to the uncoated suture.[68-70] Silicone coating of the suture and laser Doppler-guided placement of the suture could reduce the incidence of subarachnoid hemorrhage.[71] On the other hand, spontaneous hyperthermia appears to be associated with hypothalamic injury and occurs in most animals subjected to suture occlusion of MCA lasting 2 hours (h) or more, [72] so control the duration time of MCAO under 2 h will be essentially important. Sometimes inadequate MCAO may also occur due to the inconsistent suture size or the inadequate insertion depth, so keeping every parameter identical through all the experiments may secure a more reproducible outcome.

Although the Tamura's model could produce infarction similar to that induced by the intraluminal suture MCAO, the required invasive surgery, relative lower success rate, and the mild and inconsistent functional deficits it caused[73] only make it a less recommended and alternative model for the intraluminal suture MCAO model.

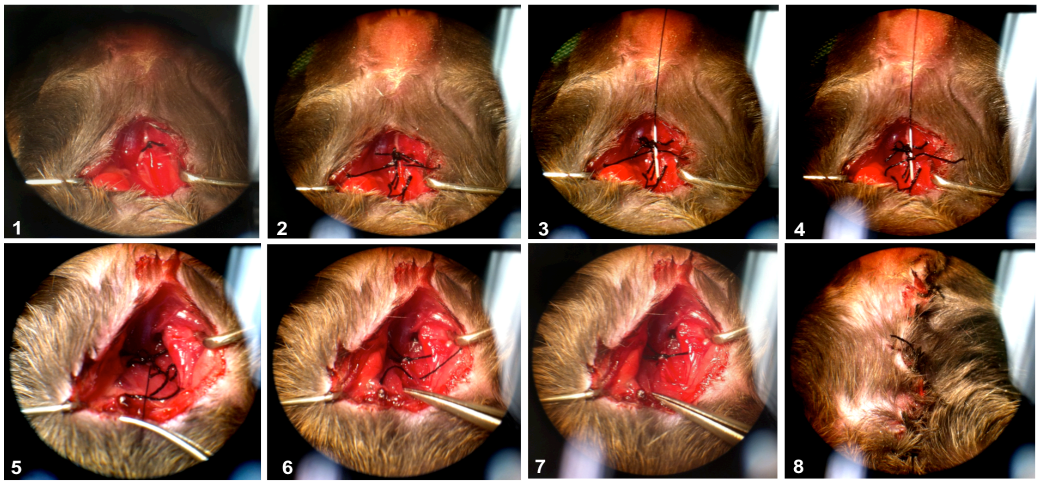

Fig 1.1 Procedures of intraluminal suture MCAO modeling on adult mice. See *Materials and Methods* for details. All the images used in the *Introduction* are original data.

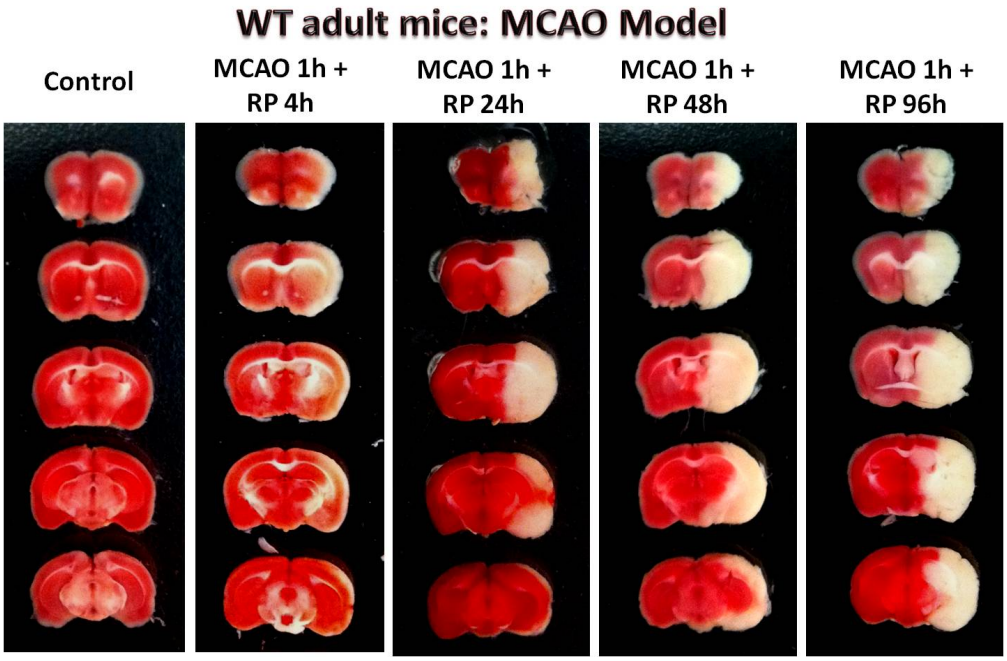

Fig 1.2 Representative images of ischemic brain infarction in pilot MCAO trials. Ischemic brains were dissected from 2-3 month old BNIP3 WT mice treated by 1 h MCAO followed by 4 h, 24 h, 48 h and 96 h recovery, respectively. Whole brains were dissected into 5 equal-thickness slices then stained by the TTC solution. Control group was treated with MCA exposure but not ligation. N = 3 for each group.

1.3.2.2.3 Embolic model

There are two types of embolic model. One is the thromboembolic model, which refers to the injection of autologous thrombi (e.g. human blood clot; homologous small clot fragments; modified fibrin-rich autologous clots) into extracranial arteries to reach the distal intracranial arteries. Another is the non-clot embolic model, refers to the injection of compounds and artificial embolic materials (e.g. viscous silicone; collagen; retractable silver ball & microspheres) into common carotid artery or internal carotid artery. [16] Both of the embolic

models mimic human stroke closely since most of the human strokes are caused by the thromboembolism. This model provides access to test thrombolytic agents and to study combination therapies (i.e. thrombolysis combined with neuroprotective drugs) on animals prior to the clinical studies on human.[74-76] Furthermore, the latest microsphere-induced embolic model is advantageous by producing a larger therapeutic window for drug testing in stroke as a result of a slow lesion development. It may also produce multifocal small cerebral lesions for the more specific stroke research.[77] Conversely, the location of infarction(s) is not consistent in the embolic model, and early spontaneous recanalization may take place. In order to avoid these weaknesses, making sure obstructing emboli is located in the proximal segment of a large feeder artery and using autolysis resistant fibrin-rich emboli might be the effective solutions.[78]

1.3.2.2.4 Photothrombosis model

This model induces a cortical infarct by the systemic injection of a photoactive dye (most often Rose Bengal) in combination with irradiation by a light beam at a specific wavelength.[79] As a consequence, the singlet oxygen has been generated leading to focal endothelial damage, platelet activation and aggregation in both pial and intraparenchymal vessels within the irradiated area.[80] By using this method, a consistent infarction in the frontoparietal cortex will be introduced while sparing the deep structures. Since the region of irradiation can be determined, any ischemic lesions in the desired cortical area could be induced and monitored selectively. The model is also less invasive given that it only requires a small craniotomy, with the dura remains intact throughout the surgical process.[29] It can be used to address specific questions,

such as in the restorative drug studies and neuronal repair evaluation. The major disadvantage of the model is the lack of penumbra due to edema and BBB breakdown in the lesion area, which is certainly undesirable for preclinical drug studies where the main target is penumbra.[81] Nevertheless, a newly designed photothrombotic ring model with modified irradiation qualities in terms of beam intensity or duration is able to induce lesions involving a penumbra.[82] Another limitation of the model is the microvascular injury resulted from the photochemical reaction, which is resistant to therapies based on the enhancement of collateral perfusion.

1.3.2.2.5 Endothelin-1 induced model

Endothelin-1 (Et-1) is an effective vasoconstrictor. When Et-1 is dropped directly onto the exposed MCA or onto the adjacent area of MCA by stereotaxic intracerebral injection, CBF in the MCA territory will be significantly reduced to around 70–93%, resulting in an ischemic lesion comparable to that induced by surgical MCAO. [83, 84] Although this model is less invasive and capable of inducing ischemia in any desired region of the brain, however, it is also inevitably dose-dependent on endothelin-1, causing a limited control over ischemia duration and intensity. Endothelin-1 application also induces astrocytosis and triggers axonal sprouting, which may retard the interpretation of the results in neural repair studies.[85]

1.3.2.3 Neonatal (Perinatal) Stroke Animal Models

Stroke attacks children, including newborns. Recent estimates suggest that ischemic stroke occurs in 1 per 4000 live birth,[86] clearly a much higher rate than in older children. Neonatal stroke refers to ischemic and hemorrhagic events resulting from disruption of either arteries or veins from early gestation

through the first month of life.[87] Perinatal stroke describes cerebrovascular lesions that occur from 20 weeks' gestation to 28 days after birth.[88] Clinically, both neonatal arterial and venous strokes often present with seizures, typically focal motor seizures, accounting for an estimated 10% of the seizures in term neonates. Children frequently have significant long-term disabilities after a neonatal stroke, including cognitive and sensory impairments, cerebral palsy, and epilepsy.[89] Some children will even present delayed development. The major risk factors for neonatal strokes include cardiac disorders, coagulation disorders, infection, trauma, drugs, maternal and placental disorders, and perinatal asphyxia.[88, 90] Well-designed clinical trials for neonatal stroke treatment are scarce, but some current studies reported the transplantation of neural stem cells and umbilical cord stem cells could be a prospective therapy. Another treatment with some proven benefits is hypothermia, although it may be more advantageous when in conjunction with pharmacological agents.[91]

Given that the neonatal brain is very different from the adult brain developmentally and functionally, it is inappropriate to simply extrapolate the adult data directly to the neonatal conditions. [92] Hence, several new models of neonatal/perinatal stroke have been developed, and an extended range of species and ages from the traditional models has also been established. In the early 1980s, **Vannucci** et al. invented the first neonatal stroke model on rat. This model is recognized as the most robust and productive model of both gray-matter and white-matter injury in the human perinatal asphyxia. [93] It uses a combination of unilateral common carotid artery ligation with a hypoxic treatment of 8% O_2 on the postnatal day 7 rat and mice pups. Since 7-day-old rat has brain maturity equal to an early third trimester human fetus in many

aspects, [94] the clinical relevance of the model could be validated moderately. Nonetheless, a marked strain difference in susceptibility to H/I injury has been detected.[95] As a consequence, a careful selection of the wild-type controls for the model could never be over-emphasized. Most of the late neurobehavioral and functional outcome studies have been performed in the neonatal rat following H/I; [96, 97] however, studies in the mice and rabbit models are also now being reported.

Recently developed models for the study of neonatal stroke also include the fetal sheep model in 2001 and near-term fetal rabbit model in 2004. The previous one mimics the human intrauterine H/I by exposing the fetuses to maternal hypoxemia[98] or to umbilical cord occlusion;[99] while the latter one mimics acute placental insufficiency in humans. Surviving newborn rabbits exhibit persistent hypertonia and motor deficits, which are striking phenotypes of cerebral palsy.[100] The neonatal stroke has also been provoked in the higher order species such as non-human primates. In the classic primate models of Myers, term monkey fetuses were exposed to true asphyxia (i.e. cessation of respiratory gas exchange) by covering their heads with a rubber sac and clamping their umbilical cord at delivery, closely resembling the clinical and pathological changes in human perinatal stroke.[101, 102] Over two decades, Myers described 4 patterns of brain damage in Rhesus monkeys that related to the degree of hypoxia/anoxia, and whether hypoxia-ischemia was combined with acidemia.[103] These experiments accurately reflect the neuropathology and mechanisms in newborn human infant and served as a priceless resource for safety and efficacy testing before trials on human.[26] In return, apparently, the cost of such models is high. They require specific facilities and equipments,

significant financial support of the animals and their care, greater ethical considerations, as well as high-skilled professional personnel who can handle them.

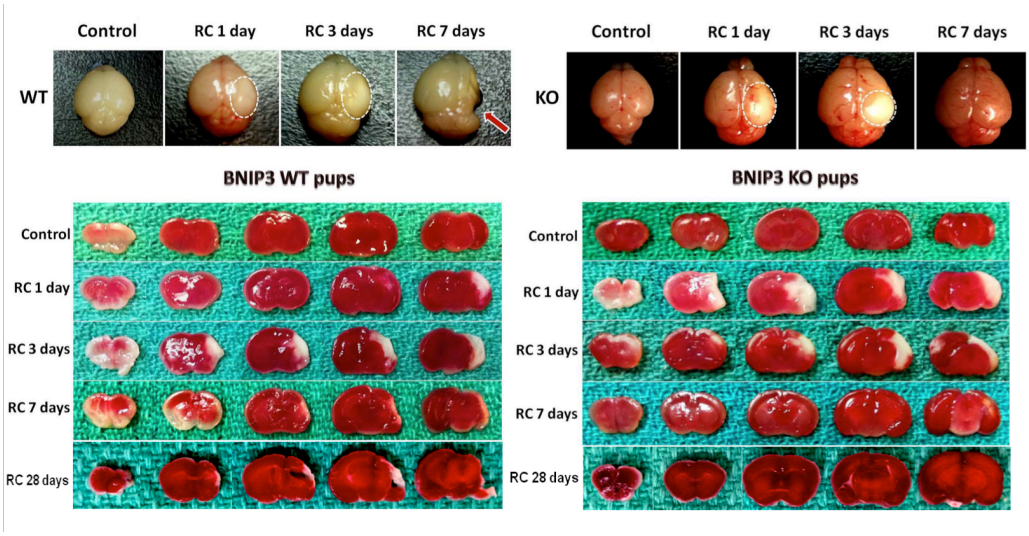

Fig 1.3 Representative images of the neonatal ischemia/hypoxia (I/H) brain injuries on postnatal day 7 mice pups. See *Materials and Methods* for detailed procedures.

1.3.2.4 Variability of *In vivo* Stroke Models

Although animal modeling has provided us most of our knowledge about pathogenic mechanisms and possible treatment of ischemic stroke, the relevance of animal stroke models to human stroke is still controversial, since many agents showing neuroprotection in preclinical animal studies have failed to show effects on stroke patients.[18] A number of factors may compromise the validity of a model by induce inter- or intra-model variability if they are not rigorously monitored. [104] Most variability in stroke modeling comes from but not limited to the animal related factors (e.g. age, strain/genetic background and gender differences), physiological parameters during the surgery, and

anaesthesia methods that are used. In experimental design, people usually tend to use the young and healthy animals with no underlying chronic diseases or any genetic predisposition to such diseases, which actually does not so resemble to the human situation. In fact, the typical stroke victims in the human population are often elderly, with many potential complications, such as diabetes, hypertension, or coronary disease. Aging is a major risk factor for stroke pathology but is frequently overlooked in studies on animals.[4] In 2005, Zhang et al. proved that aging also contributes to the reduced angiogenesis and poor neurological function recovery after stroke in rats.[105] Other researchers have revealed that rats with various strain/genetic background will response differently to a stroke attack. Certain rat strains are more sensitive to MCAO and produce more stable infarctions like the spontaneously hypertensive stroke-prone rats. Recent findings suggest that this unique strain has a genetic susceptibility to stroke even not related to blood pressure, thus could be used to investigate genetic influences on stroke.[106] On the other hand, certain rat strains may not be suitable at all for a suture MCAO model due to their distinct cerebrovascular anatomy, such as Fischer rats.[107] Additionally, the female rats develop smaller infarcts after MCAO than male rats, as a result of the potential neuroprotective effects of female hormones. [108] The physiological variability in stroke models includes temperature, blood glucose levels, arterial blood pressure and arterial blood gases. Temperature changes will affect ischemic lesion size considerably: mild to moderate hypothermia confers noticeable neuroprotection, in contrast, hyperthermia is coupled with an expansion of neuronal damage. [109, 110] Since hyperglycemia will worsen the ischemic damage in majority of experiments, using fasted animals tends to

minimize inter-animal variability of plasma glucose levels. [17] Also, the brain loses its homeostasis upon an ischemic attack and becomes more vulnerable to changes in arterial environment, parameters such as blood pressure and blood gases should be continuously controlled in any ongoing stroke experiments. [111] Finally, it has been shown that effectively monitoring the CBF by laser-Doppler flowmetry could dramatically improve the quality of an animal stroke model. [112]

Anaesthesia method is another critical factor to be considered when setting up an *in vivo* stroke model. Since most of our commonly used anaesthetics show some degree of neuroprotection,[113] selecting the best applicable anaesthesia approach with the minimum impact on result interpretation would be extremely important, especially in the preclinical neuroprotective drug studies. In the study using suture MCAO model in rats, inhalation anaesthesia under mechanical ventilation has been found to be the best anaesthesia method, as it provided a better control of physiological parameters and a lower mortality rate.[114]

1.3.3 *In Vitro* Models of Ischemic Stroke (Two Major Types)

In vitro models of ischemic stroke are differing from *in vivo* stroke models in several aspects. First of all, it requires a rather longer duration of the anoxic or hypoxic insult to kill neurons *in vitro*. Secondly, ATP depletion is less severe and the release of glutamate is delayed *in vitro* compared to ischemia *in vivo*. Thirdly, the absence of blood vessels and blood flow *in vitro* eliminates important structural and functional components of the damage process present *in vivo*, including the infiltration of inflammatory cells. Finally, the composition and responsiveness of glial cells *in vitro* differs from that in the intact brain. [27]

Although *in vivo* stroke models are more accurate in term of physiology, the technical demands and high costs make it less accessible for researchers to test the efficacy and mechanism of interested agents in a time-efficient manner. As a consequence, an *in vitro* stroke model is highly demanded and shows enormous benefits over the *in vivo* models. It provides a simple and highly controllable experimental system for the drug selection and basic mechanistic studies in a comparably low cost. It is also amenable to a wide variety of pharmacological manipulations and gene/protein functional measurements. In fact, the way isolated cells behave upon a substrate stress *in vitro* has been demonstrated to be quite similar to the way that the same cells behave under the catastrophic conditions of stroke *in vivo*. [115] The *in vivo* and *in vitro* stroke models complement one another while both of them are indispensable tools for the ischemic stroke research. Currently the most commonly used *in vitro* models of ischemic stroke are: organotypic brain slice model and primary neuronal culture plus OGD/RP model.[116]

1.3.3.1 Organotypic Brain Slice Model

Slices of developing brain tissue can be grown for several weeks as so called organotypic slice cultures (OSC). [117] To date, many OSC model systems have been used to investigate mechanisms and treatment strategies for various neuropathological states, including ischemic stroke. [118, 119] Compared to the primary cell culture model, OSC of explanted tissue (i.e. most commonly hippocampus) represent a complex multi-cellular *in vitro* environment which is advantageous in the preservation of tissue-specific cell connections, local functional circuitry and morphological architecture. [120] The two major methods for neuronal OSC are the roller-tube technique by

Gahwaler [121] and the interface cultures by Stoppini. [122] In both methods, organotypic tissues are derived from different brain regions of early postnatal (P0-P7) animals, such as rats and mice, rabbits, [123] pigs, [124] and even human fetuses. [125, 126] The conventional OSCs are mostly obtained from neonatal brains, however, attempts to culture adolescent or adult brain tissue have been made recently. [127, 128] Su et al. have reported that OSC from adult mice under conventional conditions led to a time-dependent and reproducible cell death, which was characterized by around 50% cell loss after 6 days *in vitro* (DIV) and 90% cell loss after DIV 15. [119] The cell degeneration during adult OSC can be utilized as a tool for studying neuroprotection in drug development since adult animals are more appropriate model for adult patients. [129] In addition, the OSC approach is also applicable on transgenic mice for the investigation of various gene function. [130] Since these slice cultures also reveal long-term synaptic activities and electrophysiological features of intact brain, it is compatible with physiological studies or pharmaceutical screening of the neuroprotective compounds in stroke. [131] Hence, it is a feasible alternative between primary cell culture and intact animal in terms of stroke modeling. The main shortcoming of this model is that the ischemic injury or treatments of drug are frequently limited to the surface area of brain slice but can not consistently penetrate to the inside of tissue.

1.3.3.2 Primary Neuronal Culture and OGD/RP Model

Another approach to induce stroke-like, energy failure conditions in both primary cell culture and OSC is to combine deprivation of oxygen and glucose (OGD), defining as the OGD model. [117, 132, 133] OGD model efficiently mimics the *in vivo* cerebral ischemia in which both hypoxia and hypoglycemia

are closely involved. [134, 135] In addition, during reperfusion (RP) period in stroke and brain trauma, inflammation response occurs and causes injury. Because this RP-induced injury is involved in the brain's ischemic cascade and reintroduction of oxygen within cells may cause damage to cellular proteins, DNA, and the plasma membrane, the effects of reoxygenation should be considered as well. [136] In the primary cell culture model, neurons are generally cultured in glucose-free Earle's Balanced Salt Solution (EBSS) in a hypoxic incubator for a designed length of time, until OGD is terminated by replacing the complete medium to cultures with a follow-up reperfusion injury.[137] Dissociated cortical or hippocampal neurons can be separated from embryonic 18 days (E18) rat brains or embryonic 16 days (E16) mice brains using standardized protocol. These primary cell cultures can last up to four weeks in neurobasal medium with B-27 supplement, reaching a survival rate and purity up to 95% of exclusive neurons. [138, 139]

In the OSC model, the high susceptibility of CA1 neurons to prolonged OGD is similar to their selective vulnerability to brain ischemia *in vivo*. [140] However, the OSC model failed to mimic the typical 'delayed neuronal death' pattern after global ischemia *in vivo*. [141, 142] Later, Xu and his co-workers reported this delayed cell damage in the hippocampal slice cultures subjected to OGD. [143] Similar results were also achieved by OSC from adolescent or adult rats or mice. [128, 144] Different types of neuronal death, including apoptosis, [145, 146] necrosis, [147] and a hybrid cell death have been observed in the OGD-treated OSCs, [148, 149] and neuroprotective effects of various compounds to cerebral ischemia were successfully verified in the OSC plus OGD model. [150-152]

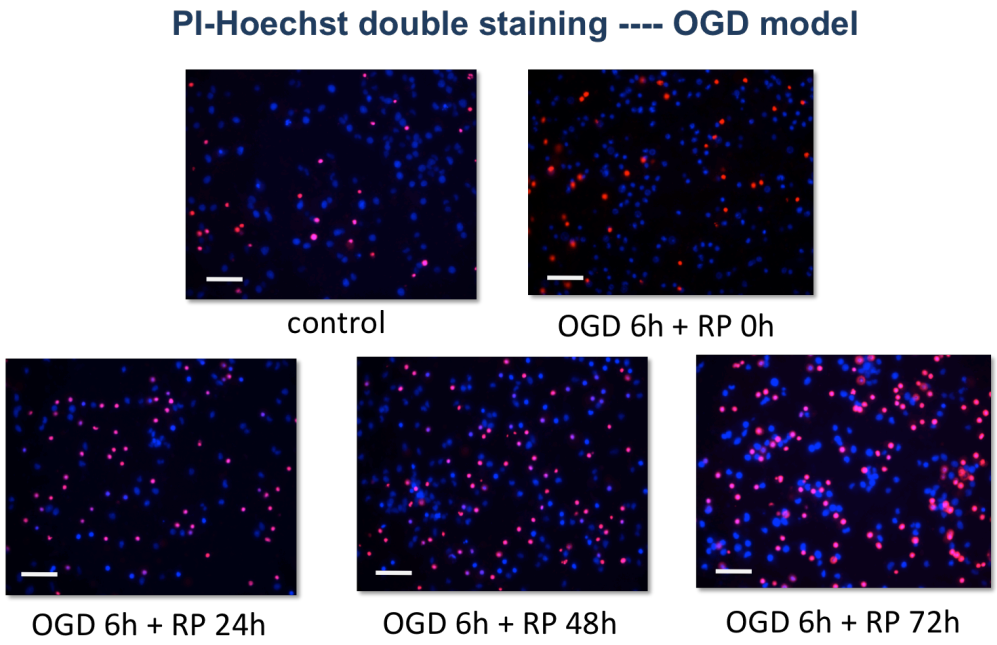

Fig 1.4 Propidium iodide (PI) and Hoechst 33342 double staining of *in vitro* cultured primary rat cortical neurons. The ratios of PI-stained (red) neurons to Hoechst-stained (blue) neurons represented the general cell death rates in the OGD/RP stroke model. Scale bars = 80 μm. Images were taken at 20× objective.

1.3.4 Measurement of Ischemic Damage in Stroke Models

Through several decades development, the methods for analyzing brain injury and dynamic changes in the ischemia/reperfusion-challenged brain thrived enormously. Due to the evolvement of modern high-resolution imaging technique, *in vivo* diagnostic and prognostic of ischemic brain damage become much easier and accurate. With different MRI techniques, detailed information on hemodynamics, tissue structure, edema formation, cell migration, gene expression, neuronal activation and other parameters can be obtained quickly. Additionally, MRI in conjunction with other imaging techniques such as optical imaging or positron emission tomography can be used to acquire complementary information. [153] Laser Doppler flowmetry are widely used to monitor the cerebral blood flow

during the ischemia; and physiological variables, including blood pressure, rectal temperature, and blood gases are measured during the operations. In order to quantify the cerebral infarction and brain edema, TTC staining on the ischemic brain slices [154] or Nissl/crystal violet staining on the brain sections should be applied, in addition to the MRI scanning. A 5-point scale neurological deficit score (i.e. 0, no deficit; 1, failure to extend right paw; 2, circling to the right; 3, falling to the right; and 4, unable to walk spontaneously) [56] and a new 14-point scoring method emphasizes the results of motor, reflex and balance tests [155] can be utilized for the neurological assessments after the surgery. BBB function is usually evaluated by the vascular albumin leakage, which known as a quantitative index of endothelial barrier dysfunction, by comparing the albumin difference in fluorescence intensity between the outside and inside of the venular segment. [156] Adhesion of leukocytes and platelets can be monitored *in vivo* using intravital video microscopy, [157] while microglia activation in stroke can be analyzed using CD11b (Mac-1/CR3) antibodies. Western Blot, ELISA, and RT-PCR will be performed for the measurement of protein and mRNA levels in the ischemic brain, respectively.

For the *in vitro* cell culture models, trypan blue exclusion test [158] and MTT-assay/LDH-assay[159] facilitate the determination of neuronal viability in stroke condition. Fluorescent analysis of nuclear marker propidium iodide (PI),[160] mitochondria-dependent tetrazolium and in situ terminal deoxytransferase-mediated dUTP nick-end labeling (TUNEL)[161] are commonly used to detect the neuronal death machinery. Like *in vivo* stroke models, apoptosis, necrosis and autophagic cell death can be distinguished and related protein markers can be detected by Western Blot or ELISA. Specifically, mitochondrial

dysfunctions triggered by oxidative stress and excessive ROS production in stroke can also be examined, by using H2DCFDA staining for the ROS production, JC-1 staining for the mitochondrial membrane potential, and Calcein AM staining for the mitochondrial permeability transition pore opening detection, respectively.

1.4 Caspase-Independent Neuronal Death Mechanisms in Ischemic Stroke

Delayed neuronal death in the penumbral region of a stroke is largely responsible for many negative implications seen in stroke victims. This type of neuronal death occurs in many forms, including apoptosis, necrosis, and alternative mechanisms. Although caspases are usually associated with apoptosis, there are several morphologically and biochemically distinct types of cell death that are independent of caspase activation. Downstream effectors and processes of mitochondrial damage, such as AIF, endonuclease G, BNIP3, mitophagy, mitochondrial biogenesis, chaperone-mediated autophagy, reactive oxygen species production as well as parallel endoplasmic reticular stress and lysosomal dysfunction, have all been shown to play a role in post-stroke delayed neuronal cell death. In this section, we attempt to summarize these caspase-independent events and their potential therapeutic applications as targets for intervention.

Caspases (cysteine aspartyl serine proteases) are a unique class of cysteine proteases that play essential roles in programmed cell death (PCD), especially in apoptosis. Although caspases are evolutionarily conserved and frequently activated during cell death,[162, 163] it appears that simply equating cell death, apoptosis, and caspase activation to one another does not apply to mammals, as the relationships between these concepts are far more complex than that. There are

several reasons for this. First of all, apoptosis is only one of many types of PCD, as mammalian cells die through several biochemically and morphologically distinct pathways. Second, caspase activation does not always necessarily lead to apoptosis.[164] Third, caspase inhibition often does not prevent cell death but rather causes a shift to caspase-independent self-destruction processes within the cell. The main reason for this is that many stimuli that promote caspase-dependent apoptosis also simultaneously provoke mitochondrial damage, leading to other caspase-independent apoptotic pathways that cannot be reversed by blocking caspase activity. Caspase-dependent self-destruction pathways are only one of many cell death pathways. Hence, in many cases, cytoprotection can only be achieved by targeting caspase-independent processes and molecules that precede activation of caspases in the first place.[165]

In addition to caspases,[166] emerging evidence from various experimental systems suggests that caspase-independent mechanisms contribute significantly to the overall cell death process.[165, 167] For example, it has been reported that, under cerebral ischemia, neuronal death was found in caspase-3 knockout mice [168] as well as wild-type mice. This indicates that there is a direct link between ischemia and cell death, regardless of whether or not there was caspase activation.[169] Caspase inhibitors, such as the broad, nonspecific caspase inhibitor zVAD-FMK, provide limited neuroprotection in brain ischemia [170] and instead often cause a switch to caspase-independent apoptotic processes. Knockouts of caspases 3 or 9, which play central roles in cell death signalling, did not ultimately alter the number of remaining cells left upon completion of the experiment. This again shows that caspases are not the sole causal factors of apoptosis.[165] In addition, caspase-independent neuronal death was identified in

Apaf-1-deficient neurons; Apaf-1 is a key factor downstream in the caspase-dependent apoptotic cascade.[171] MacManus et al. found that, after cerebral ischemia, not only was a small amount of caspase-activated DNase (CAD)-related DNA fragments with a size of 200-1,000 base pairs found, but high molecular weight (on the order of 50 kb pair magnitudes) DNA fragments that may be completely independent of caspase activity also appeared in dying neurons. This indicates that some other process is occurring.[172] These facts collectively support the notion that caspase-independent PCD is distinct from and a viable alternative to the traditional caspase-dependent apoptosis better understood in delayed neuronal cell death. In the following sections, we will critically evaluate the contribution of caspase-independent apoptotic processes in ischemic stroke and discuss the possibility of targeting caspase-independent cell death mechanisms. Inhibition of these caspase-independent processes could potentially lead to cytoprotection of neurons during times of hypoxic stress. This is a quickly developing field with several potential clinical implications. Neurons could potentially be targeted by drugs that could be used therapeutically to stave off premature cell death directly following stroke.

1.4.1 Mechanisms of Delayed Neuronal Death in Ischemic Stroke

Neurons, like other cells, have death machinery that consists of a set of genes, intracellular signalling and transduction pathways, as well as corresponding transduction factors and enzymes. To date, at least 11 prominent cell death pathways have been identified in various mammalian tissues, among which seven types are observed in the CNS.[173] We will focus on the three major well-known categories that are involved in delayed neuronal death: apoptosis, necrosis, and autophagic cell death. In addition, under certain stimuli like ischemic insults,

damaged neurons can shift from one type of cell death to another throughout the course of the chronic degeneration process. The eventual mode of death---apoptotic, necrotic, or autophagic cell death---depends upon a number of parameters. These include metabolic state, energy resources, availability of growth factors, cell maturity, stress stimuli, and several other factors.

1.4.1.1 Apoptotic Neuronal Death

Apoptosis is a form of PCD (Type I PCD). In apoptosis, a controlled and regulated sequence of events leads to the organized elimination of cells in an energy-dependent manner without releasing harmful toxins into the surrounding environment. It is widely observed that delayed neuronal death following brain ischemia shows features of apoptosis, which is marked by a well-defined sequence of morphological changes. Cell shrinkage and membrane-bound apoptotic bodies can be found under light microscopy, while nuclear chromatin condensation and fragmentation are observable through electron microscopy in dying, ischemic neurons. DNA fragmentation has also been detected during the processes of delayed neuronal death by terminal dUTP nick-end-labeling staining (TUNEL), in situ end-labeling (ISEL, in the CA1 pyramidal neurons), as well as DNA laddering on gel electrophoresis of extracted nuclear DNA.[174] Further, apoptosis-related caspases such as caspase-3 were activated in the CA1 region following transient brain ischemia.[175] Recent studies have shown that several mitochondrial proteins are released as a result of mitochondrial outer membrane permeabilization (MOMP), including apoptosis- inducing factor (AIF), Omi, and endonuclease G (Endo G), which can all promote atypical apoptotic responses in a caspase-independent fashion.[176] It is clear that AIF and/or Endo G-mediated caspase-independent cell death is characterized by large-scale DNA

fragmentation and peripheral chromatin condensation, which are distinct from oligonucleosomal DNA fragmentation and global chromatin condensation in caspase-dependent apoptosis.[177] In later stages of a brief episode of brain ischemia, phagocytosis of fragmented DNA by microglial cells in the CA1 region was also found.[174] Collectively, whether in a caspase-dependent or -independent manner, all of these observations suggest that apoptotic processes are indeed involved in delayed neuronal death due to ischemic attacks.

1.4.1.2 Necrotic Neuronal Death

In stark contrast to apoptosis, necrosis is the end result of an uncontrolled and disordered bioenergetic catastrophe resulting from ATP depletion and progressive enzymatic degradation. It is thought to be initiated mainly by toxic insults or physical damage, and is morphologically marked by vacuolation of the cytoplasm, extensive mitochondrial swelling, dilatation of the endoplasmic reticulum (ER), and early plasma membrane damage without major nuclear changes.[173, 178, 179] Although necrosis is more likely to be induced by severe ischemia at an earlier stage of insult, it is also involved in delayed neuronal death. Neurons will lose control of their ionic balance, imbibe water, and lyse eventually.[180-182] A typical necrotic neuronal cell death pathway has been found in acute excitotoxicity, which results from the over- release of neurotransmitters. The engagement of excitatory neurotransmitters and their cell membrane receptors, such as NMDA, kainite, and AMPA, are responsible for the elevated cytosolic Ca^{2+} and subsequent cell death.[183, 184] It has been reported that inhibition of Ca^{2+} uptake by mitochondria can suppress necrotic cell death, as increased Ca^{2+} levels in the cytoplasm lead to more controlled cell death pathways.[185] Moreover, the lysosomal damage and the calpain-cathepsin

liberation must play essential roles in necrotic neuronal cell death, as lysosomal protease inhibitors have been shown to protect against delayed neuronal death produced by global ischemia.[186, 187] Under some specific circumstances, necrosis may also be well regulated and is described as being "programmed necrosis" (also known as Type III PCD), a type of PCD. Necrosis is actually usually the opposite of controlled and regulated cell death; that is, spontaneous, quick, and disordered destruction/lysis of the cell.[188] This cell death pathway can be triggered by the DNA damage present after cerebral ischemia, as the DNA repair protein poly (ADP-ribose) polymerase 1 (PARP-1) is hyperactivated and actively engaged in the necrotic process, which leads to post-ischemic brain damage.[189]

1.4.1.3 Autophagic Neuronal Death

Another mechanism participating in delayed ischemic neuronal death, which has attracted attention recently, is autophagy. Autophagy is a highly regulated process that involves the degradation of a cell's own cytoplasmic macromolecules and organelles in mammalian cells via the lysosomal system. It is not only an adaptive response to nutrient limitation but also a mechanism for cell suicide.[175, 177-182] Deregulation of autophagy has been implicated in cell death in neurodegenerative disorders and is known as "autophagic cell death" [190-193] or "type II programmed cell death" (Type II PCD).[193-195] "Autophagic cell death," distinct from apoptosis and necrosis, is characterized by extensive autophagic degradation of cellular components prior to nuclear destruction. [196, 197] The most representative morphological feature of autophagy is the formation of numerous autophagosomes in the cytosol with a condensed nucleus. [198] This type of cell death can be inhibited by 3-

methyladenine (3-MA) and wortmannin or by downregulation of autophagic proteins such as Beclin 1. This implies that autophagy is a programmed death dependent on genes and is not merely a failing survival attempt. Accumulating evidence suggests that autophagy contributes to the neuronal degeneration following cerebral ischemia. The induction of autophagy has been shown in both neonatal and adult mouse cortices and hippocampi after ischemic injury; increased LC3-II (an autophagosomal marker) levels were detected as early as 8 h and were more pronounced at 24 and 72 h after hypoxic ischemia. [199, 200] Many damaged neurons showed features of autophagic cell death during cerebral hypoxia/ischemia (H/I) in adult mice (e.g., increased lysosomal cysteine proteinases, cytoplasmic autophagic vacuoles, and the induction of GFP-LC3 immunofluorescence). [174, 201] Furthermore, Puyal et al. provided evidence that inhibiting autophagy provides powerful neuroprotection in a situation where most other pharmacological treatments, including caspase inhibition, are ineffective.[202]

1.4.1.4 Crosstalk Between Different Types of Neuronal Death

The existing hybrid form of cell death that shares features of various death mechanisms and/or combines different metabolic pathways in dying neurons should not be overlooked. In particular, the crosstalk between autophagic and apoptotic processes needs to be clarified because both autophagy and apoptosis can be triggered by common upstream signals. Sometimes this results in a mixed phenotype of both cell death patterns. In many other instances, the neuron switches between the two responses in a mutually exclusive manner, perhaps as a result of variable thresholds for both processes, or as a result of a cellular "decision" between the two responses. To some extent, apoptosis and autophagic

death under ischemic conditions can be described as two sides of the same coin. It appears that simply inhibiting one type of mechanism will switch the cellular response toward the other one, and both catabolic phenomena can inhibit each other. For example, Yu et al. demonstrated that caspase inhibitors might not only arrest apoptosis but also have the unanticipated effect of promoting autophagic cell death. [203] By contrast, Yousefi et al. proved that calpain-mediated cleavage of Atg5 could switch autophagy to apoptosis.[204] Recently, several pathways that link the apoptotic and autophagic machineries have been deciphered at the molecular level. [176, 205]

Induction of autophagy may also cause necrotic cell death. Lenardo and colleagues showed that catalase, a key enzyme of the cellular antioxidant defence mechanism, was selectively eliminated during autophagic cell death and catalase depletion caused necrotic cell death, which could be prevented by autophagy inhibition as well as antioxidants. [206] To summarize, we can say that, in delayed ischemic neuronal death, the interactions and connections between multiple mechanisms will jointly seal the fate of the neurons.

1.4.2 Caspase-Independent Mechanisms and Mediators in Ischemic Delayed Neuronal Death

The term delayed neuronal death was first coined by Kirino to describe the selective loss of the hippocampal CA1 neurons that do not become morphologically obvious until 2–3 days following a brief, transient episode of brain ischemia. [207] A wealth of evidence suggests that this second round of neuronal injury, which is referred to as delayed neuronal death in the neighboring areas of the infarct core, occurs hours to days following stroke. Neurons in this penumbral area have impaired function but remain viable for a period of time

before gradually succumbing to the insult. These neurons die in a delayed manner, so targeting this damaged but salvageable region of brain tissue will potentially reduce infarct volume and improve the neurological outcome.[208]

Mitochondria are essential organelles involved in oxidative phosphorylation, calcium homeostasis, reactive oxygen species (ROS) management, and PCD. Convergence of a number of cell death pathways emanating from membrane receptors, cytosol, the nucleus, lysosome, and endoplasmic reticulum upon the mitochondria results in mitochondrial destabilization.[209] A common consequence of these death pathways is damage to the mitochondria, resulting in MOMP. A number of assays have been developed to measure MOMP as an indicator of cytotoxicity. [210] MOMP is a key event during the cell death process and often defines the point of no return.[211-213] It is lethal because it results in the release of caspase-activating molecules and caspase-independent death effectors, metabolic failure in the mitochondria, or both.[213] The effectors of mitochondria-related PCD can be divided into two categories: (1) downstream mitochondrial death effectors (including cytochrome C, AIF, and others) and (2) agents that directly target and destabilize mitochondrial membranes or through upstream signaling mechanisms. [214] The local regulation and execution of MOMP involve proteins from the Bcl-2 family, mitochondrial lipids, proteins that regulate bioenergetic metabolite flux, and putative components of the permeability transition pore.[213] Drugs designed to suppress excessive MOMP may potentially prevent pathological cell death. Identifying the category of mitochondrial-related PCD is critical for searching targets that will provide optimal protection against brain ischemia. In the following sections, we will discuss the two categories and their therapeutic potential (Fig. 7.1).

1.4.2.1 Downstream Effectors of Mitochondrial Damage (MOMP)

1.4.2.1.1 The AIF or Endo G-Mediated Atypical Apoptosis

AIF is a mitochondrial flavoprotein and normally resides in the intermembrane mitochondrial space, where it performs an oxidoreductase function.[215] Caspase- independent chromatin condensation and DNA degradation [216, 217] are promoted upon cytosolic release and subsequent nuclear translocation of AIF during MOMP (along with AIF's obligate cyclophilin A cofactor).[218, 219] Although there is sub- stantial variation among the degree to which cell death is affected by AIF (depending upon specific experimental and pathophysiological parameters), [220] this caspase-independent inducer of neuronal death following acute injury has consistently shown itself to be a major determining factor of this process. [221]

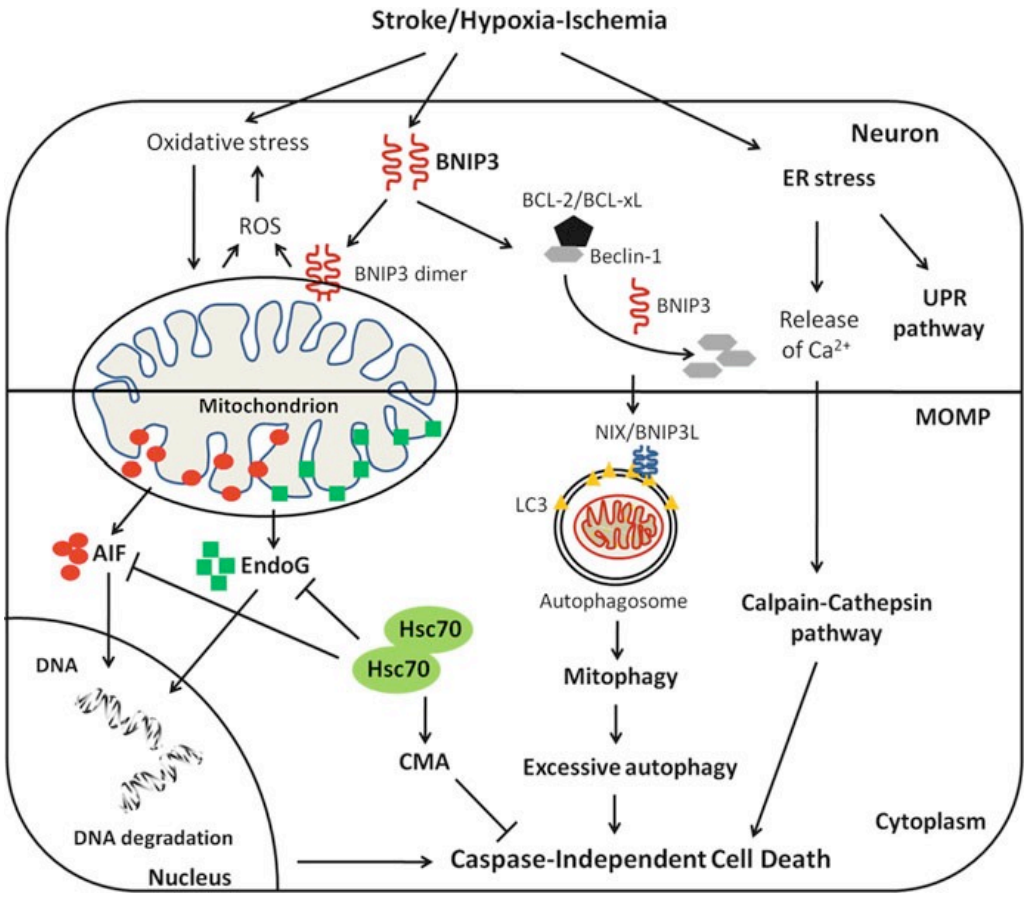

Fig 1.5 Model for caspase-independent neuronal death pathways in stroke. Hypoxia/ischemia induces HIF-1a-mediated BNIP3 expression, subsequent stable homodimerization, mitochondrial membrane insertion of the BNIP3 dimer, which results in MOMP, and the generation of reactive oxygen species (ROS). Oxidative stress can also be induced directly by H/I injury, which triggers mitochondrial damage and ROS release. As a consequence of the MOMP, neurons undergo different death pathways unrelated to caspase activation, such as the release/nuclear translocation of apoptosis-inducing factor (AIF) and endonuclease G (Endo G), mitophagy, excessive autophagy-induced cell death (by the release of Beclin 1 from the Bcl-2/Bcl-xL complex), endoplasmic reticulum (ER) stress-induced unfolded protein response (UPR), and calpain-cathepsin pathways. For each pathway, please refer to the main text for further details. *LC3* microtubule-associated protein 1 light chain 3; *Hsc70* the heat-shock cognate protein of 70 kDa, in complex with its co-chaperones; *CMA* chaperone-mediated autophagy.

Indeed, the action of AIF cannot be blocked by the broad caspase inhibitor zVAD-FMK [222] and zDEVD-FMK.[223] This is indicative of the fact that this protein is involved in caspase-independent atypical apoptosis. Inhibition of AIF reduced 37–60% of neuronal death induced by glutamate excitotoxicity and oxygen-glucose deprivation-induced neuronal death, two major contributing factors of ischemic insult. Harlequin mutant (Hq) mice, which express about 20% lower AIF levels than wild-type mice, exhibited significantly less brain damage upon MCAO.[224] Similarly, neuroprotective effects caused by AIF deficiency have been

shown to be further amplified through the utilization of broad-spectrum caspase inhibitors or antioxidants following neonatal stroke. [225, 226] The nuclear translocation of CypA that was typically observed in wild-type neurons did not manifest itself in Hq mice subjected to stroke environments. This is fully compatible with in vitro data suggesting that a proapoptotic DNA degradation complex is formed between AIF and its interacting CypA cofactor.[217] An approximately 50% reduction in infarct volume was observed in the $CypA^{-/-}$ mice, as compared to that of WT mice, which correlates quite well with the suppressed H/I-induced nuclear translocation of AIF. [216] Thus, AIF clearly acts as a lethal, caspase-independent effecter of atypical apoptosis in ischemic neuronal death.

Although there is no doubt that AIF plays a critical role in caspase-independent death, the mechanisms responsible for AIF release from the mitochondria still need to be explored further. The Bcl-2 family, which also controls caspase-dependent cell death, regulates AIF efflux and subsequently caspase-independent cell death. [227] It has been found that the anti-apoptotic protein Bcl-xL can prevent AIF translocation in neuronal cultures challenged with transient oxygen-glucose deprivation.[223] Thus, Bcl-xL may account for the acquisition of resistance to neuronal cell death following brief ischemia. Contrarily, Bax expression leads to an increase in AIF efflux from mitochondria in neurons.[171] Truncated Bid (tBid) is also associated with AIF release, and it has been demonstrated that cleavage of Bid occurs coincidently with AIF translocation from mitochondria to the nucleus.[224] Furthermore, incubation of freshly isolated mitochondria with tBid resulted in AIF release as well.[228] Accordingly, the following model of AIF release has been proposed: tBid and Bax interact with mitochondria to open mitochondrial permeability transition (MPT) pores [229] or form a membrane pore where they cleave AIF to

thereby dissociate it from the inner mitochondrial membrane.[230] The cleaved AIF then leaves the mitochondria and translocates to the nucleus to execute DNA degradation and cell death.[231]

Another mitochondrial protein that potentially contributes to caspase-independent cell death is Endo G.[232, 233] Genetic and biochemical evidence has emerged that Endo G is released from the intermembrane space of mitochondria and translocates to the nucleus to initiate a caspase-independent apoptosis during early embryogenesis [234] as well as in pathological conditions such as transient cerebral ischemia [235] with oxygen and glucose deprivation (OGD).[236] Once released from mitochondria, Endo G cleaves chromatin DNA into nucleosomal fragments independently of CAD.[232, 233] Like AIF, the release of Endo G is under the control of the Bcl-2 family.[230] The release of Endo G from mitochondria was originally described following treatment of isolated mitochondria with tBid. In the study, mitochondrial efflux of Endo G could be induced by tBid in normal mice but not in Bcl-2 transgenic knockout mice.[233] This indicates that Bcl-2 must be an important bridge between tBid and Endo G. Recently, we found that another BH3-only proapoptotic protein, Bcl2/adenovirus E1B 19-kDa interacting protein 3 (BNIP3), activated a caspase-independent neuronal death pathway mediated by Endo G in hypoxia and stroke (see Sect. 3.1.2).[237]

Human Omi/HtrA2, the stress-regulated endoprotease, has also been implicated in caspase-independent cell death mechanisms that originate from MOMP, due to its ability to promote the cleavage of caspase-unrelated substrates (e.g., cytoskeletal proteins).[238] However, the contribution of Omi/HtrA2 in acute neuronal injury is poorly characterized. Cytosolic translocation of Omi/HtrA2 and its enhanced inter- action with the X-linked inhibitor of apoptosis protein (XIAP) have

been reported to occur in vivo, in mice subjected to transient focal cerebral ischemia (tFCI).[239] Cytosolic translocation of Omi/HtrA2 and its enhanced interaction with XIAP could not be prevented by Z-VAD-fmk administration, but was significantly reduced in the brain of mice overexpressing the SOD1 gene (superoxide dismutase). Omi/ Htra2 is closely resembled by direct IAP-binding protein with a low pI (like DIABLO, whose murine ortholog is known as Smac). Cytosolic translocation of Smac/DIABLO has been shown to be promoted by tFCI in both rats [240] and mice,[241, 242] the latter case being through a pathway that can potentially be counteracted by SOD1 overexpression. Both of these results point toward a significant contribution of ROS (but not of caspases) to the molecular pathways leading to an ischemia- induced Omi/HtrA2 and Smac/DIABLO release.[243]

1.4.2.1.2 The BNIP3-Activated and Endo G-Mediated Neuronal Death Pathway

BNIP3 (formerly NIP3) is a proapoptotic, mitochondrial protein classified in the Bcl-2 family based on limited sequence homology to the Bcl-2 homology 3 (BH3) domain and C-terminal transmembrane TM domain. This subfamily includes BNIP3, NIX (also called BNIP3a and BNIP3L), BNIP3h, and a *Caenorhabditis elegans* ortholog (ceBNIP3). [244-248] When expressed, BNIP3 is able to cause cell death in a variety of cells, [246] including neurons. [237, 249] Typically, the BH3 domain of proapoptotic Bcl-2 family members mediates Bcl-2/Bcl-x(L) heterodimerization and confers proapoptotic activity. Deletion mapping of BNIP3 excluded its BH3-like domain and identified the NH2-terminus (residues 1–49) and TM domain as critical for Bcl-2 heterodimerization, and either region was sufficient for Bcl-x(L) interaction. Additionally, the removal of the BH3-like domain in BNIP3 did not diminish its apoptotic activity. The TM domain of BNIP3 is

critical for homodimerization, proapoptotic function, and mitochondrial targeting.[250] Cell transfection studies have shown that the BNIP3-induced cell death is characterized by early plasma membrane permeabilization and mitochondrial damage without cytochrome c release and caspase activation;[247, 250] this suggests that BNIP3 induces cell death through a caspase-unrelated mechanism. Integration of BNIP3 into mitochondrial membranes causes MPT pore opening, suppresses mitochondrial membrane potential, and increases ROS production.[178]

Under normal physiological conditions, BNIP3 is not detectable in healthy brain neurons. Expression of endogenous BNIP3 is induced in a variety of cells and tissues under hypoxic conditions.[251-253] Characterization of the BNIP3 gene revealed that the BNIP3 promoter contained a functional HIF-1-responsive element (HRE) and that expression of BNIP3 could be potently activated by both hypoxia and forced expression of HIF-1a.[251] In our previous studies, we reported that oxidative stress functioned as a redox signal to induce HIF-1a accumulation and subsequent activation of BNIP3.[249] We have further established a BNIP3-induced and Endo G-mediated neuronal death pathway in stroke.[237] In this pathway, BNIP3 is transcriptionally upregulated by HIF-1 in hypoxia and stroke, causing mitochondrial dysfunction, which results in mitochondrial release of Endo G. Endo G then translocates to the nucleus and cleaves chromatin DNA, which leads to a form of caspase-independent neuronal cell death. The BNIP3 pathway explains well why brain-specific knockout of HIF-1a reduces hypoxic-ischemic damage to the brain, despite the fact that HIF-1 activation is an established adaptive response to hypoxia. [254] Judging from the time-course of BNIP3 expression, it is likely that the BNIP3 pathway contributes greatly to the delayed neuronal death found in stroke.

1.4.2.1.3 Mitochondrial Dynamics and Mitophagy Pathways

Since the proteins released from the MOMP exert pleiotropic effects, ranging from caspase activation to chromatin condensation to DNA strand breakage and generation of ROS,[213, 255] successful inhibition of MOMP would be expected to prevent the release and consequent destructive effects of those caspase-dependent and caspase-independent cell death effectors. Also, considering that mitochondria are critical organelles for maintaining the cellular homeostasis and the fact that they are not static according to different physiological and pathological conditions, the mechanisms underlying the dynamic regulation of mitochondrial turnover, content, function, and number in the cells [256] will provide useful insights for therapeutic target-searching. This is especially important for postmitotic cells such as neurons; that is why we would like to introduce the concepts of mitochondrial biogenesis, mitophagy, and chaperone-mediated autophagy (CMA), and their potential roles in caspase-independent neuronal death here.

Mitochondria are dynamic organelles that move within the cell and frequently undergo fission and fusion.[257] These two processes together with the mitochondria trafficking on microtubule cytoskeleton allow the redistribution of mitochondria to meet the shifting local needs. Dynain-related protein 1 (Drp1) mediates mitochondrial fission by producing membrane scission physically; on the contrary, two distinct modulators, mitofusin 1 and 2, and optic atrophy 1 (Opa1), are necessary for fusion of the outer and inner mitochondrial membranes, respectively.[258, 259] Mitochondrial dynamics and mitophagy machinery are closely related. Usually, a mitochondrion can only be separated from the interconnected mitochondrial network (also known as mitochondrial reticulum) first, and then engulfed by the autophagosome for its mitophagic elimination. In general,

unbalanced mitochondrial dynamics toward fission rather than fusion will advance isolation of impaired mitochondria and assist their clearance by mitophagy. [257] Oxidative stress triggered by hypoxic-ischemic insult causes extensive mitochondrial fission, an event that precedes neuronal death. Interestingly, abrogation of neuronal death can occur due to overexpression of mitofusin 2, a mitochondrial fusion protein.[260] This suggests that the mitochondrial fission and fusion is tightly regulated, and crucial for neuronal viability. Furthermore, a recent study demonstrated that I/H could induce mitochondrial biogenesis. After hypoxia, increases are seen in mitochondrial DNA, total mitochondrial number, expression of the mitochondrial transcription factors downstream of PGC-1a (mitochondrial transcription factor A and nuclear respiratory factor 1), and the mitochondrial protein HSP60.[261] This exciting finding suggests that mitochondrial biogenesis is a novel endogenous neuroprotective response.

Mitophagy, the specific autophagic elimination of mitochondria, has been identified in yeast, mediated by autophagy-related 32 (Atg32), and in mammals during red blood cell differentiation, mediated by NIP-like protein X (NIX; also known as BNIP3L).[262] Lemasters and colleagues coined the term mitophagy to describe the engulfment of mitochondria into vesicles that are coated with the autophagosome marker MAP1 light chain 3 (LC3), a process that can occur within 5 min.[263] These early studies indicate that mitophagy regulates mitochondrial number to match metabolic demand and might be a core machinery of quality control to remove damaged mitochondria. Alongside mitochondrial turnover, other specialized functions of mitophagy have also been discovered. For instance, mitophagy is responsible for the complete removal of mitochondria during erythrocyte maturation[264] and the selective elimination of sperm-derived

mitochondria after oocyte fertilization.[265, 266] Mitophagy involves distinct steps to recognize defective or superfluous mitochondria and to target them to autophagosomes. In yeast, Atg32 seems to recruit redundant and/or damaged mitochondria to autophagosomes.[267] In mammals, NIX mediates developmental removal of mitochondria during erythropoiesis, [268, 269] since NIX has a WXXL-like motif, which binds to LC3 on isolation membranes and mediates the binding and sequestration of mitochondria into autophagosomes. [270, 271] Considerable evidence also shows that BNIP3, as well as NIX, can trigger mitochondrial depolarization, and that mitochondrial depolarization is sufficient to cause mitophagy. [272, 273] Lately, emerging evidence identifies a novel pathway that is mediated by the PTEN-induced putative protein kinase 1 (PINK1) and the E3 ubiquitin ligase Parkin, in the mammalian mitophagy.[274, 275] This PINK1/Parkin pathway is triggered when PINK1 is accumulated on the outer membrane of impaired mitochondria, where it induces recruitment of cytosolic Parkin. Subsequently, mitochondria present compromised motility and fusion capacity to the mitochondrial reticulum, leading to the downstream mitophagic degradation.[257] Another study found that, in neurons cultured with caspase inhibitors to prevent cell dissolution, mitochondria were completely removed by mitophagy following apoptosis induction through MOMP.[276] As MOMP occurs upstream of caspase activation, these results suggest that mitochondrial damage can induce mitophagy through alternative pathways. Taken together, after a lethal ischemic insult, mitochondrial dynamics in conjunction with selective elimination of mitochondria by mitophagy regulate the mitochondrial number required for the metabolic demand, and maintain quality control of mitochondria. Therefore, effective regulation of mitophagy and/or enhancement of mitochondrial biogenesis are potential

neuroprotective strategies.

Chaperone-mediated autophagy (CMA) is a type of autophagy responsible for the degradation of cytosolic proteins bearing a consensus motif, biochemically related to KFERQ, that targets them for lysosomal degradation.[277] This motif is recognizable by the heat-shock cognate protein of 70 kDa (i.e., hsc70), in complex with its co-chaperones.[278] The substrate/chaperone complex binds to the lysosome-associated membrane protein type-2A protein (i.e., LAMP-2A, a CMA receptor) after being delivered to the surface of lysosomes. [279] With the assistance of a resident lysosomal chaperone (lys-hsc70), the substrate protein is translocated across the lysosomal membrane in an ATP-dependent fashion, subsequent to unfolding.[280] Once in the lysosomal lumen, CMA substrates are rapidly degraded (in 5–10 min) by the broad array of lysosomal proteases. CMA is maximally upregulated under stressful conditions, such as prolonged nutrient deprivation (serum removal in cultured cells or starvation in rodents), [281, 282] mild oxidative stress, [283] and exposure to toxins.[284] Thus, CMA is part of the cellular quality control systems and is essential for the cellular responses to stress. CMA activity has been detected in several primary cell cultures including astrocytes, dopaminergic neurons, and cortical neurons, [285, 286] while impairment of CMA underlies the pathogenesis of certain human pathologies such as neurodegenerative disorders. The Hsc70 plays critical roles in CMA activity, since only a subset of lysosomes containing Hsc70 in their lumen is competent for CMA.[287] Furthermore, upon MOMP, the chaperone Hsp70 has been shown to play a critical role in sequestering AIF within the cytosol, thereby interfering with its pro-apoptotic potential.[288] Additionally, Hsp70 has been shown to act at another level, by preventing the mitochondrial release of AIF,[289] thus having

two distinct molecular mechanisms of suppressing AIF-dependent DNA degradation. As could be expected, a greater infarction volume is seen within the cortex of hsp70$^{-/-}$ mice suffering of ischemic insult than that of WT mice.[290] In the contrary scenario, Hsp70 overexpression in a neonatal H/I model has been shown to limit the mitochondrial-nuclear translocation of AIF and consequently provided significant neuroprotection. [291] All of these results suggest that the Hsp70-mediated CMA pathway is closely involved in the caspase-independent neuronal death, which provides us with another promising therapeutic target for stroke treatment.

1.4.2.2 Upstream Initiators of Mitochondrial Damage (MOMP)

1.4.2.2.1 Endoplasmic Reticulum and Lysosome Targets for Stroke: UPR Pathway / Calpain-Cathepsin Pathway

The endoplasmic reticulum (ER) serves two major functions in the cell. It facilitates the proper folding of newly synthesized proteins destined for secretion, cell surface or intracellular organelles, and it provides the cell with a Ca^{2+} reservoir.[292-294] ER stress occurs in various physiological and pathological conditions, including glucose starvation and hypoxia in stroke, where the capacity of the ER to fold proteins becomes saturated. Accumulation of unfolded proteins triggers ER stress and a subsequent evolutionarily conserved ER-to-nucleus signaling pathway, called the unfolded protein response (UPR), which reduces global protein synthesis and induces the synthesis of chaperones and other proteins that increase the capacity of the ER.[295] The signaling pathway that mediates the UPR in yeast consists of the transmembrane signaling protein inositol-requiring kinase 1 (IRE1), which can be activated by the dissociation of Grp78/BiP (ER-specific member of heat shock protein 70 family) from its ER-sensing domain in

response to accumulation of unfolded proteins. The Hac1, a transcription factor, is then expressed and transmits the signal to the nucleus.[293, 296, 297] In mammalian cells, the UPR signaling is more complicated; at least three mechanistically different ER stress transducers---RNA-dependent protein kinase (PKR)-like ER kinase (PERK), ATF6, and IRE1---operate in parallel to mediate the UPR.[295] In addition to activating the UPR, ER stress also leads to a release of Ca^{2+} from the ER into the cytosols, which, in turn, can activate various kinases and proteases possibly involved in autophagy signaling.[204, 298, 299] These activated non-caspase proteases, such as calpains and cathepsins, act as upstream MOMP triggers, which are also potential targets for neuroprotection in brain ischemia.

Calpains, a family of 14Ca^{2+}-activated neutral cysteine proteases, are activated both in physiological states and also during various pathological conditions such as in the presence of free radicals,[300, 301] brain ischemia-reperfusion,[302, 303] apoptosis, [300, 304] and Alzheimer's [305] or Parkinson's [306] diseases. Excessive activation of calpain due to an increase in free Ca^{2+} leads to cytoskeletal protein breakdown, subsequent loss of structural integrity and disturbances of axonal transport, and finally to neuronal death. Recently, Yamashima et al. reported sustained activation of m-calpain in post-ischemic CA1 neurons, which was shown to cause spillage of cathepsins (a family of hydrolytic proteases) from lysosomes.[302]

Lysosomes contain over 80 types of hydrolytic enzymes. In terms of executing neuronal death, two classes of lysosomal hydrolytic enzymes appear to be most active: aspartyl (cathepsin D) and cysteine (cathepsins B, H, L) proteases.[307] Cathepsin D mediates execution of neuronal death induced by aging, transient forebrain ischemia, and excitotoxicity, [308] while cathepsins B and L

execute hippocampal neuronal death after global ischemia.[309] The spreading of hydrolytic enzymes into the cytoplasm through injury or rupture of the lysosomal membrane was confirmed in ischemic brain injuries. This is the basis of the "calpain–cathepsin hypothesis",[187, 310] a hypothesis encompassing calpain and cathepsin as the key mediators of this process. For example, recent experiments on mice in which the endogenous calpain inhibitor calpastatin has been overexpressed or knocked out underscore the importance of calpains as an activator of lethal MOMP in neuronal cell death.[311] Cathepsin B can also act as a MOMP-inducer, linking lysosomal damage (which causes cathepsin B release) to MOMP.[312] Cathepsin B knockout cells are particularly resistant to induction of apoptosis by TNF-a, and cathepsin B knockout mice show reduced liver damage in response to TNF-a [313] or cholestasis.[314] Moreover, the cathepsin B inhibitor CA-074 can protect neurons from focal cerebral ischemia.[315]

1.4.3 Roles of the Bcl-2 Protein Family in Ischemic Delayed Neuronal Death: In Mitochondrial Impairment and Autophagic Neuronal Death

There are three functional groups of proteins comprising the BCL-2 family: the multi-domain proapoptotic effectors, BAX and BAK; the multi-BH domain pro-survival members BCL-2, BCL-xL, BCL-w, MCL-1, and A1; and the proapoptotic BH3-only members BID, BIM, BIK, BAD, NOXA, PUMA, BNIP3, and NIX. These groups of proteins work cooperatively to link the upstream signals to downstream regulators of the pro-survival and pro-death members to determine the final destiny of the cell.[316-319] Presently, Bcl-2 family proteins have been emphasized in two major models that describe the mechanisms of

MOMP. In one model, MOMP results from protein-permeable pores formed across the outer mitochondrial membrane by multi-domain proapoptotic members of BAX and BAK,[320, 321] which can interact with the proapoptotic BH3-only proteins (e.g., Bid and Bim) that function as intracellular sensors of stress.[322, 323] The other group of Bcl-2 proteins (i.e., the multi-BH domain pro-survival members; e.g., Bcl-2, Bcl-xL) exerted anti-apoptotic functions by sequestering their proapoptotic counterparts into inactive complexes [324] as well as via other mechanisms, such as by modulating Ca^{2+} fluxes at the endoplasmic reticulum.[325] In the second model, MOMP was triggered by an abrupt increase in the permeability of the mitochondrial inner membrane to low-molecular weight solutes, which is known as MPT.[326, 327] The activity of the permeability transition pore complex (PTPC), which responds to proapoptotic signals such as Ca^{2+} overload and oxidative stress, is regulated by both the pro- and anti-apoptotic Bcl-2 proteins.[328]

Besides causing mitochondrial impairment, Bcl-2 anti-apoptotic family members also target the lysosomal degradation pathway of autophagy. Bcl-2 has been shown to block caspase-independent cell death and the degradation of mitochondria, which are two processes postulated to involve autophagy. Recently, Pattingre et al. directly demonstrated the role of Bcl-2 in the negative regulation of autophagy. They showed that Bcl-2 inhibits Atg6/Beclin 1 (an autophagy-related protein) as well as the subsequent Beclin 1-dependent autophagic processes. Beclin 1 mutants incapable of binding to Bcl-2 also promote autophagic cell death through induction of autophagy, as if having been displaced by PCD-inducing proteins like BNIP3. These observations led to the hypothesis that Bcl-2 down-regulation of autophagy through its interaction with Beclin 1 may prevent cell

death from occurring.[329] This regulatory activity of Bcl-2 on autophagy is specifically attributed to its expression at the ER membrane, indicating that signaling events originating from the ER are crucial for autophagy.[330] Finally, many laboratories have now shown that ER stress triggers autophagy, and UPR stress sensors also regulate this effect.[331-334] Stimuli that increase cytosolic calcium could activate ER stress and subsequent autophagy, which can be blocked by Bcl-2.[298]

1.4.4 The BNIP3-Activated and Bcl-2-Beclin1-Mediated Autophagic Neuronal Death Pathway (Caspase-Independent)

Beclin 1 (also known as Atg6), the first identified mammalian autophagy gene product,[335] was originally isolated as a BCL-2-interacting protein.[336-338] A functional BH3-like domain was identified in Beclin 1, and its mutation disrupted the interaction of Beclin 1 with Bcl-xL.[339] Pharmacological BH3 mimetic ABT-737 could competitively inhibit the interaction between Beclin 1 and BCL-2/Bcl-xL, stimulating autophagy.[339, 340] In addition, the BH3-only proteins including BNIP3 have been shown to regulate autophagy under different settings, possibly due to disrupting the interaction between Beclin 1 and Bcl-2/Bcl-xL via their BH3 domains.[340, 341] It appears that prolonged BNIP3 expression or acute overexpression beyond an autophagic survival threshold may result in autophagic cell death. It was recently reported that prolonged exposure of several apoptosis-competent cancer lines to hypoxia induced autophagy and cell death in a BNIP3-dependent manner.[342] These results suggest that liberating Beclin 1 from BCL-2/BCL-xL may be one of the mechanisms by which BH3-only members, including BNIP3, promote autophagy.[343] On the other hand, as loss of MPT appears to induce autophagy, BNIP3 may also induce autophagy indirectly as a consequence of

such mitochondrial injury.[272]

Recently, we reported that BNIP3 contributes to delayed neuronal death following stroke and provided evidence that BNIP3 is markedly upregulated at 48 and 72 h after cerebral ischemia.[237] It is also known that BNIP3-induced neuronal death is caspase- and cytochrome C release-independent and characterized by early mitochondrial damage. We have further proposed a BNIP3-activated and Bcl-2/Beclin 1-mediated autophagic neuronal death pathway in stroke. Here are some results:

1. BNIP3 was induced in stroke, both in cultured primary neurons in an OGD model and in a neonatal cerebral H/I animal model. Levels of BNIP3 were low for up to 24 h but started to accumulate after 48 h postoperatively. The expressed BNIP3 was in its active form because it was membrane-bound and localized to mitochondria.
2. An increase of autophagy was observed as determined by the ratio of LC3-II to LC3-I, an autophagy marker protein, both in vitro and in vivo.
3. The time course and expression levels of Beclin 1 (BECN1), an autophagy-regulating protein, correlated positively with the expression of BNIP3. The expression of both proteins was accompanied by an increased autophagic neuronal death rate. This increase could be attenuated by the specific autophagy inhibitor, 3-methyladenine (3-MA).
4. The presence of large autolysosomes and numerous autophagosomes in neurons exposed to OGD injury was confirmed by electron microscopy. Autophagic cell death seemed to contribute to a great portion of the delayed neuronal death after I/H (Shi et al., *CNS Neurosciences and Therapeutics* [139]).

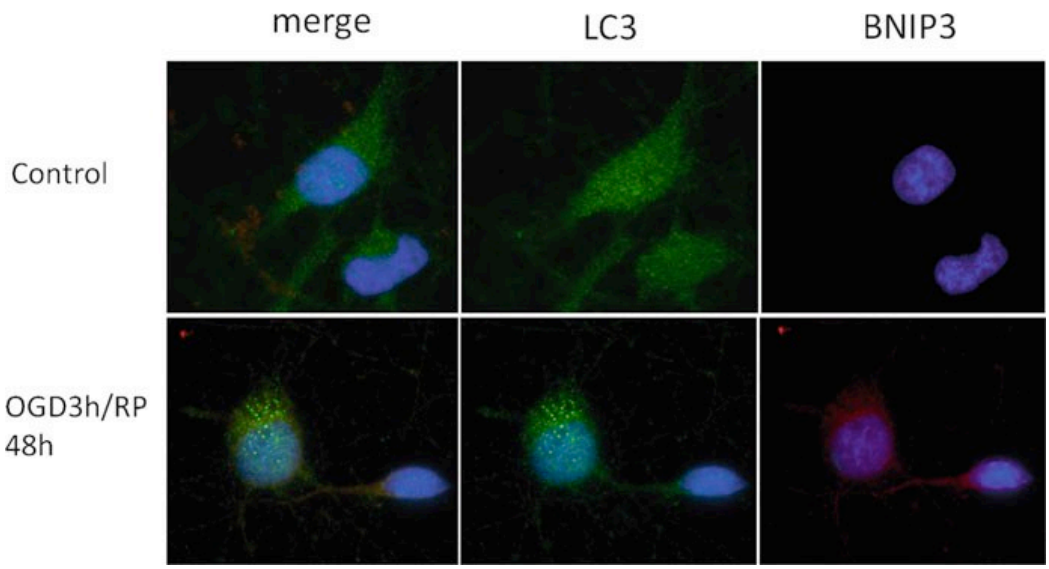

Fig 1.6 Upregulated BNIP3 expression and increased LC3 translocation after H/I and RP treatment in cortical neurons. Neurons were treated with OGD for 3 h, followed by RP for 48 h. BNIP3 was stained with *red* while LC3 and nuclei were marked by *green* and *blue*, respectively. Magnification: 100 ×

Our lab has found a unique caspase-independent cell death pathway that features the mitochondrial localization of BNIP3 then Endo G and AIF release from mitochondria and translocation into the nuclei, which results in eventual cell death (unpublished data). It is possible that autophagy also plays a part in this pathway by affecting mitochondrial stabilization. Further studies need to focus on elucidating the interactions between BNIP3, Beclin 1, and other possible intermediate autophagy-related proteins. Furthermore, molecular sequences underlying this pathway also need to be clarified in detail.

1.5 Therapy of Ischemic Stroke

1.5.1 Potential Therapeutic Applications Targeting on Mitochondrial Damage (MOMP)

In the best case scenarios, patients affected by stroke are treated within dozens of minutes, but usually treatment occurs only within hours, well after the MOMP has been initiated. Novel neuroprotective strategies that actively prevent the acute and delayed loss of neurons are urgently awaited. Such intervention should target the post-mitochondrial effectors and be administered during the first phases of cell death that occur before irreversible catabolic reactions have been ignited. Furthermore, in an early intervention that before affected neurons have undergone MOMP, combination therapies that associate MOMP blockers with post-MOMP effectors' inhibitors might achieve improved neuroprotection by preventing cell death both upstream and downstream of mitochondria.[212]

Previous studies in models of delayed neuronal death have demonstrated protective effects of inhibiting caspase activities by various caspase inhibitors or genetic inactivation of distinct caspases in transgenic mice. However, it has been proven that caspase inhibition cannot prevent impairment of the induction of long-term potentiation after ischemia. This suggests that caspase inhibition alone does not preserve functional plasticity of neurons.[344] More recently, therapeutic strategies have been directed toward the prevention of the mitochondrial release of AIF and Endo G due to the discoveries in caspase-independent cell death signaling in delayed neuronal death after cerebral ischemia. Reduction of mitochondrial AIF protein levels has led to a significant decline in neuronal cell death after ischemia. This can be directly or indirectly achieved by RNA interference,[224] inhibition of Poly (ADP-ribose) polymerase using 3-aminobenzamide, [345] expression of

hepatocyte growth factor (HGF),[346] or inhibition of neuronal NO synthase.[347] In more recent work, it has been shown that both the chaperone and ATPase domains of Hsp70 are vital in hindering the release of AIF from mitochondria, while only the latter would be required to cytosolically sequester AIF, thus preventing its nuclear translocation.[289] In addition, data obtained in vivo via an ischemic rat model (which followed the brain-targeted overexpression of different Hsp70 mutants, through plasmid transfection) suggests that the C-terminal portion of Hsp70 is in itself sufficient for neuroprotection.[348] This implies independence of both the functionality as well as the presence of its N-terminal ATPase domain. These experimental results are beginning to provide a solid foundation for the development of neuroprotective strategies through the Hsp70-mediated inhibition of AIF. Like AIF, downregulation of Endo G appears to be another promising method of neuroprotection against delayed neuronal death. Data from our laboratory showed that knockdown of BNIP3 by RNAi inhibited Endo G translocation and protected neurons from hypoxia-induced cell death.[237] Reduction in activity of cps-6, which encodes a homologue of human mitochondrial Endo G, by a genetic mutation or RNA interference, delayed appearance of cell corpses.[349] Transgenic mice with mutant Endo G heterozygous gene were more resistant to neuronal death induced by tumor necrosis factor-α (TNF-α) or staurosporine and had less DNA fragments compared to the wild-type mice.[234] Interestingly, the DNase of Endo G could be inactivated by Hsp70 in an ATP-dependent manner, which was indicated by assays based on purified cellular components,[350] backing up the potential value of targeting on Hsp70. In addition to lethal proteins, mitochondria can also generate and release highly toxic ROS, which contribute to cell death. So, ROS scavengers can have cytoprotective effects in vitro and in vivo.[351]

Inhibiting MOMP further upstream, at the initiation phase that precedes mitochondrial damage, has achieved significant levels of neuroprotection in vivo. For example, in mice lacking the neuronal nitric oxide synthase (NOS) gene,[352] pharmacological [353] and genetic [354] inhibition of the tumor suppressor protein p53 as well as systemic administration of small molecules [355] or peptides [356] designed to block the c-JunN-terminal kinase (JNK) signaling pathway showed neuroprotective effects against ischemia, trauma, and excitotoxicity. Autophagy can serve as an ER-associated degradation system in mammalian cells and play a fundamental role in regulating the accumulation of disease-associated mutant proteins in the ER. Also, non-transformed cells like primary cells may be especially sensitive to ER stress-induced autophagy. Therefore, various ER stressors being potential targets may help prevent the ER-stress-induced excessive autophagy and consequent autophagic cell death. This is based on data showing that the inhibition of autophagy by Atg5 deficiency in MEFs or by 3-methyladenine in colon epithelial cells inhibits cell death induced by ER stressors (Ca^{2+} ionophore, thapsigargin, and tunicamycin).[295, 334]

1.5.2 Potential Therapeutic Applications Targeting on Bcl-2 Family and Autophagy

It has been reported that some inhibitors of the permeability transition and/or mitochondrial ion channels inhibit cell death in models of stroke.[213, 357, 358] Seeing as BH3-only members of the Bcl-2 family seem to be important instigators of MOMP in many pathways, small-molecule antagonists of these proteins should be effective inhibitors of MOMP-triggered cell death. Pharmacological inhibitors of the pore-forming activity of Bax have been shown to exert neuroprotective effects in an animal model of global brain ischemia.[359]

Also, by inhibiting the association of Bax with mitochondria,[360] the endogenous bile acid tauroursodeoxycholic acid (TUDCA) protected rats against neurological injury after Tfci [361] and intracerebral hemorrhage.[362] For the anti-apoptotic molecules, a single injection of a DNA plasmid encoding the protective Bcl-2 gene provided neuroprotection of injured neurons in vivo.[363] Mice overexpressing anti-apoptotic members such as Bcl-2 [364, 365] or Bcl-xL [366] displayed decreased tissue damage after permanent focal ischemia. Contrarily, the main strategies for neuroprotection of the proapoptotic members may lie in the downregulation of death gene expression. Plesnila and colleagues have developed low-molecular mass 4-phenylsulfanyl-phenylamine derivatives targeting Bid and have shown that they have the ability to inhibit tBid-induced Smac release, which prevents caspase-3 activation and cell death in isolated mitochondria and in cancer cell lines.[367] The Bid inhibitors preserve mitochondrial integrity and prevent activation of caspase-3 as well as nuclear translocation of AIF and DNA condensation.[225] Neurons from Bid-null mice are resistant to cell death stimuli after oxygen-glucose deprivation and maintain a significantly reduced caspase-3 cleavage. Adult mice lack of Bid exhibit decreased cytochrome c release from mitochondria and reduced infarct volumes after transient focal ischemia as compared to wild-type mice.[368, 369] Similarly, $Bax^{-/-}$ mice had obviously less hippocampal tissue loss or controlled cortical impact [370] upon neonatal H/I [371] than $Bax^{+/-}$ and $Bax^{+/+}$ animals. Stimulation of a BH3-only protein-targeting ubiquitin ligase might be attempted.[372]

A death-promoting role of autophagy in cerebral ischemia has already been suggested by many studies. Knockdown of Atg7 can protect hippocampal pyramidal neurons against hypoxia-ischemia.[174, 199, 201, 373] Puyal et al.

reported that post-ischemic intracerebroventricular injections of autophagy inhibitor 3-MA strongly reduced the lesion volume (by 46%) even when given >4 h after the beginning of the ischemia, demonstrating for the first time that post-ischemic pharmacological inhibition of autophagy can offer neuroprotection.[374] Moreover, the neuroprotective efficacy of inhibiting autophagy more than 4 h after the onset of ischemia highlighted that autophagy should be a primary target for preventing delayed neuronal death in the ischemic penumbra.[202] This could have clinical potential, as long-term lesions and damage could be minimized despite a stroke having already occurred.

1.5.3 Other Targets and Novel Techniques

In addition to therapeutic targets discussed above, new techniques have emerged as well. Protein therapeutics combining the super anti-apoptotic factor FNK, generated from anti-apoptotic Bcl-2 gene and the protein transduction domain (PTD) of the HIV Tat protein, have been found effective in preventing delayed neuronal death in the hippocampus caused by transient global ischemia.[375] Delivery of the HGF gene to subarachnoid space prevented delayed neuronal death in gerbil hippocampal CA1 neurons after brain ischemia.[376] The Ca^{2+} channel antagonist, nimodipine, reduced brain injury and improved functional outcome in rodents [377, 378] and nonhuman primate stroke models,[379] and may improve outcome in human stroke patients.[380, 381] Dantrolene reduced ischemic injury to neurons in mice [382] and gerbils,[383] which suggests an important contribution of Ca^{2+} release from ER stores in the ischemic cell death process. Nitric oxide contributes to ischemia-induced oxidative stress and neuronal death.[384] Drugs that inhibit NOS or scavenge nitric oxide were reported to reduce neuronal damage in rodent stroke models.[385, 386] Several antioxidants have also been reported to

be effective in rodent stroke models, including vitamin E,[387] lipoate,[388] and uric acid.[389]

The tetrapeptide inhibitor tyrosine-valine-alanine-aspartate-chloromethyl ketone (Ac-YVAD-cmk) was reported to rescue cultured neurons from cell death due to oxygen/glucose deprivation by targeting lysosomal enzyme cathepsin B.[390] Based on the calpain-cathepsin hypothesis, Yamashima et al. demonstrated in the monkey brain that, other than in the CA1 region, 89.8% of caudate nucleus neurons were free from post-ischemic neuronal death on Day 5 with 4 mg/kg of CA-074 treatment, while 75.0% of the cortical V layer neurons and 91.6% of the cerebellar neurons survived with 4 mg/kg of E-64c treatment. The inhibitory effect of delayed neuronal death by E-64c was overall more remarkable than that of CA-074. This is probably because E-64c can inhibit not only cathepsins B and L but also calpains.[307] Furthermore, other approaches have been found that reduce delayed neuronal death unrelated with caspases include the actin depolymerizing agent, cytochalasin D, which was reported to be effective in reducing focal ischemic brain injury in mice,[391] and also dietary folic acid, which decreases the vulnerability of neurons to excitotoxic and oxidative insults by reducing homocysteine levels.[392]

1.6 Future Perspectives

1.6.1 Future Perspectives of the Experimental Stroke Models

Despite all the advances and conveniences that the animal models have provided us, some undeniable drawbacks of our current stroke models should never be overlooked, especially with regard to their low clinical relevance and unsuccessful translation to the human studies. The reasons for the failure of the

clinical trials are many and complex, and may due to an immature trial design that not strictly follow the manipulations proved to be successful in pre-clinical animal studies, especially in the timing of administration of the drug, therapeutic window, length of the ischemic insult and dose of drug given.[29] In order to make the animal stroke model into a more valid tool, first thing we need to consider is the increase of complexity of our existing models for a better imitation of human stroke. Before we choose a model we should begin with asking ourselves a series of questions regarding the aims of our experiments.[51] Do we need to obstruct single or multiple vessels, do we need to monitor the timing of reperfusion, or do we want to conclude whether a drug has an effect in the CNS and what its potential target would be? If we are trying to identify the limits of the drug's efficacy, we shall also consider the common co-morbidities of age, atherosclerosis, hypertension, and diabetes. Is demonstrating vigorous effects across a range of genetic backgrounds necessary to our objectives? Does variability in different modeling species matter to our experiment? Should we monitor the brain temperature in our models since changes will dramatically alter infarct size, or it is not a decisive factor thus we may perform all experiments at a fixed temperature? Thinking about what we are doing during the surgery as far as anaesthesia, and what we are changing about how that stroke is occurring is always essential. Particularly, when we are conducting any translational studies, we need to pay more attention on the recovery and behavioural tests we took on animals: whether they are the same as the assessment that are doing in clinic and humans after a stroke attack? Whether our developed physical rehabilitation therapies on the animals are relate to the rehab that is going on in the clinic? Although it is appropriate to start out with young and healthy animals, we should only take it as the starting point. Once we are confident with our techniques, we

should move on and continue with the aged, both males and females, and animals with various co-morbidities that affect the outcome. Specialized stroke modeling has been established with hypertension, hyperglycemia, and diabetes as co-morbidities; however, the broader implications of atherosclerosis and metabolic syndrome remain unknown in stroke modeling. There is still much to be resolved and every experimenter faces many choices. Howell et al. offer a guide to matching model characteristics to experimental aim and an outline of required experiments to move from identifying a candidate drug to clinical trial, and emphasize some potential questions that will be encountered and decisions that need to be made when we are studying novel and more effective therapies.[51] The arguments from the Stroke Therapy Academic Industry Roundtable (STAIR) [393, 394] and Macleod et al. [395] are recommended for reference of appropriate conduction of preclinical trials and avoidance of bias at the bench. In conclusion, the lack of translation between the animal work and clinical benefits does not lie in the animal models itself, but in how we use the models and how we apply this knowledge to design of clinical trials.[396]

1.6.2 Future Perspectives of the Caspase-Independent Stroke Targets

The delayed neuronal death (penumbral region primarily, as the infarct core undergoes inevitable necrosis) responsible for many adverse and debilitating effects in stroke victims is due to intricate interactions between several signaling and transduction pathways. These are various types of PCD, several of which are independent of caspases and apoptosis. Examples of these are autophagic cell death processes. Understanding the functionalities and interactions of these mediators can help find potential drug targets, ideally in which key PCD pathways could be inhibited or in which at least cascadic amplification could be dampened. It has

been shown that caspase inhibition in and of itself is not sufficient for maintenance of neuronal plasticity, despite some success in caspase inhibition maintaining neuronal life. If done early enough, one could target MOMP before its occurrence in ischemia with blockers, such as AIF or Endo G release. Further, the Bcl-2 family of genes has garnered great interest. BH3-only members like Bid and BNIP3 are critical instigators of MOMP, and Bcl-2 itself is an anti-apoptotic agent. By inhibiting release, downregulating or antagonizing pro-PCD intermediates, and/or upregulating expression of anti-PCD intermediates or administering anti-PCD intermediates, one can stave off or even prevent delayed neuronal death until reperfusion ensues. FNK (a derivative of Bcl-2), HGF, Ca^{2+} channel antagonists, NO synthase inhibitors, NO scavengers, cathepsin/calpain inhibitors, actin depolymerizing agents, folic acid, and numerous antioxidants (like Vitamin E, lipoate, and uric acid) have all shown neuroprotective potential in animal models. The longer the time it takes for a stroke victim to get treatment, the larger the infarct core becomes, as the surrounding penumbral tissue reaches the "point of no return." The reversibly damaged penumbra is often initially far larger than the core (due to collateral capillary networks in the area), so much of the adversity experienced after a stroke is also theoretically reversible if caught early enough. That is, the amount of tissue saved can be amplified with earlier interventions. It is possible that, in the future, we could prophylactically treat people at high risk for stroke before the infarct even occurs (as time-to-treatment equals more neuron death) by administering neuroprotective, therapeutic agents. As PCD pathways would be chronically downregulated, neurons would be protected from the very beginning of infarct, minimizing penumbral cell death and the size of the inevitable infarct core. Furthermore, the administration of therapeutic agents into the infarct

region would be facilitated through the deteriorated blood–brain barrier (which would otherwise form a barrier against distributing the agents of interest), as the integrity of the barrier is impaired through ischemic infarction processes. In conclusion, all of the aforementioned research has great potential in changing the course of treatment in stroke and the clinical implications thereof. As research continues looking into different neuroprotective ways in which to inhibit such PCD pathways, one can expect many innovative developments in the near future in this emerging field.

Chapter 2. Research Hypothesis and Objectives

2.1 Research Hypothesis

BNIP3 mediates the excessive mitophagy (autophagy) in the delayed neuronal death in neonatal stroke.

2.2 Rationales and Specific Objectives

2.2.1 Rationale of Specific Objective #1

Ischemic/Hypoxic insult following a stroke results in massive death of neurons and subsequent loss of neurological functions. [397, 398] Given that neurons are highly specialized cells with little capacity to regenerate, it is extremely important to protect them from cell death after stroke. Delayed neuronal death, a hallmark feature of stroke and the primary target for neuroprotective strategies, has been investigated by previous studies. [399] Of the diverse mechanisms that may contribute to this delayed injury, oxidative stress-induced excessive autophagy and autophagic neuron death are established features. [31, 193, 199, 201]

Autophagy refers to the degradation of a cell's cytoplasmic components via the lysosomal system. It plays a normal part in cell growth, development, and homeostasis. This highly regulated process is initiated by class III phosphoinositide 3-kinase [400, 401] and the autophagy-related gene Atg 6 (also known as Beclin-1), [336, 338] and subsequently co-regulated by Bcl-2 family members such as Bcl-2 and Bcl-xL. [329, 339] Physiological level of autophagy has a neuroprotective role, [402-404] but excessive autophagy contributes to autophagic neuron death. [191, 192, 195, 405] Recently, we published that excessive activation of autophagy contributes to neuronal death in cerebral ischemia. [139] However, the regulating mechanism of autophagic cell death is still unclear. Studies suggest that the death-inducing gene

BCL2/adenovirus E1B 19 kDa interacting protein 3 (BNIP3) may trigger the excessive autophagy-induced neuronal death in stroke. [342] BNIP3 is the only gene reported so far that has a characteristic "delayed" expression pattern in response to hypoxia and ischemia. It plays a critical role in delayed neuronal damage in stroke. [237, 406] Elmore et al. and Twig et al. have provided evidence that BNIP3 triggers mitochondrial depolarization and causes mitochondrial autophagy and clearance. [272, 273] Zhang et al. hypothesized that BNIP3 competes with Bcelin-1 for binding to Bcl-2/Bcl-xL and the released Beclin-1 in cells triggers excessive autophagy. [407] Alternatively, BNIP3 might also induce autophagy indirectly as a consequence of mitochondrial injury, as loss of mitochondrial permeability transition would induce autophagy (mitophagy). Considering the essential roles of autophagy (mitophagy) in neonatal stroke, [199] I hypothesized that BNIP3 is a primary mediator of autophagic neuron death. The proposed project is to determine how BNIP3 mediates autophagic neuron death in neonatal stroke. Targeting molecular meidators of autophagic neuron death would shed light on new therapeutic strategies for stroke.

Specific Objective #1:

The first part of the project was designed to:

Determine whether excessive autophagy contributes to neuronal death in cerebral ischemia. (*in vitro* & *in vivo*)

Determine the role of BNIP3 in Ischemia/Hypoxia (I/H)-induced neuronal autophagy and autophagic neuron death. (*in vitro* & *in vivo*)

2.2.2 Rationale of Specific Objective #2

Mitophagy, the specific autophagic elimination of mitochondria, regulates mitochondrial number to match metabolic demand and functions as a core quality control mechanism necessary for the removal of impaired mitochondria. [262] This selective degradation of malfunctioning mitochondria is of particular importance to neurons because of their constant demand for high levels of energy production. Emerging evidence indicates that impaired mitophagy plays an important role in CNS diseases. [408, 409] Intriguingly, mitophagy, like autophagy, is not always protective, as increased mitophagy leads to rapid Purkinje cell death. [410] Therefore, mitophagy can be regarded as a double-edged sword: it plays a protective role when activated by mild physiological stressors, and plays a lethal role when over-activated by a severe pathological stress such as ischemia. [405] Given the importance of precise regulation of mitochondrial turnover in the nervous system, how mitophagy is initiated and regulated represents an area of considerable interest.

BNIP3 is a member of a unique subfamily of death-inducing mitochondrial proteins. Two family members sharing 56% sequence homology have been characterized to date: BNIP3 and BNIP3L (also known as NIX). It is known that BNIP3-induced neuronal death is characterized by early mitochondrial damage. [178] Our group has previously shown that BNIP3 is markedly upregulated in a distinctive 'delayed' manner after cerebral ischemia. [237] Although several studies have postulated a possible link between BNIP3 and mitophagy, none have precisely elucidated how BNIP3 mediates mitophagy. [257, 403, 411] Interestingly, BNIP3L (NIX) directly interacts with LC3, an indicator protein localized on isolation membrane, and mediates the subsequent binding and sequestration of mitochondria

into autophagosomes. [262, 268, 269, 411] Whether BNIP3 mediates a similar function has not yet been determined and forms the basis of the current study.

Specific Objective #2:

The second part of the project was designed to:

Determine the extent to which BNIP3 gene silencing protects neurons from excessive autophagy-induced delayed neuronal death in neonatal stroke. (*in vitro* & *in vivo*)

Determine whether BNIP3 mediates the excessive autophagy (mitophagy) by interacting with LC3 in the delayed neuronal death in neonatal stroke. (*in vitro* & *in vivo*)

The methods used to accomplish the above objectives are described in:

Chapter 3: Materials & Methods.

Results are presented in the following chapters:

Chapter 4. Results (Specific Objective #1)

Chapter 5. Results (Specific Objective #2)

Significance and implications of these results are discussed with respect to the relevant scientific literature in:

Chapter 6. Discussion

Finally, summary of findings and ideas for future directions of this project are identified in:

Chapter 7. Conclusions and Future Directions

Chapter 3. Materials and Methods

3.1 Neonatal Ischemia/Hypoxia (I/H) Animal Model

All animal-involved experiments were conducted according to Canadian federal regulations and the Animal Care guidelines of the University of Manitoba. BNIP3 wild-type (B6; 129) and knockout ($BNIP3^{-/-}$) mice were developed by Dr. Gerald W. Dorn II's lab at the Center for Pharmacogenomics, Department of Internal Medicine, Washington University School of Medicine (St. Louis, MO, USA), and bred and received from Dr. Spencer B. Gibson's lab at the Manitoba Institute of Cell Biology, University of Manitoba. [342] Animals were obtained from Central Animal Care Services (CACS) of University of Manitoba, housed in a temperature-controlled environment (24±2°C) with a 12-h-light-dark cycle, and allowed free access to food and water.

Since extremely immature brains (postnatal day 1-2) are more resistant to the ischemic/hypoxic (I/H) injury, [92, 412, 413] we set up a neonatal mouse model adapted from Rice-Vannucci, [93] combining a unilateral common carotid artery ligation with a 30 min hypoxic treatment (in 8% O_2) on postnatal day 7 mice pups, when the brain maturity is equivalent to that of an early third trimester human fetus. [92, 94] This model reliably gave a well defined lesion and brain damage. Neonatal I/H brain injury was induced in 7-day old BNIP3 Wild-type and knock-out mice pups. In brief, after the mice were deeply anesthetized with isoflurane (2%), the right common carotid artery was dissected and ligated with silk sutures (4/0). After the surgical procedure, the mice pups were allowed to recover for 1 h and then placed in chambers maintained at 37°C, through which 8% humidified oxygen (balanced with nitrogen) flowed for 30 min. After hypoxic exposure, the pups were returned to their dams. The animals were allowed to recover for 24 h, 72 h, 7 days, or 28 days before

being euthanized. At each stage, brains were processed for biochemical and morphological analyses. This procedure resulted in brain injury in the ischemic hemisphere, consisting of cerebral infarction mainly in the forebrain. Control littermates were neither operated on nor subjected to hypoxia. N = 3-6 for each group.

3.2 Transient Middle Cerebral Artery Occlusion (MCAO) Animal Model

Adult focal cerebral ischemia injury was induced by intraluminal middle cerebral artery occlusion (MCAO) as described before. [61] 2-3 months old BNIP3 wild-type and knockout mice were anesthetized with isoflurane (2.5%). Body temperature was kept at 37°C using a thermostatically controlled heating platform until the animals recovered from surgery. Focal cerebral ischemia was induced by gently advancing a 6-0 Doccol monofilament (Doccol Co., Sharon, MA) from the external carotid artery into the lumen of the internal carotid artery until it blocked the origin of the middle cerebral artery (MCA). The blocking of MCA was maintained for 60 min and then the filament was withdrawn for reperfusion. The animals were allowed to recover for 48 h before being euthanized. Control animals were treated with MCA exposure but not ligation. N=3 for each group.

3.3 Infarct Volume Measurement

2, 3, 5-triphenyltetrazolium chloride (TTC) staining (Wako Pure Chemical Industries, Osaka, Japan) was performed to detect the infarct volume of ischemic brains. Briefly, the mice brains were dissected and cut into five equally spaced (2 mm) coronal sections. These sections were immersed in a 1% TTC solution for

15 min at 37°C in the dark. The ischemic infarct areas were indicated by the pale colour while the healthy brain tissues were stained in dark red. This method is acknowledged to be effective in marking damaged brain tissues even two weeks after MCAO.[414, 415] The Quantity One software from the BIO-RAD Laboratories (Mississauga, ON, Canada) was used to measure the infarct volumes. A total hemispheric infarct volume was calculated at each time point by the equation as CIV=[LT- (RT-RI)] × d, where CIV is the corrected total infarct volume, LT is the area of the left hemisphere, RT is the area of the right hemisphere, RI is the infarcted area, and d is the slice thickness (2 mm). [416, 417] Relative infarct volume was also calculated as a percentage of whole brain volume.

3.4 Brain Tissue Processing

Mice were perfused through the ascending aorta with cold 0.1M phosphate-buffered saline (PBS, pH 7.4). Brains (excluding cerebellum, pons, and medulla oblongata) were divided sagitally. The left and right hemispheres (i.e. contraleteral and ischemic hemispheres in neonatal/MCAO stroke models) were dissected into the cortex and hippocampus, and then snap frozen and stored at -80°C for protein and other biochemistry analyses. N>=3 for each time point. Meanwhile, parallel brains with the same ischemic treatment at each time point were post-fixed with freshly depolymerized 4% paraformaldehyde (PFA) in PBS for an additional 48 h at 4°C, and then was equilibrated overnight in 30% sucrose. [418, 419] The serial coronal sections were cut into 25 μm on a freezing sliding microtome (Leica Microsystems, Wetzlar, Germany) for immunohistochemistry analysis. N>=3 for each time point.

3.5 Cell Culture and Treatment

All the culture plates were purchased from Nunc and Costar. Cells were cultured in 96-well plates for cell death and autophagic parameters measurement, in 6-well plates for protein detection, in 24-well plates and on culture glasses for immunohistochemistry.

BNIP3 wild-type (B6; 129) and knockout ($BNIP3^{-/-}$) mice were obtained from Dr. Spencer B. Gibson's lab in Manitoba Institute of Cell Biology, University of Manitoba. For primary cortical neuron culture, pregnant female Sprague-Dawley rats or BNIP3 wild-type and knockout mice were anesthetized with 5% isoflurane. Primary cortical neurons were separated from embryonic 18 days (E18) rat brains or embryonic 16 days (E16) mice brains using our standardized protocol [237] and neuronal cultures were prepared as described previously.[420] Cells were plated in neurobasal medium (Invitrogen, Burlington ON, Canada) supplemented with 5 mmol/L HEPES, 1.2 mmol/L glutamine (Life Technologies), 10% fetal bovine serum (FBS, Life Technologies), 2% B27 (Life Technologies), and 25 μg/mL gentamicin (Life Technologies) at a density of 2×10^5 cells/cm^2 on plates or cover slips coated with poly-D-lysine (Sigma-Aldrich). The medium was replaced with neurobasal without FBS after 24 h. After 7 days, glutamine was removed from the medium. For OGD treatment, cells were washed twice and incubated with glucose-free Earle's Balanced Salt Solution (EBSS, Life Technologies) at pH 7.4 in a Forma Series II Water Jacketed CO_2 Incubator (Thermo Scientific Waltham, MA, USA) with an atmosphere of 94% N_2, 5% CO_2, and 1% O_2 at 37°C for the designed length of time. OGD was terminated by replacing the glucose-free EBSS with complete medium and incubating the cultures in normoxic conditions.

SH-SY5Y (human SH-SY5Y neuroblastoma cell line) cells were maintained in Dulbecco's Modified Eagle Medium plus 10% FBS in the presence of penicillin (100 units/mL), streptomycin (100 μg/mL), and 2 mM L-glutamine. [139] Cells were cultured in a humidified 5% CO_2 environment at 37 °C under the nomorxic conditions until the confluency reached around 80% of each well. Then OGD and reperfusion treatments were conducted as described above. Cell lines were passaged at a 1/5 dilution after reaching 90% confluency, and were preserved for long-term storage in liquid nitrogen at -80 °C.

3.6 Plasmid Transfection and miRNA Lentiviral Vectors

For plasmid transfection experiments, SH-SY5Y cells were seeded in 6-well plates for 72 to 96 hours until the confluency reached 70-80%. Cultures were rinsed twice with serum and antibiotics-free medium prior to transfection. Cells were transfected using Lipofectamine 2000 (Invitrogen, Burlington ON, Canada) according to the manufacturer's instructions. For each transfection, 4 g DNA and 5 μl Lipofectamine reagent were diluted in 250 μl Opti-MEM reduced serum media separately, then the DNA was added into the Lipofectamine reagent drop-wisely to produce a transfection mixture. The transfection mixture was firstly incubated for 20 min at room temperature in a microfuge tube, and then was added to each well of cells in a drop-wise manner. The cells were immersed in the transfection mixture for 6 h before replacment of a fresh complete media. Transfection efficiency was determined by immunofluorescence at approximately 70-80% in SH-SY5Y cells.

The mouse GIPZ lentiviral shRNAmir individual clone for BNIP3 gene was purchased from Thermo Scientific Open Biosystems (Catalog Number: RMM4431-99204979). Lentiviral stocks were produced using Trans-Lentiviral™ Packaging

System. Transduction of neurons was performed by adding the viral vectors (multiplicity of infection >20) to reduced medium (about 20% of normal) for one hour on the second day of culture. Then viral particles were removed by replacing culture medium. After cultured for seven days in normal neurobasal medium, neurons were treated with OGD/RP injury as described above.

3.7 Transmission Electron Microscopy

To observe I/H-induced the formation of autophagosomes and morphologic changes of cell organelles with transmission electron microscopy examination, primary cortical neurons were digested by 0.25% trypsin for 15 min and collected and compacted to solid pallets by centrifugation at 1200 g for 3 min. The pallets of neurons were then treated as tissue blocks, which were fixed first immersed in 2.5% glutaraldehyde in 0.1 mol/L phosphate buffer (pH 7.2) with 8% sucrose, postfixed in 1% osmium tetroxide in 0.1 mol/L phosphate buffer (pH 7.4), dehydrated in graded ethanol series, and flat embedded in Araldite. Ultrathin sections (40-60 nm thick) were placed on grids (200 mesh), and double stained with uranyl acetate and lead citrate. The grids containing the sections were observed under a Philips 201 (Philips Electron Optics, B.V. Eindhoven, The Netherlands) electron microscope.

3.8 Monodansylcadaverine (MDC) Staining

Cells were seeded at a density of 2×10^5 cells/cm^2 on 96-well plates. After the OGD and RP treatment, cells were incubated in 100 μM monodansylcadaverine (MDC; Fluka, Oakville, ON, Canada. Cat: 30432) solution for 1 h at 37°C in the dark. Cells were then washed with one rinse of phosphate buffered saline (PBS) and

fixed with 4% PFA for 15 min. Then cells were washed with three rinses of PBS, and measurement of fluorescence was performed on a Wallac VICTOR^3 microplate reader (Perkin Elmer Life Sciences). The excitation wavelength of MDC is 360 nm and emission wavelength is 457 nm. For each time point, there were at least 18 parallel wells and I repeated the experiment three times.

Because the total cell number changed after different lengths of OGD and RP treatment times, I added 100 μg/mL ethidium bromide (EB) solution into each well and stained nuclei of the leftover cells. Then the fluorescence was detected on a Wallac VICTOR^3 microplate reader (Perkin Elmer Life Sciences) with an excitation wavelength of 480 nm. The normalized MDC fluorescence intensity for each experiment was calculated.

3.9 Acridine Orange (AO) Staining

Cells were seeded at a density of 2×10^5 cells/cm^2 on 96-well plates. After OGD/RP, cells were incubated in PBS with 1 μg/mL acridine orange (AO; Sigma, Oakville, ON, Canada. Cat: 318337) for 10 min at room temperature (RT) in the dark. Cells were then washed with one rinse of phosphate buffered saline (PBS) and fixed with 4% PFA for 15 min. Then cells were washed with three rinses of PBS and measurement of fluorescence was performed on a Wallac VICTOR^3 microplate reader (Perkin Elmer Life Sciences). The excitation filters were 550 and 485 nm for red and green fluorescence, with emission filters 590 and 535 nm, respectively. Then the ratio of red fluorescence to green fluorescence was used to quantify autophagic activities. For each time point, at least 18 parallel wells were measured and the experiments were repeated for three times.

3.10 Fluoro-Jade C/MDC Double Staining of Autophagic Neurons and Quantification of Autophagic Neuron Death

Cells were seeded on cover slips, which were placed in 24-well plates. After the OGD and RP treatment, cells were incubated in 100 μM MDC (Fluka, Cat: 30432) solution for 1 h at 37°C in the dark. Then cells were fixed in 4% paraformaldehyde on ice for 15 min and washed with three rinses of PBS. 0.0004% Fluoro-Jade C (Millipore, Billerica, MA, USA. Cat: AG325) working solution was added in each well for 1 h at 37°C to stain the degenerating neurons. Cells were washed with two rinses of PBS (with 0.1% tween-20), 10 min each time. The cover slips were mounted on glass slides and fluorescent images were taken on a Nikon TE2000-E microscope equipped with a RETIGA camera (QImaging, Surrey, BC, Canada.). For each time point there were at least eight parallel wells, and for each well at least three pictures under different visual fields were taken. The magnification was 40×.

3.11 Quantification of Neuronal Death and Autophagy Intensity

To examine the contribution of BNIP3 to the OGD-induced neuronal death, both BNIP3 wild-type and knockout cortical neurons were collected and measured by the LDH cyto-toxicity assay. Lactate dehydrogenase (LDH) leakage was measured after 6 h of OGD followed by RP at 0, 24, 48, or 72 h. In brief, after OGD treatment, the supernatant of the cell culture was reserved. Neurons were lysed with lysis buffer at 37 ºC for 30 min. Then samples of supernatants and cell lysates were prepared following the manufacturer's instructions for the LDH-Cytotoxicity Assay Kit II (BioVision, Milpitas, CA, USA. Cat: #K313-500). The absorbance value at 450 nm was determined on a Wallac VICTOR^3 microplate reader (Perkin Elmer Life

Sciences, Waltham, MA, USA). Cell death rate was calculated according to the manufacturer's instruction.

For quantification of the autophagy intensity, both BNIP3 wild-type and knockout neurons were seeded at a density of 2×10^5 cells/cm^2 on 96-well plates. After the OGD and RP treatment, cells were incubated in 100 μM monodansylcadaverine [341, 421, 422] (MDC; Fluka, Oakville, ON, Canada. Cat: 30432) solution for 1 h at 37 °C in the dark. Cells were then washed with one rinse of phosphate buffered saline (PBS) and fixed with 4% PFA for 15 min. Then cells were washed with three rinses of PBS, and measurement of fluorescence was performed on a Wallac VICTOR^3 microplate reader (Perkin Elmer Life Sciences). The excitation wavelength of MDC is 360 nm and emission wavelength is 457 nm. For each time point, there were at least 18 parallel wells and I repeated the experiment three times. I calculated the normalized MDC fluorescence intensity as described above.

3.12 LC3-II/LysoTracker Red and LC3-II/MitoTracker Red Double Staining for Co-localization Detections in Neurons

BNIP3 wild-type and knockout cortical neurons were seeded on cover slips and placed in 24-well plates. The LC3II-GFP transgenes were transfected into neurons using the Premo™ Autophagy Sensors (LC3II-GFP) *BacMam 2.0* System (Invitrogen, Cat: P36235) according to the manufacturer's instructions. Cells were left undisturbed for at least 24 h following transfection, before treatments were administered.[423] The LC3II and LysoTracker Red double-staining were performed to detect the co-localization of autophagosomes with lysosomes in neurons, while the LC3II and MitoTracker Red double-staining were performed to detect the co-localization of autophagosomes with mitochondria in neurons. Briefly, pre-transfected

neurons showing an over-expression of LC3II protein were proceeded to the OGD/RP treatment on day 7. Upon each time point, neurons were firstly incubated in 50 nM LysoTracker Red (Invitrogen, Cat: MP-07525) solution for 1 h or incubated in 50 nM MitoTracker Red (Invitrogen, Cat: M-7512) solution for 15 min at 37 ºC in the dark. Then cells were fixed in 4% paraformaldehyde on ice for 15 min and washed with three rinses of PBS. Nuclei were stained by Hoechst 33342 (Calbiochem, Mississauga, ON, Canada). The cover slips were mounted on glass slides and cells were observed by a Carl Zeiss AxioImager. Z1 (Carl Zeiss, Gottingen, Germany) fitted with a motorized Z-stage and an apotome for optical sectioning. For high-resolution microscopy, Z-stacks were acquired at 63× magnification with 0.6 μm increments in ApoTome mode using a high-resolution AxioCam MRm digital camera, a 63× Plan-Apochromat (oil immersion) objective and Zeiss AxioVision 4.8 software (Carl Zeiss). For each time point there were at least four parallel wells, and for each well at least three pictures under different visual fields were taken.

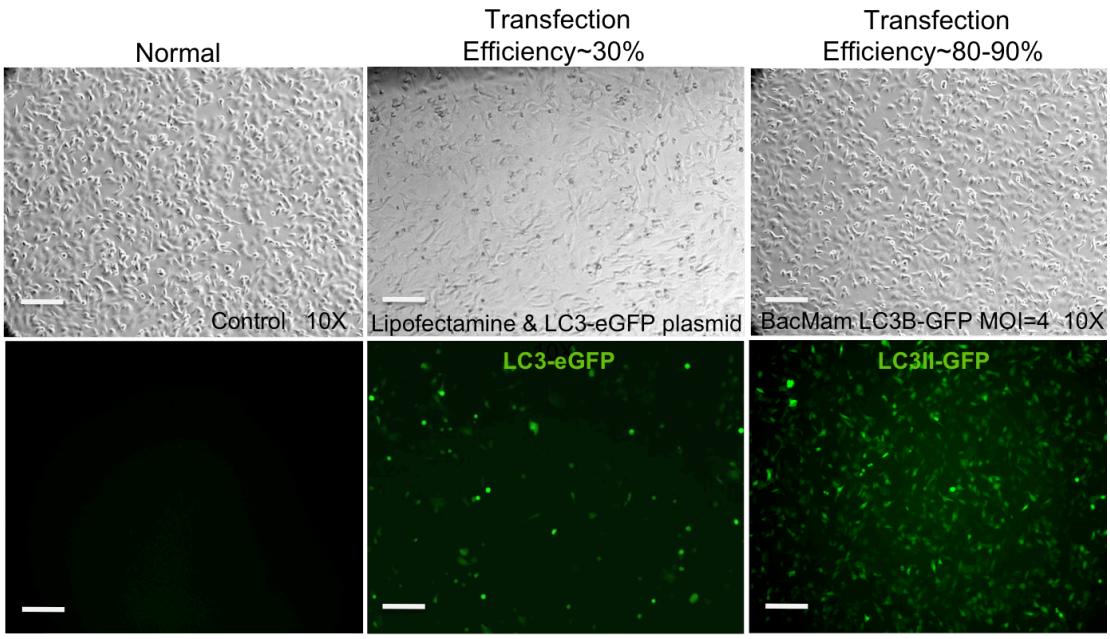

Fig 3.1 Comparision of the transfection efficiencies between tranditional plasmid transfection using Lipofectamine 2000 reagent and baculoviral vector transfection using Premo™ Autophagy Sensors (LC3II-GFP) *BacMam 2.0* System. SH-SY5Y cells were seeded in 6-well plates for 72 to 96 hours until the confluency reached 70-80% for efficient transfection. Control group without transfection. Multiplicity of infection (MOI) = 4 for the viral vector. Scale bars = 160 μm. Images were taken at 10× objective.

3.13 Immunocytochemistry

BNIP3 wild-type and knockout cortical neurons were seeded on cover slips, which were placed in 24-well plates. After OGD/RP treatment cells were fixed in 4% paraformaldehyde on ice for 20 min, washed with PBS for 3 × 5 min, then blocked with 1% BSA (Sigma) at RT for 1 h, and incubated with primary antibodies (Autophagy APG8 microtubule-associated protein 1 light chain 3 [LC3], 1:100; goat polyclonal Beclin-1 [BECN1] (Santa Cruz Biotechnology, Santa Cruz, CA, USA), 1: 100; mouse monoclonal BNIP3 antibody provided by Dr. A. Greenberg, [246] 1: 100) at 4 °C overnight. Incubation with the secondary antibody (Alexa 488-labeled goat F(ab')2 anti-(rabbit IgG), Alexa 594-labeled donkey F(ab')2 anti-(goat IgG), and Alexa 594-labeled goat F(ab')2 anti-(mouse IgG) from Invitrogen) was carried out at RT for 1 h. Nuclei were stained by Hoechst 33342 (Calbiochem, Mississauga, ON, Canada). The cover slips were mounted on glass slides and fluorescent images were taken on a Nikon TE2000-E microscope equipped with a RETIGA camera (QImaging, Surrey, BC, Canada).

3.14 Western Blotting

Total cell lysates were separated from neuronal cultures after OGD/RP treatment. Protein concentrations were determined by a reducing agent-compatible BCA assays kit (Pierce, Nepean, ON, Canada). Protein samples were separated on 12% polyacrylamide gels and electrotransferred to polyvinylidene difluoride membranes. The primary antibodies included: rabbit polyclonal autophagy APG8 (1:1000; Abgent, San Diego, CA, USA), mouse monoclonal BECN1 (1:1000; Abcam, Cambridge, MA, USA), rat monoclonal [GL2A7] LAMP-2 (1:1000; Abcam, Cambridge, MA, USA), mouse monoclonal caspase3 (1:1000; Santa Cruz Biotechnology, Santa Cruz, CA, USA), rabbit polyclonal BAX (1:1000; Santa Cruz Biotechnology, Santa Cruz, CA, USA), mouse monoclonal [7H8.2C12] Cytochrome C (1:1000; Abcam, Cambridge, MA, USA), mouse monoclonal BCL-2 (1:1000; Santa Cruz Biotechnology, Santa Cruz, CA, USA), mouse monoclonal BNIP3 (1:1000; provided by Dr. A. Greenberg),[246] mouse monoclonal NIX (H-8) (1:1000; Santa Cruz Biotechnology, Santa Cruz, CA, USA), mouse monoclonal Cox IV (1:1000; Abcam, Cambridge, MA, USA), mouse monoclonal TOMM22 (1:1000; Abcam, Cambridge, MA, USA), rabbit polyclonal VDAC1 (1:1000; Sigma-Aldrich, Oakville, Ontario, Canada), and mouse monoclonal β-actin (1:2000; Santa Cruz Biotechnology, Santa Cruz, CA, USA). The secondary antibodies were horseradish peroxidise-conjugated sheep antimouse (1:5000; GE Healthcare, Baie d'Urfe, QC, Canada) and donkey antirabbit IgG (1:5000; Thermo scientific, Ottawa ON, Canada), donkey antigoat IgG (1:5000; Santa Cruz Biotechnology, Santa Cruz, CA, USA), and goat antirat IgG (1:5000; Invitrogen Corporation, Camarillo, CA, USA). Immunoblotting was detected by Enhanced Chemiluminescence (Amersham, Baie d'Urfe, QC, Canada.) and imaged on a FluorChem 8900 imager (Alpha Innotech, San Leandro, CA, USA). Western blot

bands densities were quantified using the BIO-RAD Laboratories (Mississauga, ON, Canada) Quantity One software.

3.15 Co-immunoprecipitation Assay

For co-immunoprecipitations, neuronal cells (6×10^6/group) were digested in RIPA lysis buffer (Sigma-Aldrich, Oakville, Ontario, Canada) including 1% Halt* Protease and Phosphatase Inhibitor Cocktail (Thermo Scientific, Ottawa ON, Canada), and the total cell lysates were processed with Pierce® Co-Immunoprecipitation (Co-IP) Kit (Thermo Scientific, Ottawa ON, Canada) according to the manufacturer's instructions. The lysates were immunoprecipitated with 10 mg anti-BNIP3 antibody , 10 mg anti-BECN1 antibody, 10 mg anti-BCL-2 antibody (EMD Millipore Corporation, Billerica, MA, USA), 10 mg anti-LC3 antibody, and 10 mg anti-NIX antibody, respectively, at 4°C for 48 h. Protein-coupled resins were washed six times with lysis buffer to reduce contaminants, and prepared for western blot analysis by adding Laemmli sample buffer with 2% β-mercaptoethanol (Bio-Rad, Mississauga, Ontario, Canada) to the eluted pellet and heating at 100°C for 5 min.[424]

3.16 Enzyme-linked Immunosorbent Assay (ELISA) of LC3II

Cortical neurons or brain tissues were homogenized in RIPA lysis buffer (Sigma-Aldrich, Oakville, Ontario, Canada) including 1% Halt* Protease and Phosphatase Inhibitor Cocktail (Thermo Scientific, Ottawa ON, Canada) and then centrifuged at 5,000 × g at 4ºC for 15 min. LC3II levels were measured in the supernatants. For quantification of interactive activities of LC3II with NIX or BNIP3, the total lysates were firstly processed with Pierce® Co-Immunoprecipitation (Co-IP) Kit (Thermo

Scientific, Ottawa ON, Canada) according to the manufacturer's instructions. The eluted pellets from co-ip were then measured by the Rat Microtubule-associated proteins 1A/1B light chain 3B (MAP1LC3B) ELISA kit (CUSABIO, Wuhan, Hubei, China). Each sample was assayed in duplicate at appropriate dilutions so that relative luminescent units fell within the linear range of standard curves. [418, 425] Plate was read at 450 nm on a BioTek PowerWave XS Microplate Spectrophotometer (BioTek Instruments Inc., Winooski, VT, USA). The interactive activities of LC3II with NIX or BNIP3 were quantified as percentage of pulled-down LC3II to the total amount of LC3II.

3.17 Statistical Analysis

Statistical differences were determined using one-way ANOVA analyses and Bonferroni or Dunnett's post-tests. Comparisons between BNIP3 wild-type and knockout groups were made using two-way ANOVA analyses and Bonferroni post-tests. GraphPad Prism 5 software (GraphPad Software, Inc. La Jolla, CA, USA) was used for all the statistical analyses. A difference was considered significant at $* p < 0.05$, $** p < 0.01$, $*** p < 0.001$

Antibodies that were used for western blot (WB) and immunofluorescence (IF) are listed in Table 3.1 (primary antibodies) and Table 3.2 (secondary antibodies).

Table 3.1 Primary Antibodies

Antibody	Host Species	Application (Dilution)	Source
APG8 (LC3)	Rabbit Poly	WB 1:1000 IF 1:100	Abgent, San Diego, CA, USA
BNIP3	Mouse Mono	WB 1:1000 IF 1:100	Dr. A. Greenberg [246]

BECN1	Mouse Mono	WB 1:1000	Abcam, Cambridge, MA, USA
BECN1	Goat Poly	IF 1:100	Santa Cruz Biotechnology, USA
LAMP-2 [GL2A7]	Rat Mono	WB 1:1000	Abcam, Cambridge, MA, USA
Caspase 3	Mouse Mono	WB 1:1000	Santa Cruz Biotechnology, USA
BAX	Rabbit Poly	WB 1:1000	Santa Cruz Biotechnology, USA
Cytochrome C [7H8.2C12]	Mouse Mono	WB 1:1000	Abcam, Cambridge, MA, USA
BCL-2	Mouse Mono	WB 1:1000	Santa Cruz Biotechnology, USA
NIX (H-8)	Mouse Mono	WB 1:1000	Santa Cruz Biotechnology, USA
Cox IV	Mouse Mono	WB 1:1000	Abcam, Cambridge, MA, USA
TOMM22	Mouse Mono	WB 1:1000	Abcam, Cambridge, MA, USA
VDAC1	Rabbit Poly	WB 1:1000	Sigma-Aldrich, Ontario, Canada
β-actin	Mouse Mono	WB 1:2000	Santa Cruz Biotechnology, USA

Table 3.2 Secondary Antibodies

Antigen	Host Species	Conjugate	Dilution	Source
Mouse IgG	Sheep	Horseradish peroxidise	WB 1:5000	GE Healthcare, QC, Canada
Rabbit IgG	Donkey	Horseradish peroxidise	WB 1:5000	Thermo scientific ON, Canada
Goat IgG	Donkey	Horseradish peroxidise	WB 1:5000	Santa Cruz Biotech. , USA
Rat IgG	Goat	Horseradish peroxidise	WB 1:5000	Invitrogen Corporation, CA, USA
Rabbit IgG	Goat	Alexa Fluor® 488	IF 1:5000	Invitrogen Corporation, CA, USA
Goat IgG	Donkey	Alexa Fluor® 594	IF 1:5000	Invitrogen Corporation, CA, USA
Mouse IgG	Goat	Alexa Fluor® 594	IF 1:5000	Invitrogen Corporation, CA, USA

Chapter 4. Results (Specific Objective #1)

Conclusion: Excessive Autophagy Contributes to Neuron Death in Cerebral Ischemia

4.1 Excessive Activation of Autophagy in Primary Rat Cortical Neurons after OGD/RP Injury

TEM was used to identify ultrastructural changes in primary cortical neurons 48 and 72 h after 6 h OGD injury. Control neurons showed normal appearance of cytoplasm, organelles, nucleus, and chromatin (Figure 4.1A). After RP for 72 h, numerous autophagic vacuoles (AVs) with characteristic morphological features of autophagosomes were detected in neurons (Figure 4.1B). Swelling and dilated mitochondria were frequently found (Figure 4.1B). Abundant double-membrane structures and double-membrane autophagosomes, which surrounded parts of cytoplasm and organelles, formed in neurons following OGD/RP treatment (Figure 4.1D-H). Lysosomes showed a darkened appearance, indicating the activation of lysosomes after RP 72 h (Figure 4.1E and F). Fusion of autophagosomes with lysosomes was frequently seen (Figure 4.1E). Meanwhile, coexistence of morphological features of normal neurons (Figure 4.1C and E), autophagic cell death, necrosis, and apoptosis could be found in the same group of neurons treated by OGD for 6 h followed by RP for 48 h (Figure 4.1D).

Autophagy is also characterized by the development of acidic vesicular organelles (AVOs), which include lysosomes as well as autophagosomes that can be detected and quantified by AO staining. [426] AO is a nucleic acid selective fluorescent cationic dye useful for cell cycle determination. This pH-sensitive dye is cell permeable and stains the nucleus and cytoplasm green and any acidic

compartments red.[342, 427] In primary cortical neurons, AVO production was increased from 19.99% in normal condition to 29.19% after 6 h OGD followed by RP 72 h (Figure 4.2A). The percentage of AVO-positive neurons to total neurons in the 6 h OGD group was much greater compared to that of 3 h OGD, indicating that longer OGD injury activated higher autophagic activity. Second, we used MDC, an autofluorescent substance that accumulates in acidic AVs, as a specific marker for AVs.[341, 421, 422] Compared to the control group (con), there was a significant increase in the MDC fluorescence starting at 0 h and peaking at 48-72 h after 6 h OGD treatment (Figure 4.2B), suggesting an increase of autophagy in neurons after OGD/RP. Third, we detected the processing and translocation of endogenous LC3 protein by immunocytochemistry and Western Blotting. We observed that the level of LC3 punctate staining in the rat cortical neurons after 3 h OGD increased dramatically according to the elongation of RP time, which represents an intense activation of autophagy after H/I and RP injury (Figure 4.2D). Finally, we combined Fluoro-Jade C and MDC staining together to quantify the number of autophagic neurons. This method helped us identify those double- stained neurons, which were most possibly degenerating neurons also undergoing autophagy. We found that the increase of autophagic neurons after OGD and RP injury corresponded well to the increase of AO and MDC fluorescence (Figure 4.2C).

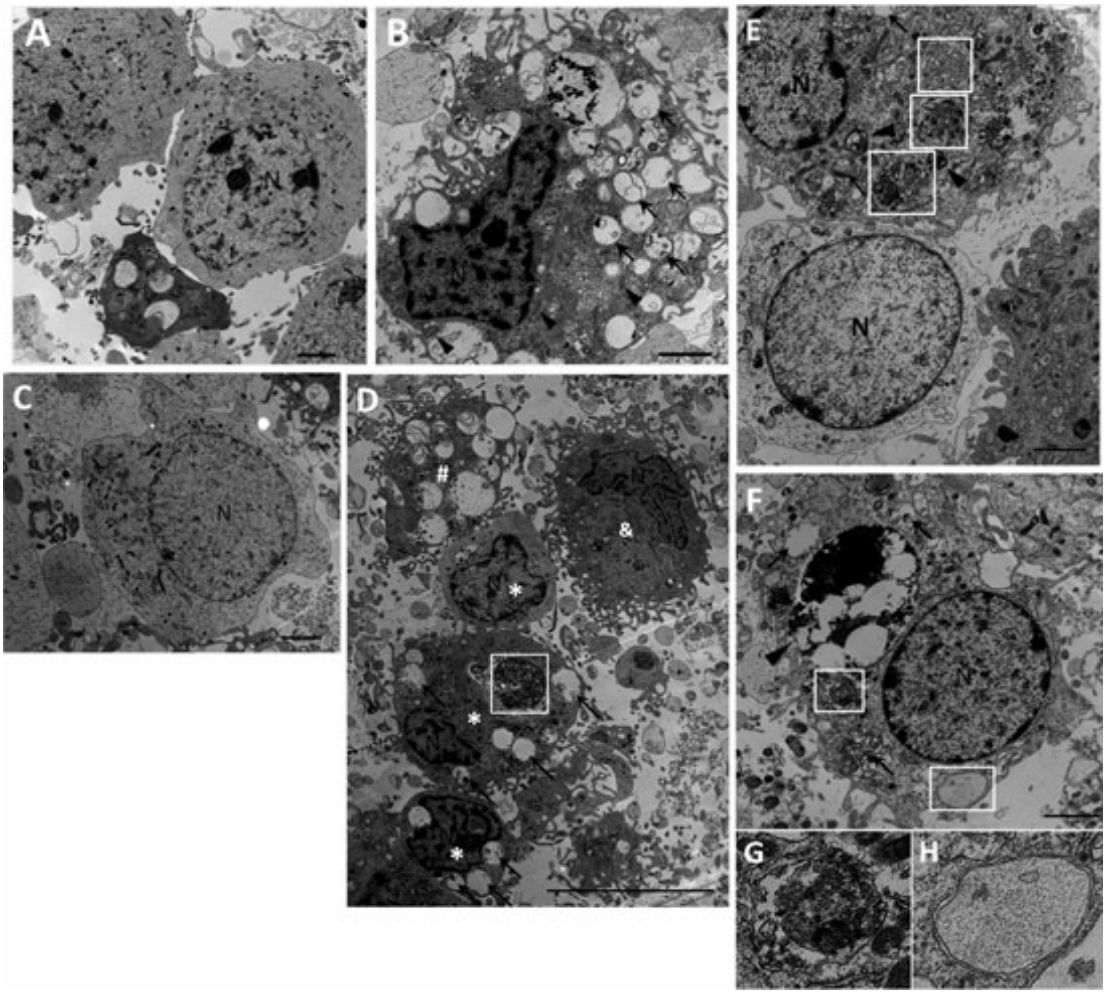

Fig 4.1 Ultrastructural changes in primary cortical neurons after OGD/RP injury. Primary neurons were subjected to OGD for 6 h then followed by RP for 48 h (D) and 72 h (B and E–H) and were fixed for EM examination. Electron microscopy (EM) images showing: Normal appearance of cytoplasm, organelles, and nucleus in control neurons (A). N, nucleus; Ultrastructural features of autophagic cell death were detected in neurons treated by OGD 6 h followed by RP 72 h. Cell shrinkage, nuclear condensation (without fragmentation), loss of cellular organelles, and formation of numer- ous autophagic vacuoles (black arrows) were shown in the picture (B, D, E, F). Mitochondria also displayed swelling and dilation as indicated

by black arrowheads (B). Coexistence of morphological features of normal neurons (C, and lower cell in E), autophagic cell death (∗), necrosis (#), and apoptosis (&) can be found in the same group of neurons treated by OGD 6 h followed by RP 48 h (D). White boxes represent autophagosomes; Black arrows represent autophagic vacuoles. Abundant double-membrane structures and double-membrane autophagosomes formed in neurons after OGD/RP treatment (D–H, as indicated by White boxes). Lysosomes stained darkened, indicating the activation of lysosomes (as shown by black arrowheads). An autophagosome fused with a lysosome. (E, as indicated by the lowest white box with beside black arrowhead). N = nucleus; Black arrows represent autophagic vacuoles; (G) and (H) showed the enlarged autophagosomes in (F). Scale bars = 2 μm in (A–C, E–F); Scale bar = 10 μm in (D).

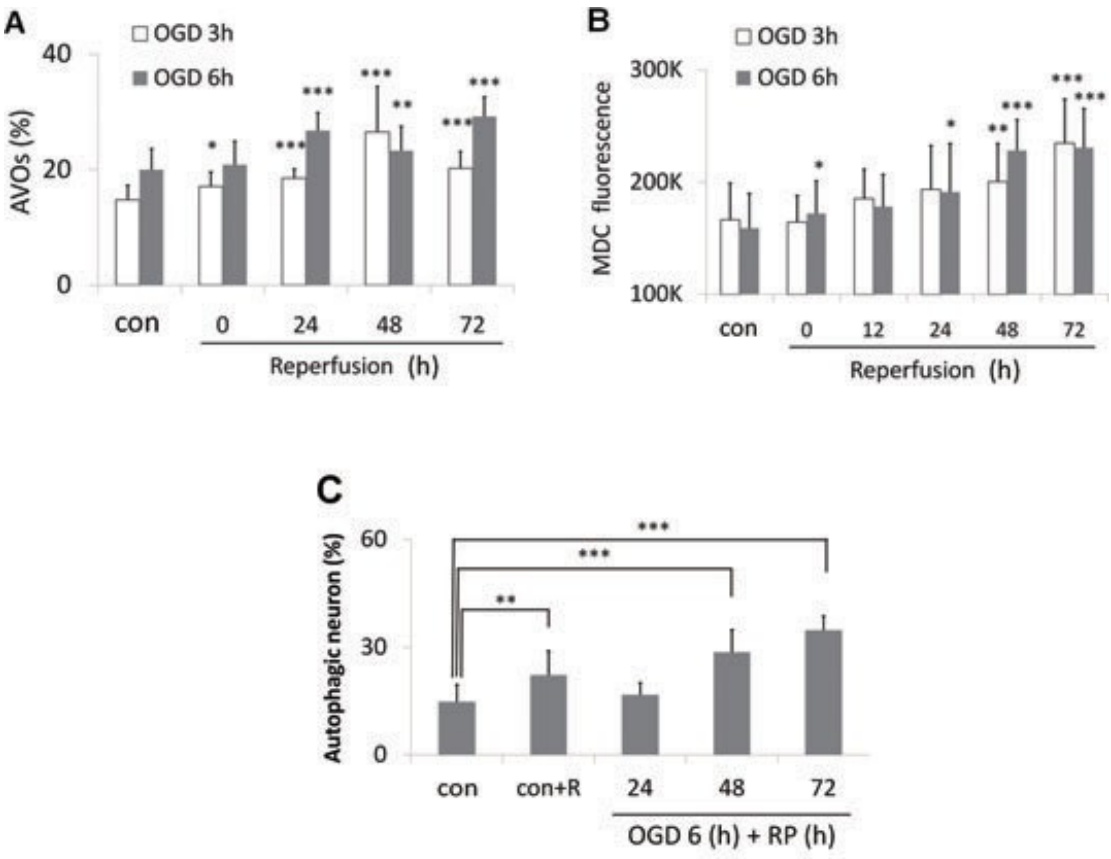
A
OGD 3h
OGD 6h
AVOs (%)
40
20
0
con
0
24
48
72
Reperfusion (h)
B
OGD 3h
OGD 6h
MDC fluorescence
300K
200K
100K
con
0
12
24
48
72
Reperfusion (h)
C
Autophagic neuron (%)
60
30
0
con
con+R
24
48
72
OGD 6 (h) + RP (h)
D
LC3/Hoechst
Control
LC3/Hoechst
OGD 3h RP 24h
LC3/Hoechst
OGD 3h RP 48h
LC3/Hoechst
OGD 3h RP 72h

Fig 4.2 The increase of autophagic activity in OGD/RP-challenged cortical neurons. Acridine orange staining (A) and MDC/EB double staining (B) were used to measure the intensity of autophagy in neurons after OGD/RP. MDC and Fluoro-Jade C double staining (C) was used to quantify the autophagic neurons under 40× magnification. * $p < 0.05$, ** $p < 0.01$, *** $p < 0.001$ versus control without OGD/RP. In (C), "control" represented "group with neither rapamycin nor OGD/RP treatment"; whereas "con+R" represented "group with rapamycin treatment (250 nM, refer to Section "OGD/RP Injury Increases Autophagy Marker Protein Levels in Cortical Neurons and SH-SY5Y Cells") but without OGD/RP." OGD/RP treatment increases punctate staining of LC3 protein (D). Neurons were treated with OGD for 3 h and followed by different times of RP (24, 48, or 72 h). Immunocytochemistry was used to demonstrate the punctate staining of LC3 protein. Control group (con) was without OGD/RP.

4.2 OGD/RP Injury Induced Autophagic Cell Death in Rat Cortical Neurons

As shown in Figure 4.3, when neurons were viewed with a fluorescence microscopy after OGD/RP treatment, the AVs labeled by MDC seemed as distinct dot-like structures distributed in the cytoplasm, in the perinuclear regions and in the processes (Figure 4.3). Fluoro-Jade C labels degenerating neurons. Some Fluoro-Jade C-positive neurons were stained with intense MDC particles. We counted these cells as autophagic neurons (Figure 4.3E-F). When the stimulus became stronger, the number of neurons with intense MDC staining and a condensed nucleus increased substantially (Figure 4.3E and G-H, red arrows). The two features were taken together as the criteria for neurons undergoing autophagic cell death. We counted the cell numbers for different morphology under 40× magnification and did the statistical analysis to get the autophagic neuron rate (Figure 4.2C) and autophagic neuronal death rate (Figure 4.3I). It was obvious that prolonged RP after OGD injury resulted in a small but significantly increase in the autophagic neuronal death rate in cortical neurons in a time-dependent fashion.

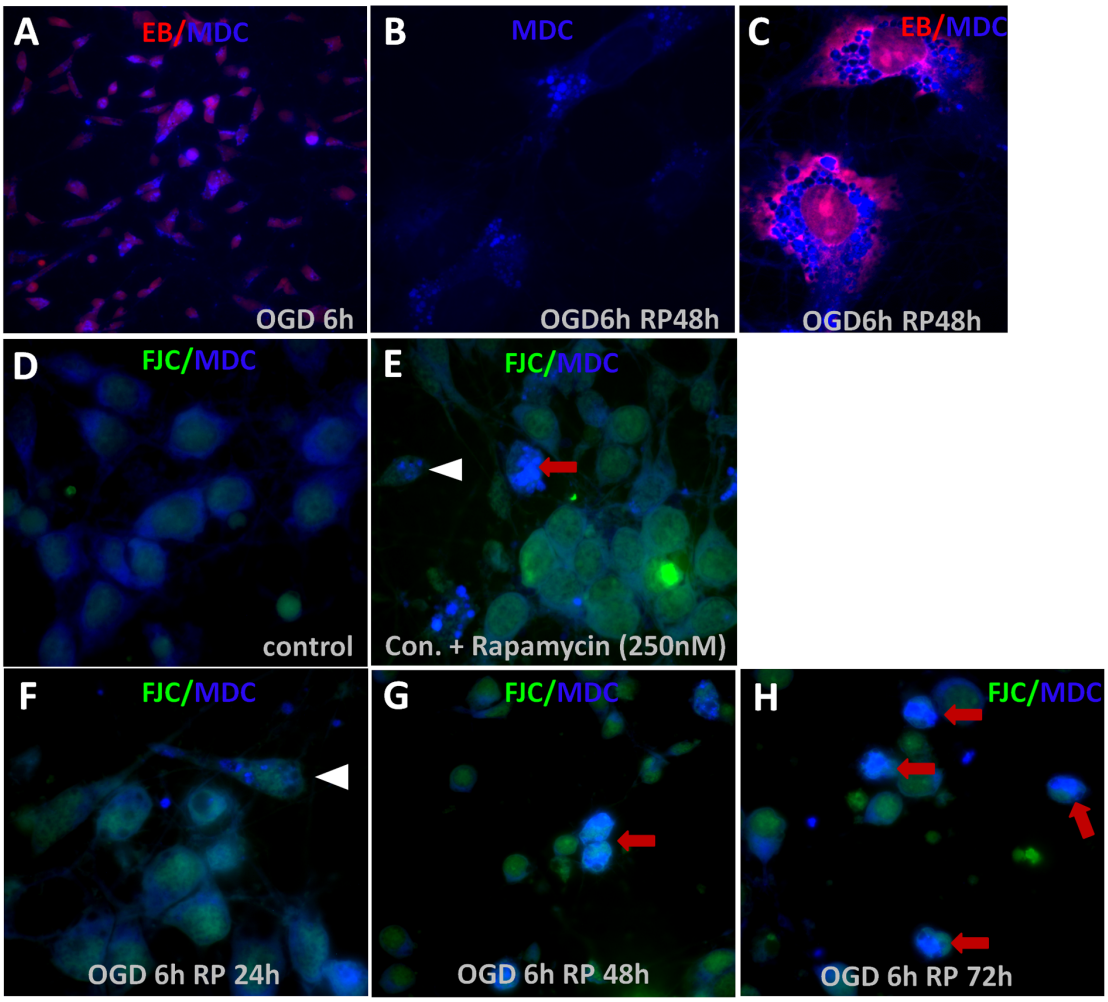
A
EB/MDC
OGD 6h
B
MDC
OGD6h RP48h
C
EB/MDC
OGD6h RP48h
D
FJC/MDC
control
E
FJC/MDC
Con. + Rapamycin (250nM)
F
FJC/MDC
OGD 6h RP 24h
G
FJC/MDC
OGD 6h RP 48h
H
FJC/MDC
OGD 6h RP 72h

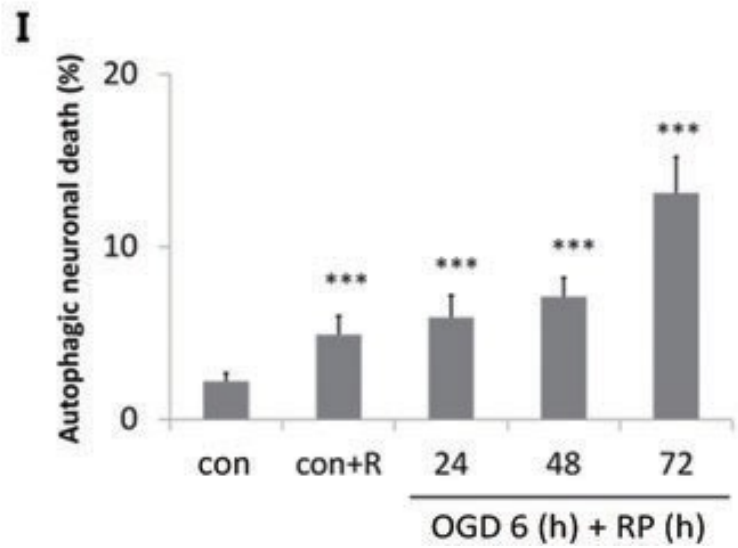
I
Autophagic neuronal death (%)
20
10
0
***
***
***
***
con
con+R
24
48
72
OGD 6 (h) + RP (h)

Fig 4.3 OGD/RP induces autophagic cell death in rat cortical neurons. Autophagic vacuoles (AVs) labeled by MDC appeared as distinct blue dot-like structures distributed in the cytoplasm. Pictures were taken under 60× (A) and 100× magnification (B-C), when nuclei were stained by EB. MDC and Fluoro-Jade C double staining was used to identify and quantify the autophagic neurons (white arrowheads) and autophagic neuron death (red arrows) under 40× magnification, D-H were representative pictures showing the different morphology under 100× magnification. Quantification of autophagic neuronal death rate (I) in cortical neurons after 6 h OGD followed by RP 24, 48, or 72 h, respectively. ∗ $p < 0.05$, ∗∗ $p < 0.01$, ∗∗∗ $p < 0.001$ versus control without OGD/RP.

4.3 OGD/RP Injury Increases Autophagy Marker Protein Levels in Cortical Neurons and SH-SY5Y Cells

As in Figure 4.4A, we proved that ammonium chloride (NH4Cl) prevented the degradation of LC3 in autophagosomes and that the accumulated amount of LC3-II increased after 6 h of OGD in rat cortical neurons compared to the control (Figure 4.4A). We determined that the optimal working concentration for NH4Cl was 20 and 30 mM on cortical neurons and SH-SY5Y cell line, respectively (data not shown). We used rapamycin, a specific autophagy inducer, in our positive control group (Figure 4.4B). The ratio of LC3-II to LC3-I was increased dramatically from 0.79 to 1.19 by rapamycin in a dose-dependent fashion (Figure 4.4C). Later, we consistently used 250 and 500 nM rapamycin as the optimal working concentrations on cortical neurons and SH-SY5Y cells, respectively.

Upon OGD/RP injury, BECN1 levels in the cortical neurons and SY5Y cells were up regulated. Changes of BECN1 levels in both cells occurred after 6 h OGD, and the expression kept increasing for at least 3 days posttreatment (Figure 4.4E and G). When cytosolic LC3-I conjugates to phosphatidyl-ethanolamine and forms LC3-II, its molecular weight will be changed from 18 to 16 kD. As shown in Figure 4.4, a dramatic increase in the ratio of LC3-II/LC3-I was observed in neurons as well as in SH-SY5Y cells after OGD/RP injury (Figure 4.4D and F). The time course and levels of BECN1 expression correlated with the increase of LC3-II to LC3-I ratios, and the time course of LC3-II to LC3-I ratios increase corresponded to the increased autophagic neuronal death rate (Figure 4.3I).

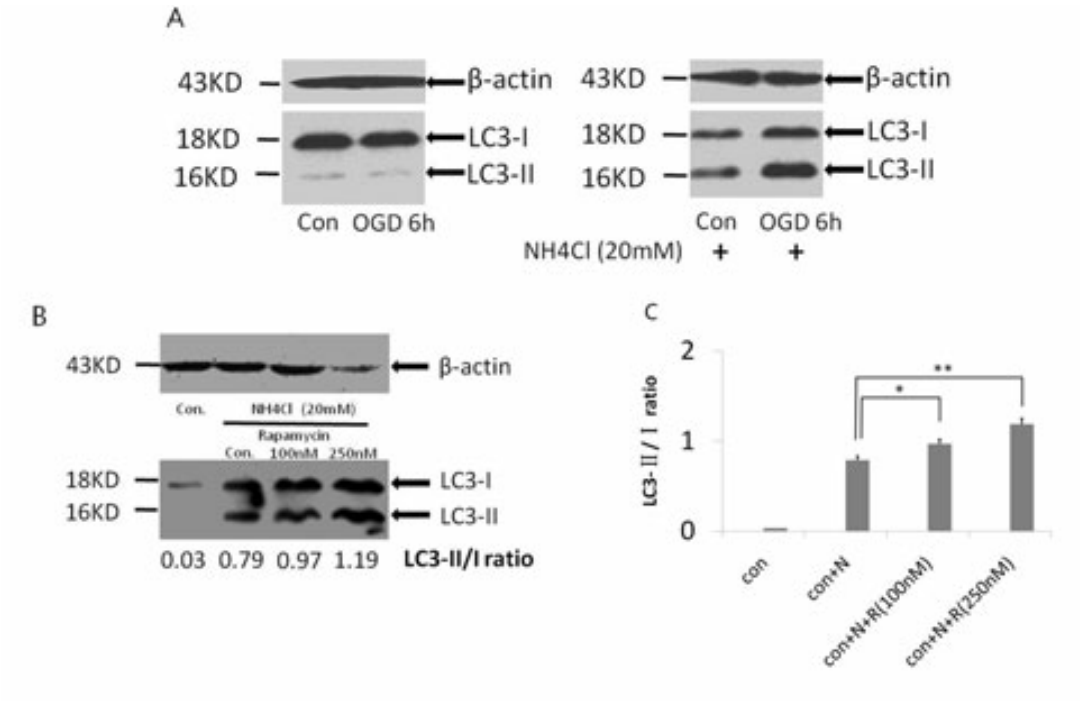

Fig 4.4 OGD/RP upregulates Beclin-1 expression and induces LC3 conversion in cortical neurons and SH-SY5Y cells. Neurons received 6 h of OGD: (A) Effects of NH_4Cl (20 mM) on accumulation of LC3-II on cortical neurons; (B) Effects of autophagy inducer rapamycin on cortical neurons; (C) Statistical analysis of (B). Cells were deprived of oxygen and glucose for 6 h and then treated with RP for different length of time. LC3 and Beclin-1 were detected by Western blot: β-actin (43 kD) was included as loading control; (D-E) Representative bands of cortical neurons; (F-G) Representative bands of SH-SY5Y cells. The ratios of LC3-II to LC3-I were calculated by Quantity One software. N = 3 for each group. ∗ $p < 0.05$, ∗∗ $p < 0.01$, ∗∗∗ $p < 0.001$ versus control group.

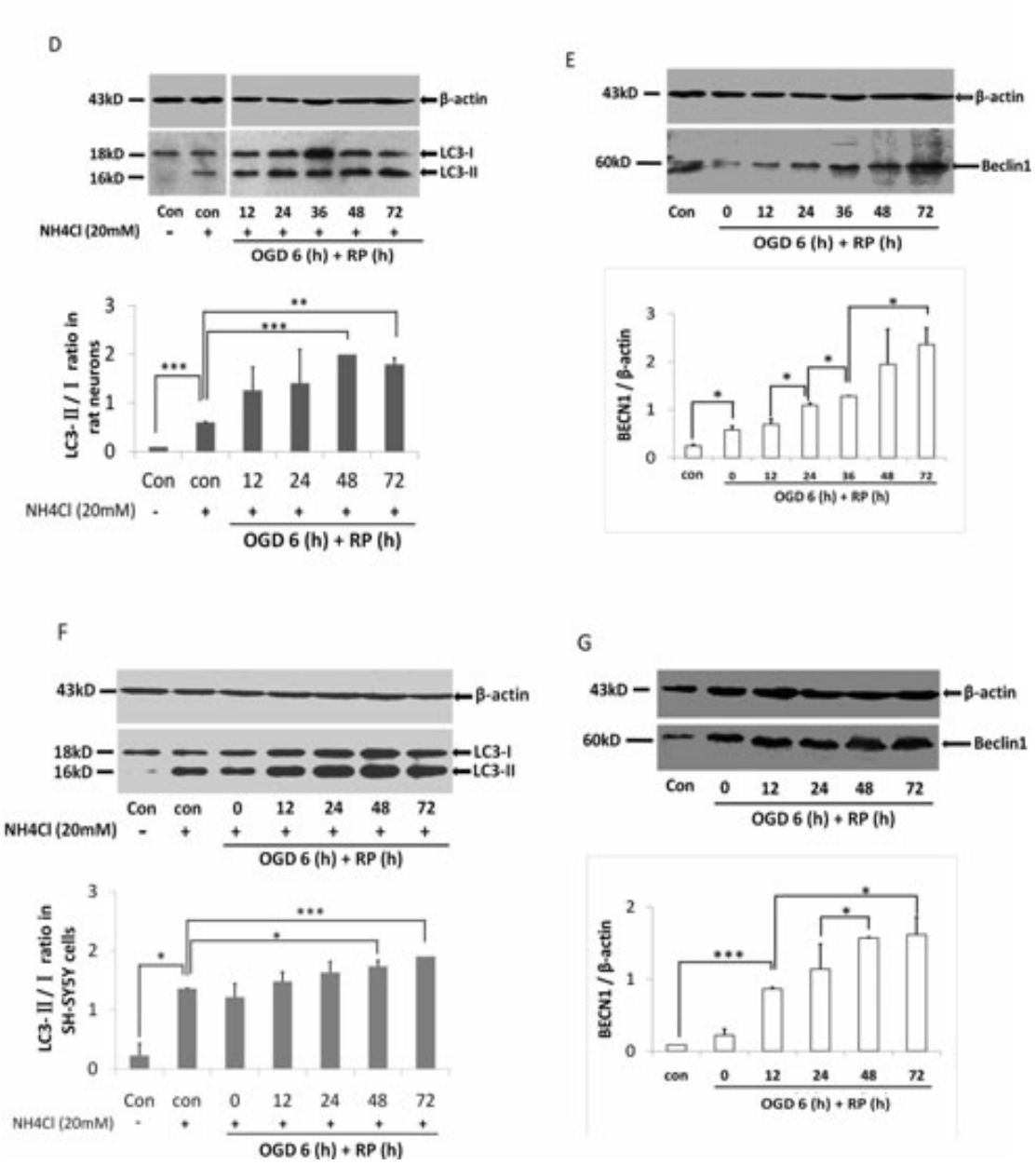
D
43kD
β-actin
18kD
16kD
LC3-I
LC3-II
Con con 12 24 36 48 72
NH4Cl (20mM) - + + + + + +
OGD 6 (h) + RP (h)
LC3- II / I ratio in rat neurons
Con con 12 24 48 72
NH4Cl (20mM) - + + + + + +
OGD 6 (h) + RP (h)
E
43kD
β-actin
60kD
Beclin1
Con 0 12 24 36 48 72
OGD 6 (h) + RP (h)
BECN1 / β-actin
con 0 12 24 36 48 72
OGD 6 (h) + RP (h)
F
43kD
β-actin
18kD
16kD
LC3-I
LC3-II
Con con 0 12 24 48 72
NH4Cl (20mM) - + + + + + +
OGD 6 (h) + RP (h)
LC3- II / I ratio in SH-SY5Y cells
Con con 0 12 24 48 72
NH4Cl (20mM) - + + + + + +
OGD 6 (h) + RP (h)
G
43kD
β-actin
60kD
Beclin1
Con 0 12 24 48 72
OGD 6 (h) + RP (h)
BECN1 / β-actin
con 0 12 24 48 72
OGD 6 (h) + RP (h)

4.4 Autophagy Inhibitor 3-MA Reduces OGD/RP-Induced Neuronal Death

To determine the role of autophagy in OGD/RP-induced neuronal injury, rat cortical neurons were treated with the autophagy inhibitors 3-MA during OGD and RP. 3-MA (PI3K inhibitor) inhibits the formation of autophagosome, thus acts as a specific inhibitor of autophagic/lysosomal protein degradation.[428] It has been useful in defining the role of autophagy under various physiological conditions, such as cerebral ischemia.[193, 429] 3-MA at the concentration of 1 mM effectively blocked the activation of autophagy as evidenced by inhibiting the production of LC3-II (Figure 4.5A and B). We also used LDH assay to quantify the effects of 3-MA on OGD-induced neuronal death. The results showed that LDH leakage was markedly increased in cortical neurons after 6 h of OGD that was followed by prolonged RP. 3-MA treatment resulted in a small but significantly decrease in the leakage of LDH in a time-dependent fashion (Figure 4.5C). Interestingly, before 24 h RP, the 3-MA treatment groups showed a higher neuronal death rate compared to the control. However, when the RP time was extended to 48 and 72 h, 3-MA demonstrated a greater protective effect on the OGD-challenged neurons. This result is most possibly because of the "role-switch" effect of autophagy during this process (see Chapter 6 "Discussion").

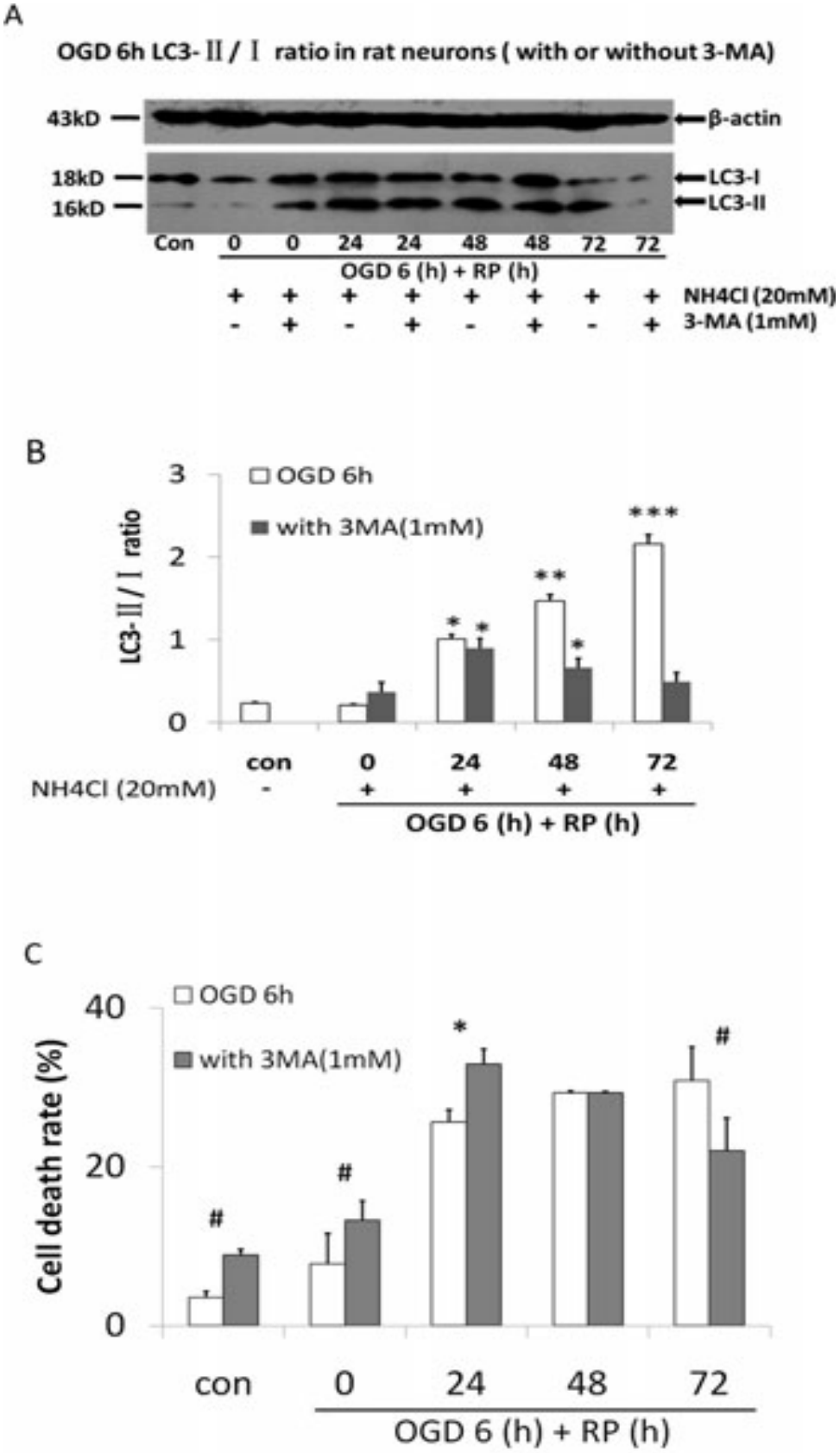
A
OGD 6h LC3- Ⅱ / Ⅰ ratio in rat neurons (with or without 3-MA)
43kD
β-actin
18kD
16kD
LC3-I
LC3-II
Con 0 0 24 24 48 48 72 72
OGD 6 (h) + RP (h)
+ + + + + + + + NH4Cl (20mM)
- + - + - + - + 3-MA (1mM)
B
LC3- Ⅱ / Ⅰ ratio
OGD 6h
with 3MA(1mM)
3
2
1
0
*** ** * * *
con 0 24 48 72
NH4Cl (20mM) - + + + +
OGD 6 (h) + RP (h)
C
Cell death rate (%)
OGD 6h
with 3MA(1mM)
40
20
0
*
con 0 24 48 72
OGD 6 (h) + RP (h)

Fig 4.5 Autophagy inhibitor 3-MA reduces OGD/RP induced-neuronal death. 3-MA (1 mM) was added into EBSS solution before OGD treatment on cortical neurons. After 6 h OGD, fresh regular culture medium with 1 mM 3-MA was used when neurons underwent prolonged RP (24, 48, or 72 h). (A) LC3 was detected by western blot. β-actin (43 kD) was included as loading control. (B) The ratios of LC3-II to LC3-I were calculated by Quantity One software. (C) Time course of cell death rate in OGD/RP-challenged neurons with or without presence of 1 mM 3-MA, by using LDH assay. N = 3 for each group. ∗ $p < 0.05$, ∗∗ $p < 0.01$, ∗∗∗ $p < 0.001$ versus control group without OGD/RP; **# P < 0.001 versus OGD/RP treatment group without 3-MA.**

4.5 Activation of Autophagy in Ischemic Brains

We challenged neonatal day 7 rats by focal cerebral ischemia and followed by whole brain hypoxia, then detected elevations of BECN1 levels at different time points postischemia in the cortex. We found the alterations in BECN1 levels in the cortex lasted for several days and peaked at 7 days postischemia. BECN1 immunoreactivity in the ipsilateral ischemic hemisphere was significantly enhanced than in the contralateral part (Figure 4.6A-D). We also probed brain sections with LC3 antibody that detects both forms of LC3. Whereas only diffused LC3 distribution was observed in contralateral side (Figure 4.6E-G), strong LC3 punctate staining was observed in ipsilateral part after RP 7 days (Figure 4.6H-J). Western blot analysis showed that BECN1 levels were increased in a time-dependent fashion according to the RP time in the ipsilateral ischemic hemisphere, whereas there is no change in

BECN1 levels between the contralateral parts (Figure 4.6K). In addition, we performed immunoblot analyses and densitometry of LC3 in whole brain extracts. With the used antibody, we detected only one band and not an obvious change in the density on the ipsilateral sides of ischemic brains (Figure 4.6K).

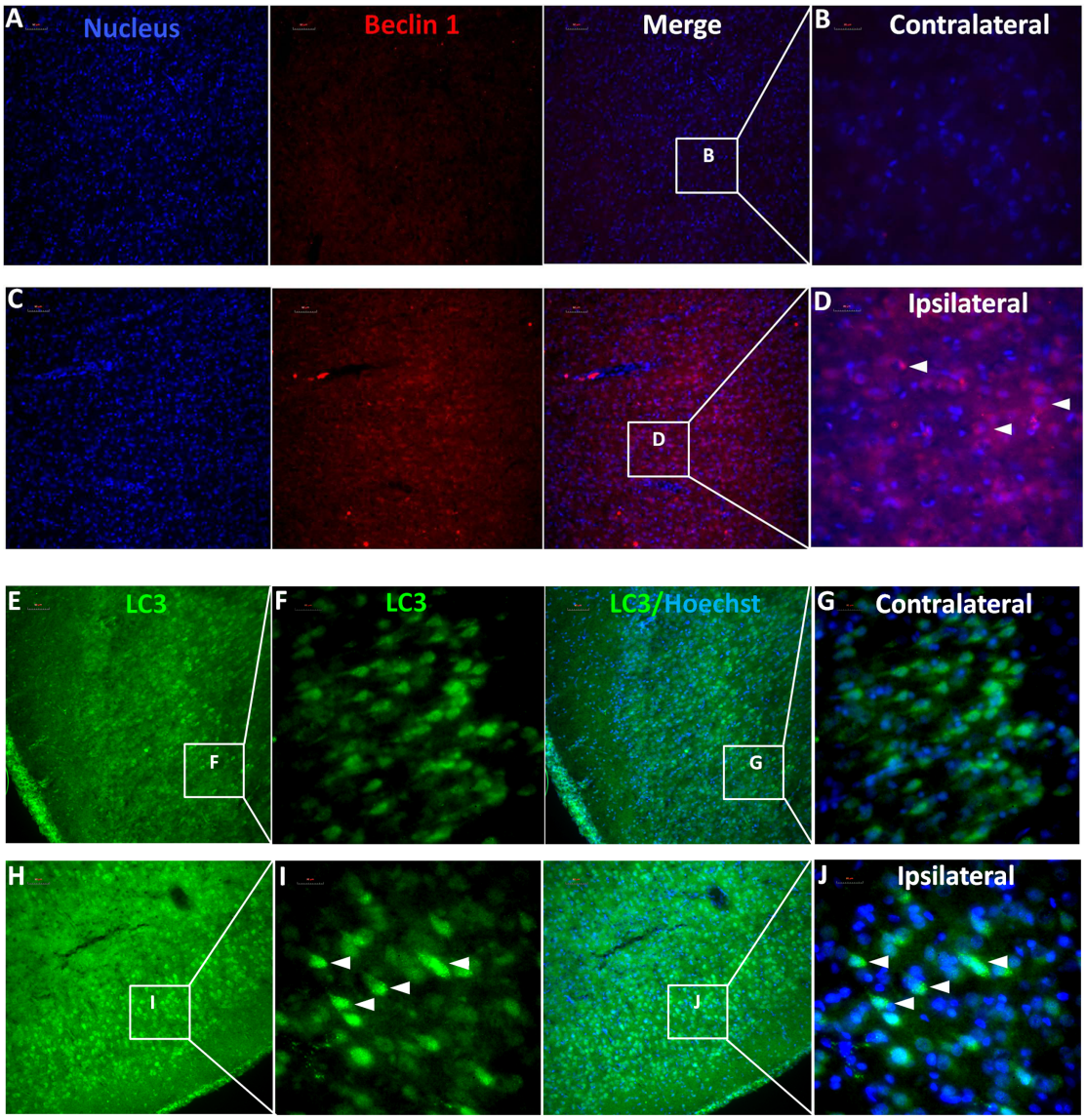

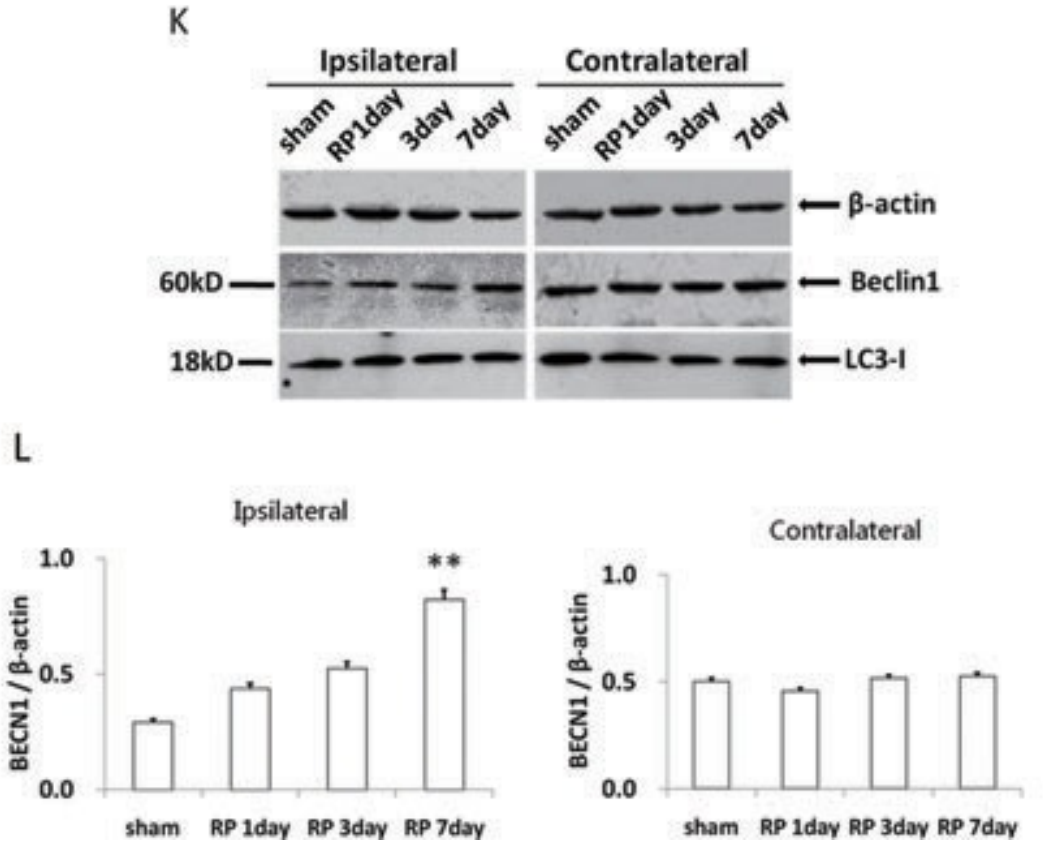

Fig 4.6 Autophagy was activated in brain tissue after neonatal hypoxia/ischemia. Beclin-1 immunoreactivity in brain sections seven days postischemia on the ischemic side (C and D) and on the contralateral side (A and B). LC3 immunoreactivity in brain sections 7 days postischemia on the ischemic side (H–J) and on the contralateral side (E-G). A, C, E, and H were taken under 20× magnification (Scale bars = 50 μm) whereas B, D, F, G, I, and J were taken under 60× magnification (Scale bars = 20 μm). Western blot analysis showed that Beclin-1 levels were increased in the ipsilateral ischemic hemisphere according to the RP time, whereas there was no change in the contralateral parts (K). N = 3 for each group. ∗ $p < 0.05$, ∗∗ $p < 0.01$, ∗∗∗ $p < 0.001$ versus sham operation group (L).

4.6 BNIP3 Competently Interacted with Bcl-2, Released BECN1 to Induce the Excessive Autophagy in Neuronal I/H Injury

In order to verify the possible molecular mechanism of BNIP3's induction of excessive autophagy, we used co-immunoprecipitation assay to detect protein-to-protein interaction. Primary rat cortical neurons were treated with OGD for 6 h followed by 24 h, 48 h, and 72 h reperfusion. Control groups proved the specificity and efficiency of each primary antibodies used in the co-ip assays. We demonstrated that the primary antibodies of monoclonal anti-BNIP3, monoclonal anti-BECN1 and monoclonal anti-BCL-2 worked well by pulling down their according antigens specifically and efficiently in the *in vitro* stroke model. Direct interaction between BNIP3 and BECN1 was not detectable in OGD/RP-treated SH-SY5Y cells as shown in Figure 4.7A. However, direct interactions between BECN1 and Bcl-2, as well as BNIP3 and Bcl-2 was confirmed by co-ip in OGD/RP-challenged rat cortical neurons, indicating that both BECN1 and BNIP3 can directly combine to Bcl-2 to exert their regulatory functions (Figure 4.7B-C). Clear bands of BECN1 were detected by using Bcl-2 as the bait protein to pull down BECN1, while clear bands of Bcl-2 were also observed by using BECN1 as the bait protein to pull down Bcl-2 (Figure 4.7B). Particularly, we found an enhanced ineraction between Bcl-2 and induced BNIP3 after OGD/RP injury, as demonstrated by the increased Bcl-2/BNIP3 complex as shown in Figure 4.7C. These enhanced interactions between BNIP3 with Bcl-2 may subsequently lead to the release of BECN1 from the previously stable Bcl-2/BECN1 complex, cause an elevated level of free BECN1 inside the cytosol, and eventually trigger the overactivation of autophagy machinary. Thus, we concluded that BNIP3 competently interacted with Bcl-2, released BECN1 to induce the excessive autophagy in neuronal I/H injury.

A

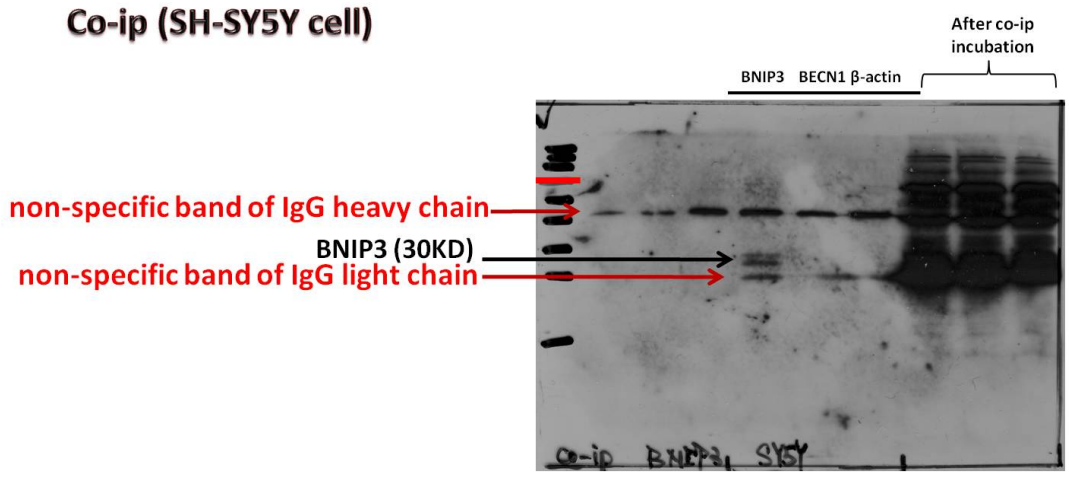

⇒ No direct interaction between BNIP3 and Beclin-1.

B

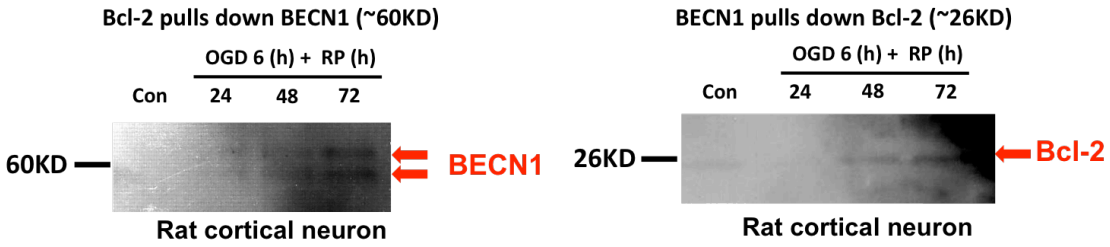

⇒ There are direct interactions between BECN1 and Bcl-2 & OGD/RP injury increases BECN1/Bcl-2 complex

C

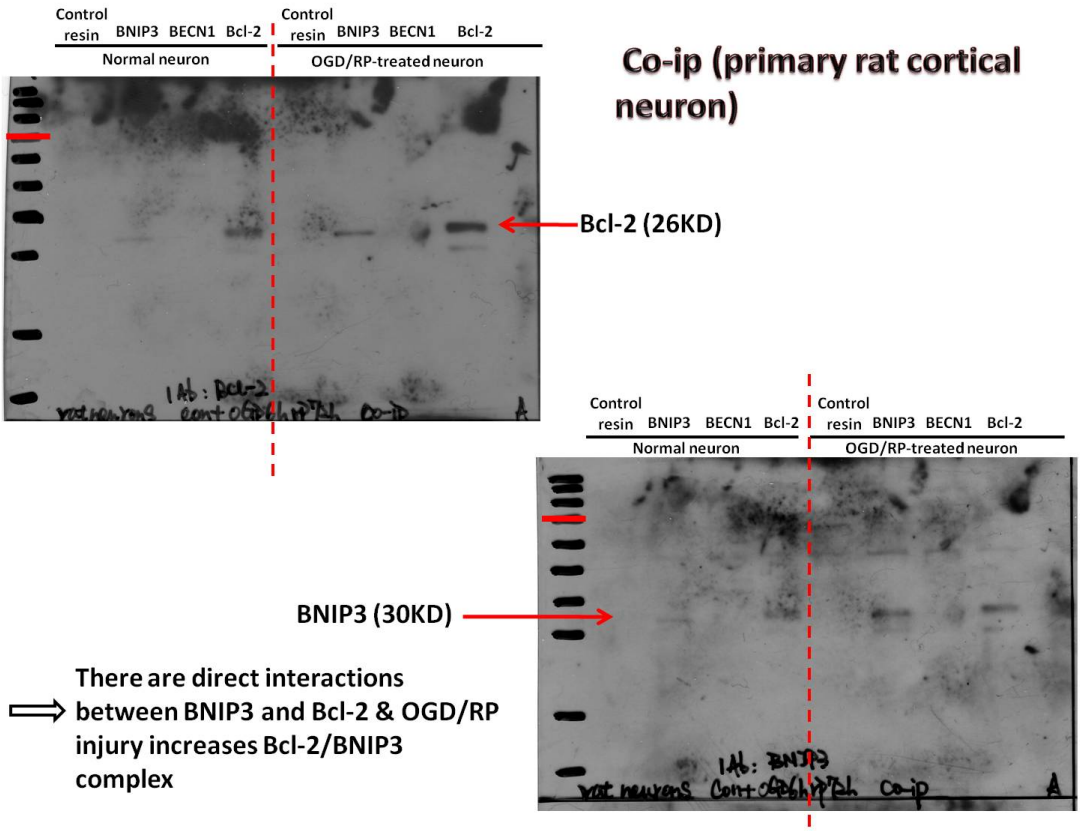

Fig 4.7 BNIP3 interacted with Bcl-2 directly to induce the excessive autophagy in OGD/RP-challenged rat cortical neuron. No direct interaction between BNIP3 and BECN1 in OGD/RP-treated SH-SY5Y cells (A). Direct interactions between BECN1 and Bcl-2, BNIP3 and Bcl-2 were detected in OGD/RP-challenged rat cortical neuron. (B-C) An enhanced interaction between Bcl-2 and induced BNIP3 was detected after the OGD/RP injury, which may induce the excessive autophagy subsequently (C). Control groups were without OGD/RP treatment. N = 3 for each group.

Chapter 5. Results (Specific Objective #2)

Conclusion: BNIP3 interacting with LC3 triggers excessive mitophagy in the delayed neuronal death in neonatal stroke

5.1 BNIP3 Gene Silencing was Neuroprotective in Neonatal Brain I/H

BNIP3 WT and KO mice pups were subjected to neonatal stroke modeling on postnatal day 7. After 1, 3, 7 and 28 days' recovery, whole brains were dissected into 5 equal-thickness slices then stained and analyzed by the TTC staining, as shown in the representative pictures (Figure 5.1A). The total infarct volumes of WT brains increased from 0 in sham-operated group to 9.45%, 29.74%, 30.73%, and 21.47% after recovery for 1, 3, 7, and 28 days, respectively; while the total infarct volumes of KO brains increased from 0 in sham-operated group to 38.16%, 22.64%, 4.72%, and 2.56% after recovery for 1, 3, 7, and 28 days, respectively (Figure 5.1B). The total infarct volume of ischemic brain significantly increased and peaked after 1 day's recovery, and then dramatically reduced after 7 and 28 days' recovery in the KO mice, indicating that BNIP3 gene silence promoted neuroprotection after brain I/H. Meanwhile, BNIP3 wild type (WT) and knockout (KO) primary cortical neurons were treated by OGD/reperfusion injuries. Light microscopy images showed observable neuronal damage in the WT group, as indicated by the shrinkage and detachment of a large amount of neurons. In contrast, the majority of the KO neurons showed normal morphology with intact attachment to the plate and fully expansion of dendrites and axons, when compared to the control group (Figure 5.1C). Neuronal death rates in OGD/RP-challenged BNIP3 WT and KO neurons were quantified by LDH assays. The cell death rates of WT neurons increased from 6.4% in control group to 28.75%,

68.71%, and 62.53% after RP for 24 h, 48 h and 72 h, respectively; while the cell death rates of KO neurons increased from 5.34% in control group to 27.26%, 55.56%, and 45.39% after RP for 24 h, 48 h and 72 h, respectively (Figure 5.1D). KO neurons showed significantly lower cell death rates after 48 and 72 h reperfusion, indicating the neuroprotection of BNIP3 gene silence in prolonged neuronal I/H. Taken together, results from both *in vitro* and *in vivo* stroke models demonstrated that BNIP3 gene silence was neuroprotective in brain I/H.

To confirm the validity and reliability of our MCAO model, we firstly conducted a series of pilot trails. A progressively increased brain infarction was detected when different RP times were carried out on WT mice treated by 1 h MCA occlusion (Figure 1.2). Later, 2-3 month old BNIP3 WT and KO mice were subjected to 1 h MCA occlusion followed by 48 h recovery specifically. We observed that before the 48 h endpoint, the BNIP3 WT mice displayed a distinctive low mobility, and a crouching gesture with hunching backs all the time (Figure 5.1Eb). Frequently, a degenerated/necrotic appearance of the right eye can be found in these mice, indicating a severe ischemic damage of the ipsilateral hemisphere. On the contrary, the BNIP3 KO mice showed much healthier behaviour post-injury. They moved around freely, and were not suffering from a great pain as the WT mice were (Figure 5.1Eb). Quantification of the brain infarct volume of WT and KO mice after MCAO modeling was also carried out. After 48 h recovery, whole brains were dissected and analyzed by TTC staining (Figure 5.1Ea). The total infarct volume of WT brain increased from 0 in sham-operated group to 35.84% after 2-day recovery, while the total infarct volume of KO brain increased from 0 in sham-operated group to 17.78% after 2-day recovery. The total infarct volume of ischemic brain reduced as much as 18% in KO mice after 48 h recovery (Figure 5.1Ec). Furthermore, direct visualization

of brain damages in the neonatal stroke model showed quite similar results, as shown in Figure 5.1Ed. Thus, we concluded that BNIP3 gene silencing effectively attenuated the brain damage in both neonatal and adult cerebral ischemia.

A

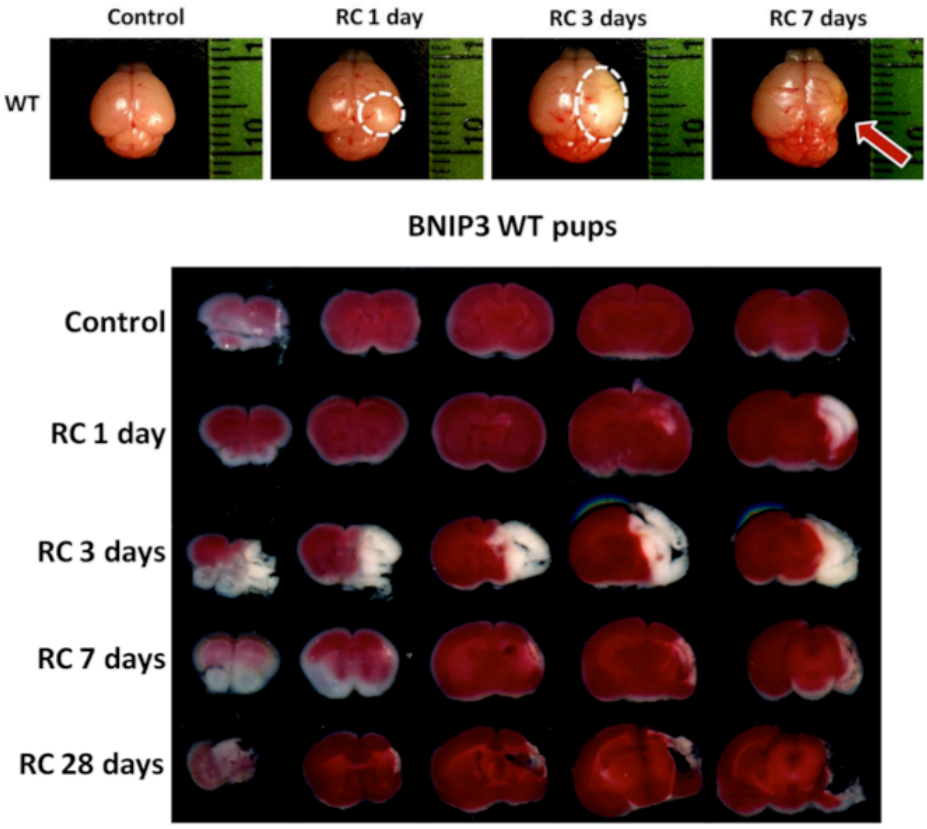

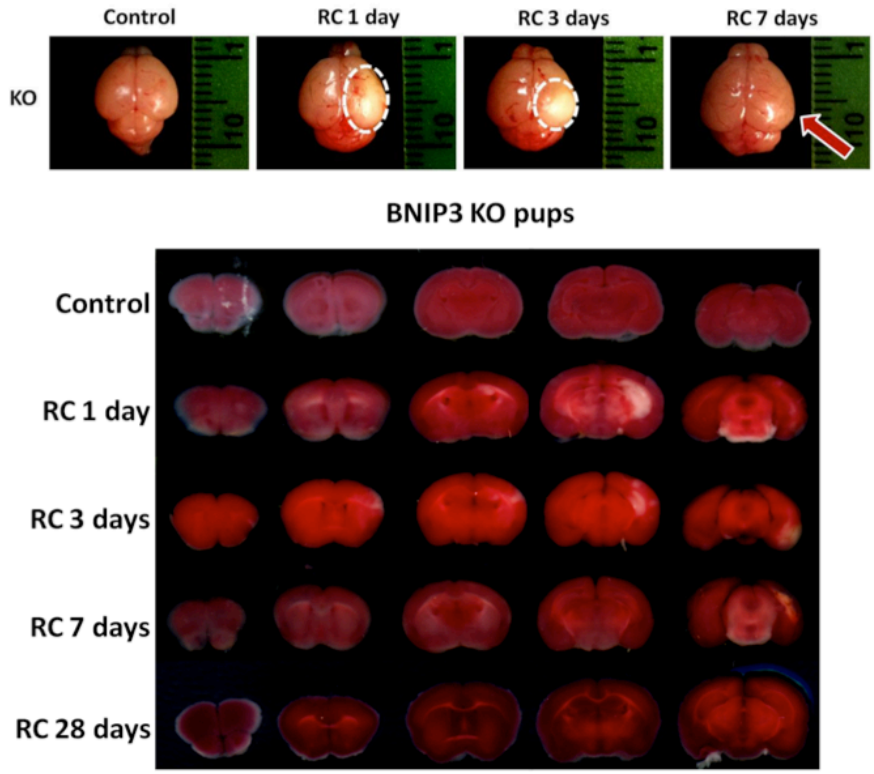
Control
RC 1 day
RC 3 days
RC 7 days
KO
BNIP3 KO pups
Control
RC 1 day
RC 3 days
RC 7 days
RC 28 days

B

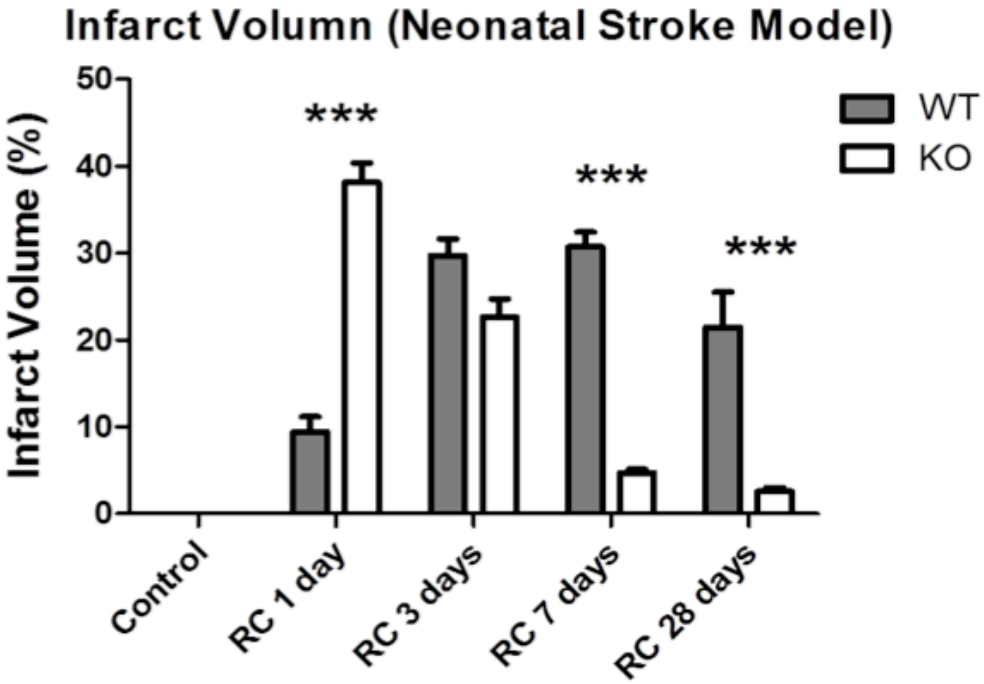
Infarct Volumn (Neonatal Stroke Model)
Infarct Volume (%)
50
40
30
20
10
0
***
***
***
WT
KO
Control
RC 1 day
RC 3 days
RC 7 days
RC 28 days

C

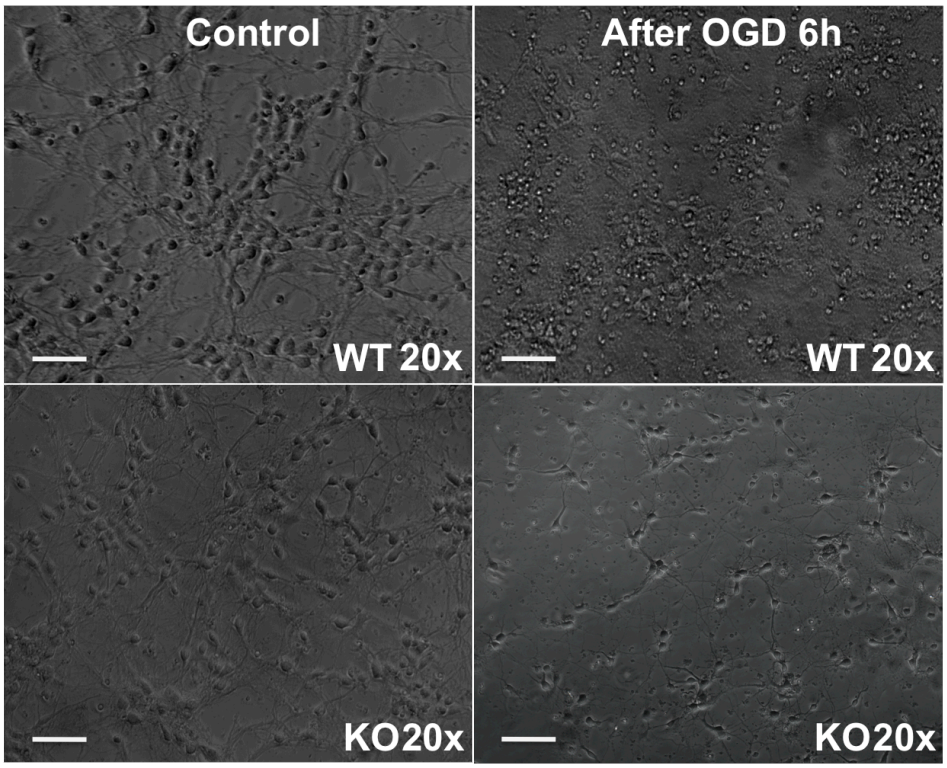
Control
After OGD 6h
WT 20x
WT 20x
KO20x
KO20x

D

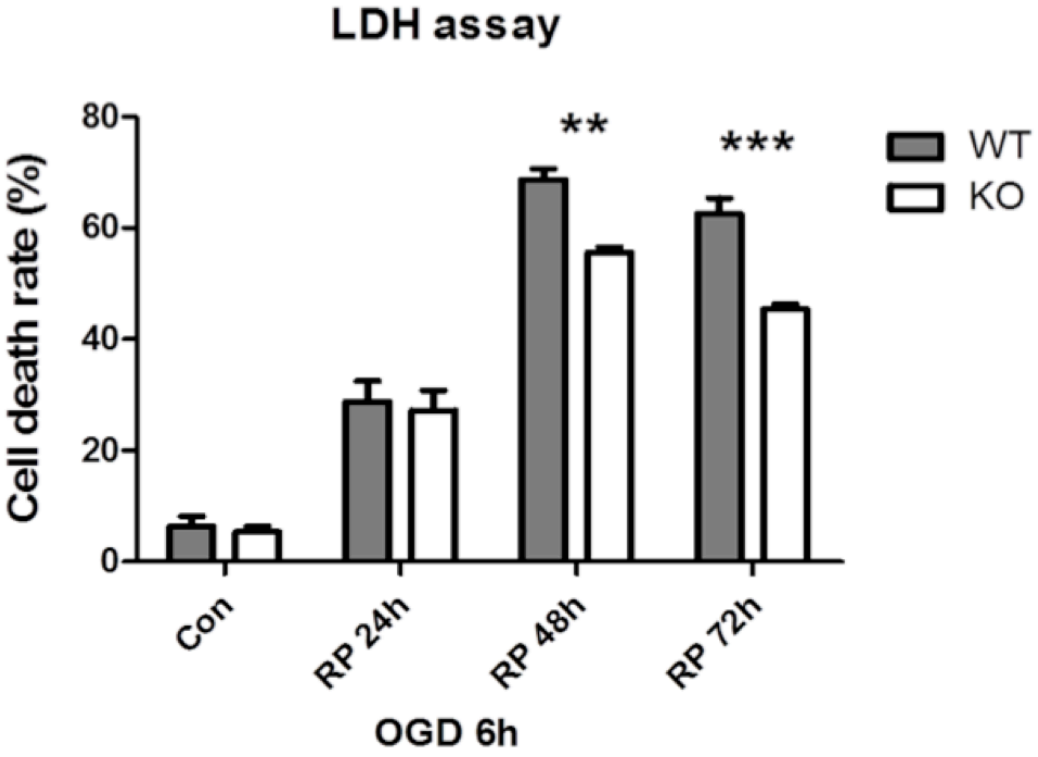
LDH assay
Cell death rate (%)
80
60
40
20
0
**
***
WT
KO
Con
RP 24h
RP 48h
RP 72h
OGD 6h

E

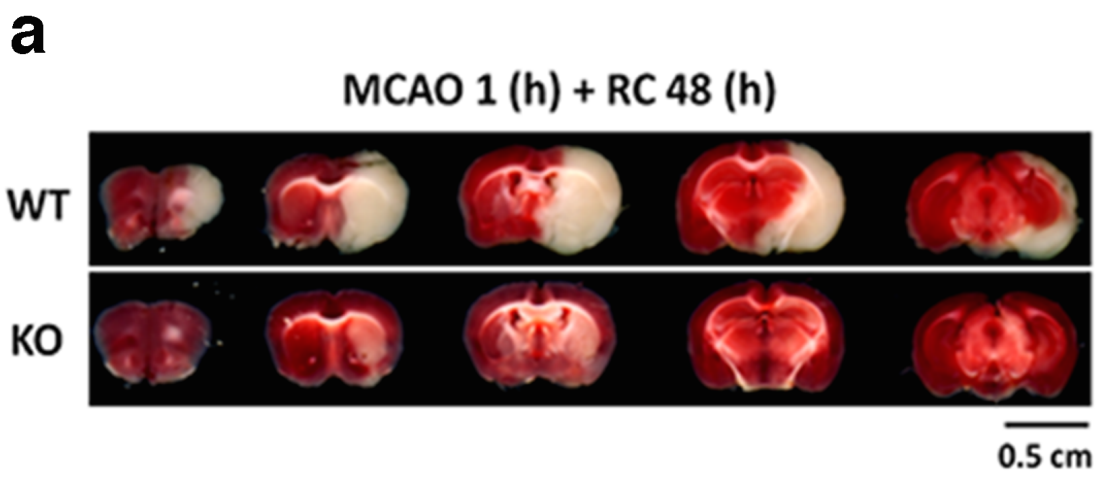
a
MCAO 1 (h) + RC 48 (h)
WT
KO
0.5 cm

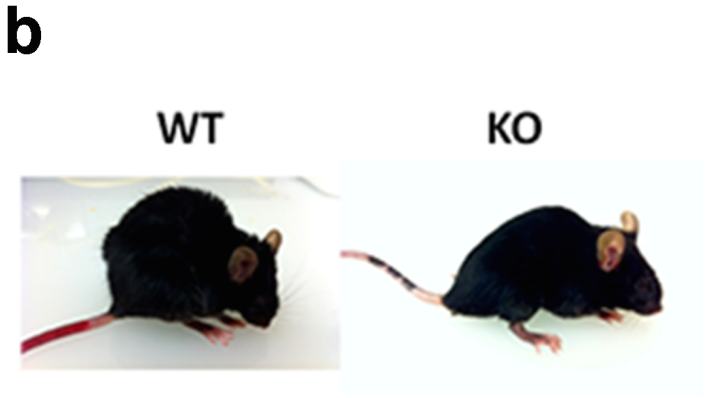
b
WT
KO

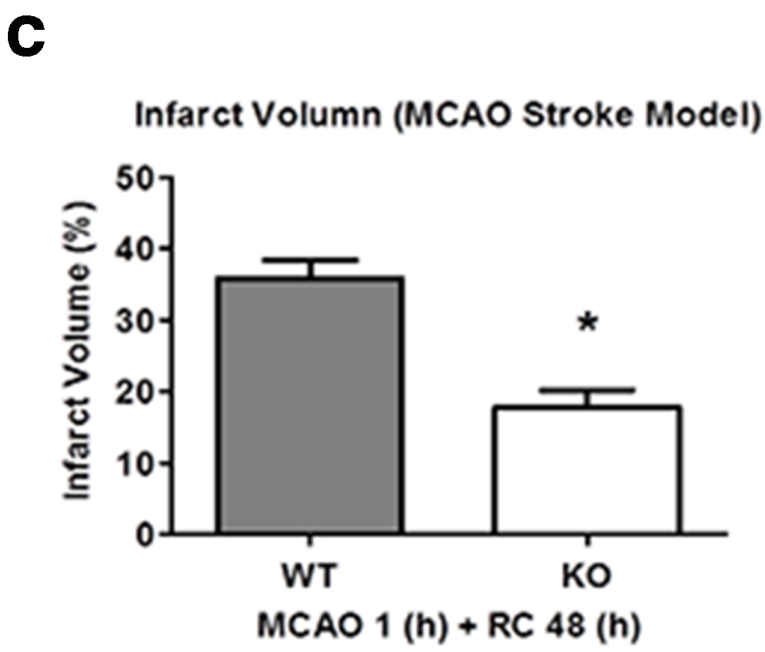
c
Infarct Volumn (MCAO Stroke Model)
Infarct Volume (%)
50
40
30
20
10
0
*
WT
KO
MCAO 1 (h) + RC 48 (h)

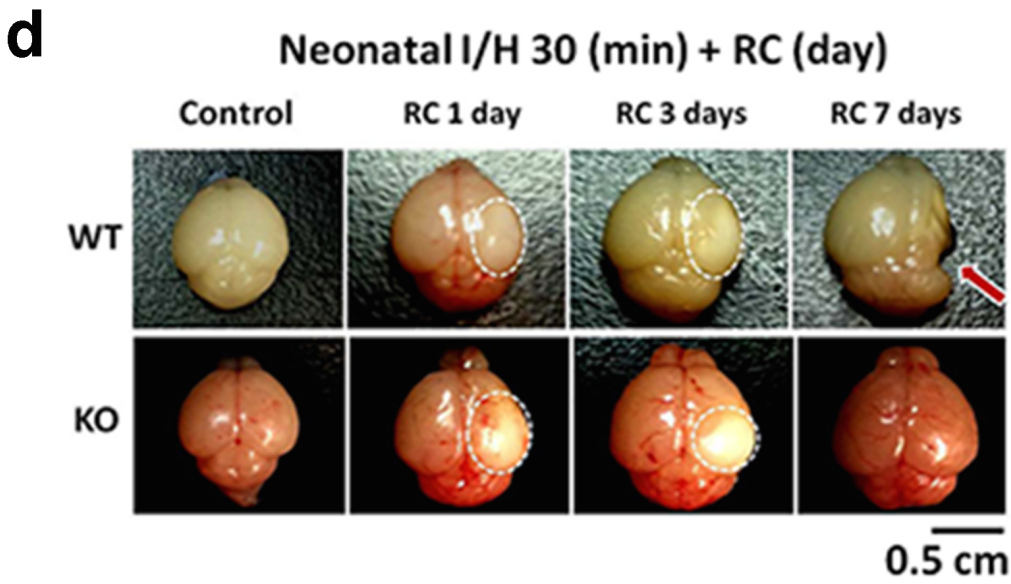

Fig 5.1 BNIP3 gene silence had neuroprotective effects in stroke models. (A-B) Measurement of the brain infarct volume on BNIP3 WT and KO mice pups in the neonatal I/H model. Two-way ANOVA analysis and Bonferroni post-tests were used to compare the total brain infarct volumes between the WT and KO groups: WT vs KO on each time point, * $p < 0.05$, ** $p < 0.01$, *** $p < 0.001$. Control groups were sham-operated and without a hypoxic treatment. N = 3-6 for each group. (C) Representative images of neuronal morphology and viability in BNIP3 WT and KO cortical neurons in the OGD/RP model. OGD 6 h with no RP treatment was induced or not. **Scale bars = 80 µm. Images were taken at 20× objective.** (D) Time course of cell death rates in OGD/RP-challenged BNIP3 WT and KO neurons, by using LDH assay. Two-way ANOVA analysis and Bonferroni post-tests were used to compare the cell death rates between the WT and KO groups: WT vs KO on each time point, *$p < 0.05$, ** $p < 0.01$, *** $p <0.001$. N = 3 for each group. (E) Measurement of the brain infarct volume on BNIP3 WT and KO adult mice in the MCAO model. (a) 2-3

month old BNIP3 WT and KO mice were treated by 1h MCA occlusion followed by 48 h recovery. Whole brains were dissected into 5 equal-thickness slices then stained and analyzed by the TTC staining. (b) Representative pictures showed the different behaviour of animals before the endpoint. (c) Infarction area of each brain slice was measured by Quantity One software, and total brain infarct volumes were calculated by GraphPad Prism 5 software. N = 3 for each group. Two-way ANOVA analysis and Bonferroni post-tests were used to compare the total brain infarct volumes between the WT and KO group: WT vs KO, * $p < 0.05$, ** $p < 0.01$, *** $p < 0.001$. (d) Representative images showed direct visualization of ischemic brain damages in neonatal stroke model. BNIP3 WT and KO mice pups were treated by unilateral common carotid artery ligation followed by 30 min hypoxia (with 8% oxygen) on postnatal day 7. After 1, 3, and 7 days' recovery, whole brains were dissected out on ice, with pictures taken immediately to record the brain morphology. Control groups were sham-operated and without a hypoxic treatment. N = 3 for each group. **Scale bars = 0.5 cm** in (a and d).

5.2 BNIP3 Expression Increased Mitophagy in Brain I/H

Primary cortical neurons were treated with OGD for 6 h followed by reperfusion for 24 h, 48 h, or 72 h. Immunocytochemistry was used to demonstrate the co-localization of mitochondria with autophagosomes inside neurons, representing the mitophagy intensity. When neurons were treated by OGD, the autophagosomes labeled by LC3-II appeared as distinct punctate structures distributed in the cytoplasm, perinuclear regions, and cell processes. This focal staining of LC3-II was distinct from the even distribution of LC3-I in the control neurons without OGD/RP. A reduced co-localization (yellow) of mitochondria (red) with autophagosomes (green) was detected in the BNIP3 KO neurons, while the WT neurons showed a significantly higher co-localization rate especially after RP for 72 h (Figure 5.2A-C). In order to determine the extent of elimination of damaged mitochondria in WT and KO neurons, markers for mitochondrial outer membrane (TOMM22) and inner membrane (COXIV) were examined by Western blot. TOMM22, the mitochondrial import receptor subunit, is an integral membrane protein of the mitochondrial outer membrane [430, 431]; COXIV, the cytochrome c oxidase, is a large transmembrane protein complex that localizes to the mitochondrial inner membrane. [432] Both of these proteins are used extensively as specific mitochondrial markers. [433-436] We found that the basal expression levels of TOMM22 and COXIV were comparable in BNIP3 WT and KO neurons. As the expression levels of these markers are precisely correlated to mitochondrial content, [437-439] the results suggest that the amount of mitochondria is not affected by loss of the BNIP3 gene. However, TOMM22 and COXIV expression levels decreased dramatically at 48 h post-OGD/RP in BNIP3 WT neurons, implying an increased mitophagy response. Meanwhile, both marker proteins were well preserved in KO neurons at each time point, showing lower mitophagy

activity after OGD/RP injury when BNIP3 was silenced (Figure 5.2D). In addition, an induced mitophagy was confirmed ultrastructurally using electron microscopy in OGD/RP-challenged WT cortical neurons (Figure 5.2F). Control neurons showed normal appearance of cytoplasm, organelles, nucleus, and chromatin (Figure 5.2F. a and e). Abundant numbers of double-membrane structures and double-membrane autophagosomes, which surrounded parts of cytoplasm and organelles, frequently formed in neurons after OGD 6 h plus RP 72 h treatment (Figure 5.2F. b-d and f, k). Healthy mitochondria were found with normal size and intact morphology in control neurons (Figure 5.2F. e, g, and h), while impaired mitochondria demonstrated swelling and dilation following the OGD/RP injury (Figure 5.2F. f, i, j, and k). Meanwhile, lysosomes showed a darkened appearance, indicating the activation of lysosomes after RP 72 h (Figure 5.2F. f and k). Fusion of an autophagosome with a lysosome was observed (Figure 5.2F. k). A forming autolysosome, which encompassed a mitochondrion, was identified, demonstrating OGD/RP-induced activation of mitophagy (Figure 5.2F. k).

Levels of mitochondrial makers were also measured in the neonatal ischemic cortex. Before neonatal stroke, we found the basal level of mitochondria was slightly higher in BNIP3 KO cortex as compared to WT cortex; yet, no statistical significance was detected, indicating that basal levels of mitochondria were comparable in these two genotypes. The TOMM22 and COXIV expression levels decreased significantly at 3 or 7 days post-ischemia in BNIP3 WT brains, implying an enhanced mitochondrial elimination. In contrast, levels of both proteins were well preserved in the ischemic hemisphere of KO pups at each time point, showing lower mitophagic activity after I/H injury when BNIP3 was silenced (Figure 5.2E). These data showed that knockout of BNIP3 decreased mitochondrial elimination, or in other words,

BNIP3 expression increased mitophagy in neonatal brain I/H.

A

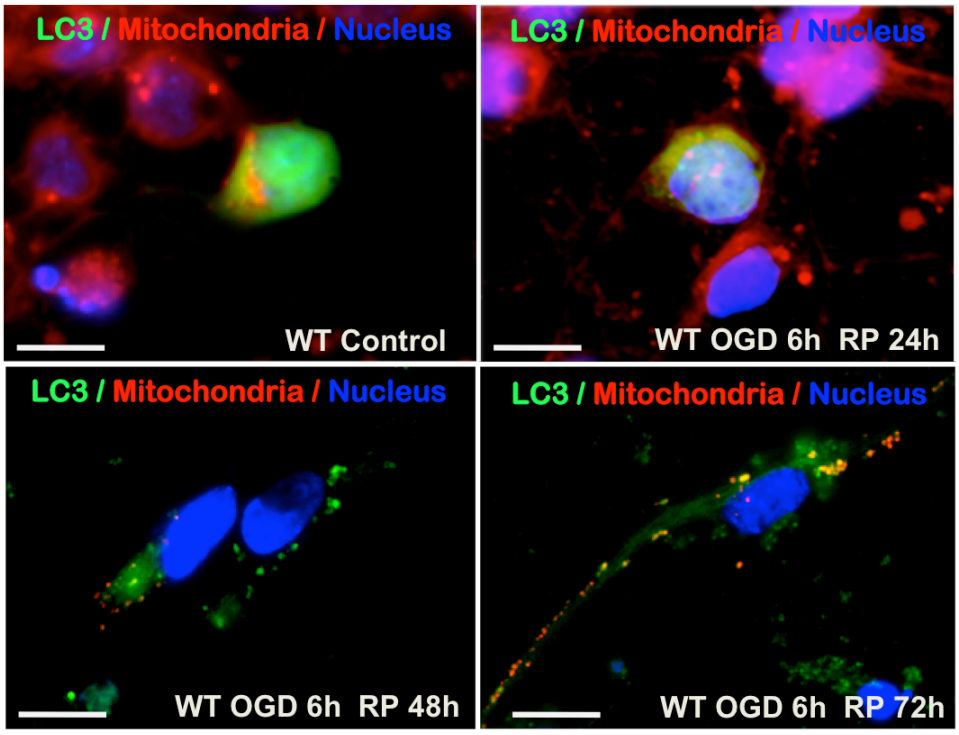

B

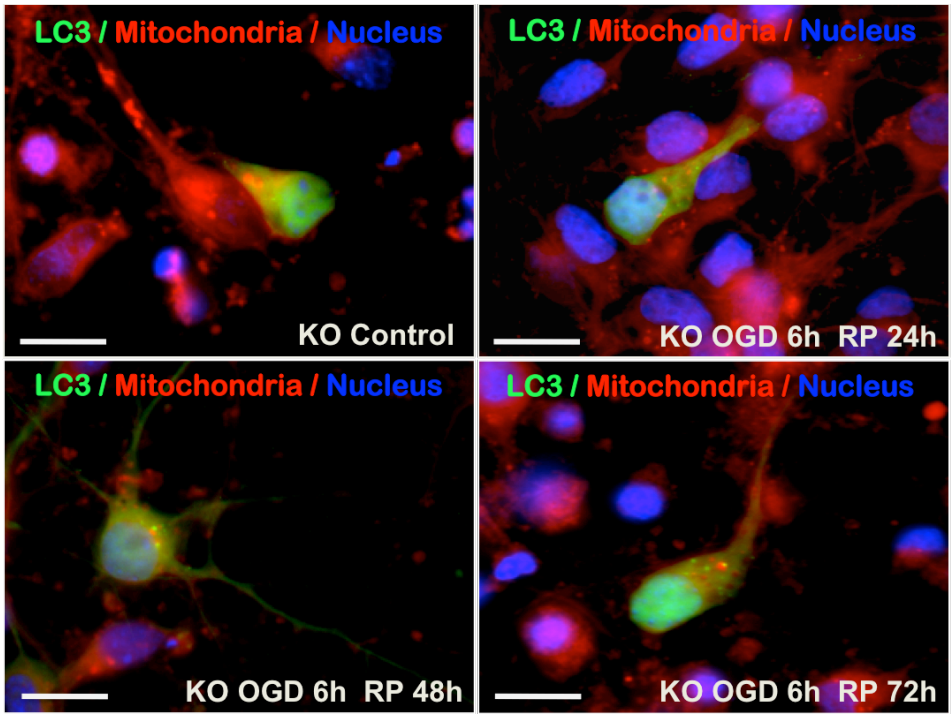

C

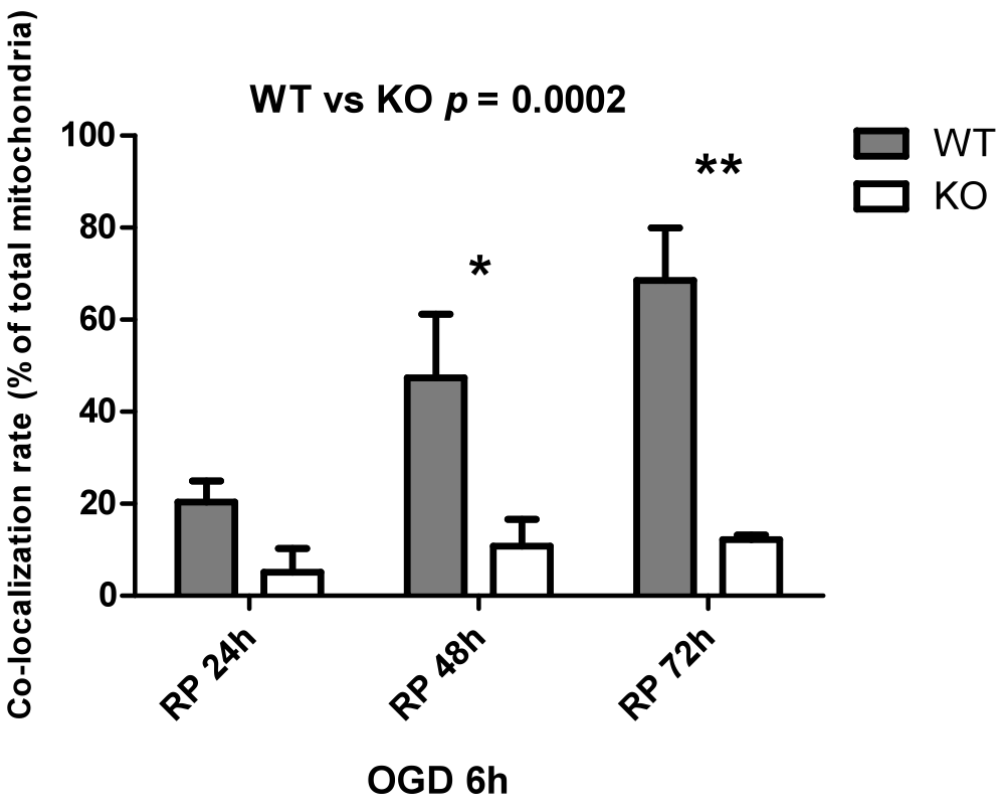
WT vs KO p = 0.0002
Co-localization rate (% of total mitochondria)
100
80
60
40
20
0
*
**
WT
KO
RP 24h
RP 48h
RP 72h
OGD 6h

D

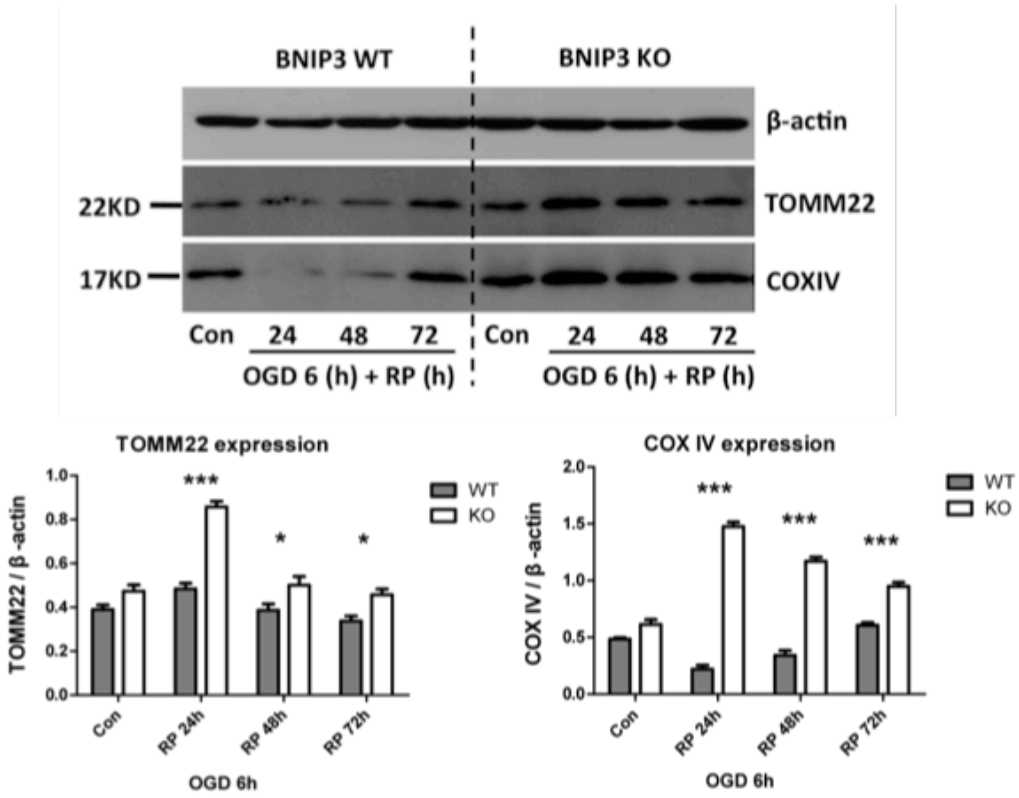
BNIP3 WT
BNIP3 KO
β-actin
22KD
TOMM22
17KD
COXIV
Con 24 48 72 Con 24 48 72
OGD 6 (h) + RP (h)
OGD 6 (h) + RP (h)
TOMM22 expression
TOMM22 / β -actin
WT
KO
Con
RP 24h
RP 48h
RP 72h
OGD 6h
COX IV expression
COX IV / β -actin
WT
KO
Con
RP 24h
RP 48h
RP 72h
OGD 6h

E

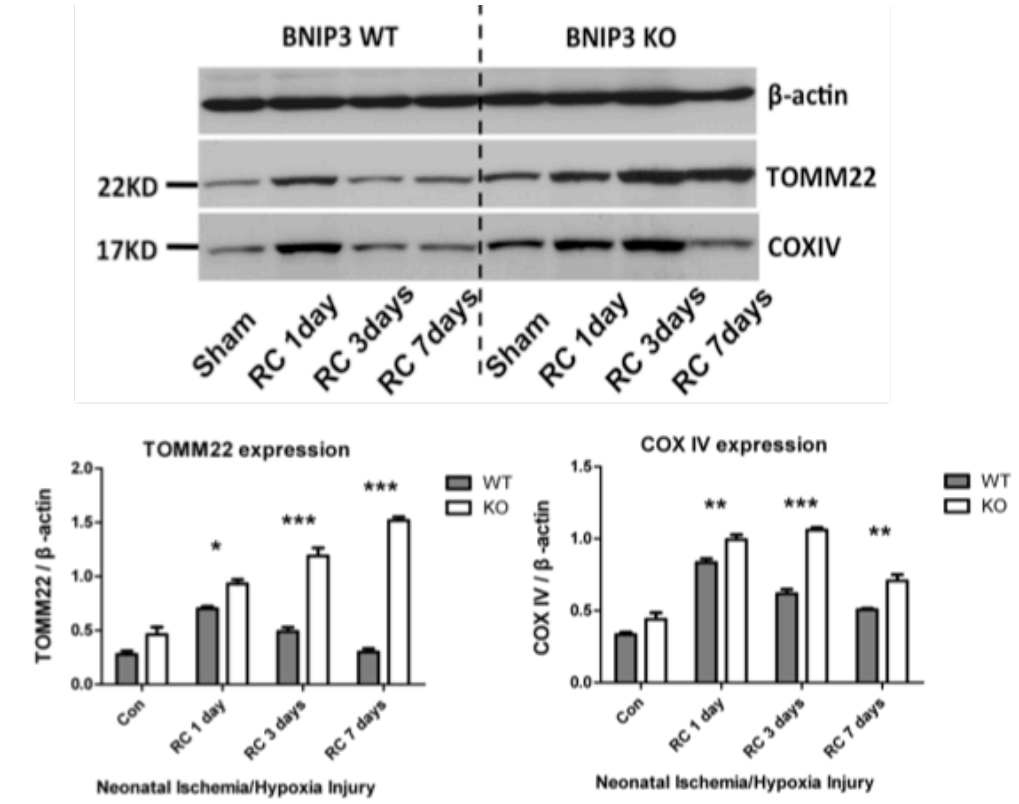
BNIP3 WT
BNIP3 KO
β-actin
22KD
TOMM22
17KD
COXIV
Sham
RC 1day
RC 3days
RC 7days
Sham
RC 1day
RC 3days
RC 7days
TOMM22 expression
TOMM22 / β -actin
WT
KO
Con
RC 1 day
RC 3 days
RC 7 days
Neonatal Ischemia/Hypoxia Injury
COX IV expression
COX IV / β -actin
WT
KO
Con
RC 1 day
RC 3 days
RC 7 days
Neonatal Ischemia/Hypoxia Injury

F

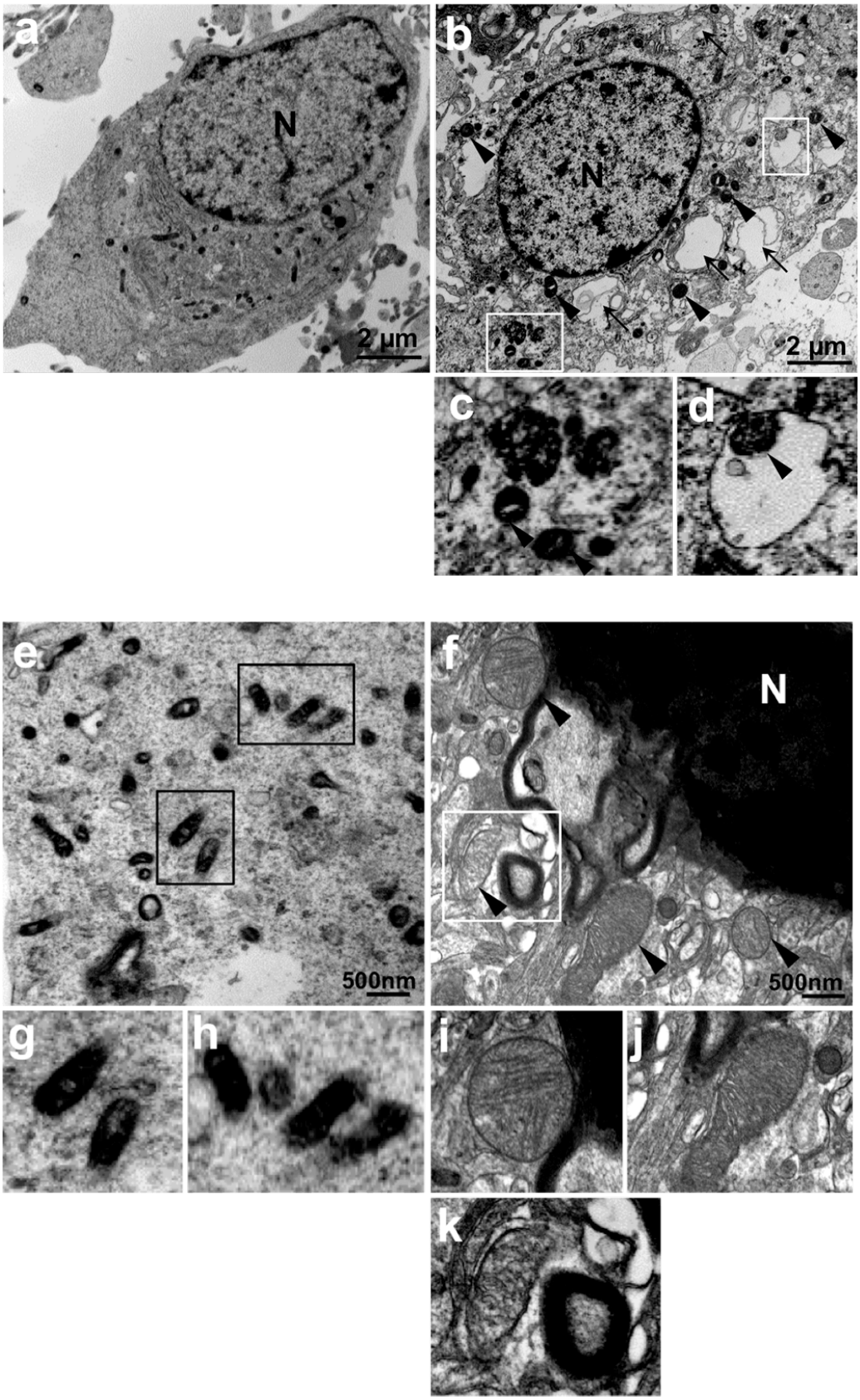

G

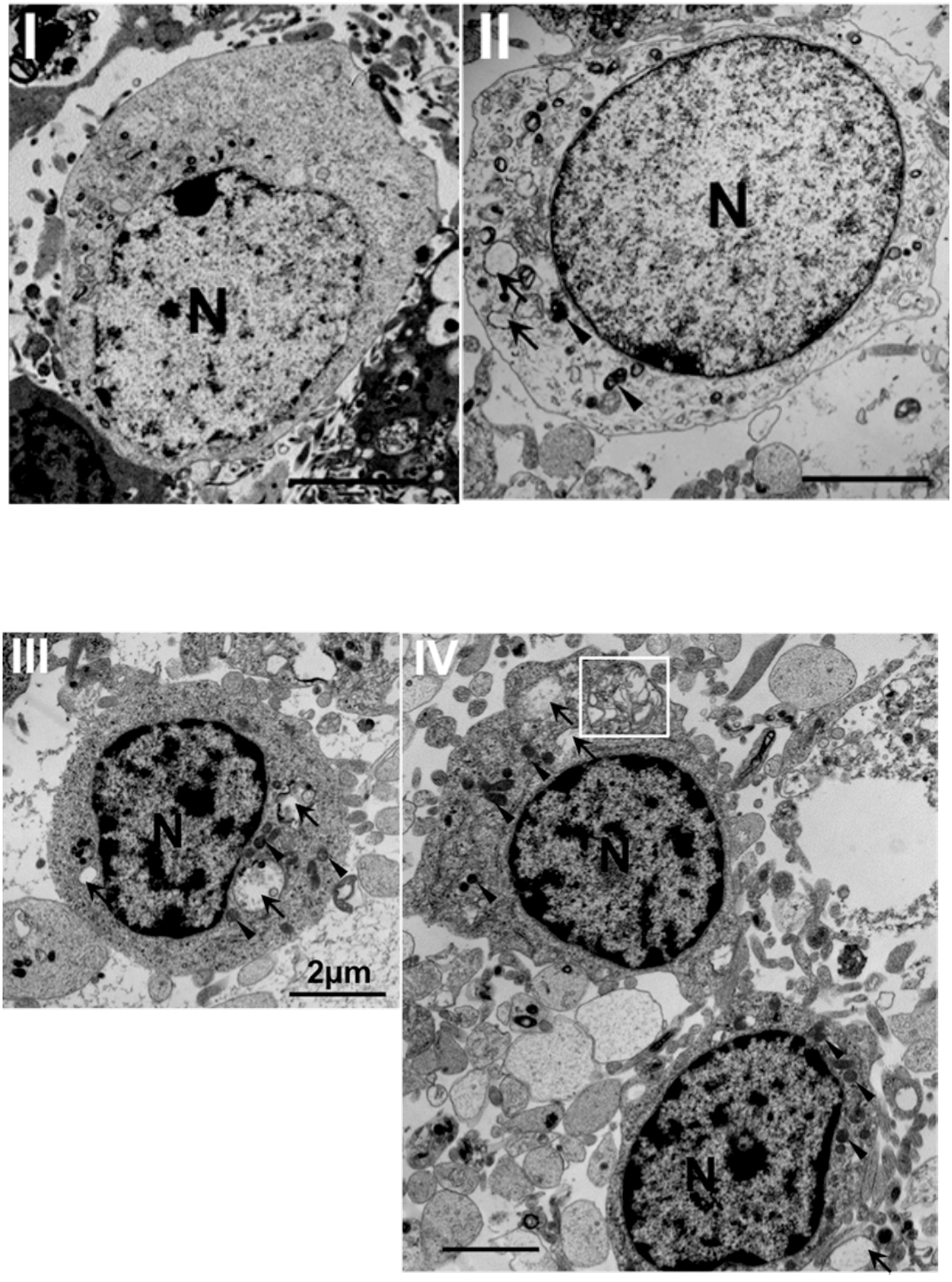

Fig 5.2 BNIP3 expression increased mitophagy in stroke models. (A-B) Immunocytochemistry was used to detect mitophagy intensity in WT/KO neurons, as shown by co-localization of mitochondria with autophagosomes. Mitochondria were stained with red; LC3 and nuclei were marked with green and blue, respectively. **Scale bars = 30 μm. Images were taken at 63× objective.** (C) Co-localization rates of mitochondria with autophagosomes in OGD/RP treated neurons. Percentage of mitochondria fused with autophagosomes (yellow dots) to the total number of mitochondria (red dots) was calculated. Two-way ANOVA analysis and Bonferroni post-tests were used to compare the WT and KO groups: WT vs KO on each time point, ***p* < 0.05, **** *p* < 0.01, ***** *p* <0.001. N = 3 for each group. (D-E) Western blot was used to determine the total amount of mitochondrial proteins *in vitro* (D) and *in vivo* (E). β-actin (43kD) was included as internal control. Band densities were measured by Quantity One software. Two-way ANOVA analysis and Bonferroni post-tests were used to compare the WT and KO groups: WT vs KO on each time point, ***p* < 0.05, **** *p* < 0.01, ***** *p* < 0.001. N = 3 for each group. Control groups were without I/H injury. (F) Group of electron micrographs (a-k) showed the occurrence of mitophagy in neurons after OGD/RP injury. White boxes represented autophagosomes; Black arrows represented autophagic vacuoles; Black arrowheads represented swelled and dilated mitochondria. Abundant double-membrane autophagosomes formed in neurons after OGD 6 h plus RP 72 h treatment (b-d, f and k, as indicated by white boxes). Healthy and functional mitochondria were stained darkened with normal sizes in control neurons (a, e, g and h, as indicated by black boxes). Lysosome was activated and fusing with autophagosome (f and k, as indicated inside the white box). N= nucleus; (c) and (d) showed the enlarged autophagosomes in (b); (g) and (h) showed the enlarged mitochondria with normal appearances in (e);

(i) and (j) showed the enlarged mitochondria with swelling and dilation appearances in (f); (k) showed an enlarged autolysosome that encompassed a mitochondrion in (f), demonstrating the ongoing process of mitophagy. Scale bars = 2 μm in (a-b), Scale bars = 500 nm in (e-f). N = 3 for each group. (G) Group of electron micrographs (I-IV) showed the progression of neuronal death after OGD/RP injury. Primary neurons were subjected to OGD for 6 h then followed by RP for 24 h (II), 48 h (III) and 72 h (IV) and were fixed for EM examination. Normal appearance of cytoplasm, organelles, and nucleus were observed in control neurons (I). N, nucleus; Ultrastructural features of autophagic cell death were detected in neurons treated by OGD 6 h followed by RP 48 h (III) and 72 h (IV), presenting a progressive shift from physiological level of autophagy (II) to the Type II programmed cell death (III-IV). Cell shrinkage, nuclear condensation (without fragmentation), loss of cellular organelles, and formation of numerous autophagic vacuoles (black arrows) were shown in the picture (II-IV). Mitochondria also displayed swelling and dilation as indicated by black arrowheads (II-IV). Mixed morphological features of autophagic cell death and apoptosis (cell membrane blebbing) were found in the same group of neurons treated by OGD 6 h followed by RP 72 h (IV), demonstrating a potential cross-talk between types I and II programmed cell death. An autophagosome was indicated by white box in (IV). **Scale bars = 2 μm** in (I-IV).

5.3 BNIP3 Expressed in a 'Delayed' Manner and Regulated Excessive Mitophagy in Brain I/H

BNIP3 WT and KO cortical neurons were cultured for 7 days then treated with 6 h OGD followed by different times of reperfusion (0-72 h). Immunocytochemistry and western blot were used to demonstrate the time course of BNIP3 and NIX expression *in vitro* (Figure 5.3A, B and D) and *in vivo* (Figure 5.3C, E). It has been shown that BNIP3 was activated after I/H injury and expressed in a 'delayed' manner in the WT tissues. The expression of BNIP3 was firstly detectable at around RP 24h and pronounced highly at RP 48 and 72 h in the OGD/RP-challenged neurons (Figure 5.3A, B and D). In the WT mice brains that were challenged by neonatal stroke modeling, BNIP3 was effectively activated after 1 day's recovery and up-regulated throughout the recovery period until reached the maximum expression at 7 days (Figure 5.3C, E). Both forms of BNIP3 protein, the cytosolic monomer (30 kD) and the mitochondria-localized homodimer (60 kD), were expressed in a similar 'delayed' pattern in the brain I/H. Immunofluorescence data verified the 'delayed' expression of BNIP3 in WT neurons, and the complete silence of BNIP3 in KO tissues after I/H injury (Figure 5.3A, D and E). Furthermore, NIX (also known as BNIP3L) was also activated and expressed in a similar pattern as BNIP3 in both stroke models. In particular, NIX expression levels were significantly higher in KO tissues compare to WT tissues at each time point after I/H, implying a compensation for the loss of the BNIP3 gene (Figure 5.3D, E). However, when BNIP3 was silenced, mitophagy levels remained unchanged at each time point after I/H and were not affected by the dramatic upregulation of NIX in KO tissues (Figure 5.2D-E), implicating that the major function of NIX is maintaining a basal/physiological level of mitophagy,

whereas excessive/pathological mitophagy is exclusively triggered by BNIP3 in brain I/H.

A

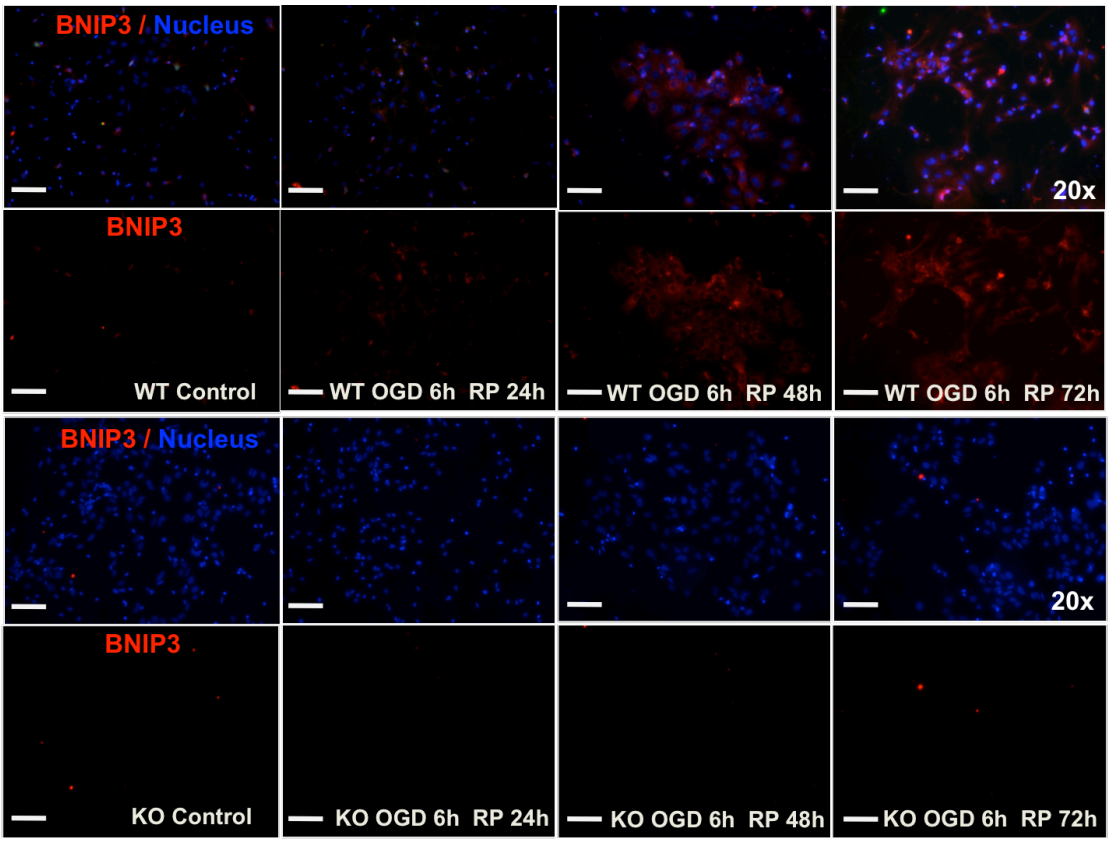

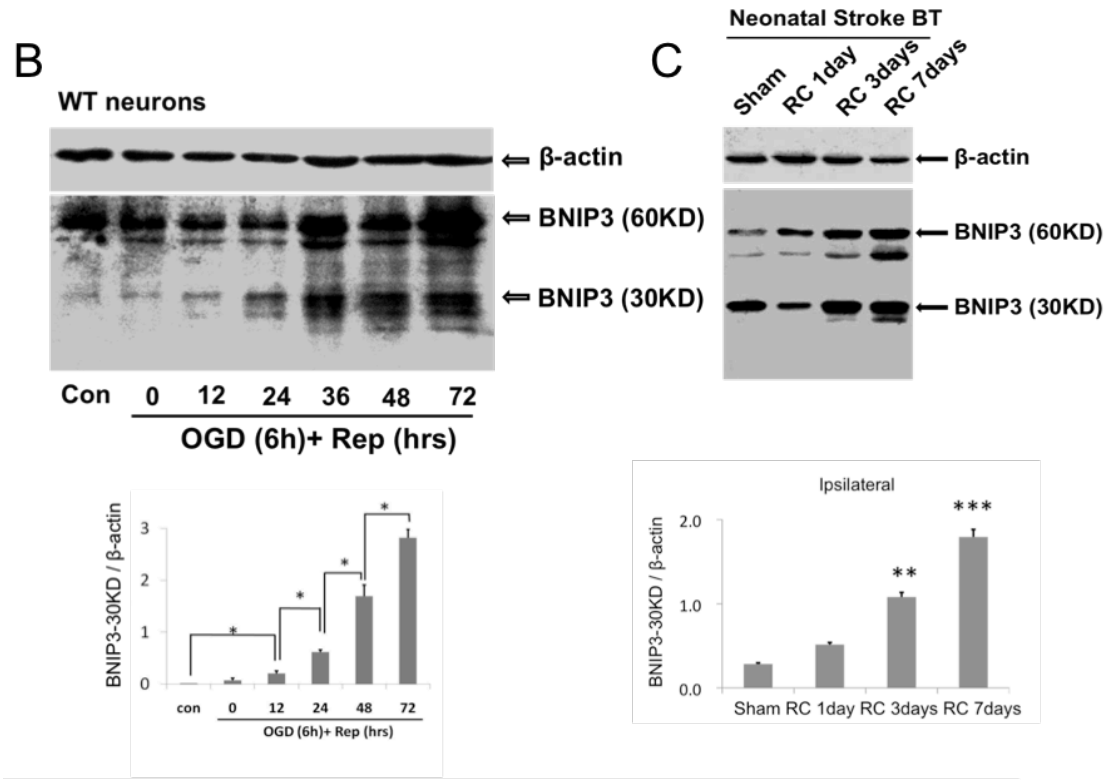
B
WT neurons
β-actin
BNIP3 (60KD)
BNIP3 (30KD)
Con 0 12 24 36 48 72
OGD (6h)+ Rep (hrs)
C
Neonatal Stroke BT
Sham
RC 1day
RC 3days
RC 7days
β-actin
BNIP3 (60KD)
BNIP3 (30KD)
BNIP3-30KD / β-actin
con 0 12 24 48 72
OGD (6h)+ Rep (hrs)
Ipsilateral
BNIP3-30KD / β-actin
Sham RC 1day RC 3days RC 7days

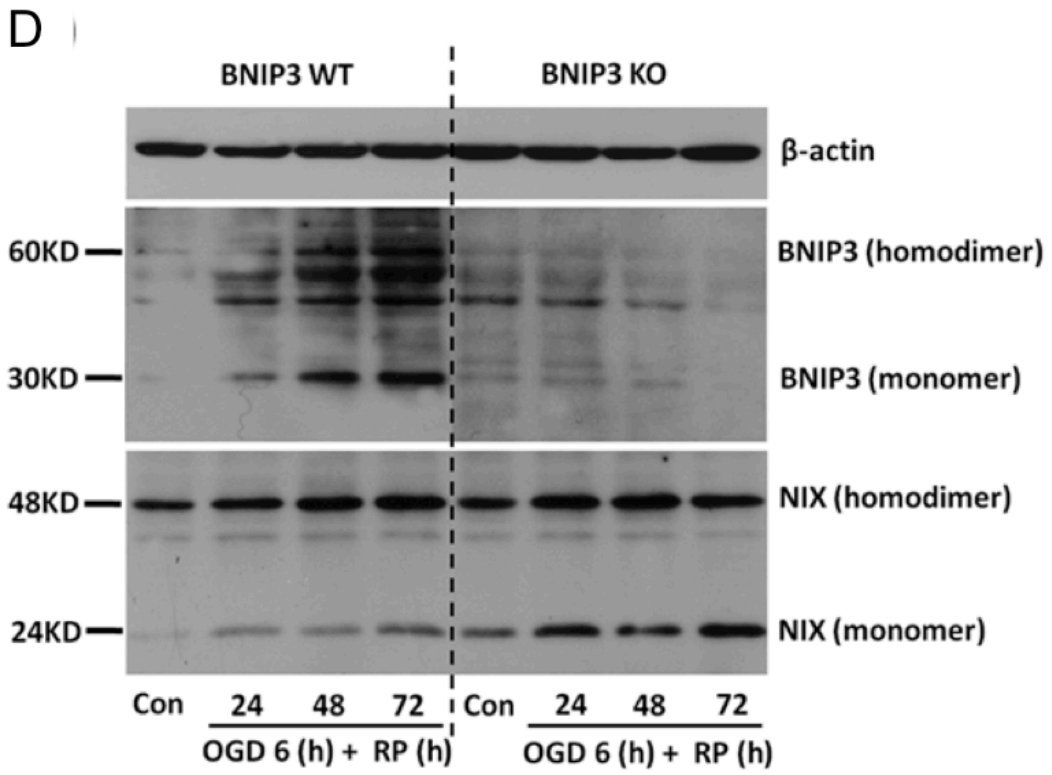
D
BNIP3 WT
BNIP3 KO
β-actin
60KD
BNIP3 (homodimer)
30KD
BNIP3 (monomer)
48KD
NIX (homodimer)
24KD
NIX (monomer)
Con 24 48 72
OGD 6 (h) + RP (h)
Con 24 48 72
OGD 6 (h) + RP (h)

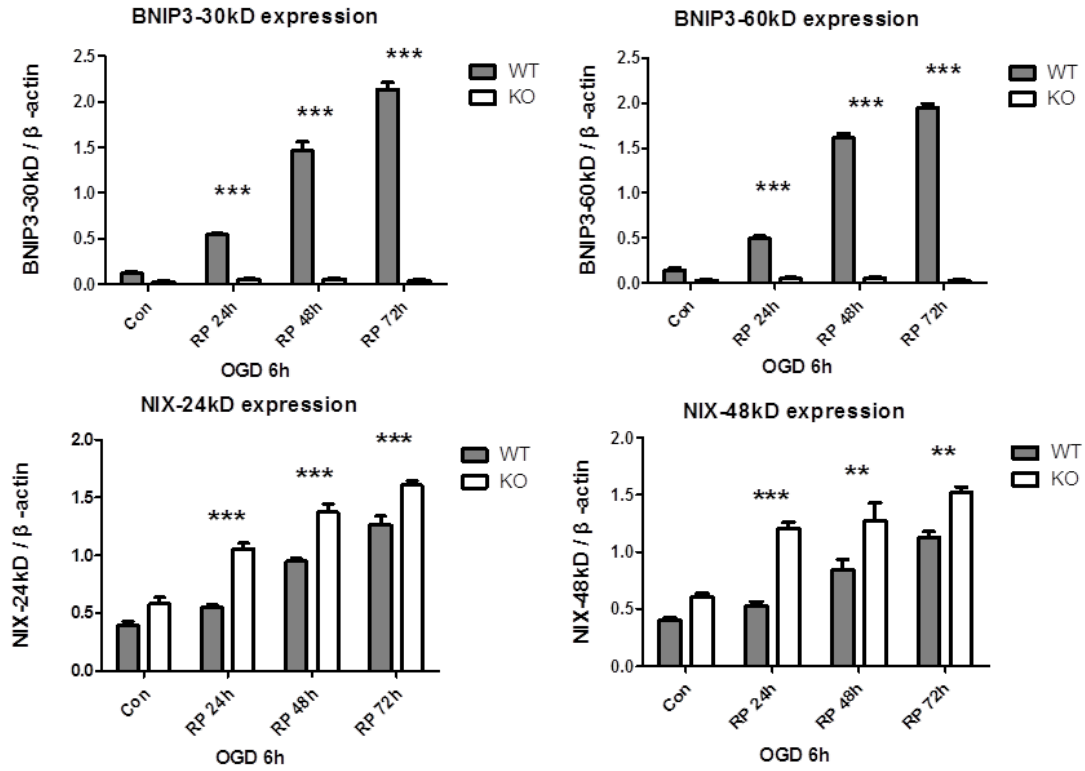
BNIP3-30kD expression
BNIP3-30kD / β -actin
WT
KO
***
Con
RP 24h
RP 48h
RP 72h
OGD 6h
BNIP3-60kD expression
BNIP3-60kD / β -actin
NIX-24kD expression
NIX-24kD / β -actin
NIX-48kD expression
NIX-48kD / β -actin
**

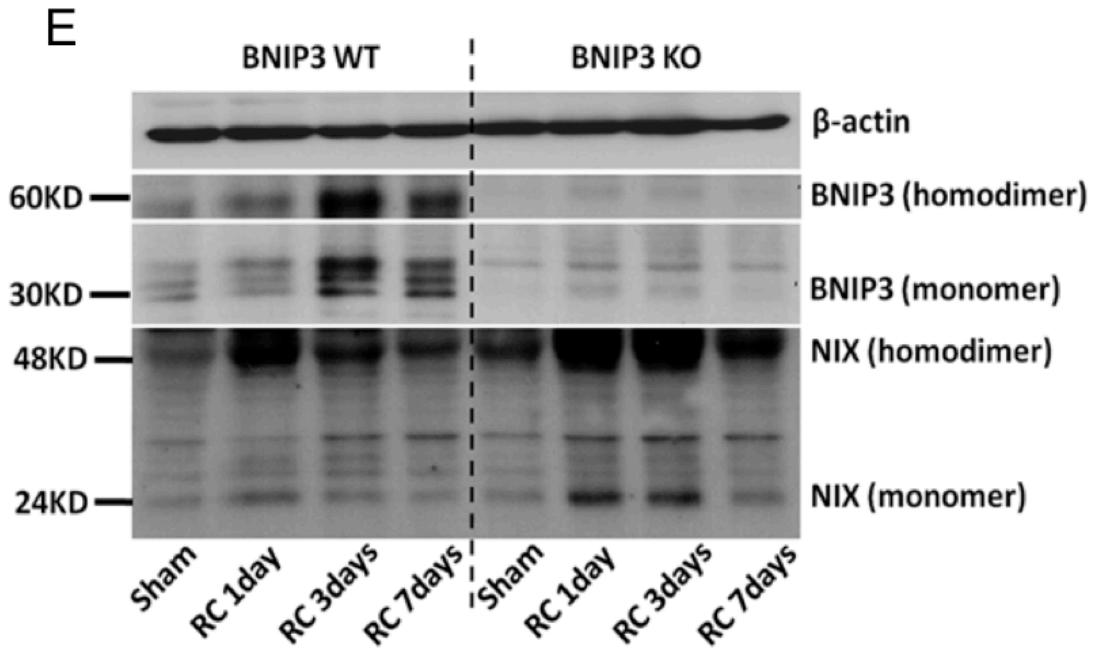
E
BNIP3 WT
BNIP3 KO
β-actin
60KD
BNIP3 (homodimer)
30KD
BNIP3 (monomer)
48KD
NIX (homodimer)
24KD
NIX (monomer)
Sham
RC 1day
RC 3days
RC 7days

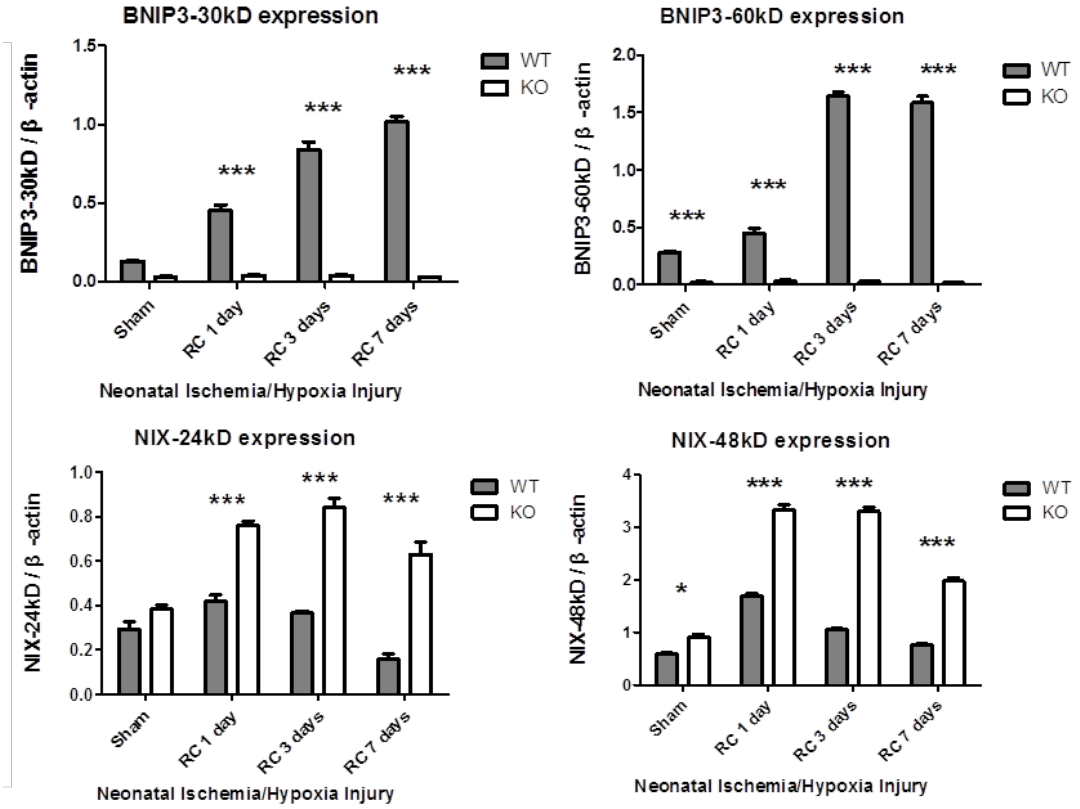

Fig 5.3 Expression patterns of BNIP3 and NIX in stroke models. (A, B and D) Primary cortical neurons were treated with OGD for 6 h followed by different times of reperfusion (0-72 h). (C, E) BNIP3 WT and KO mice pups were subjected to the neonatal stroke modeling, and brain tissues were collected and prepared for western blot assays after recovery of 1, 3 and 7 days, respectively. Immunocytochemistry (A) and Western blot (B-E) were used to demonstrate the time course of BNIP3 and NIX expression *in vitro* (A, B and D) and *in vivo* (C, E). BNIP3 was activated and expressed in a 'delayed' manner in the WT tissues, while was completely silenced in the KO tissues after I/H injury. NIX was up-regulated and expressed more to compensate for the loss of BNIP3 in KO tissues. Control and sham-operated groups without I/H. BNIP3 was stained with red, and nuclei were marked with blue. **Scale bars = 80 µm. Images were taken at 20× objective** (A). Western blot band densities

were measured by Quantity One software. Two-way ANOVA analysis and Bonferroni post-tests were used to compare the WT and KO groups: WT vs KO on each time point, $*p < 0.05$, $** p < 0.01$, $*** p < 0.001$. N = 3 for each group.

5.4 Mitochondria-localized BNIP3 Interacted with LC3 in the Neuronal Mitophagy of Stroke Models

Co-immunoprecipitation combined with ELISA assays were used to detect protein to protein interactions. Primary rat cortical neurons were treated with OGD for 6 h followed by 24 h, 48 h, and 72 h reperfusion. BNIP3 WT mice pups were subjected to the neonatal stroke, and brain tissues were collected and prepared for Co-ip assays after recovery of 1, 3 and 7 days. Control group verified that the primary antibodies of monoclonal anti-BNIP3, polyclonal anti-LC3 and monoclonal anti-NIX worked well by pulling down their according antigens specifically and efficiently in both *in vitro* and *in vivo* stroke models (Figure 5.4A). Direct interactions between NIX and LC3 were confirmed by co-ip in OGD/RP-challenged rat cortical neurons and also in I/H-challenged WT mice brain tissues, serving as positive controls (Figure 5.4B). The optimized incubation and wash conditions were used in the experimental groups, and both forms of LC3 (I and II) were probed with LC3 antibody. Our results detected clear bands of both LC3-I and LC3-II by using BNIP3 as the bait protein to pull down LC3, and the autophagosome-localized LC3-II was the major interacting target for BNIP3; on the other hand, only the single band of mitochondria-localized BNIP3 homodimer (60 kD) was detected by using LC3 as the bait protein to pull down BNIP3, suggesting that LC3 interacted specifically to the 60 KD dimer form of BNIP3. The similar results were obtained from both *in vitro* and *in vivo* stroke models,

confirming there was direct interaction between BNIP3 and LC3 in brain I/H (Figure 5.4C). By using co-ip followed by ELISA assays, the interactive intensities between NIX and LC3-II, BNIP3 and LC3-II were further quantified at each time point. The percentage of LC3-II pulled down by NIX or BNIP3 to the total amount of LC3-II was calculated as an indicator of interactive intensity (Figure 5.4D-G). In OGD/RP-challenged rat cortical neurons, significantly enhanced interactions between NIX and LC3-II, as well as BNIP3 and LC3-II were verified in a time-dependent fashion, reaching the maximum interaction at around RP 72 h (Figure 5.4D-E). In I/H-challenged neonatal cortex, significantly increased interaction between BNIP3 and LC3-II was also detected, especially after 1 day's recovery (Figure 5.4G). These enhanced interactions of mitochondria-localized BNIP3 with autophagosome-localized LC3 may subsequently contribute to the induction of excessive mitophagy.

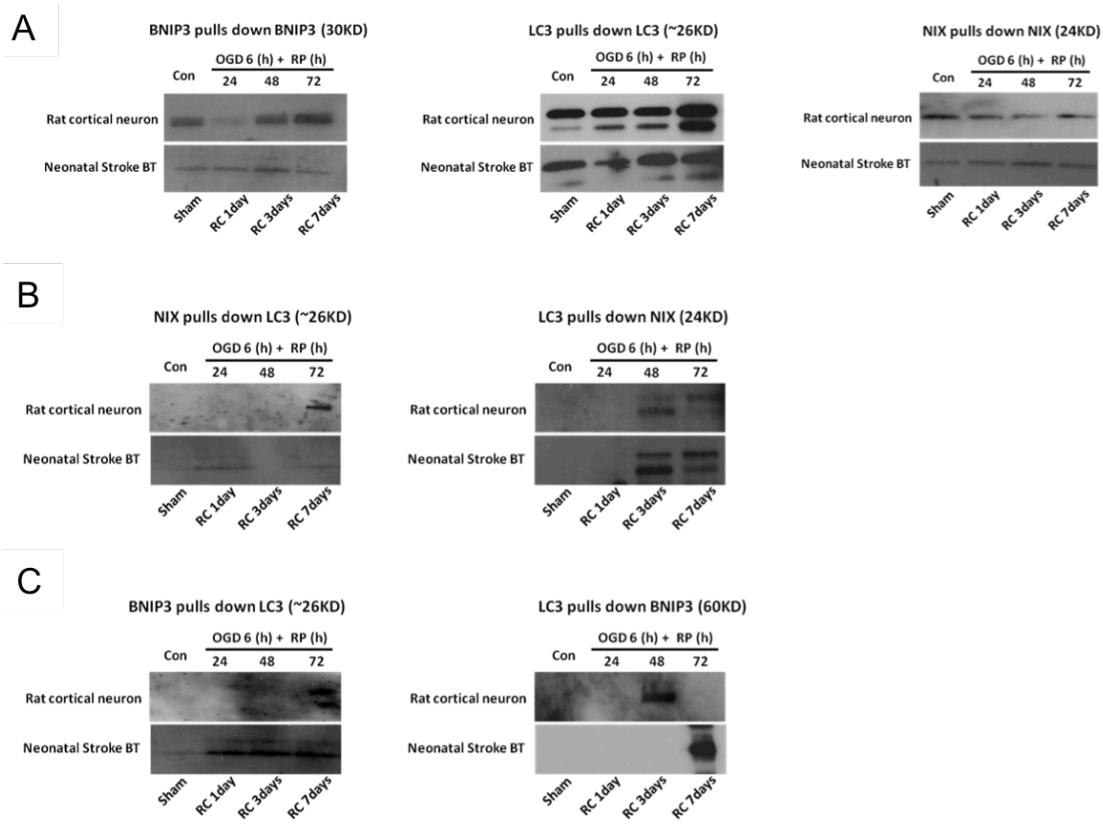

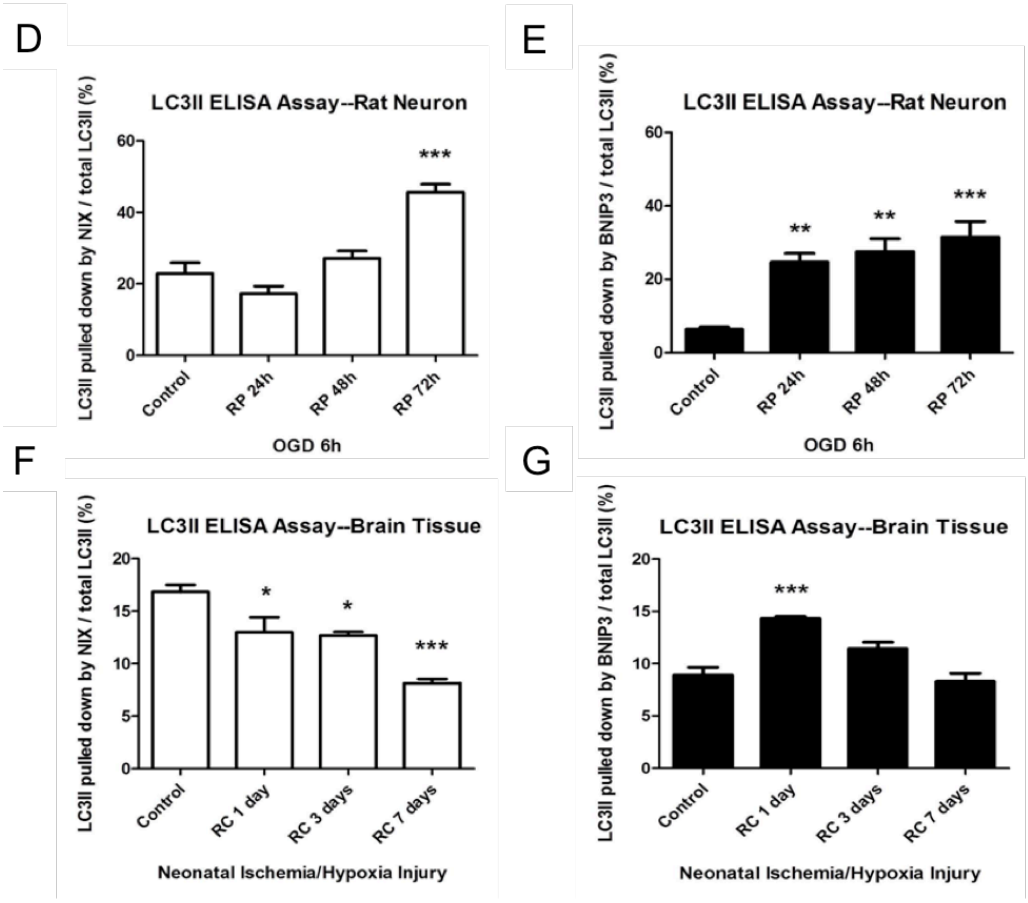

Fig 5.4 Mitochondria-localized BNIP3 interacted with LC3 directly in the neuronal mitophagy in stroke models. (A-C) Direct interactions between NIX and LC3, BNIP3 and LC3 were confirmed by Co-immunoprecipitation in both in vitro and in vivo stroke models, respectively. (A) Control groups verified the specificity and efficiency of each primary antibodies used in the co-immunoprecipitation assays. (B) Positive control group confirmed the direct interaction between NIX and LC3 in stroke models. (C) Experimental group confirmed the direct interaction between BNIP3 (60 KD homodimer form) and LC3 in stroke models. (D-G) By using co-ip followed by ELISA assays, the interactive activities between NIX and LC3, BNIP3 and LC3 were further quantified at each time point. Control and sham-operated groups were without I/H. One-way ANOVA analysis and Dunnett's post-tests were used for the statistical

analysis. * $p < 0.05$, ** $p < 0.01$, *** $p < 0.001$ versus control group. N = 3 for each group.

5.5 BNIP3 Gene Silencing Decreased Apoptosis in Cortical Neurons After OGD/RP Injury

After 6 h OGD followed by 24 h, 48 h, and 72 h reperfusion, primary cortical neurons from WT mice showed significantly activated apoptosis, as demonstrated by the increased levels of pro-apoptotic marker proteins (i.e. active caspase 3, BAX and cytochrome c) when compared to the control group. The ratios of active caspase 3, BAX, and cytochrome c to β-actins were increased dramatically from 0.34 to 1.01, 0.32 to 1.14, and 0.40 to 1.02, respectively, in a time-dependent fashion in WT neurons. However, the KO neurons displayed an opposite trend with decreased expression of the same apoptotic proteins. In OGD/RP-challenged KO neurons, the ratios of active caspase 3, BAX, and cytochrome c to β-actins were decreased dramatically from 0.71 to 0.29, 0.77 to 0.29, and 0.70 to 0.33, respectively, in a time-dependent fashion. Changes of Bcl-2 levels in WT neurons occurred after 6 h OGD, and the expression kept increasing for at least 3 days post-treatment. The time course and levels of Bcl-2 expression correlated with the increase of pro-apoptotic proteins, and this increase corresponded to the increased neuronal death rate in WT neurons (Figure 5.1D). In KO neurons, no significant difference was detected of the Bcl-2 expression at each time point, suggesting an inadequate activation of anti-apoptotic Bcl-2 after OGD/RP when BNIP3 was silenced.

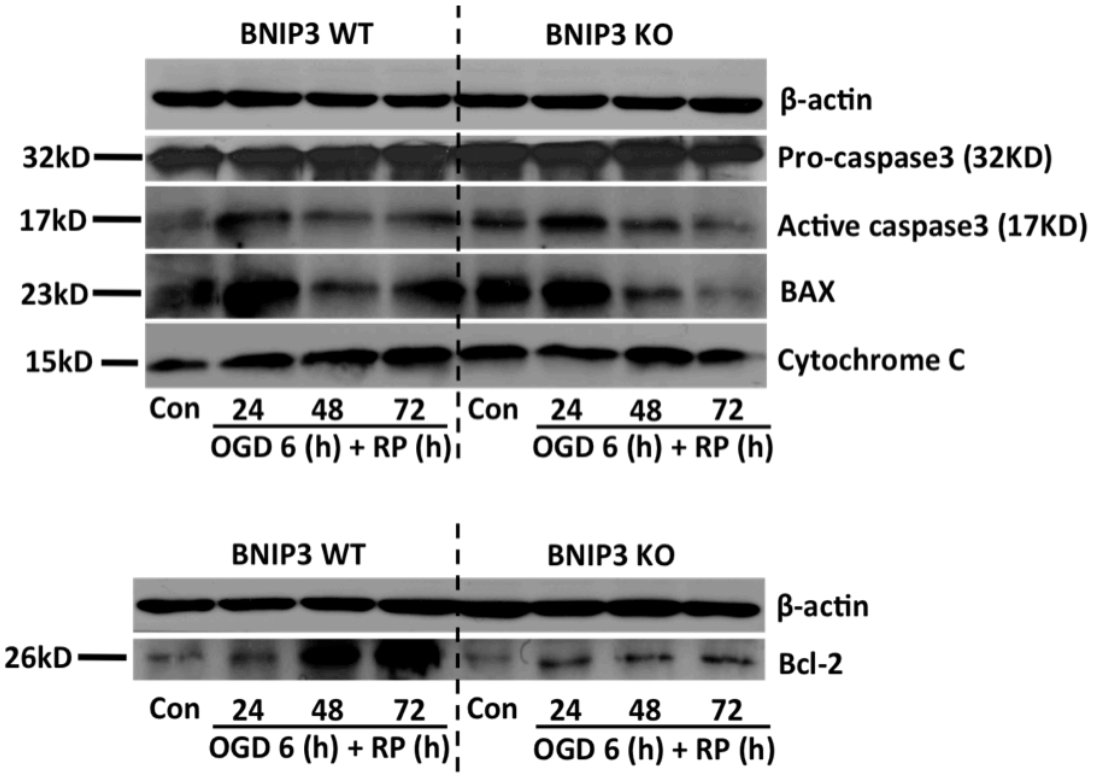
BNIP3 WT
BNIP3 KO
β-actin
32kD
Pro-caspase3 (32KD)
17kD
Active caspase3 (17KD)
23kD
BAX
15kD
Cytochrome C
Con 24 48 72 Con 24 48 72
OGD 6 (h) + RP (h)
OGD 6 (h) + RP (h)
BNIP3 WT
BNIP3 KO
β-actin
26kD
Bcl-2
Con 24 48 72 Con 24 48 72
OGD 6 (h) + RP (h)
OGD 6 (h) + RP (h)

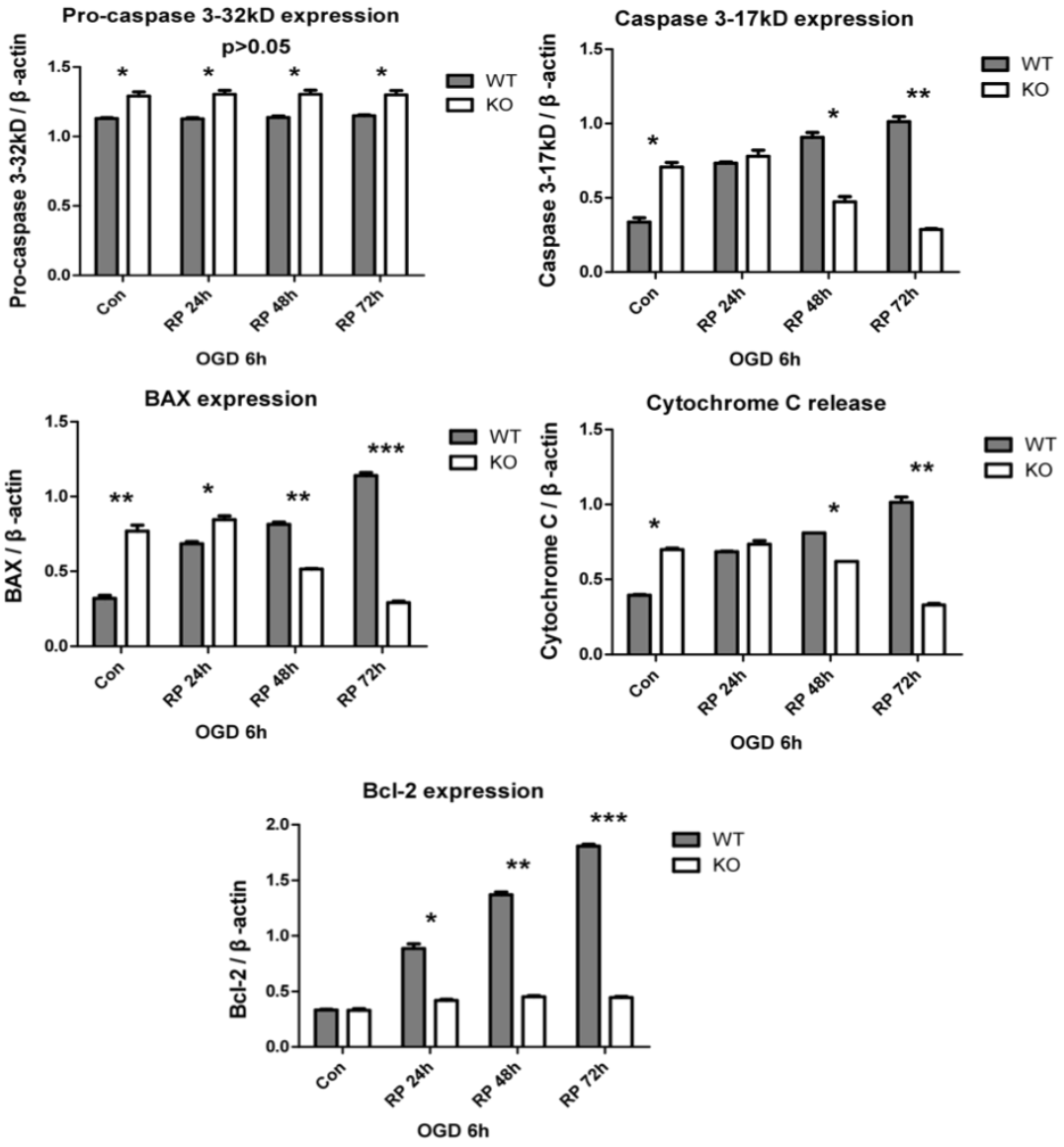

Fig 5.5 BNIP3 gene silence decreased apoptosis in cortical neurons after OGD/RP injury. Apoptosis marker protein levels were measured by western blot in BNIP3 WT and KO neurons. β-actin (43kD) was included as internal control. Decreased apoptotic activity was demonstrated by the decreased expression of pro-apoptotic proteins (Caspase-3, BAX and Cytochrome C) and anti-apoptotic protein (Bcl-2) in the BNIP3 KO neurons. Band densities were measured by Quantity One software. Two-way ANOVA analysis and Bonferroni post-tests were used to compare the WT and KO groups: WT vs KO on each time point, $*p < 0.05$, $** p < 0.01$, $*** p < 0.001$. N = 3 for each group.

5.6 BNIP3 Gene Silencing Increased Autophagy in Cortical Neurons After OGD/RP Injury

In order to detect whether BNIP3 gene silence affected general autophagy, we used several methods to testify the autophagy markers in BNIP3 WT and KO tissues. Firstly, we detected the processing and translocation of endogenous LC3 protein by immunocytochemistry. When WT and KO cortical neurons were viewed with a fluorescence microscopy after OGD/RP, the autophagosomes labeled by LC3-II seemed as distinct dot-like structures distributed in the cytoplasm, in the perinuclear regions and in the processes. This punctate staining of LC3-II was distinct from the even distribution of LC3-I in the control neurons without OGD/RP. We also observed that the levels of LC3 punctate staining in the WT and KO neurons after 6 h OGD increased dramatically according to the elongation of RP time, which represents an intense activation of general autophagy after OGD/RP injury (Figure 5.6A-B). Specifically, double labeling of BNIP3 and LC3 in WT neurons implied a correlation between BNIP3 up-regulation and autophagy activation, as indicated by the enhanced signal of BNIP3 (red) and increased punctate staining of LC3-II (green) after RP for 24, 48, and 72 h (Figure 5.6A). In KO neurons, however, much higher autophagy intensity was detected, as indicated by the substantially increased punctate-staining of LC3-II in the cytoplasm when compared to WT neurons (Figure 5.6B).

Secondly, we used MDC, an autofluorescent substance that accumulates in acidic autophagic vacuoles, as a specific marker for autophagosomes. Autophagy intensity was quantified by measuring MDC fluorescence at the emission wavelength of 457 nm. Compared to WT neurons, a significant increase in the normalized MDC fluorescence was found starting at 48 h and peaking at 72 h after 6 h OGD treatment

in KO neurons, suggesting a promoted autophagy in KO neurons after OGD/RP injury (Figure 5.6C).

Thirdly, since autophagy is characterized by the development of autophagosomes and their later-stage fusion with lysosomes, we performed immunocytochemistry by staining LC3, lysosomes, and nucleus in both OGD/RP-challenged WT and KO neurons. As shown in Figure 5.6D-E, co-localization of lysosomes with autophagosomes was represented by the overlapping of red and green signals, and as indicated by the yellowish dots inside the cytosol. We found that the percentage of colocalized lysosomes and autophagosomes was increased considerably in the KO neurons as compared to WT neurons, especially after prolonged RP of 48 or 72 h, implicating that BNIP3 gene silence increased general autophagy after OGD/RP.

Finally, Autophagy markers (i.e. Beclin1, LAMP-2, and LC3-II/I ratio) were quantified by western blot. LC3 (mammalian ATG8) is required for autophagosome formation via its conversion from LC3-I to LC3-II. [440] Cytoplasmic form LC3 (LC3-I) is distributed in the cytoplasm diffusely, [441] but, in its processed form (LC3-II), is translocated to the outer membrane of autophagosomes during autophagy activation. [440, 442] When cytosolic LC3-I is conjugated to phosphatidyl-ethanolamine and forms LC3-II, its molecular weight changes from 18 to 16 kD. Thus, an increase in the amount of the smaller molecular weight LC3-II protein and an increase in the LC3-II/I ratio are hallmarks of elevated autophagy. [440] Beclin 1, the mammalian homologue of yeast Atg6, was previously found to promote autophagy. [440] Cells with reduced Beclin 1 expression exhibit reduced autophagic activity.[404, 443] Also, a dramatic elevation in Beclin 1 levels has been found in the penumbra of rats challenged by cerebral ischemia. [444] In addition, since the fusion of

autophagosome with lysosome is the central machinery of autophagy, we also detected LAMP-2 (the lysosome-associated membrane protein 2) expression, as a marker for autophagy intensity. [278, 279, 445] Our data showed that Beclin 1 and LAMP-2 (pre-mature and mature forms) expressions, as well as LC3-II/I ratios in WT and KO neurons were upregulated after OGD/RP. Changes of Beclin 1 and LAMP-2 levels in both neurons occurred after 6 h OGD, and the expression kept rising for 72 h post-treatment in a time-dependent fashion. Specifically, KO neurons showed significantly higher levels of Beclin 1 and LAMP-2 expression, and LC3-II/I ratios as compared to WT neurons at each time point (Figure 5.6F). In general, the above results implied that BNIP3 gene silence increased general autophagy in OGD/RP-treated neurons.

A

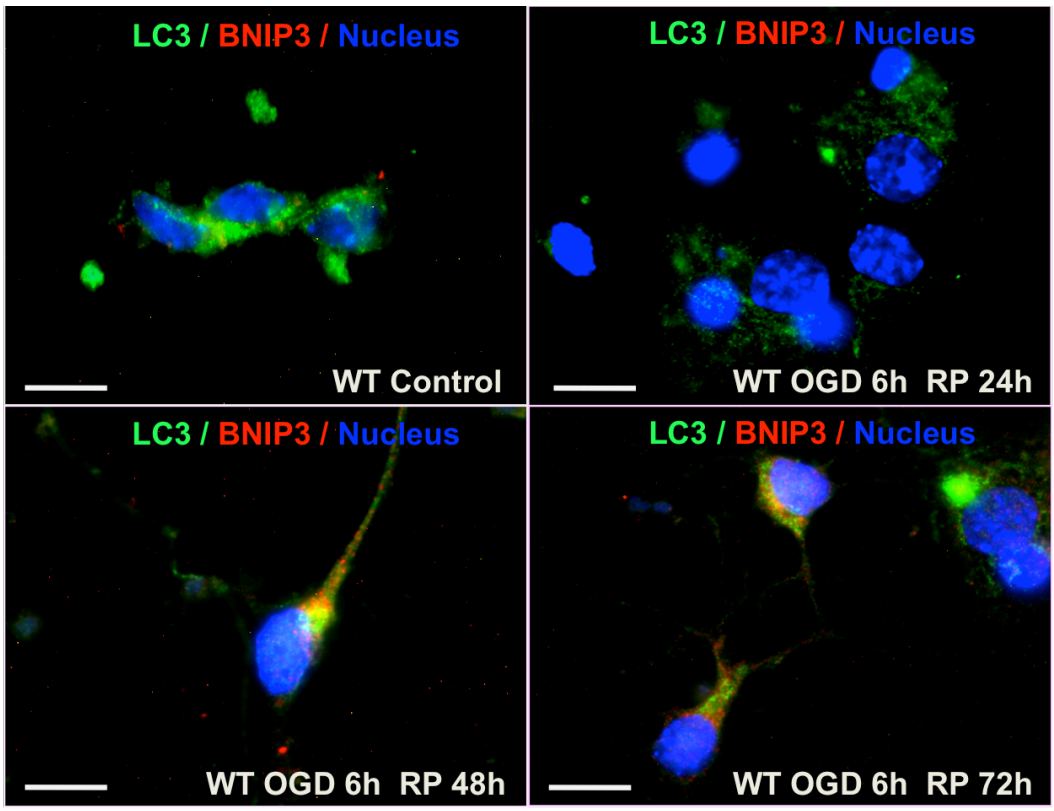

B

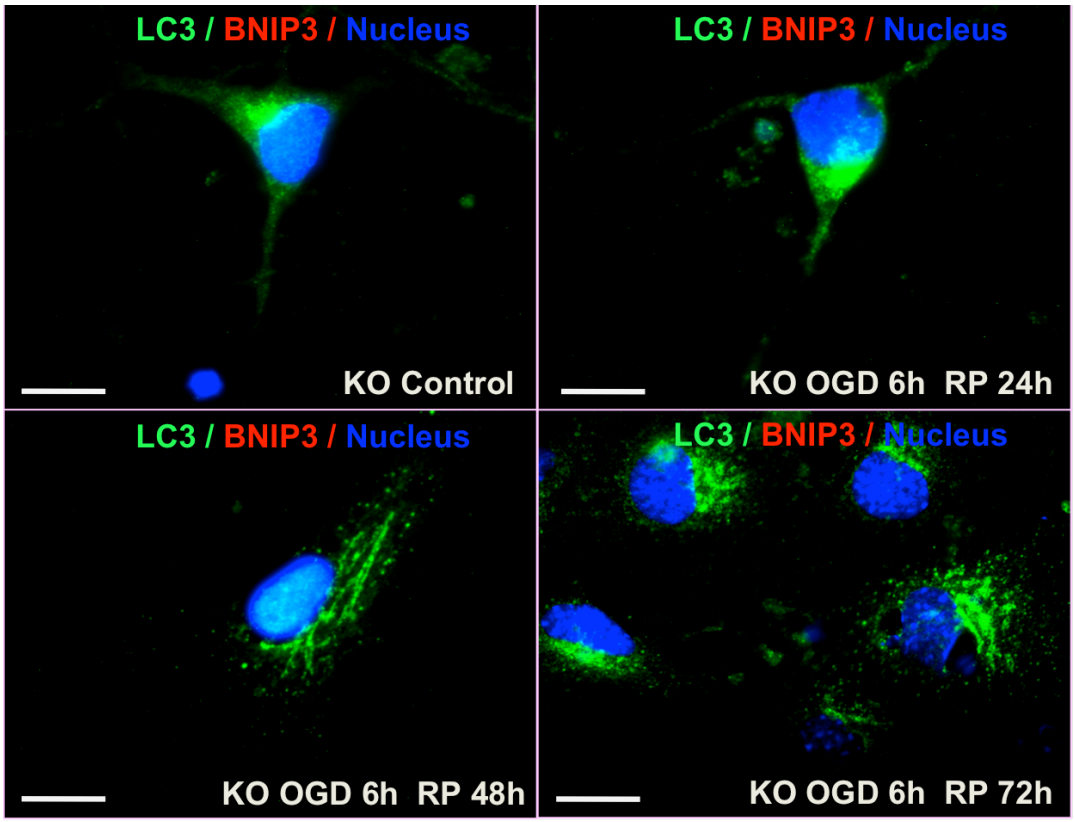
LC3 / BNIP3 / Nucleus
KO Control
LC3 / BNIP3 / Nucleus
KO OGD 6h RP 24h
LC3 / BNIP3 / Nucleus
KO OGD 6h RP 48h
LC3 / BNIP3 / Nucleus
KO OGD 6h RP 72h

C

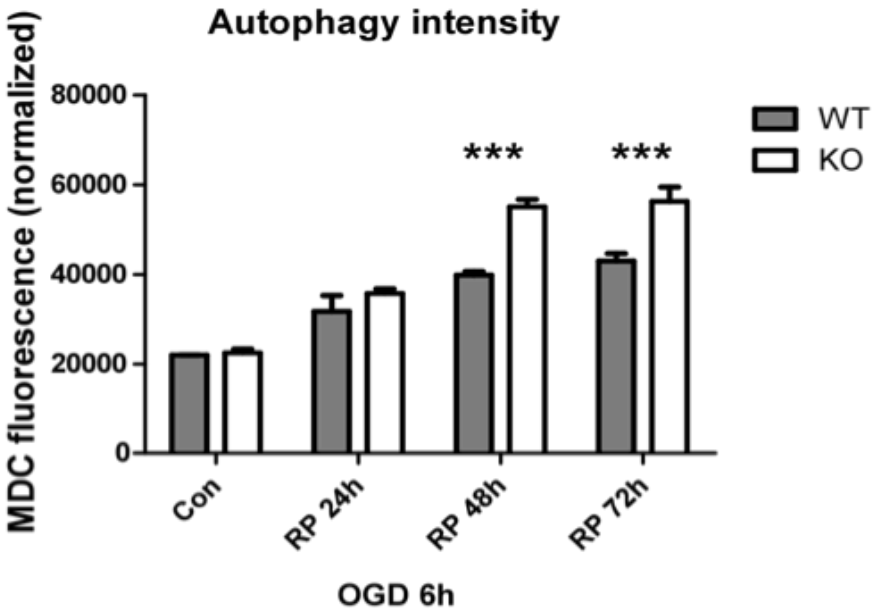
Autophagy intensity
MDC fluorescence (normalized)
80000
60000
40000
20000
0
***
***
WT
KO
Con
RP 24h
RP 48h
RP 72h
OGD 6h

D

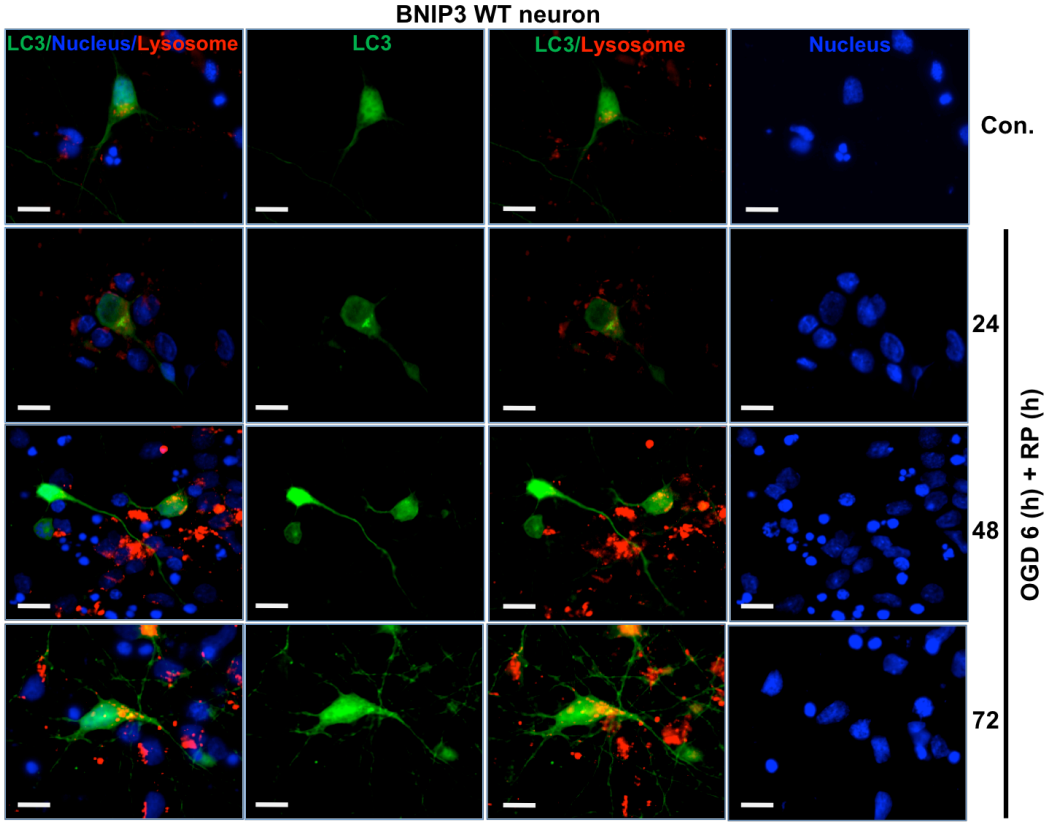
BNIP3 WT neuron
LC3/Nucleus/Lysosome
LC3
LC3/Lysosome
Nucleus
Con.
24
48
72
OGD 6 (h) + RP (h)

E

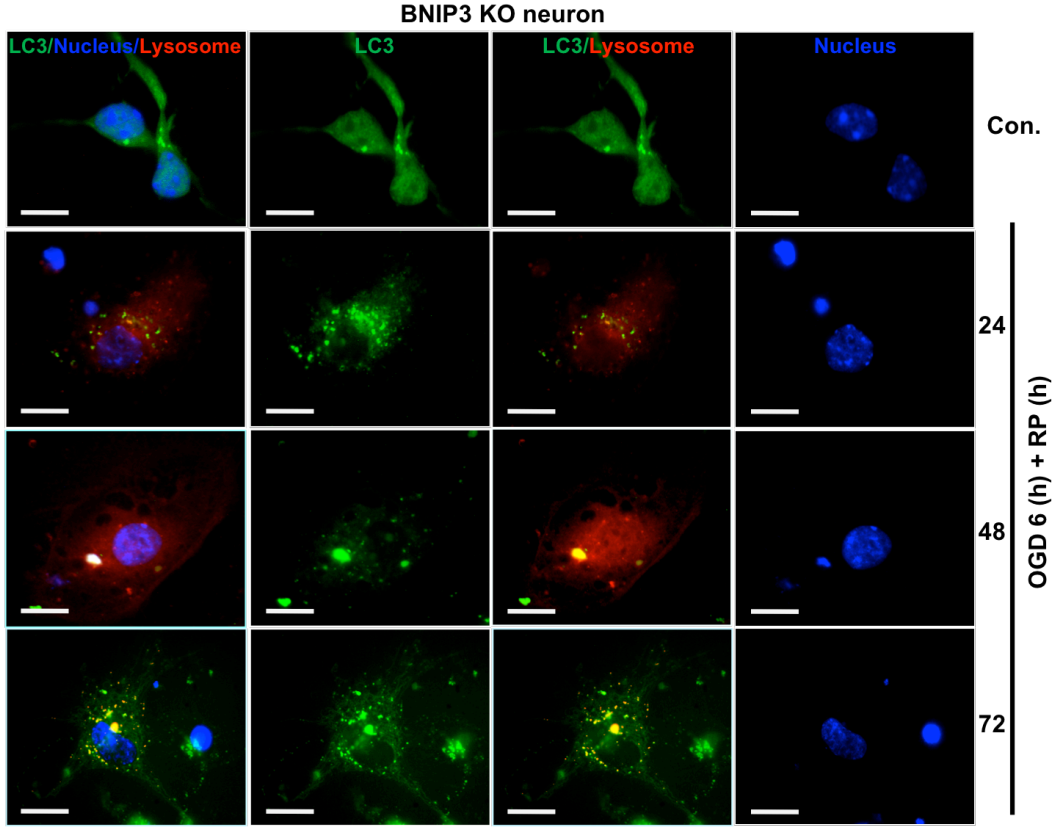
BNIP3 KO neuron
LC3/Nucleus/Lysosome
LC3
LC3/Lysosome
Nucleus
Con.
24
48
72
OGD 6 (h) + RP (h)

F

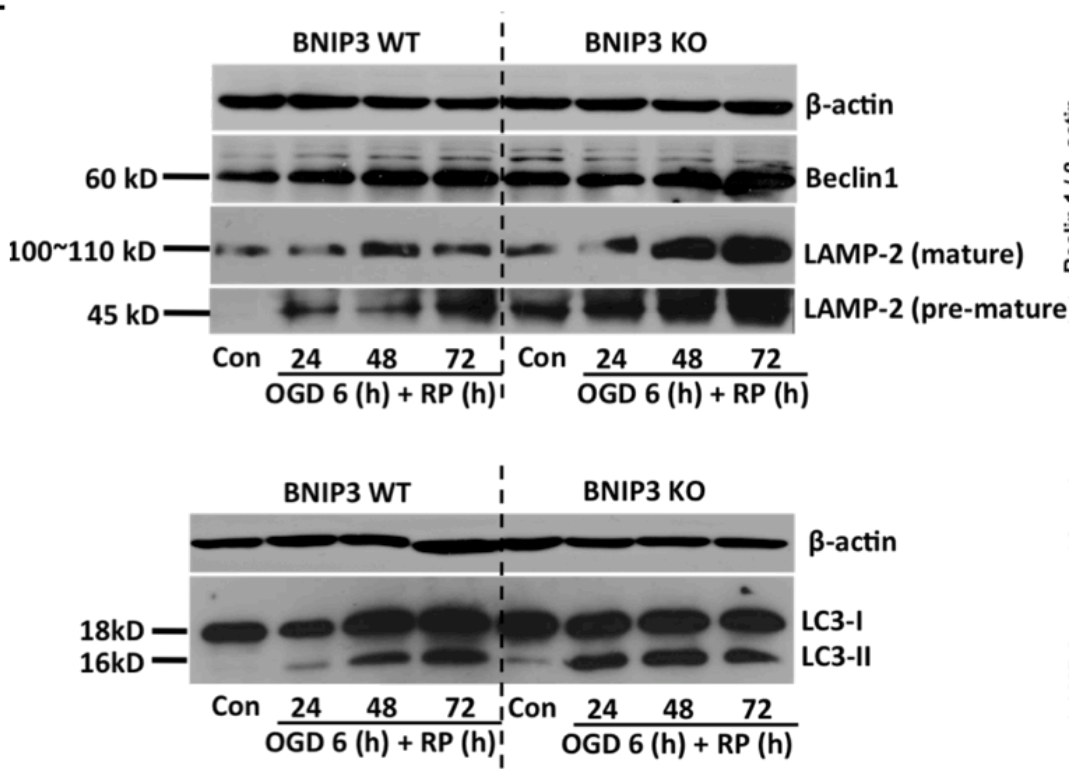
BNIP3 WT
BNIP3 KO
β-actin
60 kD
Beclin1
100~110 kD
LAMP-2 (mature)
45 kD
LAMP-2 (pre-mature
Con 24 48 72 Con 24 48 72
OGD 6 (h) + RP (h)
OGD 6 (h) + RP (h)
BNIP3 WT
BNIP3 KO
β-actin
18kD
16kD
LC3-I
LC3-II
Con 24 48 72 Con 24 48 72
OGD 6 (h) + RP (h)
OGD 6 (h) + RP (h)

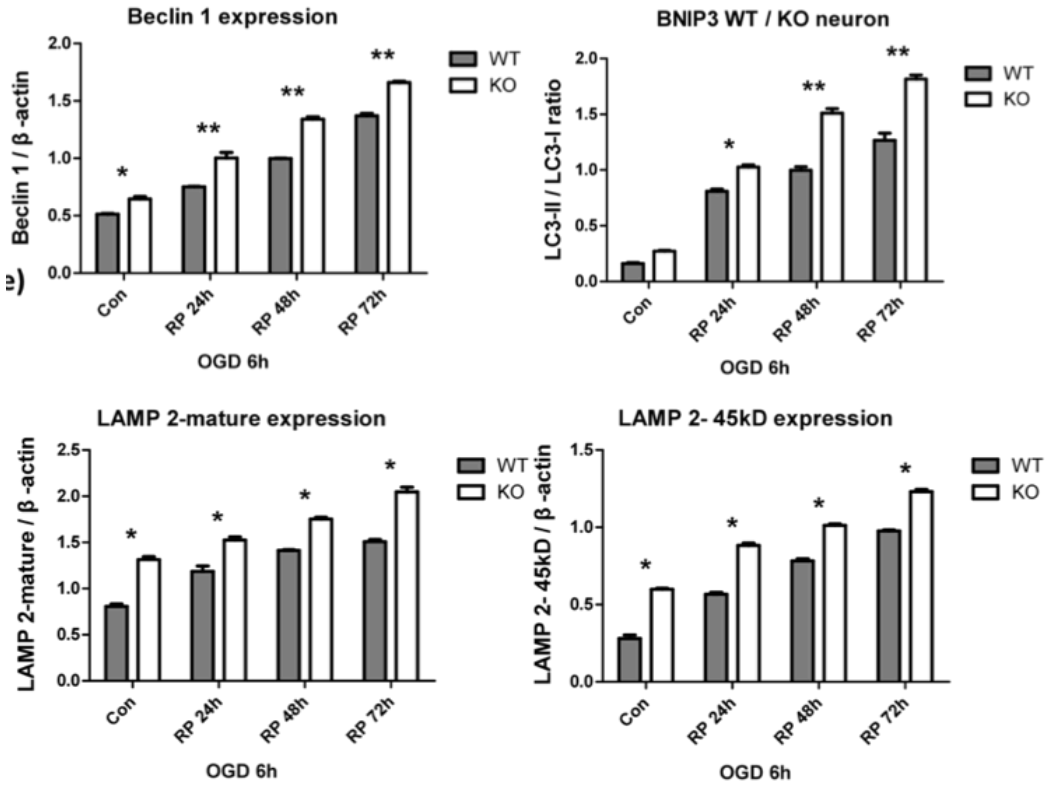
Beclin 1 expression
Beclin 1 / β -actin
WT
KO
Con
RP 24h
RP 48h
RP 72h
OGD 6h
BNIP3 WT / KO neuron
LC3-II / LC3-I ratio
WT
KO
Con
RP 24h
RP 48h
RP 72h
OGD 6h
LAMP 2-mature expression
LAMP 2-mature / β -actin
WT
KO
Con
RP 24h
RP 48h
RP 72h
OGD 6h
LAMP 2- 45kD expression
LAMP 2- 45kD / β -actin
WT
KO
Con
RP 24h
RP 48h
RP 72h
OGD 6h

Fig 5.6 BNIP3 gene silence increased general autophagy in cortical neurons after OGD/RP injury. Neurons were treated with OGD for 6h followed by 24 h, 48 h and 72 h reperfusion. (A-B) Immunocytochemistry was used to demonstrate the BNIP3 expression and punctate staining of LC3, and (D-E) the co-localization of activated lysosomes with autophagosomes inside neurons. Control group without OGD/RP. BNIP3 was stained with red, LC3 and nuclei were marked with green and blue, respectively. **Scale bars = 30 µm. Images were taken at 63× objective** in (A-B); activated lysosomes were stained with red, LC3 and nuclei were marked with green and blue, respectively. **Scale bars = 30 µm. Images were taken at 63× objective** in (D-E). (C) MDC fluorescence was measured to quantify the general autophagy intensities in BNIP3 WT and KO neurons, indicating increased autophagy intensity in KO neurons after OGD/RP. (F) Autophagy marker proteins were measured by western blot in BNIP3 WT and KO neurons. β-actin (43kD) was included as internal control. Increased autophagic activity was demonstrated by the increased expression of autophagy-related proteins (Beclin1, LAMP-2 and LC3-II/I ratio) in KO neurons. Band densities were measured by Quantity One software. Two-way ANOVA analysis and Bonferroni post-tests were used to compare the WT and KO groups: WT vs KO on each time point, $*p < 0.05$, $** p < 0.01$, $*** p < 0.001$. N = 3 for each group.

5.7 BNIP3 was an Upstream Regulator of the Neuronal Mitophagy Pathway in OGD/RP Stroke Model

Rat cortical neurons were incubated with the specific autophagy inhibitor, 3-MA, during OGD/RP treatment. Briefly, 3-MA (1 mM) was added into EBSS solution before OGD treatment and after 6 h OGD, fresh regular culture medium with 1 mM 3-MA was replaced when neurons underwent prolonged RP for 24, 48, or 72 h. Western blot was used to evaluate the expression of autophagy markers as well as BNIP3. We found that 3-MA at the concentration of 1 mM effectively blocked the activation of autophagy as evidenced by considerably reduced expression of Beclin 1 and inhibited production of LC3-II. However, the expression patterns of BNIP3 and Bcl-2 were not affected by the addition of 3-MA. Our results showed that either with or without the presence of 1mM 3-MA, BNIP3 was consistently activated and expressed in a 'delayed' manner as shown in Figure 5.7A, and no significant difference of BNIP3 or Bcl-2 expressions was detected at each time point after OGD/RP (Figure 5.7A-B). Therefore, we anticipated that BNIP3 was an upstream regulator of the neuronal mitophagy pathway in OGD/RP stroke model.

A

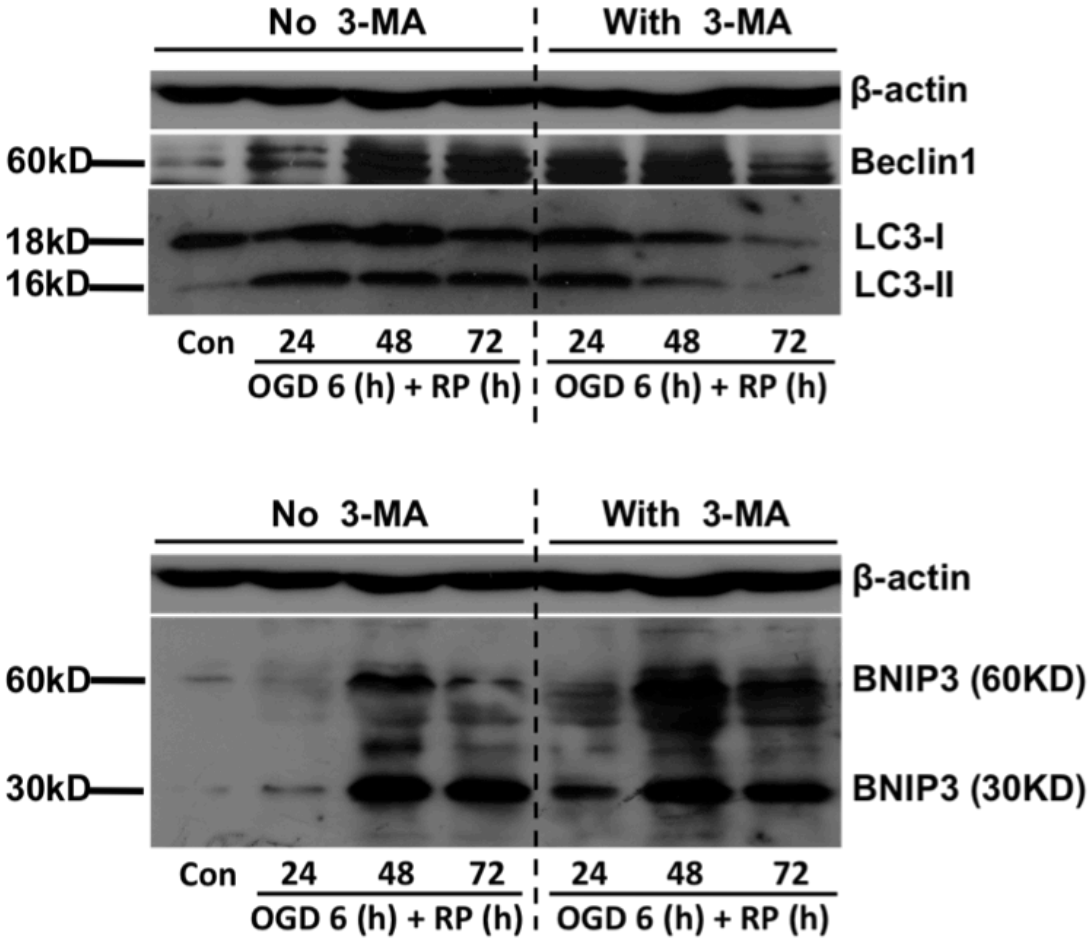
No 3-MA
With 3-MA
β-actin
60kD
Beclin1
18kD
16kD
LC3-I
LC3-II
Con
24
48
72
24
48
72
OGD 6 (h) + RP (h)
OGD 6 (h) + RP (h)
No 3-MA
With 3-MA
β-actin
60kD
30kD
BNIP3 (60KD)
BNIP3 (30KD)
Con
24
48
72
24
48
72
OGD 6 (h) + RP (h)
OGD 6 (h) + RP (h)

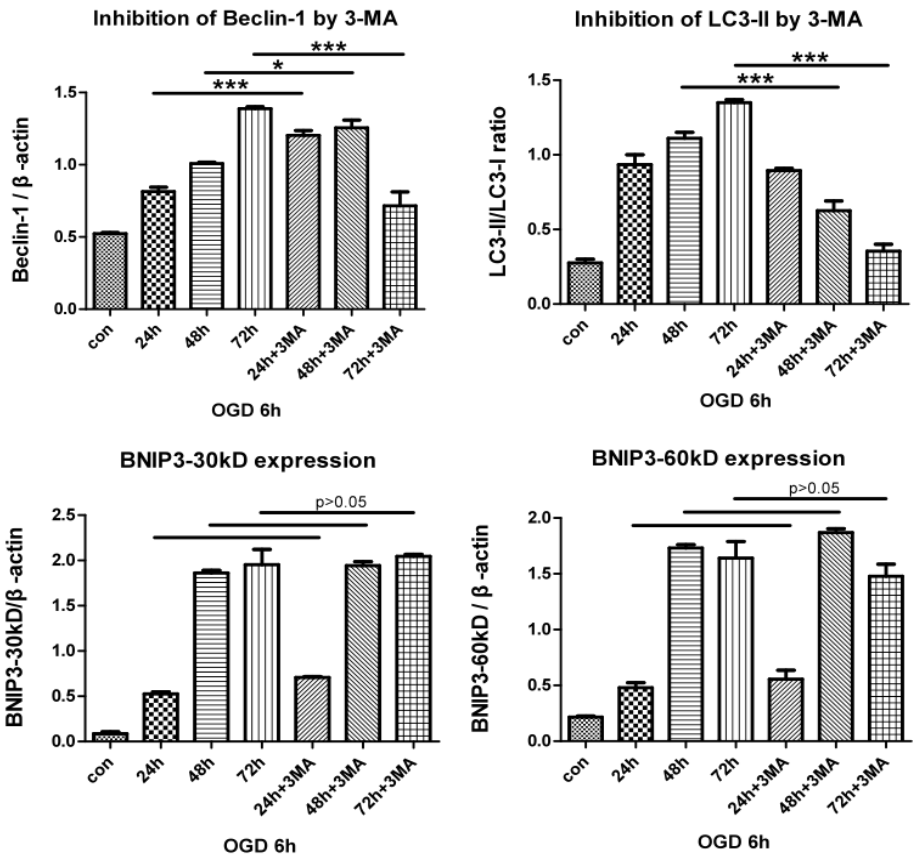
Inhibition of Beclin-1 by 3-MA
Beclin-1 / β -actin
***
*
***
con
24h
48h
72h
24h+3MA
48h+3MA
72h+3MA
OGD 6h
Inhibition of LC3-II by 3-MA
LC3-II/LC3-I ratio
***
***
OGD 6h
BNIP3-30kD expression
BNIP3-30kD/β -actin
p>0.05
OGD 6h
BNIP3-60kD expression
BNIP3-60kD / β -actin
p>0.05
OGD 6h

B

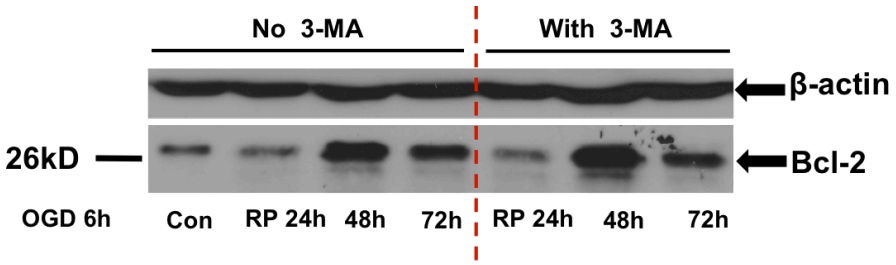
No 3-MA
With 3-MA
β-actin
26kD
Bcl-2
OGD 6h
Con
RP 24h
48h
72h
RP 24h
48h
72h

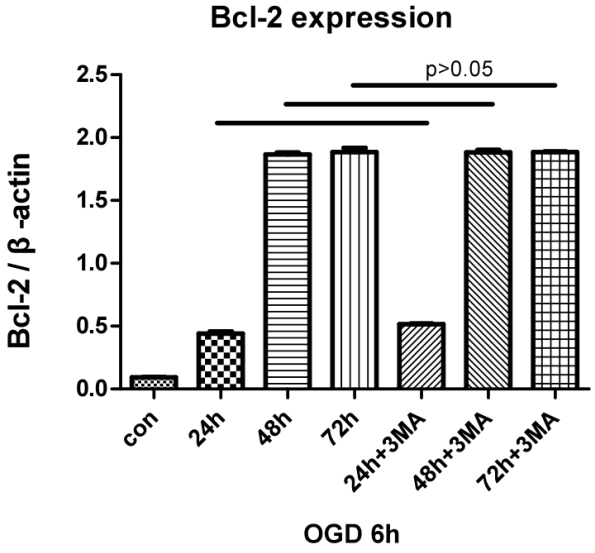
Bcl-2 expression
Bcl-2 / β -actin
p>0.05
con
24h
48h
72h
24h+3MA
48h+3MA
72h+3MA
OGD 6h

Fig 5.7 BNIP3 was an upstream regulator of the neuronal mitophagy pathway in OGD/RP stroke model. 3-MA (1 mM) was added into EBSS solution before OGD treatment on primary cortical neurons. After 6 h OGD, fresh regular culture medium with 1 mM 3-MA was used when neurons underwent prolonged RP (24, 48, or 72 h). Beclin1, LC3, BNIP3 and Bcl-2 expressions in OGD/RP-challenged neurons with or without presence of 1 mM 3-MA were detected by western blot. β-actin (43 KD) was included as internal control. 3-MA (1mM) effectively inhibited the autophagic activity by significantly decreasing the expression of Beclin1 and LC3-II/I ratio, but did not affect the expression patterns of BNIP3 (A) and Bcl-2 (B). Band densities were measured by Quantity One software. One-way ANOVA analysis and Bonferroni post-tests were used for the statistical analyses. No 3-MA group vs with 3-MA group on each time point, $*p < 0.05$, $** p < 0.01$, $*** p < 0.001$. N = 3 for each group.

Chapter 6. Discussion

6.1 Discussion of Chapter 4

In this study, we explored the role of autophagy in the OGD as well as neonatal stroke model. Although autophagy has been investigated in many contexts, it has not yet been directly studied on the OGD-challenged primary cortical neurons. Both hypoxia and hypoglycemia are involved in the ischemic stroke, accordingly we chose the OGD model in cultured cortical neurons as an in vitro approach to mimic the in vivo situation.[134, 135] In addition, during RP period in stroke and brain trauma, inflammation response occurs and causes injury. Because this RP-induced injury is involved in the brain's ischemic cascade and reintroduction of oxygen within cells may cause damage to cellular proteins, DNA, and the plasma membrane,[136] we furthermore detected the effects of reoxygenation to the cultured primary neurons as well as human neuroblastoma cells (SH-SY5Y) in our experiments. We included the well-established human neuroblastoma SH-SY5Y cell line because a remarkable feature of this cell line described so far is the expression of biochemical properties characteristic of normal neuronal cells.[446] Because 3-MA interferes with the MTT assay, we used LDH leakage as an index of cell death after OGD/RP on neurons.[447, 448] We found that our OGD/RP model works well in terms of neuronal damage so far. We therefore consistently used this model in our following experiments.

To determine whether OGD/RP can activate excessive autophagy in cortical neurons, we performed both biochemical and morphological methods combined with various autophagy-related markers. Those markers included specific fluorescent compounds (e.g., AO, MDC, EB, and Fluoro-Jade C) and autophagy marker protein, LC3. All the markers were used alone or in combination in our

OGD/RP model. Autophagosome formation involves the conversion of LC3 (mammalian ATG8) from LC3-I to LC3-II.[440] Cytoplasmic form LC3 (LC3-I) is distributed in the cytoplasm diffusely.[441] During autophagy, processed form (LC3-II) will be transported to the outer membrane of autophagosomes,[440, 442] generating a punctate pattern of LC3 expression. When cytosolic LC3-I is conjugated to phosphatidyl-ethanolamine and forms LC3-II, its molecular weight changes from 18 to 16 kD. Thus, an increase in the amount of the smaller molecular weight LC3-II protein can be detected and the increase in the LC3-II/I ratio can be used as a hallmark of up-regulated autophagy. This process is usually accompanied with an increased number of autophagosomes as well. [440] We detected the intensive signals of multiple AVs, the translocation of LC3-II to autophagosome, and the conversion of LC3-I to LC3-II and found that, at the cellular level, pronounced autophagy could accelerate damaging of cortical neurons.

Autophagic cell death or type II programmed cell death is characterized by extensive autophagic degradation of cellular organelles before nuclear destruction.[196, 197] The most representative morphological feature of autophagic cell death is the formation of numerous autophgic vacuoles or autophagosomes in the cytoplasm with condensed nucleus.[198] By transmission electron microscopy, we observed occurrence of abundant AVs in the cytoplasm, and numerous double-membrane autophagosomes formed in neurons after OGD/RP treatment. Using MDC as a specific marker for AVs and Fluoro-Jade C for degenerating neurons to identify and quantify neurons undergoing autophagic cell death after OGD/RP injury. Fluoro-Jade C, like its predecessors Fluoro-Jade and Fluoro-Jade B, was found to stain all degenerating neurons, regardless of insults or mechanisms of cell death. Specifically, Fluoro-Jade C exhibited a stain of maximal contrast and affinity

for degenerating neurons.[449] We demonstrated that prolonged RP following OGD resulted in a significant increase of autophagic neuron death rates.

Degradation and recycling of cellular constituents by autophagy is a continuous process that is usually described as "autophagic flux." To measure autophagic flux, as compared to steady-state levels of AVs, LC3-II turnover is measured at different time points in the presence and absence of a lysosomal inhibitor, NH4Cl.[191, 450, 451] We proved that NH4Cl prevented the degradation of LC3 in autophagosomes, and led to the accumulation of LC3-II after OGD/RP treatment. The amount of LC3-II that was elevated in response to the presence of degradation inhibitor represented an estimate of flux. Rapamycin (mTOR inhibitor), which mimics cellular starvation by blocking signals required for cell growth and proliferation, has become one of the most widely used autophagy inducers.[452, 453] We used rapamycin as a positive control and found the ratio of LC3-II to LC3-I increased dramatically when compare to the control group.

BECN1, the mammalian homologue of yeast Atg6, was first described as a Bcl-2-interacting protein and was formerly found to promote autophagy.[440] Cells with reduced BECN1 expression exhibit decreased autophagic activity.[404, 443] A dramatic elevation in BECN1 has been found in the penumbra of rats after cerebral ischemia.[444] As expected, we found that after OGD/RP, BECN1 expression in the cortical neurons and SY5Y cells were up regulated. Alternations in the levels of BECN1 protein in both cells occurred after 6 h OGD, and the expression kept increasing for at least 3 days of RP (Figure 4.4E-G). Interestingly, the time courses and levels of BECN1 expression correlated well with the increase of LC3-II to LC3-I ratios.

We believe that autophagy plays a death-promoting role in neuronal death after

stroke because the introduction of autophagy inhibitor, 3-MA showed obvious neuroprotective effects at the late stages of OGD/RP. This result was in agreement with Puyal and Clarke's study that postischemic intracerebro-ventricular injections of the autophagy inhibitor 3-MA blocked the ischemia-induced increment in LC3-II and powerfully reduced the lesion volume by 46%.[202] We observed the dual role of 3-MA in different stage of reoxygenation: before 24 h 3-MA triggered a higher neuronal death rates, whereas after RP 48 h and 72 h, 3-MA significantly protected neurons from dying. We believe that prolonged OGD/RP triggers autophagy to switch its role from protective to death inducing in a sequential manner. After a shorter time of RP, the role of autophagy is primarily to eliminate damaged organelles to rescue cells. Although prolonged RP triggers massive autophagy leading to autophagic cell death. As a consequence, inhibition of autophagy at an early stage may lead to further cell damage when compared to inhibition at a later stage. Our results showed the early stage (protective autophagy) lasted for around 1 day after OGD injury before autophagic cell death occurred.

BECN1 was expressed in many areas including cerebral cortex, hippocampus, and cerebellum in the rat brain.[203, 454] In neonatal cerebral H/I (unilateral common carotid artery ligation followed by whole-brain hypoxia) on postnatal day 7 rat pups, we demonstrated upregulation of BECN1 in the cortex, which lasted for several days and peaked at 7 days postischemia. We detected only one band of LC3. There was no obvious change in the LC3 density on the ipsilateral sides of ischemic brains. This is in accordance with the result of Adhami et al.[201] The lack of second bands of lipid-conjugated form of LC3 and parallel increase in LC3 density on the Western blot level might be because of the rapid turnover of LC3 proteins by autophagosome-lysosome processing after the H/I

insult.

In a recent article, we showed the contribution of BNIP3, a death-inducing mitochondrial protein, to delayed neuronal death following stroke.[237] In this chapter, we further confirmed for the first time that BNIP3 could competently interact with Bcl-2, release BECN1 to induce the excessive autophagy in neuronal ischemia/hypoxia injury (Figure 4.7). This conclusion was in agreement with Zhang et al.'s hypothesis.[407] Elmore et al. and Twig et al. have provided evidence that BNIP3 could trigger mitochondrial depolarization and cause mitochondrial autophagy and clearance.[272, 273] Alternatively, as loss of mitochondrial permeability transition would induce autophagy (mitophagy), BNIP3 might also induce autophagy indirectly as a consequence of such mitochondrial injury.

In summary, we systematically studied the extent to which autophagy contributes to neuronal death in cerebral hypoxia and ischemia. We showed that autophagy was dramatically increased in neurons after H/I injury. The increase of autophagy was accompanied with an increment of autophagic neuronal death. Inhibition of autophagy significantly reduced autophagic neuronal death. Our data suggests that excessive autophagy is a contributing factor of neuronal death in cerebral ischemia.

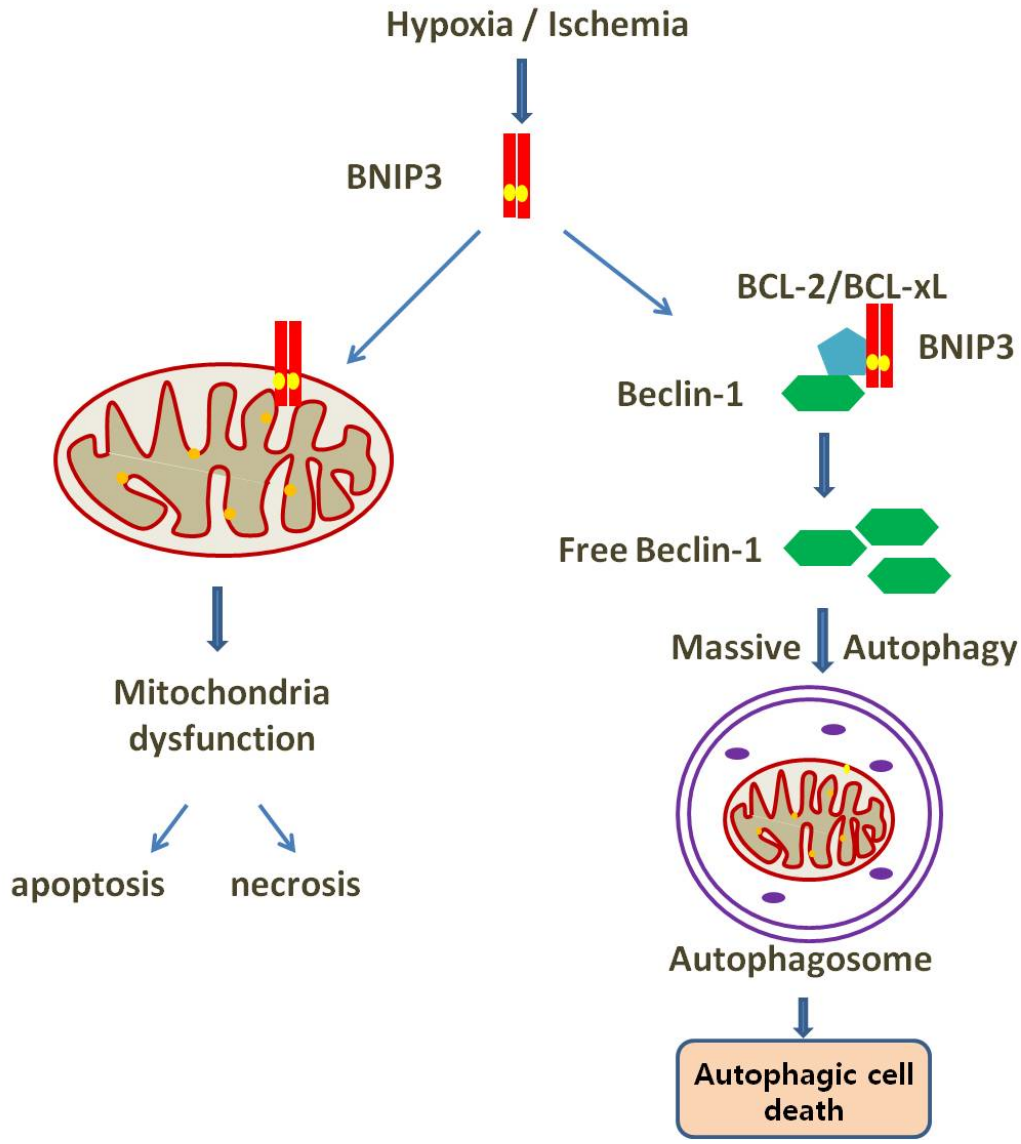

Fig 6.1 Molecular pathways regulating BNIP3 expression and autophagic cell death in hypoxia/ischemia-challenged neurons

6.2 Discussion of Chapter 5

In the present study, we have revealed a novel protective effect of knocking out BNIP3 in the response of cortical neurons to ischemic stroke. This beneficial effect is possibly through inhibition of mitophagy by decreasing interacting with LC3, as mitochondria membrane markers were strongly preserved in BNIP3 KO mice after I/H injury. Concurrently, autophagic markers such as Beclin 1, LAMP2, LC3II/I ratio were upregulated in BNIP3 KO cortical neurons after OGD, which suggests the enhanced activation of neuronal autophagy. In contrast, the autophagy activation is associated with a decreased apoptosis in KO cortical neurons.

Neonatal stroke, a type of stroke occurs in the newborn brain, is responsible for neonatal mortality and neurodevelopmental disability. [86, 398, 455-457] Similarly, perinatal stroke, which refers to the cerebrovascular lesions that occur from 20 weeks' gestation to 28 days after birth, will also cause life-long deficits to the affected children. [88] Major risk factor for neonatal strokes focuses on perinatal asphyxia. [88, 90] In this study, we slightly modified the Rice-Vannucci's model [93] by combining a unilateral common carotid artery ligation with a 30 min hypoxic treatment (in 8% O2) on postnatal day 7 mice pups, to mimic the clinical situation in human perinatal asphyxia. Compelling evidence shows that 7-day-old mice pup has brain maturity equivalent to that of an early third trimester human fetus, [92, 94] and with a body size that is easier for surgery conduction and handling. Additionally, extremely immature pups (postnatal day 1-2) are more resistant to the I/H injury compare to the older ones, with brain damages mainly in the subcortical developing white matter including oligodendrocyte progenitors and subplate neurons. [92, 412, 413] Hence, we selected to use 7-day-old pups rather that younger ones in order to match our study interest on the post-ischemic grey-matter damage. Besides a strong clinical relevance,

our *in vivo* stroke model also fulfills several other criteria listed by Aysan Durukan et al. as for the 'ideal' stroke modeling. [16] For example, the surgical technique used is relatively easy and less invasive; the cost and effort put on the modeling is reasonable. Particularly, in order to maintain the ischemic lesion size reproducible, and keep the physiological parameters monitored within a normal range, we performed all the surgeries consistently on a thermostatically controlled heating platform to avoid potential hypothermia during the procedure. Considering that neuroprotection of moderate hypothermia in neonatal strokes has been revealed in many ongoing trials,[458-461] we strictly monitored the body temperature at 37°C all through the time until pups recovered from surgery. We confirmed that this model reliably gave a well-defined lesion and brain damage.

In order to visualize and quantify the ischemic brain infarct, we selected a direct macrometric measurement of brain infarct volume by 2, 3, 5-triphenyltetrazolium chloride (TTC) staining on freshly prepared brain sections. TTC was reduced by succinate dehydrogenase in living brain tissue into a red, lipid-soluble form, while infarcted or dying tissue remains unstained. [414, 462] This method is advantageous by offering a fairly sharp contrast between damaged and healthy brain areas as early as 3 h in rats, [414, 463] and 12 h in mice. It is easy to handle and is so far the most widely used technique for direct visualization of brain infarction in stroke studies. [73] According to Gaudinski et al. and Van der Worp et al., brain infarct volume at early and late time points after ischemia can be enormously different. Cerebral edema pronounces 2-3 days after acute stroke, enlarging the normal tissue and the infarct volume to a great extent. Conversely, after one-week's recovery, decreased brain edema, together with the neuronal loss and scar formation will shrink the original infarct size. [464, 465] As a consequence, when we were comparing the

infarct volumes at various time points post-injury, the adjusted total hemispheric infarct volumes were calculated. The equation used is CIV=[LT-(RT-RI)] × d, where CIV is the corrected total infarct volume, LT is the area of the left hemisphere, RT is the area of the right hemisphere, RI is the infarct area, and d is the slice thickness (2 mm). [416, 417] Relative infarct volume was also calculated as a percentage of the whole brain volume.

Although neonatal brain is more resilient to acute ischemic insult in general, a broad delayed neuronal death in ischemic penumbra area is still inevitable. Preventing this continued neuronal loss is the key for clinical interventions but related knowledge is still incomplete. In this study, we hypothesized that I/H-induced excessive mitophagy may contribute to this progressed neuronal damage. Mitophagy, the specific autophagic elimination of mitochondria, regulates mitochondrial number to match metabolic demand and is core quality control machinery necessary for the removal of impaired mitochondria. [262] This selective degradation of mitochondria is of particular importance to neurons, because of their constant demand for high levels of energy production. Emerging evidence indicates impaired mitophagy plays an important role in CNS diseases. [408, 409] Intriguingly, however, mitophagy like autophagy not always be protective, as increased mitophagy leads to rapid Purkinje cell death. [410] Therefore, mitophagy can be regarded as a double-edged sword: it plays a protective role when activated by mild physiological stressors, whereas it plays a lethal role when over-activated by a severe pathological stress such as ischemia. [405] Given the importance of precise regulation of mitochondrial turnover in the nervous system, how mitophagy is initiated and regulated represents an area of considerable interest.

BNIP3 (Bcl-2/adenovirus E19 kD interacting protein 3) is a pro-apoptotic BH3-only protein that is associated with mitochondrial dysfunction and cell death. It has been proven that at least one form of neuronal death is activated by BNIP3. [237, 246, 466] Recent studies from our laboratory show that the death gene BNIP3 plays a role in neuronal death in hypoxia and stroke: BNIP3 is highly expressed in the middle cerebral artery occlusion (MCAO) animal model of stroke and in cultured primary neurons exposed to hypoxia, and inhibition of BNIP3 reduces hypoxia-induced cell death. [237] In transformed and cancer cells, expression of BNIP3 induces "non-apoptotic" cell death that is characterized by localization to the mitochondria, opening of the permeability transition pore, loss of membrane potential and reactive oxygen species production. Particularly, BNIP3-induced cell death is independent of caspase activation and cytochrome C release from the mitochondria in these circumstances. [178] On the other hand, BNIP3 is also reported as a potent autophagy inducer in many cells. [466] BNIP3 over-expression induces autophagy, while expression of BNIP3 siRNA or a dominant-negative form of BNIP3 reduces hypoxia-induced autophagy in cancer cells. [342] Several studies have also postulated a possible link between BNIP3 and mitophagy, however, none has precisely elucidated how BNIP3 mediates the mitophagy machinery. Interestingly, BNIP3L (NIX) directly interacts with LC3 on isolation membrane and in this way mediates the binding and sequestration of mitochondria into autophagosomes. [262, 268, 269, 411] Whether BNIP3 mediates a similar function as NIX has not yet been determined and forms the basis of the current study. [257, 403, 411] Fortunately, we obtained a powerful tool of the homozygous BNIP3 knockout mice ($BNIP3^{-/-}$) as well as their Wild type counterparts ($BNIP3^{+/+}$ in B6; 129 strain) for our investigations. Dr. Spencer B. Gibson, who shared a common interest on autophagy and BNIP3 pathways in cancer

research, provided us with the access to these transgenic animals. Later on, we primarily focused on studying BNIP3 WT and KO neuronal tissues in both *in vitro* and *in vi*vo stroke models. By making comparison and contrast to their responses to the I/H injury, we elucidated the potential underlying mechanisms as discussed in the following sections. Noticeably, the BNIP3 KO mice do not present any obvious behavioral or functional deficits as compared to the WT mice. The only structural difference that has been recorded between these two genotypes was a relatively higher astrocyte level with a comparable neuronal level in the brains of KO mice. [424, 467]

Under normal conditions, BNIP3 is not detectable in cortical neurons (Figure 5.3A, B and D), and at a very low level in glial cells of brain tissues (Figure 5.3C, E). However, BNIP3 is induced to express after stroke in a "delayed" manner, and is the only death-inducing gene that has been identified to have this "delayed" expression pattern in response to I/H. [237] Once expressed, monomer BNIP3 (30 kD) is homodimerized into its dimer form (60 kD). The later one integrated to the outer membrane of mitochondria and induced mitochondrial permeability transition, subsequently leading to release of intermembrane pro-apoptotic proteins. In cultured primary neurons, BNIP3 started to accumulate after 6 h OGD followed by 24 h RP, and the levels significantly increased to more than 10 folds after 72 h RP (Figure 5.3B, D). Immunocytochemistry results also verified the 'delayed' expression of BNIP3 in OGD/RP-challenged BNIP3 WT cortical neurons (Figure 5.3A top panel). In the neonatal stroke model, expression of BNIP3 was low for up to 1 day but started to accumulate after 3 or 7 days recovery. The active form of BNIP3 (60 kD), which was membrane-bound and localized to mitochondria, was also expressed in a similar way in the WT tissues (Figure 5.3C, E). Here a supposed 100% silence of the BNIP3 gene was confirmed in the KO ($BNIP3^{-/-}$) neurons and brains, as no signals or bands of

BNIP3 were detected using both immunofluorescence and western blot approaches (Figure 5.3A bottom panel, D, and E).

Several studies have reported that BNIP3 gene family might play important roles in mediating mitophagy and mitochondrial quality control. [257, 403, 411] BNIP3 gene family is a unique subfamily of the BH3-only members of the Bcl-2 family, which includes BNIP3, NIX (BNIP3 like protein X, also called BNIP3L), BNIP3h and a Caenorhabditis elegans ortholog, ceBNIP3. [468] NIX shares a high amino acid homology (~56%) with BNIP3, and both could homodimerize and localize to mitochondria through their transmembrane (TM) domains. [245] To date, multiple lines of evidence supports the essential role of NIX in developmental removal of mitochondria during erythrocyte maturation, [270, 271] but remain applications of NIX-mediated mitophagy are still unknown. In addition, recent evidence also shows that both NIX and BNIP3 can trigger mitochondrial depolarization, which is sufficient to initiate the phase of mitophagy. [272, 273] Our data showed that total mitochondrial proteins lost dramatically with the activation of BNIP3, but were well preserved when BNIP3 was completely silenced after both *in vitro* and *in vivo* stroke modeling (Figure 5.2D-E), implying BNIP3 gene silence decreased the mitochondrial elimination, or in other words, BNIP3 expression increased mitochondrial degradation by mitophagy in brain I/H. Although mitophagy refers to a selective targeting on mitochondria, the core autophagic machinery of autophagosome formation and a later lysosomal fusion is unchanged. Therefore, we expected to observe a co-localization between autophagosome and their engulfed mitochondria in an ongoing mitophagy process. A significantly lower co-localization rate of mitochondria with autophagosomes was observed in the BNIP3 KO neurons especially after prolonged reperfusion for 72 h (Figure 5.2A-C). We found mostly a

proximate localization but not co-localization of mitochondria with autophagosomes inside the KO neurons, suggesting a potential receptor-mediated fusion of these two organelles inside the WT neurons. In addition, by using TEM, we successfully demonstrated induced mitophagy in WT cortical neurons treated by OGD 6 h plus 72 h reperfusion (Figure 5.2F a-k), when the BNIP3 was expressed at the highest level. A forming autolysosome, which encompassed an inside mitochondrion (also known as the mitophagosome), was identified to demonstrate the continuing process (Figure 5.2F k). This result was in agreement with S Rikka et al.'s data that extensive mitophagy can be observed by EM in cells overexpressing BNIP3. [469]

Possible mechanisms have been proposed to explain how BNIP3L (NIX) regulates mitophagy. [257, 403, 411] These include NIX directly interacts with LC3 on isolation membranes through its WXXL-like motif, mediates the binding and sequestration of mitochondria into autophagosomes. [262, 268, 269] Besides the higher structural similarity between NIX and BNIP3, our data has confirmed that BNIP3 also functionally alike NIX, as BNIP3 was activated in I/H-challenged cortical neurons and neonatal brain tissues with an incremental pattern similar to that of NIX (Figure 5.3D-E). Particularly, NIX was further upregulated and expressed at a higher level in BNIP3 KO tissues at each time point post-ischemia, indicating an evident compensation for the loss of BNIP3. On the other hand, although NIX expression is elevated due to the loss of BNIP3, it cannot fully compensate for the loss of BNIP3's functions. When BNIP3 was silenced, mitophagy levels remained stable at each time point after I/H and were not affected by the dramatic upregulation of NIX in KO tissues (Figure 5.2D-E), implicating a functional discrepancy of these two homologues on mitophagy. Thus, we infer that NIX has a major function in

maintaining a basal/physiological level of mitophagy, whereas BNIP3 exclusively regulates the excessive/pathological mitophagy in brain I/H.

In light of the close resemblance between BNIP3 and NIX, a similar mechanism was found in which BNIP3 regulates the excessive mitophagy through binding to LC3. By using co-ip assays, we firstly confirmed direct interactions between NIX and LC3 in our stroke models as positive controls (Figure 5.4B). Later, we demonstrated BNIP3 successfully pulled down LC3-I/II by directly interacting with autophagosome-localized LC3-II; whereas LC3 only pulled down mitochondria-localized BNIP3 homodimer, suggesting that LC3 interacted specifically to the 60 kD mitochondria-localized BNIP3 (Figure 5.4C). Additionally, the interactive intensities between NIX and LC3-II, BNIP3 and LC3-II were proven to increase after I/H (Figure 5.4D-G). These enhanced interactions between mitochondria-localized BNIP3 with autophagosome-localized LC3 may subsequently contribute to the induction of excessive mitophagy (Figure 6.2B). It bears mentioning that NIX-induced mitophagy has a physiological role in most situations, but in others NIX may contribute to cell death as BNIP3 does. [411] However, it is still uncertain if death is always caused by excessive mitophagy, or if it is also influenced by the pro-apoptotic natures of these two proteins.

Nevertheless, another interesting finding of the present study is the significantly enhanced activation of autophagy in primary cortical neurons of BNIP3 KO mice after OGD (Figure 5.6). The role of autophagy in regulating cell death in response of stroke remains equivocal. During the early stage of stroke, autophagy was considered to alleviate the acute shortage of energy and oxygen supply. [470] In agreement with that, various autophagic markers used to determine the general autophagy levels were significantly upregulated in both BNIP3 WT and KO neurons,

but expressed higher in KO neurons at each time point (Figure 5B). Since it has been reported that an alternative spliced variant of LAMP-2, the LAMP-2A protein, is a receptor for chaperone-mediated autophagy on lysosomes, [278, 279, 445] we expected and did find increased lysosomal activation in KO neurons as well (Figure 5.6F). Mitophagy is an organelle-specific autophagic process, which constitutes a portion of total, general autophagy. Therefore, the distinct responses to stroke in mitophagy and general autophagy after silencing BNIP3 may reflect different underlying mechanisms: BNIP3-dependent mitophagy and BNIP3-independent general autophagy.

As a member of the Bcl-2 family that regulates apoptosis, BNIP3 contributes to the downstream release of pro-apoptotic effecters and promote the apoptotic response. [471, 472] It has been reported that overexpression of BNIP3 induced mitochondrial dysfunction and cytochrome C release in wild-type MEFs (mouse embryonic fibroblasts). In contrast, down-regulation of BNIP3 using RNA interference decreased activation of Bax during ischemia/reperfusion injury in myocytes. [471] Our data confirmed that BNIP3 gene silence reduced the apoptosis in OGD/reperfusion-challenged neurons, which was characterized by the down-regulation of various pro-apoptotic proteins (i.e. active caspase 3, BAX and cytochrome c) and anti-apoptotic protein (i.e. Bcl-2) in the BNIP3 KO neurons (Figure 5.5). However, it is unclear why BNIP3 silencing-induced inhibition of apoptosis was also associated with activated general autophagy, and what the consequences imply for stroke. Since the overall infarct size in the BNIP3 KO mice was significantly decreased as compared with the WT mice (Figure 5.1), it is reasonable to assume that the protective effect of knocking out BNIP3 in neurons is likely attributable to its inhibition of BNIP3-dependent mitophagy and apoptosis.

For decades, it has been accepted that the neurological dysfunctions caused by I/H insults following stroke are mainly due to the massive loss of neurons by apoptosis or necrosis. [398, 473] Until recently, several novel lines of evidence pointed out that neuronal cell damage following stroke also involves the activation of autophagy, triggering the specific "autophagic cell death" or "type II programmed cell death" (PCD II). [193-195] This specific type of cell death is characterized by the formation of numerous autophgic vacuoles or autophagosomes in the cytoplasm with condensed but not fragmented nucleus. [198] Recently, a crosstalk between apoptosis and autophagy has been proposed. Maiuri et al. believed that autophagy and apoptosis could be triggered by common upstream signals. Sometimes a mixed phenotype of both cell death patterns is visible, in many other instances, the neuron may switch between the two responses in a mutually exclusive manner as a result of variable thresholds, or as a result of a cellular 'decision' between the two responses. The same group also proposed that merely inhibit one type of these two mechanisms will switch the cellular response towards the other one and both catabolic events can inhibit each other. [176] Interestingly, this theory well explained why the complete silence of pro-apoptotic gene BNIP3 triggered a much more pronounced autophagy response in OGD/RP-challenged neurons (Figure 6.2A). Our finding was also in accordance with the result of Li Yu et al., as they found caspase inhibitors arrested apoptosis but also had the unanticipated effect of promoting autophagic cell death. [203] Oppositely, Yousefi, S. et al. proved that Calpain-mediated cleavage of Atg5 could switch autophagy to apoptosis. [204] Although several pathways that link the apoptotic and autophagic machineries have been deciphered at the molecular level, [205] however, the current knowledge on the molecular interactions between the apoptotic and autophagic pathways is still incomplete and awaits for further investigations. [176]

3-methyladenine (3-MA), a PI3K inhibitor, functions at an early stage of autophagic pathway by efficiently inhibiting the formation of autophagosome, was used as the specific autophagy inhibitor in this study. [474] 3-MA acts on the autophagic-lysosomal protein degradation [428, 429] and is useful in defining the role of autophagy under various pathological conditions, such as cerebral ischemia. [193, 429] Based upon our observation that BNIP3 expression was not affected after 3-MA treatment (Figure 5.7), we postulated that BNIP3 activation and translocation to mitochondria was the upstream of autophagosome formation and/or mitophagy initiation. Furthermore, the early stage of protective autophagy was proved to last for around one day after OGD before lethal autophagy occurred (Figure 4.5C). Combining with the 'delayed' expression features of BNIP3 in response to I/H, we inferred that the postponed expression of BNIP3 further enhanced downstream interactions between mitochondrial-localized BNIP3 (60 kD) and autophagosome-localized LC3, triggering excessive mitophagy, and contributing to the switch from protective autophagy to the death-inducing mitophagy. Consequently, by manipulating the extent of BNIP3 activation and mitophagy induction on different time windows, we may seek for potential approaches to reduce neuronal damage caused by I/H insult.

We also found that the total infarct volumes of BNIP3 WT mice brains increased continuously during the first week of recovery, and slightly decreased after a long-term recovery at 28 days. In contrast, the total brain infarct volume of KO pups peaked at post-ischemia 1 day, and then dramatically decreased in the following recovery period (Figure 5.1). Particularly, only small areas of scar tissue can be detected in KO brains after 7 and 28 days' recovery. This result leads us to hypothesize that BNIP3 gene silence not simply exert neuroprotection against I/H

injury, but also promotes the long-term neurorepair and neurorestoration capacity of brain, especially in the neonatal situation. Although accumulating evidence suggests that P6-P10 rats or mice subjected to moderate I/H show neuronal proliferation primarily in the subventricular zone (SVZ) of brain, [475-477] nevertheless, neuronal proliferation in the cortical region has also been confirmed after 1-4 weeks' recovery. [478-480] Either proliferating cells migrate from the SVZ to the cortex or that local progenitor cells proliferate due to the molecular regulation, cortical neurogenesis could always occur to compensate for the neuronal loss after I/H insult. [481] To date, very few evidence has proved that BNIP3 is one of those endogenous modulators for the neurogenesis after brain I/H. Our results from the neonatal stroke model demonstrated knocking out BNIP3 may promote the long-term neurogenesis up to 28 days. This could be explained by the death-inducing nature of BNIP3; i.e., under I/H conditions, delayed expression of BNIP3 contributes substantially to the caspase-dependent or -independent neuronal death, inhibiting progenitor cells from producing enough neurons for the tissue repair. When BNIP3 is silenced, BNIP3-mediated cell death could be wiped out, leaving more progenitors proliferate for the necessary tissue restoration.

It bears mentioning that in all the immunocytochemistry experiments, we used the "BacMam 2.0" gene delivery and expression technology from Invitrogen, by inducing baculovirus-mediated transduction of LC3II-GFP gene into primary cortical neurons. This technology uses a modified insect cell baculovirus as a vehicle to efficiently deliver and express genes in mammalian cells with minimum effort and toxicity. In addition to producing ready-to-use viral stocks, this technology has many advantages when compared to the Lipofectamine 2000 and other viral delivery methods. For instance, it produces high transduction efficiency across a broad range

of cell types including primary and stem cells, and a highly reproducible and titratable transient expression. Since baculovirus is not pathogenic to vertebrates and does not replicate in mammalian cells, it is safe for handling with only a biosafety level 1 rating, and can be used to simultaneously deliver multiple genes (Refers to the Instruction Manual from Invitrogen). In our studies, we consistently used the multiplicity of infection (MOI), the number of viral particles per cell as low as 4 for the gene transduction on both SH-SY5Y cells and primary cortical neurons. When the transduction was induced at a cell confluency of ~70%, a maximum transduction efficiency of 70-80% can be detected for best results.

In conclusion, we have demonstrated a novel and crucial role of BNIP3 in regulating the excessive mitophagy and cell death in neonatal stroke, which provides important context and targets for overall outcomes in ischemic cerebral infarct. Further studies are needed for molecular dissection of the mitophagy pathways during the delayed progression of ischemic brain damage. Detailed characterization of BNIP3's function in mitophagy would also provide clues to the emerging questions related to mitophagy.

A

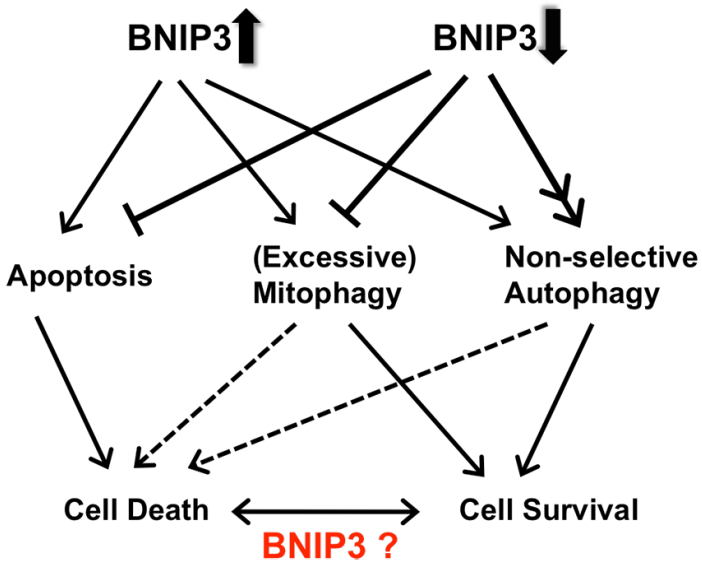

B

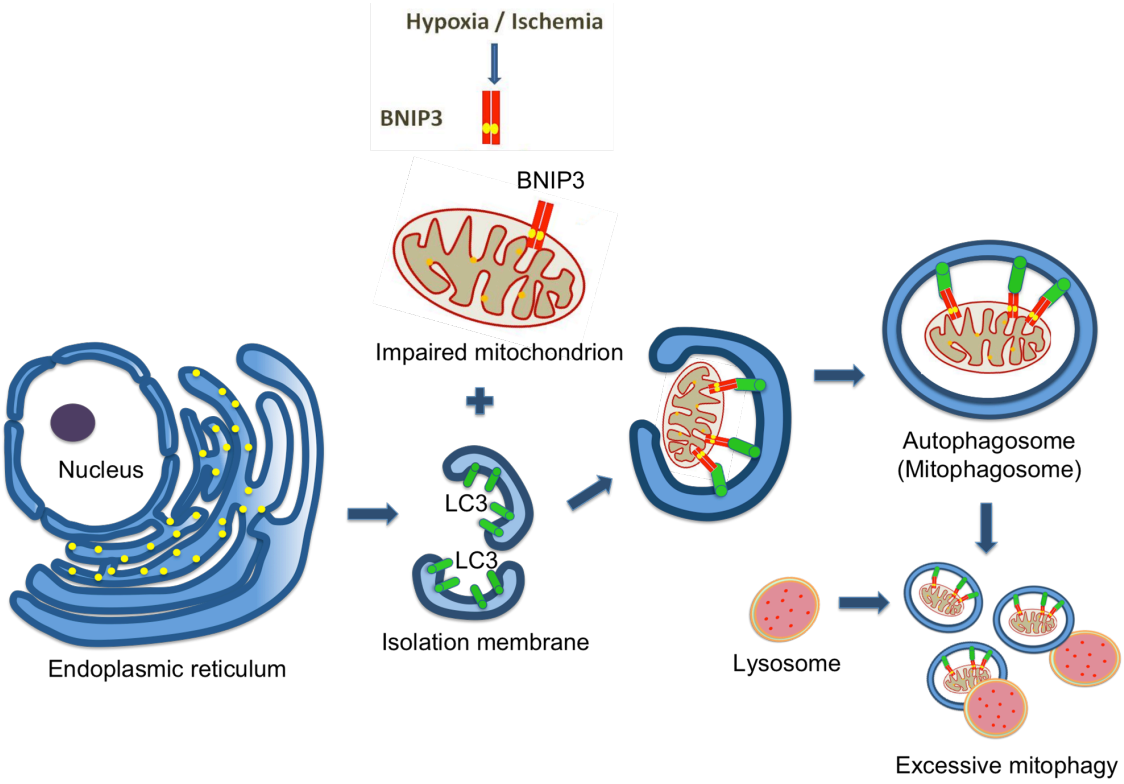

Fig 6.2 BNIP3 regulated mitophagy by interacting with LC3 in the delayed neuronal death in stroke. (A) Interactions between apoptosis, (excessive) mitophagy, general (non-selective) autophagy, cell death and cell survival when BNIP3 gene is upregulated (Left) and downregulated (right) in the stroke models. (B) Pathway depicted BNIP3's interaction with LC3 on the isolation membrane, and subsequent initiation of mitophagy machinery.

Chapter 7. Conclusions and Future Directions

Autophagy is a highly regulated process that involves the degradation of a cell's cytoplasmic macromolecules and organelles in mammalian cells by the lysosomal system. It plays a normal part in cell growth, development, and homeostasis, helping to maintain a balance between the synthesis, degradation, and subsequent recycling of cellular products. Studies reported that autophagy had a neuroprotective role. For example, suppression of basal autophagy in neural cells causes neurodegenerative disease in mice, and insufficient autophagy contributes to pathogenesis in Huntington's disease, Alzheimer disease, and amyotrophic lateral sclerosis.[402-404, 451, 482-485] Other studies, however, suggest that accelerated autophagy might contribute to neuronal death in various pathological conditions including cerebral ischemia.[31, 193, 199, 201] However, controversies exist whether increased autophagic activities contribute to autophagic neuronal death.[405]

In the first part of this study (Specific Objective #1), we aimed to investigate the activation of autophagy in primary cortical neurons and its contribution to ischemia/hypoxia (I/H) induced neuron death. I/H injury was induced by oxygen and glucose deprivation (OGD) followed by reperfusion (RP) on primary cortical neurons *in vitro*. Cerebral ischemia was induced by unilateral common carotid artery occlusion and hypoxia in neonatal rats *in vivo*. Using a combination of techniques and models, we observed a dramatic increase of autophagy in human neuroblastoma cells and in primary cortical neurons after I/H injury, which paralleled to the increment of autophagic neuron death rates. Inhibition of autophagy with 3-methyladenine (3-MA) significantly reduced neuronal death. Our data suggests that excessive

autophagy is a contributing factor of neuronal death in cerebral ischemia and hypoxia.

Our *in vivo* results, in conjugation with previous studies in a permanent middle cerebral artery occlusion model, **[193]** a transient focal cerebral ischemia model, **[374]** and an adult I/H brain injury model, **[199]** confirmed the involvement of excessive autophagy in I/H-induced brain injury. Our work systematically studied the direct effects of I/H injury-activated autophagy and autophagic cell death on primary cortical neurons for the first time. This study provides practical guidance as well as important implications for future investigations. Searching for potential target that may involve in regulation of autophagy and autophagic neuron death will be a promising direction derived from it. Given the results that late stage inhibition of autophagy may provide neuroprotection, we determined to take BNIP3, a well established delayed neuronal death mediator, and other intermediate autophagy-related proteins as our first candidates. Considering our lab's experience in elucidating BNIP3-mediated cell death pathways and based on our recent published data, studies looking into possible neuroprotective ways in which to inhibit such delayed neuron death will give certain therapeutic implications.

In the second part of this study (Specific Objective #2), we evaluated the contribution of BNIP3, a member of a unique subfamily of death-inducing mitochondrial proteins, to delayed neuronal death following stroke and provided evidence that BNIP3 was markedly upregulated in a 'delayed' manner after cerebral ischemia. It is known that BNIP3-induced neuronal death is caspase-independent and characterized by early mitochondrial

damage. According to previous work, BNIP3 can trigger mitochondrial depolarization, which in turn causes mitophagy. [272, 273] This led us to consider the possibility that BNIP3 regulates the autophagic neuron death by interacting with mitophagy pathways in I/H incident. Although several existing studies have proposed the links between BNIP3 and mitophagy, none of them has provided solid data in supporting a precise mechanism by which BNIP3 mediates mitophagy and mitophagic cell death. Our results in both *in vitro* and *in vivo* stroke models convinced our hypothesis. We confirmed a strong direct interaction between mitochondria-located BNIP3 (60kD homodimer) and autophagosome-localized LC3 by co-ip and ELISA, indicating BNIP3 was an effective LC3-binding target on damaged mitochondria. So BNIP3 may act as a receptor for targeting damaged mitochondria to autophagosomal elimination. Alternatively, as loss of mitochondrial permeability transition induces mitophagy, BNIP3 may also induce mitophagy indirectly as a consequence of mitochondrial injury. We also showed a significant neuroprotection of BNIP3 gene silence in both stroke models. Inhibition of autophagy by 3-MA didn't affect the expression patterns of BNIP3, indicating that BNIP3 was an upstream regulator of the excessive mitophagy pathway. In conclusion, our results proved for the first time that BNIP3 directly interacted with LC3, triggered a switch from the protective autophagy to the death-inducing mitophagy in the delayed neuronal death in stroke.

Future studies need to be focused on elucidating the detailed mechanisms of BNIP3-mediated mitophagy pathways. For example, the extent to which BNIP3 expression induces mitophagic neuron death can be

determined. BNIP3/BNIP3ΔTM lentivirus expression vectors will be used to examine the effect of BNIP3 over-expression. The mouse cortical neurons will be transfected on day 8 in culture with a lentiviral vector carrying the full-length mouse BNIP3 gene. Neurons transfected with a lentiviral vector carrying the truncated form of BNIP3 (BNIP3ΔTM) or the empty lentiviral vector will be used as controls. The co-staining of mitochondrial markers and BNIP3 and the quantitative measurements will be performed. This approach will allow me to detect the positive correlation between BNIP3 expression and mitophagy activation, and also test the role of ΔTM domain (which targets BNIP3 to mitochondria) in BNIP3's capacity in regulating mitophagy. In addition, knockdown BNIP3 by using RNAi technique will also be conducted. Previously we identified a BNIP3 microRNA to inhibit the expression of BNIP3. This small RNA was inserted into lentiviral vectors suitable for transduction into neurons. Thus, transduction of this miRNA would allow me to examine the effect of BNIP3 inhibition in I/H-induced neuronal mitophagy and mitophagic neuron death.

Last but not least, it will be extremely helpful to measure changes of mitochondrial functional parameters (e.g. ATP production; mitochondrial membrane potential; ROS production et al.) upon the BNIP3 over-expression or down-regulation or complete silence. In this way, I could further determine the extent to which BNIP3 regulates the mitochondrial physiology dynamically through the mitophagy pathways. Besides the pathway that was elucidated in this study, I plan to further investigate whether BNIP3 could trigger mitophagy by competitively disrupting the inhibitory interaction between Bcl-2 and Beclin 1,[329, 339] and the potential significance of this

alternative mitophagy pathway in the delayed neuronal death in stroke. The long-term outcome of the project is to establish novel cell-death pathways and to identify the organelle-specific therapeutic targets for stroke victims.

References

1. Sims, N.R. and H. Muyderman, *Mitochondria, oxidative metabolism and cell death in stroke.* Biochim Biophys Acta, 2010. 1802(1): p. 80-91.
2. Mathers, C.D., T. Boerma, and D. Ma Fat, *Global and regional causes of death.* Br Med Bull, 2009. 92: p. 7-32.
3. Donnan, G.A., et al., *Stroke.* Lancet, 2008. 371(9624): p. 1612-23.
4. Casals, J.B., et al., *The use of animal models for stroke research: a review.* Comp Med, 2011. 61(4): p. 305-13.
5. B, D.V., *Sur la signification morphologique des artères cerebrales.* Arch Biol 1905. 21(21): p. 357-457.
6. Vrselja, Z., et al., *Function of circle of Willis.* J Cereb Blood Flow Metab, 2014.
7. Windle, B.C., *The Arteries Forming the Circle of Willis.* J Anat Physiol, 1888. 22(Pt 2): p. 289-93.
8. A, M., *Neuroanatomia funcional.* Rio de Janeiro (Brazil): Atheneu, 1988.
9. Fisher, C.M., *The arterial lesions underlying lacunes.* Acta Neuropathol, 1968. 12(1): p. 1-15.
10. Shuaib, A. and V.C. Hachinski, *Mechanisms and management of stroke in the elderly.* CMAJ, 1991. 145(5): p. 433-43.
11. Stam, J., *Thrombosis of the cerebral veins and sinuses.* N Engl J Med, 2005. 352(17): p. 1791-8.
12. Bamford, J., et al., *Classification and natural history of clinically identifiable subtypes of cerebral infarction.* Lancet, 1991. 337(8756): p. 1521-6.
13. Bamford, J.M., *The role of the clinical examination in the subclassification of stroke.* Cerebrovasc Dis, 2000. 10 Suppl 4: p. 2-4.
14. Ross, S., et al., *Postmortem whole-body CT angiography: evaluation of two contrast media solutions.* AJR Am J Roentgenol, 2008. 190(5): p. 1380-9.
15. Wain, R.A., et al., *Angiographic criteria reliably predict when carotid endarterectomy can be safely performed without a shunt.* J Am Coll Surg, 1999. 189(1): p. 93-100; discussion 100-1.
16. Durukan, A. and T. Tatlisumak, *Acute ischemic stroke: overview of major experimental rodent models, pathophysiology, and therapy of focal cerebral ischemia.* Pharmacol Biochem Behav, 2007. 87(1): p. 179-97.
17. Ginsberg, M.D. and R. Busto, *Rodent models of cerebral ischemia.* Stroke, 1989. 20(12): p. 1627-42.
18. Li F, F.M., *Animal modeling for developing stroke therapy.* Stroke therapy, 2001. Woburn,MA: Butterworth-Heinemann;: p. 83-96.
19. Fukuda, S. and G.J. del Zoppo, *Models of focal cerebral ischemia in the nonhuman primate.* ILAR J, 2003. 44(2): p. 96-104.
20. Cook, D.J. and M. Tymianski, *Nonhuman primate models of stroke for translational neuroprotection research.* Neurotherapeutics, 2012. 9(2): p. 371-9.
21. MS, L., *Impact of noninvasive technology on animal research.* ILAR Journal, 2001. 42: p. 187-262.
22. Ferreira JR, P.I., *Nomenclatura proposta para denominar as artérias da base do encéfalo do macaco-prego.* Acta Scientiarum Biol Sci, 2001. 23: p. 635-643.
23. Iwaniuk, A.N. and I.Q. Whishaw, *On the origin of skilled forelimb movements.* Trends Neurosci, 2000. 23(8): p. 372-6.
24. Cenci, M.A., I.Q. Whishaw, and T. Schallert, *Animal models of neurological deficits: how relevant is the rat?* Nat Rev Neurosci, 2002. 3(7): p. 574-9.

25. Redgrave, P., T.J. Prescott, and K. Gurney, *The basal ganglia: a vertebrate solution to the selection problem?* Neuroscience, 1999. 89(4): p. 1009-23.
26. Inder, T., et al., *Non-human primate models of neonatal brain injury.* Semin Perinatol, 2004. 28(6): p. 396-404.
27. Woodruff, T.M., et al., *Pathophysiology, treatment, and animal and cellular models of human ischemic stroke.* Mol Neurodegener, 2011. 6(1): p. 11.
28. McBean, D.E. and P.A. Kelly, *Rodent models of global cerebral ischemia: a comparison of two-vessel occlusion and four-vessel occlusion.* Gen Pharmacol, 1998. 30(4): p. 431-4.
29. Traystman, R.J., *Animal models of focal and global cerebral ischemia.* ILAR J, 2003. 44(2): p. 85-95.
30. Cimino, M., et al., *Neuroprotective effect of simvastatin in stroke: a comparison between adult and neonatal rat models of cerebral ischemia.* Neurotoxicology, 2005. 26(5): p. 929-33.
31. Uchiyama, Y., M. Koike, and M. Shibata, *Autophagic neuron death in neonatal brain ischemia/hypoxia.* Autophagy, 2008. 4(4): p. 404-8.
32. Aronowski, J., R. Strong, and J.C. Grotta, *Reperfusion injury: demonstration of brain damage produced by reperfusion after transient focal ischemia in rats.* J Cereb Blood Flow Metab, 1997. 17(10): p. 1048-56.
33. Gursoy-Ozdemir, Y., A. Can, and T. Dalkara, *Reperfusion-induced oxidative/nitrative injury to neurovascular unit after focal cerebral ischemia.* Stroke, 2004. 35(6): p. 1449-53.
34. Nagel, S., et al., *Therapeutic hypothermia in experimental models of focal and global cerebral ischemia and intracerebral hemorrhage.* Expert Rev Neurother, 2008. 8(8): p. 1255-68.
35. Kitagawa, K., et al., *Cerebral ischemia after bilateral carotid artery occlusion and intraluminal suture occlusion in mice: evaluation of the patency of the posterior communicating artery.* J Cereb Blood Flow Metab, 1998. 18(5): p. 570-9.
36. Pulsinelli, W.A. and J.B. Brierley, *A new model of bilateral hemispheric ischemia in the unanesthetized rat.* Stroke, 1979. 10(3): p. 267-72.
37. Pulsinelli, W.A., J.B. Brierley, and F. Plum, *Temporal profile of neuronal damage in a model of transient forebrain ischemia.* Ann Neurol, 1982. 11(5): p. 491-8.
38. Pulsinelli, W.A., D.E. Levy, and T.E. Duffy, *Cerebral blood flow in the four-vessel occlusion rat model.* Stroke, 1983. 14(5): p. 832-4.
39. Krakovsky, M., et al., *Effect of hyperbaric oxygen therapy on survival after global cerebral ischemia in rats.* Surg Neurol, 1998. 49(4): p. 412-6.
40. Kirino, T., *Delayed neuronal death.* Neuropathology, 2000. 20 Suppl: p. S95-7.
41. Eklof, B. and B.K. Siesjo, *The effect of bilateral carotid artery ligation upon acid-base parameters and substrate levels in the rat brain.* Acta Physiol Scand, 1972. 86(4): p. 528-38.
42. Eklof, B. and B.K. Siesjo, *The effect of bilateral carotid artery ligation upon the blood flow and the energy state of the rat brain.* Acta Physiol Scand, 1972. 86(2): p. 155-65.
43. Smith, M.L., R.N. Auer, and B.K. Siesjo, *The density and distribution of ischemic brain injury in the rat following 2-10 min of forebrain ischemia.* Acta Neuropathol, 1984. 64(4): p. 319-32.
44. Smith, M.L., et al., *Models for studying long-term recovery following forebrain ischemia in the rat. 2. A 2-vessel occlusion model.* Acta Neurol Scand, 1984. 69(6): p. 385-401.
45. Sheng, H., et al., *Characterization of a recovery global cerebral ischemia model in the mouse.* J Neurosci Methods, 1999. 88(1): p. 103-9.

46. Kirino, T., *Delayed neuronal death in the gerbil hippocampus following ischemia.* Brain Res, 1982. 239(1): p. 57-69.
47. Levine, S. and D. Sohn, *Cerebral ischemia in infant and adult gerbils. Relation to incomplete circle of Willis.* Arch Pathol, 1969. 87(3): p. 315-7.
48. Herrmann, M., et al., *Effect of inherent epileptic seizures on brain injury after transient cerebral ischemia in Mongolian gerbils.* Exp Brain Res, 2004. 154(2): p. 176-82.
49. Bottiger, B.W., et al., *Global cerebral ischemia due to cardiocirculatory arrest in mice causes neuronal degeneration and early induction of transcription factor genes in the hippocampus.* Brain Res Mol Brain Res, 1999. 65(2): p. 135-42.
50. Lowry, O.H., et al., *EFFECT OF ISCHEMIA ON KNOWN SUBSTRATES AND COFACTORS OF THE GLYCOLYTIC PATHWAY IN BRAIN.* J Biol Chem, 1964. 239: p. 18-30.
51. Howells, D.W., et al., *Different strokes for different folks: the rich diversity of animal models of focal cerebral ischemia.* J Cereb Blood Flow Metab, 2010. 30(8): p. 1412-31.
52. Chiang, T., R.O. Messing, and W.H. Chou, *Mouse model of middle cerebral artery occlusion.* J Vis Exp, 2011(48).
53. Tamura, A., et al., *Focal cerebral ischaemia in the rat: 1. Description of technique and early neuropathological consequences following middle cerebral artery occlusion.* J Cereb Blood Flow Metab, 1981. 1(1): p. 53-60.
54. Tamura, A., et al., *Focal cerebral ischaemia in the rat: 2. Regional cerebral blood flow determined by [14C]iodoantipyrine autoradiography following middle cerebral artery occlusion.* J Cereb Blood Flow Metab, 1981. 1(1): p. 61-9.
55. Bolander, H.G., et al., *Regional cerebral blood flow and histopathologic changes after middle cerebral artery occlusion in rats.* Stroke, 1989. 20(7): p. 930-7.
56. Bederson, J.B., et al., *Rat middle cerebral artery occlusion: evaluation of the model and development of a neurologic examination.* Stroke, 1986. 17(3): p. 472-6.
57. Weinstein, P.R., G.G. Anderson, and D.A. Telles, *Neurological deficit and cerebral infarction after temporary middle cerebral artery occlusion in unanesthetized cats.* Stroke, 1986. 17(2): p. 318-24.
58. Shigeno, T., et al., *Recirculation model following MCA occlusion in rats. Cerebral blood flow, cerebrovascular permeability, and brain edema.* J Neurosurg, 1985. 63(2): p. 272-7.
59. Hossmann, K.A., *Cerebral ischemia: models, methods and outcomes.* Neuropharmacology, 2008. 55(3): p. 257-70.
60. Koizumi J, Y.Y., Nakazawa T, Ooneda G, *Experimental studies of ischemic brain edema. 1. A new experimental model of cerebral embolism in rats in which recirculation can be introduced in the ischemic area.* Jpn J Stroke, 1986. 8: p. 1-8.
61. Longa, E.Z., et al., *Reversible middle cerebral artery occlusion without craniectomy in rats.* Stroke, 1989. 20(1): p. 84-91.
62. Abraham, H., et al., *Filament size influences temperature changes and brain damage following middle cerebral artery occlusion in rats.* Exp Brain Res, 2002. 142(1): p. 131-8.
63. Zarow, G.J., et al., *Endovascular suture occlusion of the middle cerebral artery in rats: effect of suture insertion distance on cerebral blood flow, infarct distribution and infarct volume.* Neurol Res, 1997. 19(4): p. 409-16.
64. He, Z., et al., *Experimental model of small deep infarcts involving the hypothalamus in rats: changes in body temperature and postural reflex.* Stroke, 1999. 30(12): p. 2743-51; discussion 2751.
65. Belayev, L., et al., *Middle cerebral artery occlusion in the rat by intraluminal*

suture. Neurological and pathological evaluation of an improved model. Stroke, 1996. 27(9): p. 1616-22; discussion 1623.

66. Memezawa, H., et al., *Ischemic penumbra in a model of reversible middle cerebral artery occlusion in the rat.* Exp Brain Res, 1992. 89(1): p. 67-78.
67. DeVries, A.C., et al., *Cognitive and behavioral assessment in experimental stroke research: will it prove useful?* Neurosci Biobehav Rev, 2001. 25(4): p. 325-42.
68. Shimamura, N., et al., *Comparison of silicon-coated nylon suture to plain nylon suture in the rat middle cerebral artery occlusion model.* J Neurosci Methods, 2006. 156(1-2): p. 161-5.
69. Laing, R.J., J. Jakubowski, and R.W. Laing, *Middle cerebral artery occlusion without craniectomy in rats. Which method works best?* Stroke, 1993. 24(2): p. 294-7; discussion 297-8.
70. Takano, K., et al., *Reproducibility and reliability of middle cerebral artery occlusion using a silicone-coated suture (Koizumi) in rats.* J Neurol Sci, 1997. 153(1): p. 8-11.
71. Schmid-Elsaesser, R., et al., *A critical reevaluation of the intraluminal thread model of focal cerebral ischemia: evidence of inadvertent premature reperfusion and subarachnoid hemorrhage in rats by laser-Doppler flowmetry.* Stroke, 1998. 29(10): p. 2162-70.
72. Li, F., T. Omae, and M. Fisher, *Spontaneous hyperthermia and its mechanism in the intraluminal suture middle cerebral artery occlusion model of rats.* Stroke, 1999. 30(11): p. 2464-70; discussion 2470-1.
73. Liu, S., et al., *RODENT STROKE MODEL GUIDELINES FOR PRECLINICAL STROKE TRIALS (1ST EDITION).* J Exp Stroke Transl Med, 2009. 2(2): p. 2-27.
74. Overgaard, K., *Thrombolytic therapy in experimental embolic stroke.* Cerebrovasc Brain Metab Rev, 1994. 6(3): p. 257-86.
75. Brinker, G., et al., *Thrombolysis of cerebral clot embolism in rat: effect of treatment delay.* Neuroreport, 1999. 10(16): p. 3269-72.
76. Zhang, L., et al., *Intravenous administration of a GPIIb/IIIa receptor antagonist extends the therapeutic window of intra-arterial tenecteplase-tissue plasminogen activator in a rat stroke model.* Stroke, 2004. 35(12): p. 2890-5.
77. Mayzel-Oreg, O., et al., *Microsphere-induced embolic stroke: an MRI study.* Magn Reson Med, 2004. 51(6): p. 1232-8.
78. Busch, E., K. Kruger, and K.A. Hossmann, *Improved model of thromboembolic stroke and rt-PA induced reperfusion in the rat.* Brain Res, 1997. 778(1): p. 16-24.
79. Watson, B.D., et al., *Induction of reproducible brain infarction by photochemically initiated thrombosis.* Ann Neurol, 1985. 17(5): p. 497-504.
80. Dietrich, W.D., et al., *Photochemically induced cerebral infarction. II. Edema and blood-brain barrier disruption.* Acta Neuropathol, 1987. 72(4): p. 326-34.
81. Dietrich, W.D., et al., *Photochemically induced cerebral infarction. I. Early microvascular alterations.* Acta Neuropathol, 1987. 72(4): p. 315-25.
82. Hilger, T., et al., *Characterization of a novel chronic photothrombotic ring stroke model in rats by magnetic resonance imaging, biochemical imaging, and histology.* J Cereb Blood Flow Metab, 2004. 24(7): p. 789-97.
83. Macrae, I.M., et al., *Endothelin-1-induced reductions in cerebral blood flow: dose dependency, time course, and neuropathological consequences.* J Cereb Blood Flow Metab, 1993. 13(2): p. 276-84.
84. Sharkey, J., I.M. Ritchie, and P.A. Kelly, *Perivascular microapplication of endothelin-1: a new model of focal cerebral ischaemia in the rat.* J Cereb Blood Flow Metab, 1993. 13(5): p. 865-71.
85. Carmichael, S.T., *Rodent models of focal stroke: size, mechanism, and purpose.* NeuroRx, 2005. 2(3): p. 396-409.

86. Nelson, K.B. and J.K. Lynch, *Stroke in newborn infants.* Lancet Neurol, 2004. 3(3): p. 150-8.
87. Aden, U., *Neonatal stroke is not a harmless condition.* Stroke, 2009. 40(6): p. 1948-9.
88. Sehgal, A., *Perinatal stroke: a case-based review.* Eur J Pediatr, 2012. 171(2): p. 225-34.
89. Chauvier, D., et al., *Targeting neonatal ischemic brain injury with a pentapeptide-based irreversible caspase inhibitor.* Cell Death Dis, 2011. 2: p. e203.
90. Chabrier, S. and A. Buchmuller, *Editorial comment--specificities of the neonatal stroke.* Stroke, 2003. 34(12): p. 2892-3.
91. Rees, S., R. Harding, and D. Walker, *The biological basis of injury and neuroprotection in the fetal and neonatal brain.* Int J Dev Neurosci, 2011. 29(6): p. 551-63.
92. Northington, F.J., *Brief update on animal models of hypoxic-ischemic encephalopathy and neonatal stroke.* ILAR J, 2006. 47(1): p. 32-8.
93. Rice, J.E., 3rd, R.C. Vannucci, and J.B. Brierley, *The influence of immaturity on hypoxic-ischemic brain damage in the rat.* Ann Neurol, 1981. 9(2): p. 131-41.
94. Clancy, B., R.B. Darlington, and B.L. Finlay, *Translating developmental time across mammalian species.* Neuroscience, 2001. 105(1): p. 7-17.
95. Sheldon, R.A., C. Sedik, and D.M. Ferriero, *Strain-related brain injury in neonatal mice subjected to hypoxia-ischemia.* Brain Res, 1998. 810(1-2): p. 114-22.
96. Balduini, W., et al., *Simvastatin protects against long-lasting behavioral and morphological consequences of neonatal hypoxic/ischemic brain injury.* Stroke, 2001. 32(9): p. 2185-91.
97. Yang, S.N., et al., *Impaired SynGAP expression and long-term spatial learning and memory in hippocampal CA1 area from rats previously exposed to perinatal hypoxia-induced insults: beneficial effects of A68930.* Neurosci Lett, 2004. 371(1): p. 73-8.
98. Harris, A.P., et al., *Fetal cerebral and peripheral circulatory responses to hypoxia after nitric oxide synthase inhibition.* Am J Physiol Regul Integr Comp Physiol, 2001. 281(2): p. R381-90.
99. Gonzalez, H., et al., *Cerebral oxygenation during postasphyxial seizures in near-term fetal sheep.* J Cereb Blood Flow Metab, 2005. 25(7): p. 911-8.
100. Derrick, M., et al., *Preterm fetal hypoxia-ischemia causes hypertonia and motor deficits in the neonatal rabbit: a model for human cerebral palsy?* J Neurosci, 2004. 24(1): p. 24-34.
101. Myers, R.E., *Two patterns of perinatal brain damage and their conditions of occurrence.* Am J Obstet Gynecol, 1972. 112(2): p. 246-76.
102. Myers, R.E., *Atrophic cortical sclerosis associated with status marmoratus in a perinatally damaged monkey.* Neurology, 1969. 19(12): p. 1177-88.
103. Myers, *Experimental models of perinatal brain damage: Relevance to human pathology.* Intrauterine Asphyxia and the Developing Fetal Brain., 1977. Chicago, IL, Year Book: p. 37-97.
104. Mhairi Macrae, I., *New models of focal cerebral ischaemia.* Br J Clin Pharmacol, 1992. 34(4): p. 302-8.
105. Zhang, L., et al., *Functional recovery in aged and young rats after embolic stroke: treatment with a phosphodiesterase type 5 inhibitor.* Stroke, 2005. 36(4): p. 847-52.
106. Nabika, T., Z. Cui, and J. Masuda, *The stroke-prone spontaneously hypertensive rat: how good is it as a model for cerebrovascular diseases?* Cell Mol Neurobiol, 2004. 24(5): p. 639-46.

107. **Dittmar, M.S., et al., *Fischer-344 rats are unsuitable for the MCAO filament model due to their cerebrovascular anatomy.* J Neurosci Methods, 2006. 156(1-2): p. 50-4.**

108. **Merchenthaler, I., T.L. Dellovade, and P.J. Shughrue, *Neuroprotection by estrogen in animal models of global and focal ischemia.* Ann N Y Acad Sci, 2003. 1007: p. 89-100.**

109. **Krieger, D.W. and M.A. Yenari, *Therapeutic hypothermia for acute ischemic stroke: what do laboratory studies teach us?* Stroke, 2004. 35(6): p. 1482-9.**

110. **McIlvoy, L.H., *The effect of hypothermia and hyperthermia on acute brain injury.* AACN Clin Issues, 2005. 16(4): p. 488-500.**

111. **PulsinelliW, J.M., *Animal models of brain ischemia.* Stroke: pathophysiology, diagnosis, and management., 1992. New York, NY, USA: Churchill Livingstone;: p. 49-67.**

112. **Woitzik, J. and L. Schilling, *Control of completeness and immediate detection of bleeding by a single laser-Doppler flow probe during intravascular middle cerebral artery occlusion in rats.* J Neurosci Methods, 2002. 122(1): p. 75-8.**

113. **Kirsch, J.R., R.J. Traystman, and P.D. Hurn, *Anesthetics and cerebroprotection: experimental aspects.* Int Anesthesiol Clin, 1996. 34(4): p. 73-93.**

114. **Zausinger, S., A. Baethmann, and R. Schmid-Elsaesser, *Anesthetic methods in rats determine outcome after experimental focal cerebral ischemia: mechanical ventilation is required to obtain controlled experimental conditions.* Brain Res Brain Res Protoc, 2002. 9(2): p. 112-21.**

115. **Arumugam, T.V., et al., *Intravenous immunoglobulin (IVIG) protects the brain against experimental stroke by preventing complement-mediated neuronal cell death.* Proc Natl Acad Sci U S A, 2007. 104(35): p. 14104-9.**

116. **Lipton, P., *Ischemic cell death in brain neurons.* Physiol Rev, 1999. 79(4): p. 1431-568.**

117. **Noraberg, J., et al., *Organotypic hippocampal slice cultures for studies of brain damage, neuroprotection and neurorepair.* Curr Drug Targets CNS Neurol Disord, 2005. 4(4): p. 435-52.**

118. **Holopainen, I.E., *Organotypic hippocampal slice cultures: a model system to study basic cellular and molecular mechanisms of neuronal cell death, neuroprotection, and synaptic plasticity.* Neurochem Res, 2005. 30(12): p. 1521-8.**

119. **Su, T., et al., *Evaluation of cell damage in organotypic hippocampal slice culture from adult mouse: a potential model system to study neuroprotection.* Brain Res, 2011. 1385: p. 68-76.**

120. **Gahwiler, B.H., et al., *Organotypic slice cultures: a technique has come of age.* Trends Neurosci, 1997. 20(10): p. 471-7.**

121. **Gahwiler, B.H., *Organotypic monolayer cultures of nervous tissue.* J Neurosci Methods, 1981. 4(4): p. 329-42.**

122. **Stoppini, L., P.A. Buchs, and D. Muller, *A simple method for organotypic cultures of nervous tissue.* J Neurosci Methods, 1991. 37(2): p. 173-82.**

123. **Savas, A., et al., *The effects of continuous and single-dose radiation on choline uptake in organotypic tissue slice cultures of rabbit hippocampus.* Neurol Res, 2001. 23(6): p. 669-75.**

124. **Meyer, M., et al., *Improved survival of embryonic porcine dopaminergic neurons in coculture with a conditionally immortalized GDNF-producing hippocampal cell line.* Exp Neurol, 2000. 164(1): p. 82-93.**

125. **Bauer, M., et al., *Liposome-mediated gene transfer to fetal human ventral mesencephalic explant cultures.* Neurosci Lett, 2001. 308(3): p. 169-72.**

126. **Walsh, K.H. and C.J. McDougle, *Pharmacological strategies for trichotillomania.* Expert Opin Pharmacother, 2005. 6(6): p. 975-84.**

127. Leutgeb, J.K., J.U. Frey, and T. Behnisch, *LTP in cultured hippocampal-entorhinal cortex slices from young adult (P25-30) rats.* J Neurosci Methods, 2003. 130(1): p. 19-32.
128. Hassen, G.W., et al., *A new model of ischemic preconditioning using young adult hippocampal slice cultures.* Brain Res Brain Res Protoc, 2004. 13(3): p. 135-43.
129. Brewer, G.J., *Isolation and culture of adult rat hippocampal neurons.* J Neurosci Methods, 1997. 71(2): p. 143-55.
130. Olsson, T., et al., *Deletion of the adenosine A1 receptor gene does not alter neuronal damage following ischaemia in vivo or in vitro.* Eur J Neurosci, 2004. 20(5): p. 1197-204.
131. Bahr, B.A., et al., *Stable maintenance of glutamate receptors and other synaptic components in long-term hippocampal slices.* Hippocampus, 1995. 5(5): p. 425-39.
132. Dwyer, T.A., D.E. Earl, and L. Wang, *The utility of a new in vitro model of the stroke penumbra.* J Neurosci, 2008. 28(26): p. 6537-8.
133. Yang, L., K.K. Shah, and T.J. Abbruscato, *An in vitro model of ischemic stroke.* Methods Mol Biol, 2012. 814: p. 451-66.
134. Hossmann, K.A., *Pathophysiology and therapy of experimental stroke.* Cell Mol Neurobiol, 2006. 26(7-8): p. 1057-83.
135. Lin, C.H., P.S. Chen, and P.W. Gean, *Glutamate preconditioning prevents neuronal death induced by combined oxygen-glucose deprivation in cultured cortical neurons.* Eur J Pharmacol, 2008. 589(1-3): p. 85-93.
136. Wieloch, T. and B.K. Siesjo, *Ischemic brain injury: the importance of calcium, lipolytic activities, and free fatty acids.* Pathol Biol (Paris), 1982. 30(5): p. 269-77.
137. Zhao, S.T., et al., *Mitochondrial BNIP3 upregulation precedes endonuclease G translocation in hippocampal neuronal death following oxygen-glucose deprivation.* BMC Neurosci, 2009. 10: p. 113.
138. Xie, C., W.R. Markesbery, and M.A. Lovell, *Survival of hippocampal and cortical neurons in a mixture of MEM+ and B27-supplemented neurobasal medium.* Free Radic Biol Med, 2000. 28(5): p. 665-72.
139. Shi, R., et al., *Excessive autophagy contributes to neuron death in cerebral ischemia.* CNS Neurosci Ther, 2012. 18(3): p. 250-60.
140. Newell, D.W., A.T. Malouf, and J.E. Franck, *Glutamate-mediated selective vulnerability to ischemia is present in organotypic cultures of hippocampus.* Neurosci Lett, 1990. 116(3): p. 325-30.
141. Siesjo, B.K., et al., *Mechanisms of secondary brain damage in global and focal ischemia: a speculative synthesis.* J Neurotrauma, 1995. 12(5): p. 943-56.
142. Hunter, A.J., A.R. Green, and A.J. Cross, *Animal models of acute ischaemic stroke: can they predict clinically successful neuroprotective drugs?* Trends Pharmacol Sci, 1995. 16(4): p. 123-8.
143. Xu, G.P., et al., *Improvement in neuronal survival after ischemic preconditioning in hippocampal slice cultures.* Brain Res, 2002. 952(2): p. 153-8.
144. Xiang, Z., et al., *Long-term maintenance of mature hippocampal slices in vitro.* J Neurosci Methods, 2000. 98(2): p. 145-54.
145. Meli, E., et al., *Poly(ADP-ribose) polymerase as a key player in excitotoxicity and post-ischemic brain damage.* Toxicol Lett, 2003. 139(2-3): p. 153-62.
146. Cho, S., et al., *Spatiotemporal evidence of apoptosis-mediated ischemic injury in organotypic hippocampal slice cultures.* Neurochem Int, 2004. 45(1): p. 117-27.
147. Bonde, C., et al., *Ionotropic glutamate receptors and glutamate transporters are involved in necrotic neuronal cell death induced by oxygen-glucose deprivation of hippocampal slice cultures.* Neuroscience, 2005. 136(3): p. 779-94.
148. Runden, E., et al., *Regional selective neuronal degeneration after protein*

phosphatase inhibition in hippocampal slice cultures: evidence for a MAP kinase-dependent mechanism. J Neurosci, 1998. 18(18): p. 7296-305.

149. Moroni, F., et al., *Poly(ADP-ribose) polymerase inhibitors attenuate necrotic but not apoptotic neuronal death in experimental models of cerebral ischemia.* Cell Death Differ, 2001. 8(9): p. 921-32.
150. Moroni, F., et al., *The novel and systemically active metabotropic glutamate 1 (mGlu1) receptor antagonist 3-MATIDA reduces post-ischemic neuronal death.* Neuropharmacology, 2002. 42(6): p. 741-51.
151. Moroni, F., et al., *Neuroprotective effects of kynurenine-3-hydroxylase inhibitors in models of brain ischemia.* Adv Exp Med Biol, 1999. 467: p. 199-206.
152. Vallieres, L., et al., *Reduced hippocampal neurogenesis in adult transgenic mice with chronic astrocytic production of interleukin-6.* J Neurosci, 2002. 22(2): p. 486-92.
153. Dijkhuizen, R.M. and K. Nicolay, *Magnetic resonance imaging in experimental models of brain disorders.* J Cereb Blood Flow Metab, 2003. 23(12): p. 1383-402.
154. Arumugam, T.V., et al., *Age and energy intake interact to modify cell stress pathways and stroke outcome.* Ann Neurol, 2010. 67(1): p. 41-52.
155. Li, Y., et al., *Intrastriatal transplantation of bone marrow nonhematopoietic cells improves functional recovery after stroke in adult mice.* J Cereb Blood Flow Metab, 2000. 20(9): p. 1311-9.
156. Thompson, R.J., N. Zhou, and B.A. MacVicar, *Ischemia opens neuronal gap junction hemichannels.* Science, 2006. 312(5775): p. 924-7.
157. Arumugam, T.V., et al., *Contributions of LFA-1 and Mac-1 to brain injury and microvascular dysfunction induced by transient middle cerebral artery occlusion.* Am J Physiol Heart Circ Physiol, 2004. 287(6): p. H2555-60.
158. Siniscalchi, A., et al., *Neuroprotective effects of riluzole: an electrophysiological and histological analysis in an in vitro model of ischemia.* Synapse, 1999. 32(3): p. 147-52.
159. Badiola, N., et al., *Activation of caspase-8 by tumour necrosis factor receptor 1 is necessary for caspase-3 activation and apoptosis in oxygen-glucose deprived cultured cortical cells.* Neurobiol Dis, 2009. 35(3): p. 438-47.
160. Laake, J.H., et al., *A simple in vitro model of ischemia based on hippocampal slice cultures and propidium iodide fluorescence.* Brain Res Brain Res Protoc, 1999. 4(2): p. 173-84.
161. Krassioukov, A.V., et al., *An in vitro model of neurotrauma in organotypic spinal cord cultures from adult mice.* Brain Res Brain Res Protoc, 2002. 10(2): p. 60-8.
162. Boyce, M., A. Degterev, and J. Yuan, *Caspases: an ancient cellular sword of Damocles.* Cell Death Differ, 2004. 11(1): p. 29-37.
163. Golstein, P., L. Aubry, and J.P. Levraud, *Cell-death alternative model organisms: why and which?* Nat Rev Mol Cell Biol, 2003. 4(10): p. 798-807.
164. Garrido, C. and G. Kroemer, *Life's smile, death's grin: vital functions of apoptosis-executing proteins.* Curr Opin Cell Biol, 2004. 16(6): p. 639-46.
165. Kroemer, G. and S.J. Martin, *Caspase-independent cell death.* Nat Med, 2005. 11(7): p. 725-30.
166. Lo, E.H., T. Dalkara, and M.A. Moskowitz, *Mechanisms, challenges and opportunities in stroke.* Nat Rev Neurosci, 2003. 4(5): p. 399-415.
167. Lang-Rollin, I.C., et al., *Mechanisms of caspase-independent neuronal death: energy depletion and free radical generation.* J Neurosci, 2003. 23(35): p. 11015-25.
168. Le, D.A., et al., *Caspase activation and neuroprotection in caspase-3- deficient mice after in vivo cerebral ischemia and in vitro oxygen glucose deprivation.* Proc Natl

Acad Sci U S A, 2002. 99(23): p. 15188-93.
169. Didenko, V.V., et al., *Caspase-3-dependent and -independent apoptosis in focal brain ischemia.* Mol Med, 2002. 8(7): p. 347-52.
170. Himi, T., Y. Ishizaki, and S. Murota, *A caspase inhibitor blocks ischaemia-induced delayed neuronal death in the gerbil.* Eur J Neurosci, 1998. 10(2): p. 777-81.
171. Cregan, S.P., et al., *Apoptosis-inducing factor is involved in the regulation of caspase-independent neuronal cell death.* J Cell Biol, 2002. 158(3): p. 507-17.
172. MacManus, J.P., et al., *Detection of higher-order 50- and 10-kbp DNA fragments before apoptotic internucleosomal cleavage after transient cerebral ischemia.* J Cereb Blood Flow Metab, 1997. 17(4): p. 376-87.
173. Repici, M., J. Mariani, and T. Borsello, *Neuronal death and neuroprotection: a review.* Methods Mol Biol, 2007. 399: p. 1-14.
174. Nitatori, T., et al., *Delayed neuronal death in the CA1 pyramidal cell layer of the gerbil hippocampus following transient ischemia is apoptosis.* J Neurosci, 1995. 15(2): p. 1001-11.
175. Chen, J., et al., *Induction of caspase-3-like protease may mediate delayed neuronal death in the hippocampus after transient cerebral ischemia.* J Neurosci, 1998. 18(13): p. 4914-28.
176. Maiuri, M.C., et al., *Self-eating and self-killing: crosstalk between autophagy and apoptosis.* Nat Rev Mol Cell Biol, 2007. 8(9): p. 741-52.
177. Cho, B.B. and L.H. Toledo-Pereyra, *Caspase-independent programmed cell death following ischemic stroke.* J Invest Surg, 2008. 21(3): p. 141-7.
178. Vande Velde, C., et al., *BNIP3 and genetic control of necrosis-like cell death through the mitochondrial permeability transition pore.* Mol Cell Biol, 2000. 20(15): p. 5454-68.
179. Kerr, J.F., A.H. Wyllie, and A.R. Currie, *Apoptosis: a basic biological phenomenon with wide-ranging implications in tissue kinetics.* Br J Cancer, 1972. 26(4): p. 239-57.
180. Garcia, J.H., et al., *Incomplete infarct and delayed neuronal death after transient middle cerebral artery occlusion in rats.* Stroke, 1997. 28(11): p. 2303-9; discussion 2310.
181. Nedergaard, M., *Neuronal injury in the infarct border: a neuropathological study in the rat.* Acta Neuropathol, 1987. 73(3): p. 267-74.
182. Sairanen, T., et al., *Apoptosis dominant in the periinfarct area of human ischaemic stroke--a possible target of antiapoptotic treatments.* Brain, 2006. 129(Pt 1): p. 189-99.
183. Bennett, B.L., et al., *SP600125, an anthrapyrazolone inhibitor of Jun N-terminal kinase.* Proc Natl Acad Sci U S A, 2001. 98(24): p. 13681-6.
184. Sattler, R. and M. Tymianski, *Molecular mechanisms of glutamate receptor-mediated excitotoxic neuronal cell death.* Mol Neurobiol, 2001. 24(1-3): p. 107-29.
185. Stout, A.K., et al., *Glutamate-induced neuron death requires mitochondrial calcium uptake.* Nat Neurosci, 1998. 1(5): p. 366-73.
186. Syntichaki, P., et al., *Specific aspartyl and calpain proteases are required for neurodegeneration in C. elegans.* Nature, 2002. 419(6910): p. 939-44.
187. Yamashima, T., et al., *Inhibition of ischaemic hippocampal neuronal death in primates with cathepsin B inhibitor CA-074: a novel strategy for neuroprotection based on 'calpain-cathepsin hypothesis'.* Eur J Neurosci, 1998. 10(5): p. 1723-33.
188. Yuan, J., M. Lipinski, and A. Degterev, *Diversity in the mechanisms of neuronal cell death.* Neuron, 2003. 40(2): p. 401-13.
189. de Murcia, G., et al., *Structure and function of poly(ADP-ribose) polymerase.* Mol Cell Biochem, 1994. 138(1-2): p. 15-24.

190. !!! INVALID CITATION !!!
191. Chu, C.T., et al., *Autophagy in neurite injury and neurodegeneration: in vitro and in vivo models.* Methods Enzymol, 2009. 453: p. 217-49.
192. Chu, C.T., *Eaten alive: autophagy and neuronal cell death after hypoxia-ischemia.* Am J Pathol, 2008. 172(2): p. 284-7.
193. Qin, A.P., et al., *Autophagy was activated in injured astrocytes and mildly decreased cell survival following glucose and oxygen deprivation and focal cerebral ischemia.* Autophagy, 2010. 6(6).
194. Canu, N., et al., *Role of the autophagic-lysosomal system on low potassium-induced apoptosis in cultured cerebellar granule cells.* J Neurochem, 2005. 92(5): p. 1228-42.
195. Uchiyama, Y., *Autophagic cell death and its execution by lysosomal cathepsins.* Arch Histol Cytol, 2001. 64(3): p. 233-46.
196. Schwartz, L.M., et al., *Do all programmed cell deaths occur via apoptosis?* Proc Natl Acad Sci U S A, 1993. 90(3): p. 980-4.
197. Bursch, W., et al., *Programmed cell death (PCD). Apoptosis, autophagic PCD, or others?* Ann N Y Acad Sci, 2000. 926: p. 1-12.
198. Bursch, W., et al., *Autophagic and apoptotic types of programmed cell death exhibit different fates of cytoskeletal filaments.* J Cell Sci, 2000. 113 (Pt 7): p. 1189-98.
199. Koike, M., et al., *Inhibition of autophagy prevents hippocampal pyramidal neuron death after hypoxic-ischemic injury.* Am J Pathol, 2008. 172(2): p. 454-69.
200. Zhu, C., et al., *The influence of age on apoptotic and other mechanisms of cell death after cerebral hypoxia-ischemia.* Cell Death Differ, 2005. 12(2): p. 162-76.
201. Adhami, F., et al., *Cerebral ischemia-hypoxia induces intravascular coagulation and autophagy.* Am J Pathol, 2006. 169(2): p. 566-83.
202. Puyal, J. and P.G. Clarke, *Targeting autophagy to prevent neonatal stroke damage.* Autophagy, 2009. 5(7): p. 1060-1.
203. Yu, L., et al., *Regulation of an ATG7-beclin 1 program of autophagic cell death by caspase-8.* Science, 2004. 304(5676): p. 1500-2.
204. Yousefi, S., et al., *Calpain-mediated cleavage of Atg5 switches autophagy to apoptosis.* Nat Cell Biol, 2006. 8(10): p. 1124-32.
205. Rubinsztein, D.C., et al., *Autophagy and its possible roles in nervous system diseases, damage and repair.* Autophagy, 2005. 1(1): p. 11-22.
206. Yu, L., et al., *Autophagic programmed cell death by selective catalase degradation.* Proc Natl Acad Sci U S A, 2006. 103(13): p. 4952-7.
207. Kirino, T., A. Tamura, and K. Sano, *A reversible type of neuronal injury following ischemia in the gerbil hippocampus.* Stroke, 1986. 17(3): p. 455-9.
208. Lo, E.H., *A new penumbra: transitioning from injury into repair after stroke.* Nat Med, 2008. 14(5): p. 497-500.
209. Horbinski, C. and C.T. Chu, *Kinase signaling cascades in the mitochondrion: a matter of life or death.* Free Radic Biol Med, 2005. 38(1): p. 2-11.
210. Galluzzi, L., et al., *Methods for the assessment of mitochondrial membrane permeabilization in apoptosis.* Apoptosis, 2007. 12(5): p. 803-13.
211. Kroemer, G. and J.C. Reed, *Mitochondrial control of cell death.* Nat Med, 2000. 6(5): p. 513-9.
212. Galluzzi, L., et al., *Targeting post-mitochondrial effectors of apoptosis for neuroprotection.* Biochim Biophys Acta, 2009. 1787(5): p. 402-13.
213. Green, D.R. and G. Kroemer, *The pathophysiology of mitochondrial cell death.* Science, 2004. 305(5684): p. 626-9.
214. Vosler, P.S., et al., *Mitochondrial targets for stroke: focusing basic science research*

toward development of clinically translatable therapeutics. Stroke, 2009. 40(9): p. 3149-55.

215. Krantic, S., et al., *Apoptosis-inducing factor: a matter of neuron life and death.* Prog Neurobiol, 2007. 81(3): p. 179-96.
216. Zhu, C., et al., *Cyclophilin A participates in the nuclear translocation of apoptosis-inducing factor in neurons after cerebral hypoxia-ischemia.* J Exp Med, 2007. 204(8): p. 1741-8.
217. Cande, C., et al., *AIF and cyclophilin A cooperate in apoptosis-associated chromatinolysis.* Oncogene, 2004. 23(8): p. 1514-21.
218. Lorenzo, H.K., et al., *Apoptosis inducing factor (AIF): a phylogenetically old, caspase-independent effector of cell death.* Cell Death Differ, 1999. 6(6): p. 516-24.
219. Susin, S.A., et al., *Molecular characterization of mitochondrial apoptosis-inducing factor.* Nature, 1999. 397(6718): p. 441-6.
220. Penninger, J.M. and G. Kroemer, *Mitochondria, AIF and caspases--rivaling for cell death execution.* Nat Cell Biol, 2003. 5(2): p. 97-9.
221. Hisatomi, T., et al., *Relocalization of apoptosis-inducing factor in photoreceptor apoptosis induced by retinal detachment in vivo.* Am J Pathol, 2001. 158(4): p. 1271-8.
222. Daugas, E., et al., *Mitochondrio-nuclear translocation of AIF in apoptosis and necrosis.* FASEB J, 2000. 14(5): p. 729-39.
223. Cao, G., et al., *Translocation of apoptosis-inducing factor in vulnerable neurons after transient cerebral ischemia and in neuronal cultures after oxygen-glucose deprivation.* J Cereb Blood Flow Metab, 2003. 23(10): p. 1137-50.
224. Culmsee, C., et al., *Apoptosis-inducing factor triggered by poly(ADP-ribose) polymerase and Bid mediates neuronal cell death after oxygen-glucose deprivation and focal cerebral ischemia.* J Neurosci, 2005. 25(44): p. 10262-72.
225. Zhu, C., et al., *Involvement of apoptosis-inducing factor in neuronal death after hypoxia-ischemia in the neonatal rat brain.* J Neurochem, 2003. 86(2): p. 306-17.
226. Zhu, C., et al., *Apoptosis-inducing factor is a major contributor to neuronal loss induced by neonatal cerebral hypoxia-ischemia.* Cell Death Differ, 2007. 14(4): p. 775-84.
227. Tsujimoto, Y., *Cell death regulation by the Bcl-2 protein family in the mitochondria.* J Cell Physiol, 2003. 195(2): p. 158-67.
228. van Loo, G., et al., *Caspases are not localized in mitochondria during life or death.* Cell Death Differ, 2002. 9(11): p. 1207-11.
229. Crompton, M., *The mitochondrial permeability transition pore and its role in cell death.* Biochem J, 1999. 341 (Pt 2): p. 233-49.
230. Donovan, M. and T.G. Cotter, *Control of mitochondrial integrity by Bcl-2 family members and caspase-independent cell death.* Biochim Biophys Acta, 2004. 1644(2-3): p. 133-47.
231. Cande, C., et al., *Apoptosis-inducing factor (AIF): key to the conserved caspase-independent pathways of cell death?* J Cell Sci, 2002. 115(Pt 24): p. 4727-34.
232. Li, L.Y., X. Luo, and X. Wang, *Endonuclease G is an apoptotic DNase when released from mitochondria.* Nature, 2001. 412(6842): p. 95-9.
233. van Loo, G., et al., *Endonuclease G: a mitochondrial protein released in apoptosis and involved in caspase-independent DNA degradation.* Cell Death Differ, 2001. 8(12): p. 1136-42.
234. Zhang, J., et al., *Endonuclease G is required for early embryogenesis and normal apoptosis in mice.* Proc Natl Acad Sci U S A, 2003. 100(26): p. 15782-7.
235. Lee, B.I., et al., *Early nuclear translocation of endonuclease G and subsequent DNA fragmentation after transient focal cerebral ischemia in mice.* Neurosci Lett, 2005.

386(1): p. 23-7.
236. Tanaka, S., et al., *Mitochondrial impairment induced by poly(ADP-ribose) polymerase-1 activation in cortical neurons after oxygen and glucose deprivation.* J Neurochem, 2005. 95(1): p. 179-90.
237. Zhang, Z., et al., *BNIP3 upregulation and EndoG translocation in delayed neuronal death in stroke and in hypoxia.* Stroke, 2007. 38(5): p. 1606-13.
238. Vande Walle, L., et al., *Proteome-wide Identification of HtrA2/Omi Substrates.* J Proteome Res, 2007. 6(3): p. 1006-15.
239. Saito, A., et al., *Modulation of the Omi/HtrA2 signaling pathway after transient focal cerebral ischemia in mouse brains that overexpress SOD1.* Brain Res Mol Brain Res, 2004. 127(1-2): p. 89-95.
240. Siegelin, M.D., et al., *Regulation of XIAP and Smac/DIABLO in the rat hippocampus following transient forebrain ischemia.* Neurochem Int, 2005. 46(1): p. 41-51.
241. Saito, A., et al., *Interaction between XIAP and Smac/DIABLO in the mouse brain after transient focal cerebral ischemia.* J Cereb Blood Flow Metab, 2003. 23(9): p. 1010-9.
242. Shibata, M., et al., *Subcellular localization of a promoter and an inhibitor of apoptosis (Smac/DIABLO and XIAP) during brain ischemia/reperfusion.* Neuroreport, 2002. 13(15): p. 1985-8.
243. Saito, A., et al., *Oxidative stress is associated with XIAP and Smac/DIABLO signaling pathways in mouse brains after transient focal cerebral ischemia.* Stroke, 2004. 35(6): p. 1443-8.
244. Boyd, *Adenovirus E1B 19 kDa and Bcl-2 proteins interact with a common set of cellular proteins.* Cell, 1994. 79(6): p. 1121.
245. Chen, G., et al., *Nix and Nip3 form a subfamily of pro-apoptotic mitochondrial proteins.* J Biol Chem, 1999. 274(1): p. 7-10.
246. Chen, G., et al., *The E1B 19K/Bcl-2-binding protein Nip3 is a dimeric mitochondrial protein that activates apoptosis.* J Exp Med, 1997. 186(12): p. 1975-83.
247. Cizeau, J., et al., *The C. elegans orthologue ceBNIP3 interacts with CED-9 and CED-3 but kills through a BH3- and caspase-independent mechanism.* Oncogene, 2000. 19(48): p. 5453-63.
248. Yasuda, M., et al., *Regulation of apoptosis by a Caenorhabditis elegans BNIP3 homolog.* Oncogene, 1998. 17(19): p. 2525-30.
249. Zhang, S., et al., *Evidence of oxidative stress-induced BNIP3 expression in amyloid beta neurotoxicity.* Brain Res, 2007. 1138: p. 221-30.
250. Ray, R., et al., *BNIP3 heterodimerizes with Bcl-2/Bcl-X(L) and induces cell death independent of a Bcl-2 homology 3 (BH3) domain at both mitochondrial and nonmitochondrial sites.* J Biol Chem, 2000. 275(2): p. 1439-48.
251. Bruick, R.K., *Expression of the gene encoding the proapoptotic Nip3 protein is induced by hypoxia.* Proc Natl Acad Sci U S A, 2000. 97(16): p. 9082-7.
252. Guo, K., et al., *Hypoxia induces the expression of the pro-apoptotic gene BNIP3.* Cell Death Differ, 2001. 8(4): p. 367-76.
253. Sowter, H.M., et al., *HIF-1-dependent regulation of hypoxic induction of the cell death factors BNIP3 and NIX in human tumors.* Cancer Res, 2001. 61(18): p. 6669-73.
254. Helton, R., et al., *Brain-specific knock-out of hypoxia-inducible factor-1alpha reduces rather than increases hypoxic-ischemic damage.* J Neurosci, 2005. 25(16): p. 4099-107.
255. Saelens, X., et al., *Toxic proteins released from mitochondria in cell death.* Oncogene, 2004. 23(16): p. 2861-74.
256. Diaz, F. and C.T. Moraes, *Mitochondrial biogenesis and turnover.* Cell Calcium,

2008. 44(1): p. 24-35.
257. Ashrafi, G. and T.L. Schwarz, *The pathways of mitophagy for quality control and clearance of mitochondria.* Cell Death Differ, 2013. 20(1): p. 31-42.
258. Okamoto, K. and J.M. Shaw, *Mitochondrial morphology and dynamics in yeast and multicellular eukaryotes.* Annu Rev Genet, 2005. 39: p. 503-36.
259. Hoppins, S., L. Lackner, and J. Nunnari, *The machines that divide and fuse mitochondria.* Annu Rev Biochem, 2007. 76: p. 751-80.
260. Jahani-Asl, A., et al., *Mitofusin 2 protects cerebellar granule neurons against injury-induced cell death.* J Biol Chem, 2007. 282(33): p. 23788-98.
261. Yin, W., et al., *Rapidly increased neuronal mitochondrial biogenesis after hypoxic-ischemic brain injury.* Stroke, 2008. 39(11): p. 3057-63.
262. Youle, R.J. and D.P. Narendra, *Mechanisms of mitophagy.* Nat Rev Mol Cell Biol, 2011. 12(1): p. 9-14.
263. Kim, I., S. Rodriguez-Enriquez, and J.J. Lemasters, *Selective degradation of mitochondria by mitophagy.* Arch Biochem Biophys, 2007. 462(2): p. 245-53.
264. Sandoval, H., et al., *Essential role for Nix in autophagic maturation of erythroid cells.* Nature, 2008. 454(7201): p. 232-5.
265. Sato, M. and K. Sato, *Degradation of paternal mitochondria by fertilization-triggered autophagy in C. elegans embryos.* Science, 2011. 334(6059): p. 1141-4.
266. Al Rawi, S., et al., *Postfertilization autophagy of sperm organelles prevents paternal mitochondrial DNA transmission.* Science, 2011. 334(6059): p. 1144-7.
267. Nowikovsky, K., et al., *Mdm38 protein depletion causes loss of mitochondrial K+/H+ exchange activity, osmotic swelling and mitophagy.* Cell Death Differ, 2007. 14(9): p. 1647-56.
268. Schweers, R.L., et al., *NIX is required for programmed mitochondrial clearance during reticulocyte maturation.* Proc Natl Acad Sci U S A, 2007. 104(49): p. 19500-5.
269. Kundu, M., et al., *Ulk1 plays a critical role in the autophagic clearance of mitochondria and ribosomes during reticulocyte maturation.* Blood, 2008. 112(4): p. 1493-502.
270. Schwarten, M., et al., *Nix directly binds to GABARAP: a possible crosstalk between apoptosis and autophagy.* Autophagy, 2009. 5(5): p. 690-8.
271. Novak, I., et al., *Nix is a selective autophagy receptor for mitochondrial clearance.* EMBO Rep, 2010. 11(1): p. 45-51.
272. Elmore, S.P., et al., *The mitochondrial permeability transition initiates autophagy in rat hepatocytes.* FASEB J, 2001. 15(12): p. 2286-7.
273. Twig, G., et al., *Fission and selective fusion govern mitochondrial segregation and elimination by autophagy.* EMBO J, 2008. 27(2): p. 433-46.
274. Greene, J.C., et al., *Mitochondrial pathology and apoptotic muscle degeneration in Drosophila parkin mutants.* Proc Natl Acad Sci U S A, 2003. 100(7): p. 4078-83.
275. Park, J., et al., *Mitochondrial dysfunction in Drosophila PINK1 mutants is complemented by parkin.* Nature, 2006. 441(7097): p. 1157-61.
276. Tolkovsky, A.M., et al., *Mitochondrial disappearance from cells: a clue to the role of autophagy in programmed cell death and disease?* Biochimie, 2002. 84(2-3): p. 233-40.
277. Dice, J.F., *Peptide sequences that target cytosolic proteins for lysosomal proteolysis.* Trends Biochem Sci, 1990. 15(8): p. 305-9.
278. Chiang, H.L., et al., *A role for a 70-kilodalton heat shock protein in lysosomal degradation of intracellular proteins.* Science, 1989. 246(4928): p. 382-5.
279. Cuervo, A.M. and J.F. Dice, *A receptor for the selective uptake and degradation of proteins by lysosomes.* Science, 1996. 273(5274): p. 501-3.
280. Agarraberes, F.A., S.R. Terlecky, and J.F. Dice, *An intralysosomal hsp70 is required*

for a selective pathway of lysosomal protein degradation. J Cell Biol, 1997. 137(4): p. 825-34.

281. Cuervo, A.M., et al., *Activation of a selective pathway of lysosomal proteolysis in rat liver by prolonged starvation.* Am J Physiol, 1995. 269(5 Pt 1): p. C1200-8.
282. Wing, S.S., et al., *Proteins containing peptide sequences related to Lys-Phe-Glu-Arg-Gln are selectively depleted in liver and heart, but not skeletal muscle, of fasted rats.* Biochem J, 1991. 275 (Pt 1): p. 165-9.
283. Kiffin, R., et al., *Activation of chaperone-mediated autophagy during oxidative stress.* Mol Biol Cell, 2004. 15(11): p. 4829-40.
284. Cuervo, A.M., et al., *Direct lysosomal uptake of alpha 2-microglobulin contributes to chemically induced nephropathy.* Kidney Int, 1999. 55(2): p. 529-45.
285. Cuervo, A.M., et al., *Impaired degradation of mutant alpha-synuclein by chaperone-mediated autophagy.* Science, 2004. 305(5688): p. 1292-5.
286. Martinez-Vicente, M., et al., *Dopamine-modified alpha-synuclein blocks chaperone-mediated autophagy.* J Clin Invest, 2008. 118(2): p. 777-88.
287. Cuervo, A.M., J.F. Dice, and E. Knecht, *A population of rat liver lysosomes responsible for the selective uptake and degradation of cytosolic proteins.* J Biol Chem, 1997. 272(9): p. 5606-15.
288. Ravagnan, L., et al., *Heat-shock protein 70 antagonizes apoptosis-inducing factor.* Nat Cell Biol, 2001. 3(9): p. 839-43.
289. Ruchalski, K., et al., *Distinct hsp70 domains mediate apoptosis-inducing factor release and nuclear accumulation.* J Biol Chem, 2006. 281(12): p. 7873-80.
290. Lee, S.H., et al., *Effects of hsp70.1 gene knockout on the mitochondrial apoptotic pathway after focal cerebral ischemia.* Stroke, 2004. 35(9): p. 2195-9.
291. Matsumori, Y., et al., *Hsp70 overexpression sequesters AIF and reduces neonatal hypoxic/ischemic brain injury.* J Cereb Blood Flow Metab, 2005. 25(7): p. 899-910.
292. Berridge, M.J., *The endoplasmic reticulum: a multifunctional signaling organelle.* Cell Calcium, 2002. 32(5-6): p. 235-49.
293. Bernales, S., F.R. Papa, and P. Walter, *Intracellular signaling by the unfolded protein response.* Annu Rev Cell Dev Biol, 2006. 22: p. 487-508.
294. Momoi, T., *Conformational diseases and ER stress-mediated cell death: apoptotic cell death and autophagic cell death.* Curr Mol Med, 2006. 6(1): p. 111-8.
295. Hoyer-Hansen, M. and M. Jaattela, *Connecting endoplasmic reticulum stress to autophagy by unfolded protein response and calcium.* Cell Death Differ, 2007. 14(9): p. 1576-82.
296. Bertolotti, A., et al., *Dynamic interaction of BiP and ER stress transducers in the unfolded-protein response.* Nat Cell Biol, 2000. 2(6): p. 326-32.
297. Bertolotti, A. and D. Ron, *Alterations in an IRE1-RNA complex in the mammalian unfolded protein response.* J Cell Sci, 2001. 114(Pt 17): p. 3207-12.
298. Hoyer-Hansen, M., et al., *Control of macroautophagy by calcium, calmodulin-dependent kinase kinase-beta, and Bcl-2.* Mol Cell, 2007. 25(2): p. 193-205.
299. Demarchi, F., et al., *Calpain is required for macroautophagy in mammalian cells.* J Cell Biol, 2006. 175(4): p. 595-605.
300. Ray, S.K., et al., *Oxidative stress and Ca2+ influx upregulate calpain and induce apoptosis in PC12 cells.* Brain Res, 2000. 852(2): p. 326-34.
301. Schoonbroodt, S., et al., *Crucial role of the amino-terminal tyrosine residue 42 and the carboxyl-terminal PEST domain of I kappa B alpha in NF-kappa B activation by an oxidative stress.* J Immunol, 2000. 164(8): p. 4292-300.
302. Yamashima, T., et al., *Sustained calpain activation associated with lysosomal rupture executes necrosis of the postischemic CA1 neurons in primates.* Hippocampus, 2003. 13(7): p. 791-800.

303. Yamashima, T., et al., *Transient brain ischaemia provokes Ca2+, PIP2 and calpain responses prior to delayed neuronal death in monkeys.* Eur J Neurosci, 1996. 8(9): p. 1932-44.
304. Ray, S.K., et al., *Diverse stimuli induce calpain overexpression and apoptosis in C6 glioma cells.* Brain Res, 1999. 829(1-2): p. 18-27.
305. Lee, M.S., et al., *Neurotoxicity induces cleavage of p35 to p25 by calpain.* Nature, 2000. 405(6784): p. 360-4.
306. Mouatt-Prigent, A., et al., *Increased M-calpain expression in the mesencephalon of patients with Parkinson's disease but not in other neurodegenerative disorders involving the mesencephalon: a role in nerve cell death?* Neuroscience, 1996. 73(4): p. 979-87.
307. Yamashima, T., *Ca2+-dependent proteases in ischemic neuronal death: a conserved 'calpain-cathepsin cascade' from nematodes to primates.* Cell Calcium, 2004. 36(3-4): p. 285-93.
308. Adamec, E., et al., *Up-regulation of the lysosomal system in experimental models of neuronal injury: implications for Alzheimer's disease.* Neuroscience, 2000. 100(3): p. 663-75.
309. Yamashima, T., *Implication of cysteine proteases calpain, cathepsin and caspase in ischemic neuronal death of primates.* Prog Neurobiol, 2000. 62(3): p. 273-95.
310. Chan, P.H., *Role of oxidants in ischemic brain damage.* Stroke, 1996. 27(6): p. 1124-9.
311. Takano, J., et al., *Calpain mediates excitotoxic DNA fragmentation via mitochondrial pathways in adult brains: evidence from calpastatin mutant mice.* J Biol Chem, 2005. 280(16): p. 16175-84.
312. Muntener, K., et al., *Exon skipping of cathepsin B: mitochondrial targeting of a lysosomal peptidase provokes cell death.* J Biol Chem, 2004. 279(39): p. 41012-7.
313. Guicciardi, M.E., et al., *Cathepsin B knockout mice are resistant to tumor necrosis factor-alpha-mediated hepatocyte apoptosis and liver injury: implications for therapeutic applications.* Am J Pathol, 2001. 159(6): p. 2045-54.
314. Canbay, A., et al., *Cathepsin B inactivation attenuates hepatic injury and fibrosis during cholestasis.* J Clin Invest, 2003. 112(2): p. 152-9.
315. Benchoua, A., et al., *Activation of proinflammatory caspases by cathepsin B in focal cerebral ischemia.* J Cereb Blood Flow Metab, 2004. 24(11): p. 1272-9.
316. Danial, N.N. and S.J. Korsmeyer, *Cell death: critical control points.* Cell, 2004. 116(2): p. 205-19.
317. Leber, B., J. Lin, and D.W. Andrews, *Embedded together: the life and death consequences of interaction of the Bcl-2 family with membranes.* Apoptosis, 2007. 12(5): p. 897-911.
318. Reed, J.C., *Proapoptotic multidomain Bcl-2/Bax-family proteins: mechanisms, physiological roles, and therapeutic opportunities.* Cell Death Differ, 2006. 13(8): p. 1378-86.
319. Youle, R.J. and A. Strasser, *The BCL-2 protein family: opposing activities that mediate cell death.* Nat Rev Mol Cell Biol, 2008. 9(1): p. 47-59.
320. Lalier, L., et al., *Bax activation and mitochondrial insertion during apoptosis.* Apoptosis, 2007. 12(5): p. 887-96.
321. Tajeddine, N., et al., *Hierarchical involvement of Bak, VDAC1 and Bax in cisplatin-induced cell death.* Oncogene, 2008. 27(30): p. 4221-32.
322. Zamzami, N., et al., *Bid acts on the permeability transition pore complex to induce apoptosis.* Oncogene, 2000. 19(54): p. 6342-50.
323. Kuwana, T., et al., *BH3 domains of BH3-only proteins differentially regulate Bax-mediated mitochondrial membrane permeabilization both directly and indirectly.*

Mol Cell, 2005. 17(4): p. 525-35.
324. Kim, R., *Unknotting the roles of Bcl-2 and Bcl-xL in cell death.* Biochem Biophys Res Commun, 2005. 333(2): p. 336-43.
325. Pinton, P. and R. Rizzuto, *Bcl-2 and Ca2+ homeostasis in the endoplasmic reticulum.* Cell Death Differ, 2006. 13(8): p. 1409-18.
326. Zamzami, N., N. Larochette, and G. Kroemer, *Mitochondrial permeability transition in apoptosis and necrosis.* Cell Death Differ, 2005. 12 Suppl 2: p. 1478-80.
327. Zoratti, M., I. Szabo, and U. De Marchi, *Mitochondrial permeability transitions: how many doors to the house?* Biochim Biophys Acta, 2005. 1706(1-2): p. 40-52.
328. Brenner, C., et al., *Bcl-2 and Bax regulate the channel activity of the mitochondrial adenine nucleotide translocator.* Oncogene, 2000. 19(3): p. 329-36.
329. Pattingre, S., et al., *Bcl-2 antiapoptotic proteins inhibit Beclin 1-dependent autophagy.* Cell, 2005. 122(6): p. 927-39.
330. Rodriguez, D., D. Rojas-Rivera, and C. Hetz, *Integrating stress signals at the endoplasmic reticulum: The BCL-2 protein family rheostat.* Biochim Biophys Acta, 2011. 1813(4): p. 564-74.
331. Kouroku, Y., et al., *ER stress (PERK/eIF2alpha phosphorylation) mediates the polyglutamine-induced LC3 conversion, an essential step for autophagy formation.* Cell Death Differ, 2007. 14(2): p. 230-9.
332. Ogata, M., et al., *Autophagy is activated for cell survival after endoplasmic reticulum stress.* Mol Cell Biol, 2006. 26(24): p. 9220-31.
333. Yorimitsu, T., et al., *Endoplasmic reticulum stress triggers autophagy.* J Biol Chem, 2006. 281(40): p. 30299-304.
334. Ding, W.X., et al., *Differential effects of endoplasmic reticulum stress-induced autophagy on cell survival.* J Biol Chem, 2007. 282(7): p. 4702-10.
335. Aita, V.M., et al., *Cloning and genomic organization of beclin 1, a candidate tumor suppressor gene on chromosome 17q21.* Genomics, 1999. 59(1): p. 59-65.
336. Liang, X.H., et al., *Induction of autophagy and inhibition of tumorigenesis by beclin 1.* Nature, 1999. 402(6762): p. 672-6.
337. Qu, X., et al., *Promotion of tumorigenesis by heterozygous disruption of the beclin 1 autophagy gene.* J Clin Invest, 2003. 112(12): p. 1809-20.
338. Yue, Z., et al., *Beclin 1, an autophagy gene essential for early embryonic development, is a haploinsufficient tumor suppressor.* Proc Natl Acad Sci U S A, 2003. 100(25): p. 15077-82.
339. Maiuri, M.C., et al., *Functional and physical interaction between Bcl-X(L) and a BH3-like domain in Beclin-1.* EMBO J, 2007. 26(10): p. 2527-39.
340. Maiuri, M.C., et al., *BH3-only proteins and BH3 mimetics induce autophagy by competitively disrupting the interaction between Beclin 1 and Bcl-2/Bcl-X(L).* Autophagy, 2007. 3(4): p. 374-6.
341. Bellot, G., et al., *Hypoxia-induced autophagy is mediated through hypoxia-inducible factor induction of BNIP3 and BNIP3L via their BH3 domains.* Mol Cell Biol, 2009. 29(10): p. 2570-81.
342. Azad, M.B., et al., *Hypoxia induces autophagic cell death in apoptosis-competent cells through a mechanism involving BNIP3.* Autophagy, 2008. 4(2): p. 195-204.
343. Chinnadurai, G., S. Vijayalingam, and S.B. Gibson, *BNIP3 subfamily BH3-only proteins: mitochondrial stress sensors in normal and pathological functions.* Oncogene, 2008. 27 Suppl 1: p. S114-27.
344. Gillardon, F., et al., *Inhibition of caspases prevents cell death of hippocampal CA1 neurons, but not impairment of hippocampal long-term potentiation following global ischemia.* Neuroscience, 1999. 93(4): p. 1219-22.
345. Strosznajder, R. and B. Gajkowska, *Effect of 3-aminobenzamide on Bcl-2, Bax and*

AIF localization in hippocampal neurons altered by ischemia-reperfusion injury. the immunocytochemical study. Acta Neurobiol Exp (Wars), 2006. 66(1): p. 15-22.

346. Niimura, M., et al., *Prevention of apoptosis-inducing factor translocation is a possible mechanism for protective effects of hepatocyte growth factor against neuronal cell death in the hippocampus after transient forebrain ischemia.* J Cereb Blood Flow Metab, 2006. 26(11): p. 1354-65.
347. Li, X., et al., *Influence of duration of focal cerebral ischemia and neuronal nitric oxide synthase on translocation of apoptosis-inducing factor to the nucleus.* Neuroscience, 2007. 144(1): p. 56-65.
348. Sun, Y., et al., *The carboxyl-terminal domain of inducible Hsp70 protects from ischemic injury in vivo and in vitro.* J Cereb Blood Flow Metab, 2006. 26(7): p. 937-50.
349. Parrish, J., et al., *Mitochondrial endonuclease G is important for apoptosis in C. elegans.* Nature, 2001. 412(6842): p. 90-4.
350. Kalinowska, M., et al., *Regulation of the human apoptotic DNase/RNase endonuclease G: involvement of Hsp70 and ATP.* Apoptosis, 2005. 10(4): p. 821-30.
351. Rustin, P., *The use of antioxidants in Friedreich's ataxia treatment.* Expert Opin Investig Drugs, 2003. 12(4): p. 569-75.
352. Elibol, B., et al., *Nitric oxide is involved in ischemia-induced apoptosis in brain: a study in neuronal nitric oxide synthase null mice.* Neuroscience, 2001. 105(1): p. 79-86.
353. Culmsee, C., et al., *A synthetic inhibitor of p53 protects neurons against death induced by ischemic and excitotoxic insults, and amyloid beta-peptide.* J Neurochem, 2001. 77(1): p. 220-8.
354. Morrison, R.S., et al., *Loss of the p53 tumor suppressor gene protects neurons from kainate-induced cell death.* J Neurosci, 1996. 16(4): p. 1337-45.
355. Gao, Y., et al., *Neuroprotection against focal ischemic brain injury by inhibition of c-Jun N-terminal kinase and attenuation of the mitochondrial apoptosis-signaling pathway.* J Cereb Blood Flow Metab, 2005. 25(6): p. 694-712.
356. Guan, Q.H., et al., *Neuroprotection against ischemic brain injury by a small peptide inhibitor of c-Jun N-terminal kinase (JNK) via nuclear and non-nuclear pathways.* Neuroscience, 2006. 139(2): p. 609-27.
357. Mattson, M.P. and G. Kroemer, *Mitochondria in cell death: novel targets for neuroprotection and cardioprotection.* Trends Mol Med, 2003. 9(5): p. 196-205.
358. Stavrovskaya, I.G., et al., *Clinically approved heterocyclics act on a mitochondrial target and reduce stroke-induced pathology.* J Exp Med, 2004. 200(2): p. 211-22.
359. Hetz, C., et al., *Bax channel inhibitors prevent mitochondrion-mediated apoptosis and protect neurons in a model of global brain ischemia.* J Biol Chem, 2005. 280(52): p. 42960-70.
360. Rodrigues, C.M., et al., *Tauroursodeoxycholic acid prevents Bax-induced membrane perturbation and cytochrome C release in isolated mitochondria.* Biochemistry, 2003. 42(10): p. 3070-80.
361. Rodrigues, C.M., et al., *Neuroprotection by a bile acid in an acute stroke model in the rat.* J Cereb Blood Flow Metab, 2002. 22(4): p. 463-71.
362. Rodrigues, C.M., et al., *Tauroursodeoxycholic acid reduces apoptosis and protects against neurological injury after acute hemorrhagic stroke in rats.* Proc Natl Acad Sci U S A, 2003. 100(10): p. 6087-92.
363. Saavedra, R.A., et al., *In vivo neuroprotection of injured CNS neurons by a single injection of a DNA plasmid encoding the Bcl-2 gene.* Prog Brain Res, 2000. 128: p. 365-72.
364. Martinou, J.C., et al., *Overexpression of BCL-2 in transgenic mice protects neurons*

from naturally occurring cell death and experimental ischemia. Neuron, 1994. 13(4): p. 1017-30.

365. Zhao, H., et al., *Bcl-2 overexpression protects against neuron loss within the ischemic margin following experimental stroke and inhibits cytochrome c translocation and caspase-3 activity.* J Neurochem, 2003. 85(4): p. 1026-36.
366. Wiessner, C., et al., *Neuron-specific transgene expression of Bcl-XL but not Bcl-2 genes reduced lesion size after permanent middle cerebral artery occlusion in mice.* Neurosci Lett, 1999. 268(3): p. 119-22.
367. Culmsee, C. and N. Plesnila, *Targeting Bid to prevent programmed cell death in neurons.* Biochem Soc Trans, 2006. 34(Pt 6): p. 1334-40.
368. Plesnila, N., et al., *BID mediates neuronal cell death after oxygen/ glucose deprivation and focal cerebral ischemia.* Proc Natl Acad Sci U S A, 2001. 98(26): p. 15318-23.
369. Plesnila, N., et al., *Function of BID -- a molecule of the bcl-2 family -- in ischemic cell death in the brain.* Eur Surg Res, 2002. 34(1-2): p. 37-41.
370. Tehranian, R., et al., *Disruption of Bax protein prevents neuronal cell death but produces cognitive impairment in mice following traumatic brain injury.* J Neurotrauma, 2008. 25(7): p. 755-67.
371. Gibson, M.E., et al., *BAX contributes to apoptotic-like death following neonatal hypoxia-ischemia: evidence for distinct apoptosis pathways.* Mol Med, 2001. 7(9): p. 644-55.
372. Fischer, S.F., et al., *Chlamydia inhibit host cell apoptosis by degradation of proapoptotic BH3-only proteins.* J Exp Med, 2004. 200(7): p. 905-16.
373. Rami, A., A. Langhagen, and S. Steiger, *Focal cerebral ischemia induces upregulation of Beclin 1 and autophagy-like cell death.* Neurobiol Dis, 2008. 29(1): p. 132-41.
374. Puyal, J., et al., *Postischemic treatment of neonatal cerebral ischemia should target autophagy.* Ann Neurol, 2009. 66(3): p. 378-89.
375. Asoh, S., et al., *Protection against ischemic brain injury by protein therapeutics.* Proc Natl Acad Sci U S A, 2002. 99(26): p. 17107-12.
376. Hayashi, K., et al., *Gene therapy for preventing neuronal death using hepatocyte growth factor: in vivo gene transfer of HGF to subarachnoid space prevents delayed neuronal death in gerbil hippocampal CA1 neurons.* Gene Ther, 2001. 8(15): p. 1167-73.
377. Nuglisch, J., et al., *Protective effect of nimodipine against ischemic neuronal damage in rat hippocampus without changing postischemic cerebral blood flow.* J Cereb Blood Flow Metab, 1990. 10(5): p. 654-9.
378. Mossakowski, M.J. and R. Gadamski, *Nimodipine prevents delayed neuronal death of sector CA1 pyramidal cells in short-term forebrain ischemia in Mongolian gerbils.* Stroke, 1990. 21(12 Suppl): p. IV120-2.
379. Hadley, M.N., et al., *The efficacy of intravenous nimodipine in the treatment of focal cerebral ischemia in a primate model.* Neurosurgery, 1989. 25(1): p. 63-70.
380. Nag, D., R.K. Garg, and M. Varma, *A randomized double-blind controlled study of nimodipine in acute cerebral ischemic stroke.* Indian J Physiol Pharmacol, 1998. 42(4): p. 555-8.
381. Kakarieka, A., E.H. Schakel, and J. Fritze, *Clinical experiences with nimodipine in cerebral ischemia.* J Neural Transm Suppl, 1994. 43: p. 13-21.
382. Mattson, M.P., et al., *Presenilin-1 mutation increases neuronal vulnerability to focal ischemia in vivo and to hypoxia and glucose deprivation in cell culture: involvement of perturbed calcium homeostasis.* J Neurosci, 2000. 20(4): p. 1358-64.
383. Wei, H. and D.C. Perry, *Dantrolene is cytoprotective in two models of neuronal cell*

death. J Neurochem, 1996. 67(6): p. 2390-8.
384. Huang, Z., et al., *Effects of cerebral ischemia in mice deficient in neuronal nitric oxide synthase.* Science, 1994. 265(5180): p. 1883-5.
385. Satoh, K., et al., *Edarabone scavenges nitric oxide.* Redox Rep, 2002. 7(4): p. 219-22.
386. Kamii, H., et al., *Effects of nitric oxide synthase inhibition on brain infarction in SOD-1-transgenic mice following transient focal cerebral ischemia.* J Cereb Blood Flow Metab, 1996. 16(6): p. 1153-7.
387. Hara, H., H. Nagasawa, and K. Kogure, *Nimodipine prevents postischemic brain damage in the early phase of focal cerebral ischemia.* Stroke, 1990. 21(12 Suppl): p. IV102-4.
388. Wolz, P. and J. Krieglstein, *Neuroprotective effects of alpha-lipoic acid and its enantiomers demonstrated in rodent models of focal cerebral ischemia.* Neuropharmacology, 1996. 35(3): p. 369-75.
389. Yu, Z.F., et al., *Uric acid protects neurons against excitotoxic and metabolic insults in cell culture, and against focal ischemic brain injury in vivo.* J Neurosci Res, 1998. 53(5): p. 613-25.
390. Gray, J., et al., *Evidence that inhibition of cathepsin-B contributes to the neuroprotective properties of caspase inhibitor Tyr-Val-Ala-Asp-chloromethyl ketone.* J Biol Chem, 2001. 276(35): p. 32750-5.
391. Endres, M., et al., *Neuroprotective effects of gelsolin during murine stroke.* J Clin Invest, 1999. 103(3): p. 347-54.
392. Kruman, II, et al., *Homocysteine elicits a DNA damage response in neurons that promotes apoptosis and hypersensitivity to excitotoxicity.* J Neurosci, 2000. 20(18): p. 6920-6.
393. Fisher, M., et al., *Update of the stroke therapy academic industry roundtable preclinical recommendations.* Stroke, 2009. 40(6): p. 2244-50.
394. STAIR, *Recommendations for standards regarding preclinical neuroprotective and restorative drug development.* Stroke, 1999. 30(12): p. 2752-8.
395. Macleod, M.R., et al., *Good laboratory practice: preventing introduction of bias at the bench.* Stroke, 2009. 40(3): p. e50-2.
396. Willing, A.E., *Experimental models: help or hindrance.* Stroke, 2009. 40(3 Suppl): p. S152-4.
397. Graham, S.H. and J. Chen, *Programmed cell death in cerebral ischemia.* J Cereb Blood Flow Metab, 2001. 21(2): p. 99-109.
398. Ferriero, D.M., *Neonatal brain injury.* N Engl J Med, 2004. 351(19): p. 1985-95.
399. Jiequn Weng, J.K., *Delayed neuronal death in stroke: Molecular pathways.*, in *Advancements in neurological research.* , J.H. Zhang, Editor 2008, Research Signpost: Kerala. p. pp. 1-22.
400. Petiot, A., et al., *Distinct classes of phosphatidylinositol 3'-kinases are involved in signaling pathways that control macroautophagy in HT-29 cells.* J Biol Chem, 2000. 275(2): p. 992-8.
401. Juhasz, G., et al., *The class III PI(3)K Vps34 promotes autophagy and endocytosis but not TOR signaling in Drosophila.* J Cell Biol, 2008. 181(4): p. 655-66.
402. Hara, T., et al., *Suppression of basal autophagy in neural cells causes neurodegenerative disease in mice.* Nature, 2006. 441(7095): p. 885-9.
403. Green, D.R., L. Galluzzi, and G. Kroemer, *Mitochondria and the autophagy-inflammation-cell death axis in organismal aging.* Science, 2011. 333(6046): p. 1109-12.
404. Komatsu, M., et al., *Loss of autophagy in the central nervous system causes neurodegeneration in mice.* Nature, 2006. 441(7095): p. 880-4.

405. Wong, E. and A.M. Cuervo, *Autophagy gone awry in neurodegenerative diseases.* Nat Neurosci, 2010. 13(7): p. 805-11.
406. Althaus, J., et al., *Expression of the gene encoding the pro-apoptotic BNIP3 protein and stimulation of hypoxia-inducible factor-1alpha (HIF-1alpha) protein following focal cerebral ischemia in rats.* Neurochem Int, 2006. 48(8): p. 687-95.
407. Zhang, H., et al., *Mitochondrial autophagy is an HIF-1-dependent adaptive metabolic response to hypoxia.* J Biol Chem, 2008. 283(16): p. 10892-903.
408. Chu, C.T., H. Bayir, and V.E. Kagan, *LC3 binds externalized cardiolipin on injured mitochondria to signal mitophagy in neurons: Implications for Parkinson disease.* Autophagy, 2013. 10(2).
409. Batlevi, Y. and A.R. La Spada, *Mitochondrial autophagy in neural function, neurodegenerative disease, neuron cell death, and aging.* Neurobiol Dis, 2011. 43(1): p. 46-51.
410. Chakrabarti, L., et al., *Autophagy activation and enhanced mitophagy characterize the Purkinje cells of pcd mice prior to neuronal death.* Mol Brain, 2009. 2: p. 24.
411. Zhang, J. and P.A. Ney, *Role of BNIP3 and NIX in cell death, autophagy, and mitophagy.* Cell Death Differ, 2009. 16(7): p. 939-46.
412. Sheldon, R.A., J. Chuai, and D.M. Ferriero, *A rat model for hypoxic-ischemic brain damage in very premature infants.* Biol Neonate, 1996. 69(5): p. 327-41.
413. McQuillen, P.S., et al., *Selective vulnerability of subplate neurons after early neonatal hypoxia-ischemia.* J Neurosci, 2003. 23(8): p. 3308-15.
414. Bederson, J.B., et al., *Evaluation of 2,3,5-triphenyltetrazolium chloride as a stain for detection and quantification of experimental cerebral infarction in rats.* Stroke, 1986. 17(6): p. 1304-8.
415. Kurozumi, K., et al., *Mesenchymal stem cells that produce neurotrophic factors reduce ischemic damage in the rat middle cerebral artery occlusion model.* Mol Ther, 2005. 11(1): p. 96-104.
416. Swanson, R.A., et al., *A semiautomated method for measuring brain infarct volume.* J Cereb Blood Flow Metab, 1990. 10(2): p. 290-3.
417. Zhao, M.Z., et al., *Novel therapeutic strategy for stroke in rats by bone marrow stromal cells and ex vivo HGF gene transfer with HSV-1 vector.* J Cereb Blood Flow Metab, 2006. 26(9): p. 1176-88.
418. Zhu, S., et al., *Therapeutic effects of quetiapine on memory deficit and brain beta-amyloid plaque pathology in a transgenic mouse model of Alzheimer's disease.* Curr Alzheimer Res, 2013. 10(3): p. 270-8.
419. Qing, H., et al., *Valproic acid inhibits Abeta production, neuritic plaque formation, and behavioral deficits in Alzheimer's disease mouse models.* J Exp Med, 2008. 205(12): p. 2781-9.
420. Brewer, G.J., *Serum-free B27/neurobasal medium supports differentiated growth of neurons from the striatum, substantia nigra, septum, cerebral cortex, cerebellum, and dentate gyrus.* J Neurosci Res, 1995. 42(5): p. 674-83.
421. Biederbick, A., H.F. Kern, and H.P. Elsasser, *Monodansylcadaverine (MDC) is a specific in vivo marker for autophagic vacuoles.* Eur J Cell Biol, 1995. 66(1): p. 3-14.
422. Munafo, D.B. and M.I. Colombo, *A novel assay to study autophagy: regulation of autophagosome vacuole size by amino acid deprivation.* J Cell Sci, 2001. 114(Pt 20): p. 3619-29.
423. Delk, N.A. and M.C. Farach-Carson, *Interleukin-6: a bone marrow stromal cell paracrine signal that induces neuroendocrine differentiation and modulates autophagy in bone metastatic PCa cells.* Autophagy, 2012. 8(4): p. 650-63.
424. Burton, T.R., et al., *BNIP3 acts as transcriptional repressor of death receptor-5 expression and prevents TRAIL-induced cell death in gliomas.* Cell Death Dis, 2013.

4: p. e587.

425. Hellstrom-Lindahl, E., M. Viitanen, and A. Marutle, *Comparison of Abeta levels in the brain of familial and sporadic Alzheimer's disease.* Neurochem Int, 2009. 55(4): p. 243-52.

426. Paglin, S., et al., *A novel response of cancer cells to radiation involves autophagy and formation of acidic vesicles.* Cancer Res, 2001. 61(2): p. 439-44.

427. Parks, D.R., et al., *Antigen-specific identification and cloning of hybridomas with a fluorescence-activated cell sorter.* Proc Natl Acad Sci U S A, 1979. 76(4): p. 1962-6.

428. Seglen, P.O. and P.B. Gordon, *3-Methyladenine: specific inhibitor of autophagic/lysosomal protein degradation in isolated rat hepatocytes.* Proc Natl Acad Sci U S A, 1982. 79(6): p. 1889-92.

429. Scarlatti, F., et al., *Ceramide-mediated macroautophagy involves inhibition of protein kinase B and up-regulation of beclin 1.* J Biol Chem, 2004. 279(18): p. 18384-91.

430. Yano, M., et al., *Identification and functional analysis of human Tom22 for protein import into mitochondria.* Mol Cell Biol, 2000. 20(19): p. 7205-13.

431. Saeki, K., et al., *Identification of mammalian TOM22 as a subunit of the preprotein translocase of the mitochondrial outer membrane.* J Biol Chem, 2000. 275(41): p. 31996-2002.

432. Tsukihara, T., et al., *Structures of metal sites of oxidized bovine heart cytochrome c oxidase at 2.8 A.* Science, 1995. 269(5227): p. 1069-74.

433. Chatre, L. and M. Ricchetti, *Large heterogeneity of mitochondrial DNA transcription and initiation of replication exposed by single-cell imaging.* J Cell Sci, 2013. 126(Pt 4): p. 914-26.

434. Bender, A., et al., *TOM40 mediates mitochondrial dysfunction induced by alpha-synuclein accumulation in Parkinson's disease.* PLoS One, 2013. 8(4): p. e62277.

435. Chacko, A.D., et al., *Voltage dependent anion channel-1 regulates death receptor mediated apoptosis by enabling cleavage of caspase-8.* BMC Cancer, 2010. 10: p. 380.

436. Hornig-Do, H.T., et al., *Isolation of functional pure mitochondria by superparamagnetic microbeads.* Anal Biochem, 2009. 389(1): p. 1-5.

437. Liu, S., et al., *Parkinson's disease-associated kinase PINK1 regulates Miro protein level and axonal transport of mitochondria.* PLoS Genet, 2012. 8(3): p. e1002537.

438. Zu, L., et al., *Ischemic preconditioning attenuates mitochondrial localization of PTEN induced by ischemia-reperfusion.* Am J Physiol Heart Circ Physiol, 2011. 300(6): p. H2177-86.

439. Franko, A., et al., *Efficient Isolation of Pure and Functional Mitochondria from Mouse Tissues Using Automated Tissue Disruption and Enrichment with Anti-TOM22 Magnetic Beads.* PLoS One, 2013. 8(12): p. e82392.

440. Kabeya, Y., et al., *LC3, a mammalian homologue of yeast Apg8p, is localized in autophagosome membranes after processing.* EMBO J, 2000. 19(21): p. 5720-8.

441. Mann, S.S. and J.A. Hammarback, *Molecular characterization of light chain 3. A microtubule binding subunit of MAP1A and MAP1B.* J Biol Chem, 1994. 269(15): p. 11492-7.

442. Mizushima, N., *Methods for monitoring autophagy.* Int J Biochem Cell Biol, 2004. 36(12): p. 2491-502.

443. Levine, B. and D.J. Klionsky, *Development by self-digestion: molecular mechanisms and biological functions of autophagy.* Dev Cell, 2004. 6(4): p. 463-77.

444. Rami, A., *Upregulation of Beclin 1 in the ischemic penumbra.* Autophagy, 2008. 4(2): p. 227-9.

445. Eskelinen, E.L., et al., *Unifying nomenclature for the isoforms of the lysosomal*

membrane protein LAMP-2. Traffic, 2005. 6(11): p. 1058-61.
446. Biedler, J.L., et al., *Multiple neurotransmitter synthesis by human neuroblastoma cell lines and clones.* Cancer Res, 1978. 38(11 Pt 1): p. 3751-7.
447. Zheng, Z., et al., *Anti-inflammatory effects of the 70 kDa heat shock protein in experimental stroke.* J Cereb Blood Flow Metab, 2008. 28(1): p. 53-63.
448. Yan, C.H., et al., *Contributions of autophagic and apoptotic mechanisms to CrTX-induced death of K562 cells.* Toxicon, 2006. 47(5): p. 521-30.
449. Schmued, L.C., et al., *Fluoro-Jade C results in ultra high resolution and contrast labeling of degenerating neurons.* Brain Res, 2005. 1035(1): p. 24-31.
450. Chen, Y., et al., *Mitochondrial electron-transport-chain inhibitors of complexes I and II induce autophagic cell death mediated by reactive oxygen species.* J Cell Sci, 2007. 120(Pt 23): p. 4155-66.
451. Kabuta, T., Y. Suzuki, and K. Wada, *Degradation of amyotrophic lateral sclerosis-linked mutant Cu,Zn-superoxide dismutase proteins by macroautophagy and the proteasome.* J Biol Chem, 2006. 281(41): p. 30524-33.
452. Jung, C.H., et al., *mTOR regulation of autophagy.* FEBS Lett, 2010. 584(7): p. 1287-95.
453. Law, B.K., *Rapamycin: an anti-cancer immunosuppressant?* Crit Rev Oncol Hematol, 2005. 56(1): p. 47-60.
454. Liang, X.H., et al., *Protection against fatal Sindbis virus encephalitis by beclin, a novel Bcl-2-interacting protein.* J Virol, 1998. 72(11): p. 8586-96.
455. Platt, M.J., et al., *Trends in cerebral palsy among infants of very low birthweight (<1500 g) or born prematurely (<32 weeks) in 16 European centres: a database study.* Lancet, 2007. 369(9555): p. 43-50.
456. Allin, M., et al., *Cognitive maturation in preterm and term born adolescents.* J Neurol Neurosurg Psychiatry, 2008. 79(4): p. 381-6.
457. Larroque, B., et al., *Neurodevelopmental disabilities and special care of 5-year-old children born before 33 weeks of gestation (the EPIPAGE study): a longitudinal cohort study.* Lancet, 2008. 371(9615): p. 813-20.
458. Azzopardi, D.V., et al., *Moderate hypothermia to treat perinatal asphyxial encephalopathy.* N Engl J Med, 2009. 361(14): p. 1349-58.
459. Edwards, A.D., et al., *Neurological outcomes at 18 months of age after moderate hypothermia for perinatal hypoxic ischaemic encephalopathy: synthesis and meta-analysis of trial data.* BMJ, 2010. 340: p. c363.
460. Gluckman, P.D., et al., *Selective head cooling with mild systemic hypothermia after neonatal encephalopathy: multicentre randomised trial.* Lancet, 2005. 365(9460): p. 663-70.
461. Shankaran, S., et al., *Whole-body hypothermia for neonates with hypoxic-ischemic encephalopathy.* N Engl J Med, 2005. 353(15): p. 1574-84.
462. Liszczak, T.M., et al., *Limitations of tetrazolium salts in delineating infarcted brain.* Acta Neuropathol, 1984. 65(2): p. 150-7.
463. Liu, S., et al., *Interstitial pO2 in ischemic penumbra and core are differentially affected following transient focal cerebral ischemia in rats.* J Cereb Blood Flow Metab, 2004. 24(3): p. 343-9.
464. Gaudinski, M.R., et al., *Establishing final infarct volume: stroke lesion evolution past 30 days is insignificant.* Stroke, 2008. 39(10): p. 2765-8.
465. van der Worp, H.B., et al., *Methodological quality of animal studies on neuroprotection in focal cerebral ischaemia.* J Neurol, 2005. 252(9): p. 1108-14.
466. Quinsay, M.N., et al., *Bnip3-mediated mitochondrial autophagy is independent of the mitochondrial permeability transition pore.* Autophagy, 2010. 6(7): p. 17-24.
467. Azad, M.B. and S.B. Gibson, *Role of BNIP3 in proliferation and hypoxia-induced*

autophagy: implications for personalized cancer therapies. **Ann N Y Acad Sci, 2010. 1210: p. 8-16.**

468. Zhang, H.M., et al., ***BNips: a group of pro-apoptotic proteins in the Bcl-2 family.*** **Apoptosis, 2003. 8(3): p. 229-36.**

469. Rikka, S., et al., ***Bnip3 impairs mitochondrial bioenergetics and stimulates mitochondrial turnover.*** **Cell Death Differ, 2011. 18(4): p. 721-31.**

470. He, S., et al., ***Immune-related GTPase M (IRGM1) regulates neuronal autophagy in a mouse model of stroke.*** **Autophagy, 2012. 8(11): p. 1621-7.**

471. Kubli, D.A., J.E. Ycaza, and A.B. Gustafsson, ***Bnip3 mediates mitochondrial dysfunction and cell death through Bax and Bak.*** **Biochem J, 2007. 405(3): p. 407-15.**

472. Burton, T.R. and S.B. Gibson, ***The role of Bcl-2 family member BNIP3 in cell death and disease: NIPping at the heels of cell death.*** **Cell Death Differ, 2009. 16(4): p. 515-23.**

473. Graham, S.H. and J. Chen, ***Programmed cell death in cerebral ischemia.*** **J Cereb Blood Flow Metab, 2001. 21(2): p. 99-109.**

474. Sarkar, S., et al., ***Lithium induces autophagy by inhibiting inositol monophosphatase.*** **J Cell Biol, 2005. 170(7): p. 1101-11.**

475. Ong, J., et al., ***Hypoxic-ischemic injury stimulates subventricular zone proliferation and neurogenesis in the neonatal rat.*** **Pediatr Res, 2005. 58(3): p. 600-6.**

476. Plane, J.M., et al., ***Neonatal hypoxic-ischemic injury increases forebrain subventricular zone neurogenesis in the mouse.*** **Neurobiol Dis, 2004. 16(3): p. 585-95.**

477. Yang, Z. and S.W. Levison, ***Hypoxia/ischemia expands the regenerative capacity of progenitors in the perinatal subventricular zone.*** **Neuroscience, 2006. 139(2): p. 555-64.**

478. Kadam, S.D., et al., ***Neurogenesis and neuronal commitment following ischemia in a new mouse model for neonatal stroke.*** **Brain Res, 2008. 1208: p. 35-45.**

479. Hayashi, T., et al., ***Neural precursor cells division and migration in neonatal rat brain after ischemic/hypoxic injury.*** **Brain Res, 2005. 1038(1): p. 41-9.**

480. Yang, Z., et al., ***Sustained neocortical neurogenesis after neonatal hypoxic/ischemic injury.*** **Ann Neurol, 2007. 61(3): p. 199-208.**

481. Donega, V., et al., ***The endogenous regenerative capacity of the damaged newborn brain: boosting neurogenesis with mesenchymal stem cell treatment.*** **J Cereb Blood Flow Metab, 2013. 33(5): p. 625-34.**

482. Martinez-Vicente, M., et al., ***Cargo recognition failure is responsible for inefficient autophagy in Huntington's disease.*** **Nat Neurosci, 2010. 13(5): p. 567-76.**

483. Fornai, F., et al., ***Autophagy and amyotrophic lateral sclerosis: The multiple roles of lithium.*** **Autophagy, 2008. 4(4): p. 527-30.**

484. Pickford, F., et al., ***The autophagy-related protein beclin 1 shows reduced expression in early Alzheimer disease and regulates amyloid beta accumulation in mice.*** **J Clin Invest, 2008. 118(6): p. 2190-9.**

485. Nixon, R.A., et al., ***Extensive involvement of autophagy in Alzheimer disease: an immuno-electron microscopy study.*** **J Neuropathol Exp Neurol, 2005. 64(2): p. 113-22.**